Petrogenesis of kimberlites from South Africa and lamproites from Western Australia and North America

Thesis

Petrogenesis of Kimberlites from South Africa and Lamproites from Western Australia and North America

A thesis presented for the degree of
Doctor of Philosophy

by

Kirsten Jane Fraser

BSc. Hons. (Edinburgh) 1983

Department of Earth Sciences
The Open University
September 1987

Acknowledgements

This work was initially funded by the De Beers Mining Corporation. They also provided the majority of the samples for this study. I would like to express my thanks to the following:

Chris Hawkesworth, my supervisor, for his help and encouragement throughout this research and for critical comments on earlier drafts of this thesis.

John Bristow, Mike Skinner, Jock Robey, Simon Shee and Barry Hawthorne (De Beers Geology Department, Kimberley), together with Tony Erlank (UCT), Craig Smith (BPI) and, in particular, Barbara Scott Smith, for their hospitality in South Africa and for introducing me, with enthusiasm, to the world of kimberlites and lamproites.

Nick Rogers, at the O.U., for help with INAA, for many valuable discussions and critical comments on earlier drafts. Peter van Calsteren, Andy Gledhill and Zen Palacz for support in the O.U. isotope laboratories. John Taylor and Andrew Lloyd for cartographic advice.

Godfrey Fitton and Dodie James for letting me use the Edinburgh University XRF facilities, and for their advice. Mike Saunders at Edinburgh University for help in wet chemical techniques and the use of the atomic absorption equipment.

Nick Walsh (Kings College, London) for providing ICP analyses and Roger Mitchell (Lakehead University, Canada) for samples from Smoky Butte.

Sue Brooks (O.U. Academic Computing Service) for help with the LaTeX production scheme used to produce this thesis.

My thanks go to the O.U. overseas travel fund, the O.U Earth Sciences department and the organisers of the 4th International Kimberlite Conference for money to attend the 4IKC in Perth Australia (1986) and to Pete Nixon (Leeds University) for including me in the 1986 Royal Society Expedition to the Soloman Islands.

Finally, I would like to express my thanks to Ray Burgess, Fiona M. McGibbon and Bramley J. Murton who, in the final stages of this work, contributed to the typing, proof-reading or compilation of this thesis.

Abstract

Group 2 kimberlites from South Africa, and lamproites from Western Australia and North America are relatively unfractionated mantle-derived igneous rocks, situated on or close to ancient cratonic areas. They are characterised by high trace element contents, while the range in Nd and Sr isotopes encompasses much of that reported for various upper and lower crustal rocks. It is argued that these features are not due to crustal contamination during magma ascent, rather they are source and extraction phenomena.

The mantle source regions of these rocks were ancient ($\simeq$ 1.0 to 2.5 Ga) and variably trace element enriched. Preservation of such regions within the mantle is most probable in the relatively 'cold' and 'rigid' subcontinental mantle lithosphere, which is believed to have been isolated from the convecting asthenosphere for a long time. The source regions of the kimberlites and lamproites were situated at various depths within the subcontinental mantle lithosphere, from within the amphibole stability field ($<$ 100 km) to within the diamond stability field ($>$ 150 km). Low degrees of partial melting ($<$ 1%), together with volatile composition and depth of melting, have significantly influenced the composition of the resultant kimberlite and lamproite magmas. Those magmas that originated from within the diamond stability field contain abundant entrained and disaggregated mantle peridotite. This feature is related to melt migration and rapid ascent to the surface, from these mantle depths.

The Sr, Nd and Pb isotope data record evidence of variable, but related trace element enrichment styles. The origin of these trace elements is either from recycled continental crust (e.g. pelagic sediment), or from intra-mantle processes (e.g. the migration and crystallisation of small volume silicate melts with variable volatile compositions). The available data are insufficient to determine between the models and further work in this area is required.

Nomenclature

GP	=	garnet peridotite
GPP	=	garnet phlogopite peridotite
PP	=	phlogopite peridotite
PKP	=	phlogopite K-richterite peridotite
MARID	=	mica-amphibole-rutile-ilmenite-diopside mantle xenolith
TKB	=	tuffisitic kimberlite breccia
EPD	=	external precursor dyke
LOI	=	loss on ignition
OIB	=	ocean island basalt
MORB	=	mid-ocean ridge basalt
KLMZ	=	King Leopold Mobile Zone
HCMZ	=	Halls Creek Mobile Zone
4IKC	=	Fourth International Kimberlite conference
REE	=	rare earth elements
LREE	=	light rare earth elements
HREE	=	heavy rare earth elements
HFSE	=	high field strength elements
LILE	=	large ion lithophile elements
PPL	=	plane polarised light
XPL	=	cross polarised light
RO	=	Millipore reverse osmosis system
TD	=	teflon distilled

Contents

List of Figures

List of Tables

Chapter 1

Introduction

1.1 Background

Study of mantle derived volcanics and entrained xenoliths has rewarded scientists with a better understanding of the nature and evolution of the upper mantle portion of the earth. The information is fragmentary and far from complete, yet the plethora of evidence acquired in recent years has effected a considerable shift away from simple two component (crust and depleted mantle) models to explain the radiogenic isotope variations in mantle-derived rocks (O'Nions et al., 1979; Allègre, 1982; Zindler et al., 1982). Xenoliths from the subcontinental mantle have been shown to preserve a wide range in Sr, Nd and Pb isotope ratios, which are thought to have developed in old mantle material within the continental lithosphere (Kramers et al., 1983; Menzies, 1983; Richardson et al., 1984). However, questions remain over the processes responsible for the inferred fractionation in Rb/Sr, Sm/Nd, U/Pb and Th/Pb and concerning the extent to which such lithosphere is remobilised during continental magmatism.

Geophysical considerations suggest that the continental lithosphere is 100 to 250 km thick and that 60% to 80% of it consists of upper mantle rocks attached to the base of the continental crust (Jordan, 1978). Ancient ages from inclusions in diamonds (Richardson et al., 1984) and thermal considerations (Bickle, 1986) intimate that a thick continental lithosphere has been preserved since Archaean times. Bickle (op. cit.) proposed that the substantial increase in depth range of melting for a hotter Archaean mantle resulted in anomalously thick residual lithosphere under Archaean cratons. The residual major element chemistry of peridotite xenoliths from the subcontinental lithosphere is consistent with them having been depleted by melt extraction (Nixon et al., 1981; Harte, 1983). Temperatures recorded from geothermometry of mantle peridotites are low with respect to their high pressures (e.g. Shee et al., 1982). This is compatible with low geothermal gradients inferred for ancient cratonic areas from surface heat flow measure-

ments (e.g. Chapman and Pollack, 1977). That many Archaean medium and high grade metamorphic rocks crystallised at similar pressures and temperatures to much younger metamorphic rocks, has prompted the suggestion that the thermal state of the continental crust and lithosphere has changed little during the ca. 3500 Ma of the geological record (Windley, 1977; Bickle, 1978; Burke and Kidd, 1978). Thus, the subcontinental lithosphere is cold and rigid to the depth of the diamond stability field and presumably isolated from the areas of convection (the asthenosphere) within the upper mantle.

Study of mantle xenoliths from kimberlites and continental alkaline magmatism provides evidence that the subcontinental mantle lithosphere has been subjected to numerous trace element enrichment events over a long period of time. The role of metasomatic processes in the mantle has received much attention of late e.g. Menzies and Hawkesworth (1987) and references therein. Dawson (1984) proposes that the effects of mantle metasomatism, as recorded in numerous xenoliths, could be termed either patent or cryptic.

Patent metasomatism, similar to modal metasomatism coined by Harte (1983), is accompanied by the crystallisation of phases such as amphibole (e.g. K-richterite and kaersutite), phlogopite, clinopyroxene and ore minerals, such as sulphides. Such metasomatised xenoliths have been extensively collected from continental alkali basalts (e.g. Lloyd and Bailey, 1975; Bergman et al., 1981; Cohen et al., 1984; Kempton, 1987; Menzies et al., 1987 and references therein) and from kimberlites (Carswell, 1975; Erlank and Rickard, 1977; Harte et al., 1975, 1987; Erlank et al., 1982, 1987; Waters, 1986, 1987).

Cryptic metasomatism has been identified in a wide range of xenoliths from both basalts and kimberlites (e.g. Frey and Green, 1974; Shimizu, 1975; Nixon et al., 1981; Cohen et al., 1984). These xenoliths are characterised by a depletion in major elements, or 'basaltic' elements, such as Ca, Al, Fe, Ti and Na, but are enriched in incompatible elements e.g. REE (Nixon et al., 1981), Rb, Cs, Sr and Ba (Shimizu, 1975).

Most pertinent to this study has been the work on the mantle xenoliths carried by kimberlites. The majority can be divided into two main groups, sheared and coarse textured (Nixon and Boyd, 1973a; Harte, 1983). The sheared peridotites are generally fertile in basaltic components, relatively depleted in incompatible trace elements and appear to have an origin closely associated with asthenospheric mantle. On the other hand, the coarse peridotites tend to be depleted in major elements and enriched in trace elements and are believed to represent cryptically metasomatised, depleted lithosphere mantle (Shimizu, 1975; Nixon et al., 1981; Richardson et al., 1985). This trace element enrichment cannot be totally ascribed to contamination by the host magmas, since high trace element concentra-

tions and enriched isotope signatures are observed within the mineral phases (Shimizu, 1975; Kramers, 1977; Menzies and Murthy, 1980; Cohen et al., 1984; Richardson et al., 1985).

Patent metasomatism has been attributed to the migration of fluids and small volume silicate melts. The origin of cryptic metasomatism is unclear, as suggested by its name, but is probably due to migration of fluids. The enrichment cannot, on the basis of known crystal/silicate liquid partition coefficients, be ascribed to silicate melts (Dawson, 1984).

Given sufficient time, changes in parent/daughter ratios, resulting from trace element enrichment events can be mirrored by the radiogenic isotope systematics. Isotopic studies of metasomatised xenoliths have investigated the timing of these metasomatic events and their relation to their host magmas. Although, in a number of cases, isotope analyses of patently metasomatised veined xenoliths have indicated enrichment shortly prior to magma extraction (Bergman et al., 1981; Cohen et al., 1984), there is also isotopic evidence that some cryptic and patent metasomatic enrichments, recorded by xenoliths and xenocrysts, significantly predate the time of magma genesis (Menzies and Murthy, 1980; Cohen et al., 1984; Erlank et al., 1982, 1987; Richardson et al., 1985).

Work on mantle derived inclusions within kimberlites from South Africa, with particular emphasis on those from the Kimberley area, reveal that the South African subcontinental lithosphere in this area has undergone a long and complex polyphase evolution. Model ages recorded for various mantle enrichment events in this region vary from 3.3 Ga (syngenetic mineral inclusions within diamonds; Richardson et al., 1984) to 150 Ma (PKP and PP metasomatised xenoliths; Erlank et al., 1982).

An alternative, albeit more indirect approach to investigating mantle enrichment processes, has come from the study of mantle derived volcanic rocks. Relatively unradiogenic Sr and radiogenic Nd isotope ratios testify that many OIB were derived, at least in part, from time-integrated, low Rb/Sr and high Sm/Nd mantle derived material. However, their high trace element abundances e.g. LREE enrichment and relatively high Rb/Sr ratios indicate that their source regions were enriched in incompatible elements shortly before or during magma genesis (Norry and Fitton, 1983).

Interest in continental volcanic rocks has increased with the knowledge that they too may record more than simply crustal contamination of magmas from depleted mantle sources. Detailed trace element and isotope studies have been utilised to show that a number of rocks within flood basalt provinces could have been derived from heterogeneous trace element enriched source regions (Hawkesworth et al., 1983; Cox, 1983; Weaver and Tarney, 1983; Mantovani et al., 1985).

In a review, Hawkesworth et al. (1984) combined Sr and Nd isotope and

selected trace element data from within-plate basalts and mantle xenoliths and they tentatively identified two mantle enrichment processes. One is characterised by high Ti/K, low Rb/Sr and Rb/Ba and concentrates trace elements such as K, Rb, Ba, through Nb, Ta and LREE to Zr and Ti. It occurs in both oceanic and continental areas and evidence from spinel lherzolites and megacrysts indicates that it reflects the migration of small volumes of silicate, possibly basanitic, melts. The other, as evidenced by the high K rocks from Vulsini, Italy (Rogers et al., 1985) and K-richterite bearing mantle xenoliths (Erlank et al., 1982, 1987; Jones et al., 1982) exhibit low Ti/K, but high Rb/Ba and Rb/Sr ratios and may be attributed to the migration of H_2O-rich fluids.

Kimberlites are important in the study of the evolution of the subcontinental mantle, because they contain diamond and are therefore derived from the deepest mantle source regions known (> 150 km). Until recently, as outlined above, most attention has been focussed on the xenolithic content of these rocks: the megacryst suite, peridotites, eclogites and xenocrysts such as diamond, which Harte (1983) envisages as tantalising 'twigs and leaves from trees of the mantle forests'. However, the isotopic (Sr-Nd-Pb) study, of South African Cretaceous kimberlites, by Smith (1983a, b) has shown that the two groups of kimberlite, termed 'basaltic' and 'micaceous' by Wagner (1914), are also different in terms of age and isotopic composition. Group 1 ('basaltic') kimberlites are younger and are believed to originate from asthenospheric sources. Group 2 kimberlites have radiogenic Sr and unradiogenic Nd and Pb isotopic signatures and are believed to originate from ancient trace element enriched sources within the mantle portion of the continental lithosphere.

The recent refutation of the widely held view that kimberlite was the only known terrestrial source of diamonds has stimulated much scientific interest. The diamondiferous Prairie Creek kimberlite or mica peridotite (Bolivar and Brookins, 1979) has been re-identified as an olivine lamproite body (Scott Smith and Skinner, 1984a). The initially termed diamondiferous kimberlites or kimberlitic bodies (Atkinson et al., 1982; Jaques et al., 1982; McCulloch et al., 1983; Nixon et al., 1984) of the West Kimberley area (Western Australia) have also been reclassified as olivine lamproites (Scott Smith and Skinner, 1984b).

The discovery of diamonds in these lamproites means that there are now two known distinct rock-types which are derived from great depth in the mantle (> 150 km). These findings have posed many questions; what are the relationships between kimberlite and lamproite magmas? Do the observed differences arise within the source regions, or from extraction processes? What can these rocks tell us of the deep subcontinental mantle, its characteristics and evolution?

Some indication of the interest in these problems can be gained from the number of papers on lamproites given at the previous two international kimberlite conferences. Four out of fifty-seven papers (7%) in the proceedings of the 3IKC (Kornprobst, 1984a, b) refer to lamproites, which contrasts with a total of thirty-one out of one hundred and fifty-four papers (20%) at the 4IKC (Fourth International Kimberlite Conference; 1986, abstract volume).

A number of recent geochemical studies consider that lamproites from North America and Western Australia, like Group 2 kimberlites from South Africa, are derived from ancient trace element enriched sources situated deep within the subcontinental mantle lithosphere (McCulloch et al., 1983; Vollmer et al., 1984; Fraser et al., 1985; Nelson et al., 1986a). The large variations in Sr-Nd-Pb isotope geochemistry between localities testify to heterogeneity in parent/daughter ratios and perhaps age.

Hawkesworth et al. (1985) extended the work on enrichment styles by Hawkesworth et al. (1984), to include lamproite and kimberlite data and suggested that these rocks are extreme endmembers of mantle enrichment processes. A number of authors have also postulated that sediment can be recycled back into the lithospheric mantle, contributing to Island Arc volcanism (McClennan and Taylor, 1981; Brown et al., 1982; Cohen and O'Nions, 1982), Back Arc Basin volcanism (Mattey et al., 1984; Exley et al., 1986; Mattey et al., 1987), formation of diamonds (Schulz, 1986 and see reviews in Meyer, 1985 and Mattey, 1987), eclogites (Ringwood, 1975; MacGregor and Manton, 1986) and continental ultrapotassic volcanism (Nelson et al., 1986b).

This study has been concerned with using petrographic and geochemical evidence from selected suites of kimberlites and lamproites in order to determine the processes involved in setting up the mantle source regions and those which occur during melt formation and ascent to the surface.

The following sections in this chapter detail relevant background information regarding kimberlites and lamproites and summarise the lines of evidence used to compare and contrast these two distinct rock-types. Finally, there is a section outlining the aims of this project and the localities studied.

1.2 Kimberlites

1.2.1 Setting and geology

Kimberlites, named after their type locality in the Kimberley area, South Africa (Lewis, 1888), are rare and volumetrically insignificant igneous rocks. They are usually situated on, or close to, ancient (> 2.5 Ga) cratonic regions and are emplaced in areas which have undergone epeirogenic uplift.

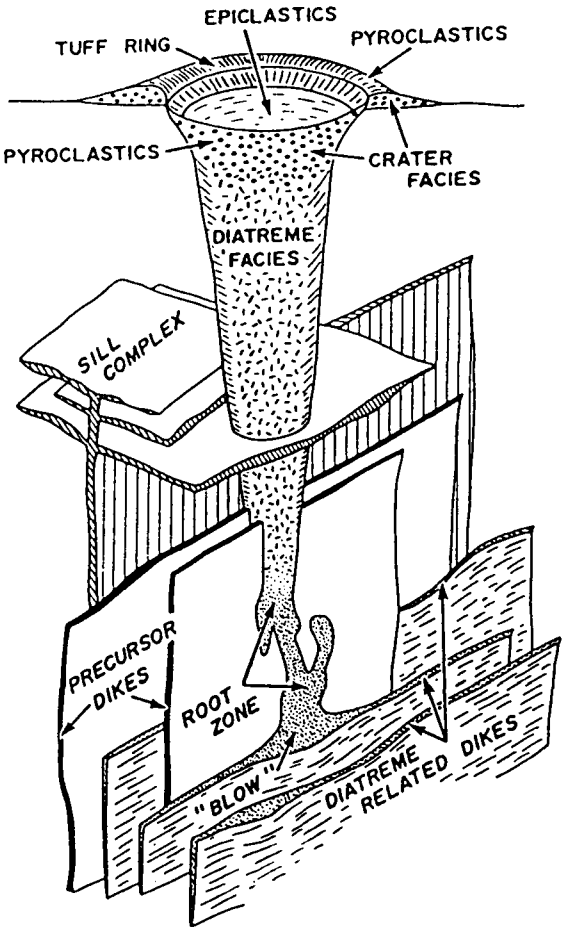

Figure 1.1 Model of an idealised kimberlite magmatic system illustrating the relationships between crater, diatreme and hypabyssal facies rocks (not to scale). Hypabyssal facies rocks include sills, dykes, root zone and "blow" (after Mitchell, 1986).

Kimberlites have been the subject of much research for two main reasons. Firstly, an economic impetus, resulting from the presence of diamonds in some intracratonic kimberlites. Secondly, they are hybrid rocks, carrying to the surface a multitude of ultrabasic xenoliths, thus sampling portions of the mantle otherwise inaccessible.

Detailed mapping during mining of the kimberlite pipes in South Africa has established the geology of the pipes (Dawson, 1967a; Hawthorne, 1975; Clement, 1982). Figure 1.1 shows the model of an idealised kimberlite magmatic system. Kimberlites may occur as diatremes, dykes and more rarely sills. Three textural-genetic groups have been identified: crater facies, diatreme facies and hypabyssal facies (Hawthorne, 1975; Clement and Skinner, 1985). Details of the crater and diatreme facies can be found in Clement and Skinner (1985), Dawson (1980), Mitchell (1986) and references therein.

1.2.2 Petrography and definition

Only the hypabyssal facies kimberlite found in sills and dykes and in the root zones to the pipes, are considered sufficiently fresh for petrographic and geochemical studies interested in the origin of kimberlitic magmas.

Kimberlites are complex hybrid rocks. In addition to a magmatic component, they contain abundant mantle and crustal xenolithic material, megacrysts and xenocrysts (from disaggregation of xenolithic material). Where the origin of a grain (xenocryst or phenocryst) is in doubt, the term macrocryst is applied (Clement et al., 1984). A note of warning, in previous literature these so-called macrocrysts are sometimes called megacrysts (e.g. Dawson, 1980). In this thesis, the term megacryst is reserved for the monomineralic crystals generally too large to be derived from peridotites and which are believed to have crystallised from melts which were probably situated near the base of the lithosphere (Boyd and Nixon, 1973; Nixon and Boyd, 1973b; Harte, 1983; Hunter and Taylor, 1984). Since the relationship of the megacryst suite to the host kimberlite is debated (phenocryst – Dawson and Stevens, 1975; Gurney et al., 1979a; Kramers et al., 1981: or xenocryst – Boyd and Nixon, 1973; Pasteris, 1980), the term megacryst also has no genetic significance.

As a result of the hybrid composition of kimberlite an accurate definition of this rock-type has been elusive. The most recent definition proposed by Mitchell (1986) is a modification of those suggested by Mitchell (1979) and Clement et al. (1984):

> 'Kimberlites are a clan of volatile-rich (dominantly CO_2) potassic ultrabasic rocks. Commonly, they exhibit a distinctive inequigranular texture resulting from the presence of macrocrysts (and in some cases megacrysts) set in a fine-grained matrix. The megacryst/macrocryst assemblage consists of rounded anhedral crystals of magnesian ilmenite, Cr-poor titanian pyrope, olivine, Cr-poor clinopyroxene, phlogopite, enstatite and Ti-poor chromite. Olivine is the dominant member of the macrocryst assemblage. The matrix minerals include: second generation euhedral primary olivine and/or phlogopite, together with perovskite, spinel (titaniferous magnesian ulvöspinel-ulvöspinel-magnetite series), diopside (Al- and Ti-poor), monticellite, apatite, calcite and primary late-stage serpentine (commonly Fe-rich). Some kimberlites contain late-stage poikilitic eastonitic phlogopites. Nickeliferous sulphides and rutile are common accessory minerals. The replacement of early-formed olivine, phlogopite, monticellite and apatite by deuteric serpentine and calcite is common. Evolved members of the clan may be devoid of, or poor

in, macrocrysts, and composed essentially of calcite, serpentine and magnetite, together with minor phlogopite, apatite and perovskite.'

Wagner (1914) divided kimberlites into basaltic and micaceous groups based on the amount of matrix phlogopite present. Basaltic is a misnomer as it implies the presence of plagioclase, which (apart from rare xenocrysts) is absent from kimberlite (Skinner and Clement, 1979, Dawson, 1980). Skinner and Clement (1979) proposed a classification scheme in which fresh hypabyssal kimberlites are classified solely on the basis of their groundmass mineralogy: five subdivisions are made on the modal predominance of diopside, monticellite ($CaMgSiO_4$), phlogopite, calcite and serpentine. Further subdivision can be made if one or more of these, or any other mineral is present in sufficient abundance for it to qualify as a characterising accessory. Olivine is an essential mineral and is omitted from the classification.

Mitchell (1986) observed that the above classification is useful in providing a rational terminology which allows comparison of kimberlites on a worldwide basis. However, he noted that the drawbacks to this system are that neither the modal variation of phenocrystal olivine, nor the textural relationships of mica (phenocryst/macrocryst or groundmass) are considered.

1.2.3 Composition

It is very doubtful if any bulk rock analyses will reflect pristine kimberlite composition, owing to the ubiquitous presence of abundant extraneous material. Investigation of the geochemistry of kimberlites is hampered by various problems including; their mode of emplacement and interaction with groundwater, their high xenolith and xenocryst content, the loss of volatiles (H_2O and CO_2) together with mobile elements that may be concentrated and transported in the gas phase and the inhomogeneous segregation texture of some kimberlites (Dawson, 1980). Although not without problems, most kimberlite geologists now recognise that the analysis of fresh hypabyssal kimberlite is the best approach to dealing with the geochemistry of kimberlites.

Kimberlites show a wide range in composition and a number of general statements can be made regarding their chemistry. They are volatile rich (CO_2 and H_2O), undersaturated ultrabasic rocks ($SiO_2 \simeq$ 25–30 wt%, although certain diopside- and phlogopite-rich varieties may approach, or in rare instances exceed 40 wt%). They have low Al_2O_3 (usually $<$ 5 wt%) and very low Na_2O contents (usually $<$ 1 wt%), but high P_2O_5 contents and K_2O/Na_2O ratios (>2)(Dawson, 1967b, Dawson, 1980; Clement, 1982; Mitchell, 1986).

A number of authors (Dawson, 1967b, 1980; Wedepohl and Muramatsu, 1979) have shown that the trace elements in kimberlites can be divided into two groups:

1. Those in amounts usually found in ultramafic rocks e.g. Sc, V, Cr, Co, Ni, Cu, Zn and Cd.

2. Those in amounts greater than normally found in ultramafic rocks e.g. Cl, B, Mo, Pt, Y, Sc, Bi, REE, Zr, Hf, F, Tl, Sr, Ba, Pb, Rb, Nb, Ta, U, Th and Cs.

Kimberlites are highly LREE enriched and have La and Yb enriched 100–1000 and 2–10 times chondrite respectively. La/Yb ratios vary from 50–500, with the majority ranging from 80–200 (Mitchell, 1986). This dual nature of kimberlite is a paradox. Compatible trace elements are concentrated in large degree partial melts, whereas incompatible trace elements (e.g. the alkaline earths, LREE and alkali and volatile elements) are concentrated in initial small partial melts or late-stage residual melts.

Early isotope studies were hampered by the belief that the earth could be modelled as an isotopically two component system of depleted mantle and enriched crust. Thus, any high $(^{87}Sr/^{86}Sr)_i$ ratios (> 0.704) in kimberlites were attributed to contamination of bulk crustal components (Powell, 1966; Brookins, 1967). Mitchell and Crocket (1971) and Barrett and Berg (1975) argued that high initial Sr isotope ratios could not always be attributed to assimilation of bulk crust and the preferred interpretation was that these ratios were due to alteration of the kimberlite by groundwaters subsequent to intrusion (Berg and Allsopp, 1972; Barrett and Berg, 1975). Interestingly, Barrett and Berg (1975) observed that the low ($\simeq 0.704$) Sr isotope ratios were recorded in 'basaltic' kimberlites, whereas high ratios occur in seemingly fresh micaceous kimberlites. More recent Sr-Nd-Pb isotope studies on fresh hypabyssal kimberlite have been carried out by Kramers (1977), Basu and Tatsumoto (1980) and Smith (1983a, b).

1.2.4 Group 1 and 2 kimberlites

Smith (op. cit.) showed that the Cretaceous kimberlites of South Africa can be divided into two groups on the basis of mineralogy, age and isotopes, which cannot be attributed to crustal contamination. The Group 1, generally non-micaceous kimberlites tend to be younger (90–114 Ma) and are isotopically (Sr-Nd-Pb) similar to many OIB. These kimberlites, apparently in contrast to the Group 2 kimberlites, contain Fe-Ti rich peridotites and the Cr-poor megacryst suite. These factors indicate that the Group 1 kimberlites have a close relationship to asthenospheric mantle. The older

(114–150 Ma) micaceous Group 2 kimberlites, on the other hand, exhibit radiogenic Sr, but unradiogenic Nd and Pb contents and it is suggested that they are derived from ancient (> 1 Ga) trace element enriched sources situated within the subcontinental lithosphere. Thus, the two-fold division of kimberlites proposed by Wagner (1914) appears to be maintained. The Group 1 and 2 kimberlite terminology is adopted in this work, although mineral classification of individual samples is made using the classification scheme of Skinner and Clement (1979).

1.2.5 Diamonds

A number of kimberlites contain diamond and two schools of thought have emerged concerning the relationship of diamond (phenocryst or xenocryst) to the kimberlite magma. This problem has been reviewed by Dawson (1980), Meyer (1985) and Mitchell (1986). In addition to the discovery of diamonds in eclogites and more rarely peridotites (Bonney, 1899; Gurney et al., 1968; Rickwood and Mathais, 1970; Dawson and Smith, 1975a; McCallum and Eggler, 1976; Reid et al., 1976; Shee et al., 1982), the most convincing argument for a xenocrystic origin, at least for some diamonds, has recently come from Proterozoic to Archaean Nd and Pb model ages from syngenetic silicate and sulphide inclusions in diamonds (Kramers, 1979; Richardson et al., 1984; Smith et al., 1986). These ages, indicating a number of discrete diamond formation events, are significantly older than those determined for their host South African kimberlites which were emplaced in Cretaceous times. In these cases, kimberlite was only the transporting vehicle in which diamond ascended rapidly from mantle depths to the crust. However, recent carbon and nitrogen isotope studies on diamond 'coats' and cubic microdiamonds may suggest that this diamond is actually phenocrystal to the host kimberlite (Boyd et al., 1986).

In addition to advancing our knowledge of the nature of the subcontinental mantle lithosphere, the study of xenoliths and xenocrysts such as diamond has also placed constraints on the generation and movement of small volume kimberlite melts. It has been argued that rapid rates of ascent are required to preserve diamond and dense mantle xenoliths within the kimberlite magmas (Anderson, 1979: Artyushkov and Sobolev, 1984). Rapid ascent is also proposed from studies of olivine annealing, exsolution phenomena in pyroxene from kimberlites and the megacryst suites which show evidence of rapid quenching from high temperatures (see review in Harte, 1983 and references therein). Assuming rapid ascent, Mitchell (1986) tentatively proposed that the intersection of a 40 mW m^{-2} shield geotherm with the stishovite-coesite and diamond-graphite inversion curves, constrains kimberlite genesis to pressures of about 45–100 Kb. Furthermore, estimated

conditions of equilibration for coexisting inclusions of the ultramafic suite in diamond give temperatures of 900–1300°C and pressures of 45–65 Kb (Prinz et al., 1975; Hervig et al., 1980; Boyd and Finnerty, 1980). These values lie within the region of the diamond stability field and are similar to those obtained for diamond-bearing and diamond-free garnet lherzolite xenoliths (e.g. Shee et al., 1982).

1.2.6 Affinities with other rock-types

Kimberlites have petrographic and chemical affinities with a diverse group of ultrabasic alkaline rocks of lamprophyric aspect e.g. alnöites and mica-peridotites (Mitchell, 1986). However, the latter rock groups are typically richer in Al, Ti, Na and Fe and/or can be distinguished by distinctive mineralogy and spinel compositions (Mitchell, op. cit.).

It has previously been suggested that kimberlites may be genetically related to a number of other intracontinental volcanic rocks believed to originate from mantle depths; in particular carbonatites (Dawson, 1967b; Gaspar and Wyllie, 1984) and melilitites (McIver and Ferguson, 1979; McIver, 1981). Dawson (1980) and Mitchell (1986) have reviewed these problems and despite a number of geochemical and mineralogical similarities, kimberlites do not appear to be related to either rock-type. The basic premises on which these ideas were originally based have been refuted: the central-complex type kimberlite in alkaline rock carbonatite complexes is in fact alnöite and calcite in kimberlites is primary magmatic and not a secondary replacement of melilite. Evidence against direct relationships between these rocks and kimberlite is also provided from studies of mineralogy, tectonic setting and experimental petrology (Mitchell, 1979 and see discussions in Dawson, 1980 and Mitchell, 1986).

1.2.7 Petrogenesis

Any model attempting to explain the petrogenesis of kimberlites has to consider the origin of the various components within kimberlite, the trigger to magmatism and the mechanism of extraction from mantle depths to the surface. Factors to be considered in the first of these problems include:

1. The hybrid nature of kimberlites.
2. The volatile-rich (CO_2 and H_2O), ultrabasic composition of kimberlites.
3. The high incompatible and compatible trace element contents.
4. The relatively 'depleted' major element chemistry of kimberlites.

5. The small volume of kimberlites and lack of associated rock-types.

In view of their complexity, a large number of petrogenetic models for kimberlite genesis have been proposed. Dawson (1980) and Mitchell (1986) reviewed a number of earlier hypotheses, in addition to those postulated in more recent years. The latter appear to fall into the following four broad categories. *Hybridisation* where kimberlites are believed to be mixtures between, for example, xenolithic material and olivine melilitites (Holmes, 1936) or 'crystal-mush' magmas (Boyd and Nixon, 1973; Nixon and Boyd, 1973b) and between granite and carbonatites (Dawson, 1967b). *Fractional crystallisation* of bimineralic eclogite from a partial melt of a four phase garnet lherzolite (O'Hara and Yoder, 1967). *Zone refining* within the mantle (Harris and Middlemost, 1969; Alibert et al., 1983). *Partial melting* of mantle material (e.g. Wyllie, 1980; Bailey, 1984, 1985).

In the light of recent investigations and the much improved understanding of the relationship between various components (matrix, macrocrysts, xenoliths and xenocrysts) within kimberlite, most authors currently favour some form of partial melting model to generate kimberlite magmas. However, there are very few constraints that can be placed on such models. For example, with regard to the composition of parental upper mantle source material, the composition of the vapour phase during melting and the depth and degree of melting.

Kramers et al. (1981) attempted to generate kimberlite compositions from 'ordinary' mantle by invoking melting with extremely low K_D values. However, the volatile-rich nature and high incompatible element content of kimberlites, combined with increasing evidence of trace element enriched subcontinental lithosphere from mantle xenoliths, has led a number of geologists to propose trace element enriched source regions for kimberlite magmas. Geochemical investigations have led to suggestions of source regions which contain phlogopite (Dawson, 1971, 1972; Mitchell and Brunfelt, 1975), apatite and titanates (Fesq et al., 1975a; Kable et al., 1975). Experimental studies have shown that carbonation reactions can occur in the system peridotite-H_2O-CO_2 (Wyllie and Huang, 1976; Wyllie, 1979; Brey et al., 1983; Olafsson and Eggler, 1983) and Wyllie (1980) suggests that the most likely source for a kimberlite is a phlogopite-carbonate-garnet lherzolite. Support for ancient trace element enriched source regions, for at least some kimberlites, comes from the Sr-Nd-Pb isotope signatures of Group 2 kimberlites.

Metasomatism caused by volatile fluxing has been proposed by Lloyd and Bailey (1975), Boettcher et al. (1979) and Bailey (1980, 1982, 1984, 1985) as a precursor to alkaline and kimberlite magmatism. Alternatively, Green and Gueguen (1974) and Wyllie (1980) have considered that kimberlite mag-

matism occurs via melting at the top of asthenospheric derived peridotite diapirs rising through the mantle, and Wyllie (op. cit.) further proposed that kimberlite magmatism itself could result in mantle metasomatism.

For reasons outlined above, kimberlite magmas must ascend rapidly, in a matter of hours, from within the diamond stability zone to the surface. Most authors envisage that this occurs through a crack (Anderson, 1979; Wyllie, 1980; Artyushkov and Sobolev, 1984). Initial magmatism would generate a conduit which could permit rapid extraction of kimberlites from depth (Wyllie, 1980). Either a physical or thermal perturbation could trigger kimberlite activity. Smith (1983b) attempted to relate the timing of Cretaceous kimberlite emplacement in South Africa to rifting of the South Atlantic (Group 2 kimberlites) and hotspot trails under the South African craton (Group 1 kimberlites). Le Roex (1986) extended the latter argument suggesting there is a relationship between hotspot activity and both groups in South Africa and argued that perhaps all kimberlites are derived from sources situated within the asthenosphere.

1.3 Lamproites

Lamproites are K- and Mg-rich igneous rocks that possess an exotic and diagnostic mineralogy and geochemistry. The term lamproite was initially coined by Niggli (1923) in his detailed chemical system of igneous rock classification. Lamproites were leucite-bearing rocks from Spain and Wyoming with very high ($\geq$ 0.8) niggli, *mg* and *k* numbers. Subsequently, Tröger (1935) refered to lamproite as a potassium-, magnesium-rich lamprophyric rock and Wade and Prider (1940) used lamproite to describe rocks from Western Australia. The discovery in the mid-late 1970's of diamonds within lamproites from the Kimberley region of Western Australia (Scott Smith and Skinner, 1984b; Atkinson et al., 1984; Jaques et al., 1984a) has renewed interest and stimulated further research into the petrogenesis of these rocks and their relationship to kimberlites. Much of the recent work has been reviewed in Bergman (1987), Mitchell (1985), Jaques et al. (1986a) and the abstract volume of the 4IKC also details numerous studies.

Lamproites are known to occur in twenty major suites and range in age from Proterozoic (Holsteinborg, Greenland and Chelima, India) to Quaternary (Leucite Hills, Wyoming and Gaussberg, Antarctica). They all occur in continental regions and they tend to be localised marginal to cratonic areas (Bergman, 1987).

Lamproites generally occur in volcanic fields and exhibit a wide range in geological form: flows, pyroclastics, cinder cones, dykes, sills and diatremes. The diamondiferous lamproites typically form diatremes. Figure

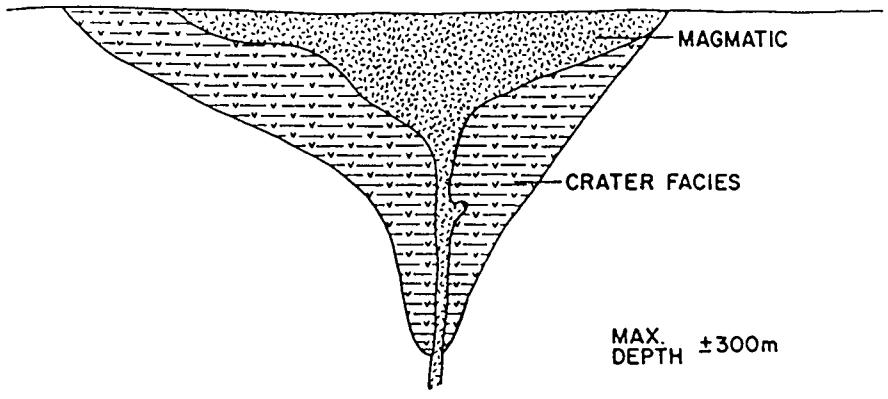

Figure 1.2 Model of a lamproite diatreme illustrating the relationship between the crater and hypabyssal facies material (after Scott Smith and Skinner, 1984b).

1.2 is a schematic simplified model of a lamproite pipe based on occurrences in South-eastern Spain, Leucite hills (Wyoming) and Prairie Creek (Arkansas)(Scott Smith and Skinner, 1984b). A shallow irregular, approximately champagne-glass shaped crater is dominantly filled with pyroclastic material. The later quiet intrusion of magmatic lamproite may form ponded lava lakes. In some cases, the pipes are more complex owing to multiple intrusion (Scott Smith and Skinner, op. cit.). Within individual diamondiferous pipes, the diamond grade is always higher in the early pyroclastic phase relative to the later magmatic phase (Atkinson et al., 1984; Jaques et al., 1986a).

The petrographic diversity of lamproites has generally hindered development of a concise and universal definition, classification and nomenclature for these rocks. Individual areas have generally been characterised by local names. Thus, petrographically similar rocks may be given quite different names e.g. madupite (Leucite Hills) $\simeq$ jumillite (Spain) (Mitchell, 1985). Recently, a number of authors have attempted to rectify these classification problems. Mitchell (1985) suggests the following definition of lamproites as a revision to that proposed by Scott Smith and Skinner (1984a):

> 'Lamproite clan—A group of ultrapotassic mafic rocks characterised by the presence of widely varying modal amounts of titanian (2–10% TiO_2), Al_2O_3-poor (5-12%) phlogopite, titanian (5–10%) tetraferriphlogopite, potassian (ca. 5% K_2O) titanian (3–5% TiO_2) richterite, forsteritic olivine, diopside, sanidine and leucite as the major phases. Minor and accessory phases include enstatite, priderite, apatite, wadeite, magnesiochromite, titanian magnesiochromite, ilmenite, scherbakovite, armalcolite, perovskite and jeppeite. Analcime is common as a sec-

ondary mineral replacing leucite and/or sanidine. Other secondary phases include carbonate, chlorite, zeolites and barite.

Important textural features of petrographic significance are, the occurrence of phlogopite as either phenocrysts or poikilitic groundmass plates and the late (post-phlogopite) crystallisation of potassian titanian richterite.'

Scott Smith and Skinner (1984a) have proposed a classification scheme similar to that developed for kimberlites by Skinner and Clement (1979). Six divisions are made on the modal predominance of phlogopite, amphibole, clinopyroxene, olivine, sanidine and glass. Further subdivisions can be made if a mineral is present in sufficient abundance to qualify as a characterising accessory. Leucite was considered an essential mineral and therefore, excluded from the classification.

Subsequent work on the Western Australia lamproites has shown that leucite is not an essential mineral and Scott Smith and Skinner (1984b) suggested it be included as a classifying constituent. Bergman (1987) and Mitchell (1985) propose that as glass is not a mineral it should be used solely as a textural term. Furthermore, they point out the classification does not take into account the variations in texture of phlogopite and the following terminology is suggested: phlogopite lamproite should be used when phlogopite occurs as phenocrysts, and madupite lamproite should be used when phlogopite is a poikilitic groundmass phase.

Scott Smith and Skinner (1984a) and Bergman (1987) suggest that whole-rock chemistry can also be used to characterise the lamproite suite i.e. $K_2O/Al_2O_3 > 0.7$ (wt%), $K_2O/Na_2O > 4$ and mg numbers > 65. Thus, they are ultrapotassic and in many cases perpotassic rocks. They have low Al, Fe, Ca, Na and CO_2, but high Ti, P and K contents. The vast majority of lamproites fall in the following ranges; 45–55 wt% SiO_2, 4–10 wt% Al_2O_3, 1–5 wt% TiO_2, 2–10 wt% CaO, 5–10 wt% K_2O, 0.2–1.5 wt% Na_2O, 0.5–2.0 wt% P_2O_5 and 1.0–3.0 wt% BaO. CO_2 appears to be absent (Bergman, 1987).

The unusual major element geochemistry of these rocks is reflected in their mineralogy and mineral chemistry. Lamproite mineralogy has been studied in detail by Mitchell (1981, 1985) and Wagner and Velde (1986). Mitchell (1981, 1985) has shown that although each locality has its own characteristics, there are some distinctive features common to all lamproite minerals. Phlogopite is the only mineral which shows extensive compositional variation with evolutionary trends of decreasing Al_2O_3 and FeO_T with increasing TiO_2 (Mitchell, 1981, 1985). Their combined high TiO_2, low Al_2O_3, relatively low FeO_T contents and evolutionary trends distinguish lamproite micas from those of most other parageneses e.g. micas of the Ro-

man Province, from New South Wales leucitites, kimberlite phenocrysts, primary or secondary micas in lherzolites and MARID micas (Mitchell, 1985).

The Al-bearing silicate minerals in lamproites from early to late crystallising phases (e.g. spinel, diopside, phlogopite and K-richterite) show a general tetrahedral deficiency, the sum Si + Al being systematically lower than its theoretical value (Wagner and Velde, 1986). This, together with the frequent glassy textures observed in lamproites, led Wagner and Velde (op. cit.) to suggest a primary origin for the peralkaline character of the lamproite magmas.

Lamproites are highly enriched in trace elements (Carmichael, 1967; Carmichael et al., 1974; Jaques et al., 1984a, 1986b; Nixon et al., 1984; Bergman, 1987). Carmichael et al. (1974) observed that lamproites from southeast Spain, Leucite Hills (Wyoming) and the West Kimberley region (Western Australia) were similar to kimberlites in that they are both enriched in compatible trace elements such as Ni and Cr (typical of ultrabasic rocks) and also incompatible trace elements such as Rb, Ba, Sr, Nb, Zr and F (more typical of highly fractionated or acid rocks).

Although values overlap, lamproites tend to be even more LREE enriched than kimberlites with La enriched by factors of 200 to 2000 × chondrite and low HREE values, Yb = 1.5 to 12 × chondrite (Collerson and McCulloch, 1983; Jaques et al., 1984a; Nixon et al., 1984; Fraser et al., 1985; Bergman, 1987)

Nd and Sr isotope studies have revealed that lamproite suites are characterised by low εNd and variable εSr. Powell and Bell (1970) first showed that the Leucite Hills (Wyoming), Western Australia and southeast Spain lamproites were characterised by very different initial Sr isotope ratios. They showed that the Leucite Hills lamproites had relatively low $(^{87}Sr/^{86}Sr)_i \simeq$ 0.7055 to 0.7070, whereas those from Jumilla (Spain) and the West Kimberley have extremely high $(^{87}Sr/^{86}Sr)_i \simeq$ 0.7136 to 0.7158 and 0.7125 to 0.7215 respectively. More recently, Nelson et al. (1986a) have extended the range for the Spanish lamproites (0.71688 to 0.72083) and Collerson and McCulloch (1983) report $(^{87}Sr/^{86}Sr)_i$ ratios of 0.70923 to 0.70978 for the Gaussberg (Antarctica) lamproites. Nd isotope studies have further shown that all the above lamproite suites are characterised by unradiogenic Nd contents (εNd= −7.3 to −17.0; Collerson and McCulloch, 1983; McCulloch et al., 1983; Nixon et al., 1984; Vollmer et al., 1984; Fraser et al., 1985; Nelson et al., 1986a). Thus, these lamproites all contain a predominant contribution from old LREE enriched material with highly variable Rb/Sr ratios.

It has long been argued that lamproite magmas are derived from the mantle. High liquidus temperatures (1320°C) at 1 Kb (Sobolev et al., 1975), high Mg, Ni and Cr contents and the presence of mantle xenoliths and

xenocrysts testify to a mantle origin for these rocks (e.g. Carmichael, 1967; McCulloch et al., 1983).

In contrast to the abundant literature concerned with the petrogenesis of kimberlites, there is relatively little which addresses the origin of the lamproite group. Models which have been proposed are often along similar lines to those proposed for kimberlites. Geochemical modelling for individual localities revealed that the unusual geochemistry of these rocks could not readily be explained by simple bulk crustal contamination of mantle derived rocks (Powell and Bell, 1970; McCulloch et al., 1983; Collerson and McCulloch, 1983; Vollmer et al., 1984). Early models proposed zone refining in the crust (Powell and Bell, 1970), or the migration of alkalis in a volatile phase to a peridotite magma (Prider, 1960). Wade and Prider (1940) and Prider (1960) suggested that the West Kimberley lamproites were closely akin to kimberlites and Wade and Prider (1940) proposed that kimberlite magmas fractionated to produce more potassic silica-rich lamproite magmas.

In the light of current views on the nature of the subcontinental mantle lithosphere, recent authors have tended to infer an origin for lamproites predominantly from partial melting of ancient, variably enriched source regions situated in the subcontinental lithosphere (Collerson and McCulloch, 1983; McCulloch et al., 1983; Nixon et al., 1984; Vollmer et al., 1984; Jaques et al., 1984a, 1986b; Fraser et al., 1985; Nelson et al., 1986a). Interestingly, the major element chemistry of these rocks reveals that they are depleted in Ca, Al, Fe and Na, i.e. in basaltic components. Therefore, it has been proposed that the source regions of these rocks were depleted by melt extraction prior to trace element enrichment (Jaques et al., 1984a, 1986a; Bergman, 1987). High pressure experimental studies on a magnesium-rich leucite lamproite from Western Australia, led Arima and Edgar (1983) to suggest these rocks originated from metasomatised mantle consisting of phlogopite and rutile $\pm$ olivine $\pm$ orthopyroxene.

McCulloch et al. (1983) and Vollmer at al. (1984) used Nd and Sr isotope arguments to suggest mixing models between enriched and depleted mantle to generate the Leucite Hills and Western Australia lamproites respectively. Nelson et al. (1986a) used Pb isotope data to suggest that the mixing in the Western Australia lamproites occurred at some time in the past ($\simeq$ 1.00 to 1.25 Ga). McCulloch et al. (1983) further maintained that there is a relationship between kimberlites and the Western Australia lamproites. The isotope variations between these rock groups were attributed to different proportions of enriched and depleted mantle endmembers. The preservation of diamond and mantle xenoliths and the volatile-rich nature of lamproites are consistent with their rapid ascent to the surface from mantle depths.

1.4 Comparing and contrasting kimberlites and lamproites

The recent discovery of diamonds within lamproites from North America and Western Australia has directed research towards assessing the relationship of kimberlites and lamproites. The misidentification of both the Prairie Creek (Arkansas) and West Kimberley (Western Australia) olivine lamproites as kimberlites indicates there are close mineralogical affinities. However, recent studies have revealed significant differences between the two rock-types. This section outlines the important similarities and distinctions found to exist between kimberlites and lamproites. The main features which can be used to distinguish these rock-types include; geology of the intrusions, petrography, mineral chemistry and whole-rock chemistry (Scott Smith and Skinner, 1984a, b)

Geology: The mode of emplacement of the lamproites differs from that of kimberlites. Kimberlite diatremes are carrot-shaped (Figure 1.1) while lamproite diatremes are champagne-glass shaped (Figure 1.2). The shallower depth to the lamproite diatremes is believed to reflect the lower volatile content and slower ascent rates of these magmas. Slower ascent rates for lamproites can also be inferred from the highly resorbed nature of the diamonds present (S. R. Boyd pers. comm., Jaques et al., 1986a) and the rarity of mantle xenoliths. Garnet peridotites which are retrieved have re-equilibrated in the spinel stability field (O'Neill et al., 1986). There is little evidence for extrusive kimberlite (Dawson, 1980; Mitchell, 1986), but lamproites frequently form lava flows and lava lakes apparently formed within some craters (Scott Smith and Skinner, 1984b).

Petrography: The occurrence of two generations of olivine within diamondiferous lamproites makes these rocks superficially resemble kimberlites. However as discussed by Scott Smith and Skinner (1984a, b), lamproites exhibit a number of features atypical of kimberlites. Lamproite olivine phenocrysts can form complex crystal aggregates and the olivine macrocrysts often exhibit a complex euhedral outline. This contrasts with olivine morphology in kimberlites, where the olivine phenocrysts are euhedral and the macrocrysts are generally anhedral and rounded. The presence of amphibole (typically K-richterite), glass, priderite [$(K,Ba)(Ti,Fe)_8O_{16}$)], wadeite ($Zr_2K_4Si_6O_{16}$) and armalcolite (ferropseudobrookite ($FeTi_2O_5$) - kerroite ($MgTi_2O_5$) series), the paucity of ilmenite and rutile and the absence of minerals such as primary serpentine or carbonate are also features characteristic of lamproites, but atypical of kimberlites (Scott Smith and Skinner, 1984a, b). The pyroclastic rock-types (breccias and tuffs) found within lamproite diatremes have not been identified in kimberlites and the nature of the lapilli, with abundant glass and vesicles, is extremely unusual for kimberlite

(Scott Smith and Skinner, 1984a).

Mineral chemistry: In lamproites the spinels have lower Al_2O_3 and MgO, while the phlogopites lower Al_2O_3, higher TiO_2, Fe_2O_3 and Na_2O compared with the same phases within kimberlite and they exhibit different evolutionary trends (Mitchell, 1986; Scott Smith and Skinner, 1984a). The groundmass diopsides in lamproites are higher in TiO_2 (Dawson, 1987).

Whole-rock geochemistry: Scott Smith and Skinner (1984a) showed that geochemically the diamondiferous olivine lamproites from Prairie Creek (Arkansas) are intermediate in composition between kimberlites and lamproites from Holsteinburg (Greenland). Bergman (1987) compares the average major element composition of diamondiferous lamproites (number = 46) and kimberlites (number = 325) which reveals that these primitive lamproites tend to be richer in SiO_2, TiO_2, P_2O_5, BaO and in particular K_2O, but lower in Al_2O_3, FeO_T, MgO and volatiles. These features are confirmed by other studies, however, although unclear in Bergman's study, most authors consider that fresh hypabyssal lamproite has much lower CaO and CO_2 (the latter sometimes termed absent) than kimberlites (Dawson, 1987; Scott Smith and Skinner, 1984a; Mitchell, 1985)

Dawson (1987) suggests that the micaceous Group 2 kimberlites of South Africa have closer geochemical similarities to olivine lamproites from Western Australia than with the generally non-micaceous Group 1 kimberlites. Ancient trace element enriched source regions situated deep within the subcontinental lithosphere have been postulated for both Group 2 kimberlites and lamproites.

1.5 Aims of thesis

Group 2 kimberlites and lamproites are generally believed to be partial melts of ancient trace element enriched subcontinental lithospheric source regions. Their unusual geochemistry offers the opportunity to determine whether and to what extent their trace element contents are source or extraction phenomena. Preliminary Nd–Sr isotope data for these mantle derived rocks reveals an extreme range of compositions encompassing much of that reported for various upper and lower crustal rocks.

The aims of this thesis, are to evaluate melt extraction processes and the evolution of the mantle source regions of selected Group 2 kimberlites and lamproites, using a combination of geochemical (radiogenic isotopes, major and trace elements) and petrographic evidence. First, important factors in melt formation and extraction processes are considered, e.g. the volatiles present during melting, degree of partial melting, depth of melting and the mode of extraction. Secondly, the questions which will be addressed

regarding source evolution are;

1. Characteristics and age of trace element enrichment events.

2. Source of these trace element enrichments. Do they originate from recycled upper and lower continental crust to the depths of diamond stability, or can they be evaluated in terms of different melt and fluid related mantle processes?

To answer these questions, this study involved analysis of Group 2 kimberlites from Finsch mine (South Africa) and lamproites from North America (Leucite Hills, Wyoming; Prairie Creek, Arkansas; Smoky Butte, Montana) and Western Australia (West Kimberley Province). Details of sample localities can be found in subsequent chapters and within the appendices. Information regarding analytical techniques used in this study, together with the petrographic and isotope data generated are also to be found in the appendices.

Chapter 2

Kimberlites: Finsch Mine, South Africa

2.1 Introduction

This chapter considers the petrogenesis of micaceous Group 2 kimberlites from Finsch mine, South Africa. Unlike earlier studies, this work concentrates on a number of hypabyssal samples from a single pipe. This offers a unique opportunity to use integrated petrographic and geochemical data to evaluate the nature and evolution of a kimberlite source region via the processes operating prior to, during and subsequent to melting.

The majority of these kimberlites are not significantly contaminated by crust and they represent primitive mantle melts. They are however, derived from ancient trace element enriched source regions, situated within the mantle portion of the Kaapvaal craton. Consideration of extraction processes demonstrates that mixing of a highly incompatible trace element enriched, small volume partial melt with abundant entrained and disaggregated peridotite explains the dichotomy of high compatible and incompatible trace element contents of these rocks.

Comparison with the petrography and geochemistry of other kimberlites indicates that they all undergo similar extraction processes, although the melt components of Group 1 and 2 kimberlites appear to be derived from distinct mantle source regions. The geochemistry of Group 1 and 2 kimberlites suggests that the volatile (H_2O and CO_2) composition during source evolution and subsequent melting is important. The role of volatiles is discussed more fully in Chapter 5.

2.2 Review of previous literature

2.2.1 The Finsch mine kimberlites

The diamondiferous Finsch kimberlite pipe is situated on the Kaapvaal craton, near Postmasburg, Cape Province, 170 km west of Kimberley (28°16′

S, 23°06′ E) South Africa. It is the second largest pipe in South Africa after Premier and it was discovered in 1960 on the farm "Brits". Opencast mining started in 1962 under De Beers mining corporation and at present they are in the process of converting to underground mining. Diamond production is in excess of 2 million carats per year and 4 million carats were produced in 1981 (Shee et al., 1982).

The pipe surface is roughly circular in cross section (Figure 2.1a) and covers an area of 17.9 Ha. This area decreases regularly from the surface (average inward dip of the walls $\simeq 82°$; Hawthorne, 1975) to at least a depth of 350 m and probably to 500 m as is suggested by exploratory drilling (Clement, 1982). Estimates imply that the original surface area may have been over 100 Ha (Clement op. cit.).

The pipe is intrusive into the banded ironstones of the lower Griquatown (Pretoria) Group. These persist to a depth of 140 m where they are underlain by 30 m of a mixed transition horizon termed the Passage beds. These in turn are underlain by Ghaaplateau dolomite.

The weathered kimberlite encountered during initial sampling of the pipe has been described by Ruotsala (1975). Mining to greater depths has exposed fresher material and enabled detailed mapping of the pipe. A number of discrete intrusions and radial dykes have been identified between the surface and the 348 m level of the mine and two dykes, external to the main pipe, have been intersected in the shaft/pipe haulage on the 350 m level (De Beers Internal Report). The intrusions were initially labelled F1 to F8 according to the order in which they were recognised as separate intrusions. Their distribution within the pipe and age relations are shown in Figure 2.1b-d, while information regarding their texture and petrography is given in Table 2.1. The Finsch tuffisitic kimberlite breccias (TKB) contain abundant highly micaceous globular or pellet-like segregations, many of which have centrally located kernels, mainly of olivine (often serpentinised). These segregations, together with scattered mica crystals, occasional grains of serpentine, olivine and country rock xenoliths, are enclosed in a matrix of calcite and serpentine (Clement, 1975).

In a more recent detailed study, Clement (1982) observed mineralogical differences between hypabyssal facies, phlogopite kimberlites from the Finsch mine and hypabyssal facies kimberlites from the Kimberley area (De Beers, Wesselton, Bultfontein and Dutoitspan) and the Koffiefontein intrusion (80 km SSE of Kimberley) South Africa. In contrast to the others, Finsch kimberlites contain abundant matrix phlogopite (phenocrysts and groundmass) and varied, but usually substantial, amounts of diopside accompanied by a paucity of perovskites and opaques.

The most reliable emplacement age for Finsch mine is a Rb-Sr phlogopite age of 118 ± 2.2 Ma obtained from groundmass micas of a fresh hypabyssal

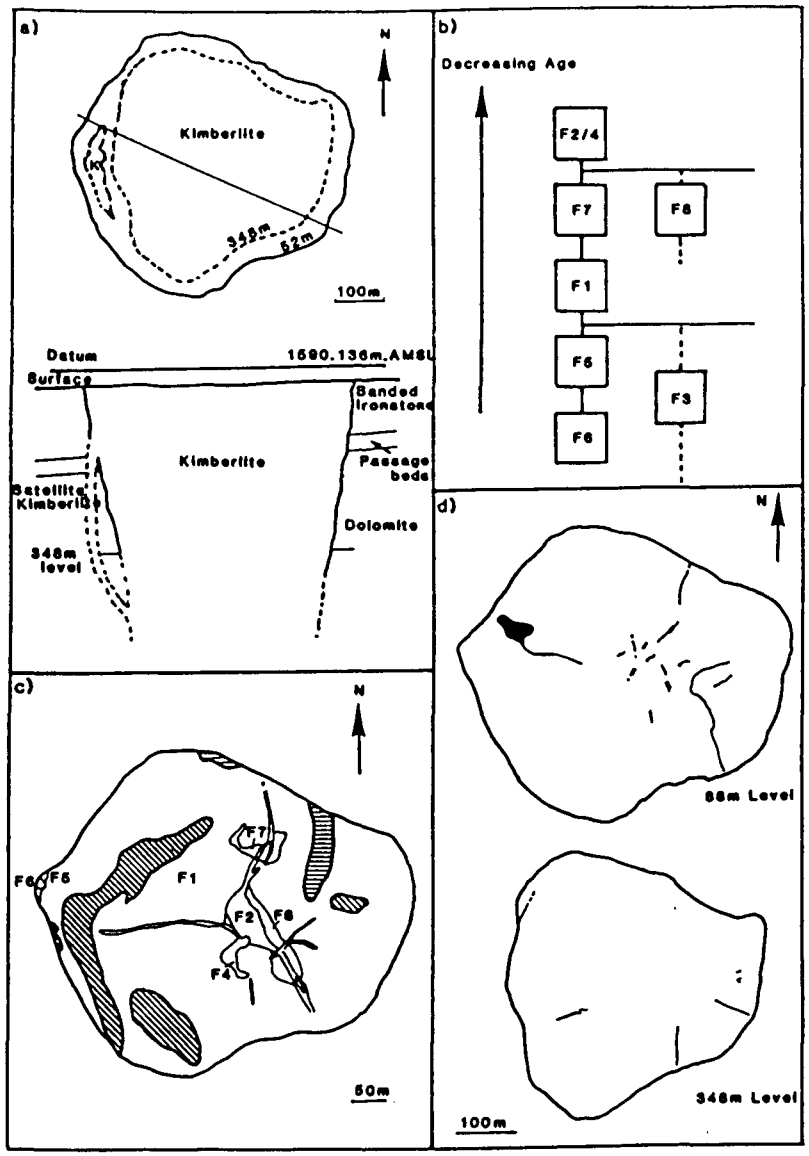

Figure 2.1 Geology of the Finsch pipe: a) Shape and size of the Finsch pipe between the surface and 348 m level. b) The relative ages of the various intrusions. Position of F3 and F8 in sequence are uncertain (see also Table 2.1) though tie-lines indicate F8 and F3 predate F2/4 and F1 respectively. c) Geology of the open pit; composite plan showing the distribution of kimberlite intrusions and major floating reef bodies in the pipe, between the 196 and 220 m levels of the open pit. Note the tendency for floating reef bodies of Ventersdorp lava (diagonal hatching) and Karoo sediments (shale and/or mudstone; horizontal hatching) to be located near the margins of the pipe. The F3 intrusion is not exposed at these levels. d) Distribution of internal dykes on the 88 and 348 m levels. The paucity of dykes on the 348 m level is probably, at least in part, an artifact of exposure, which is restricted to a 90 m square tunnel grid. The irregular nature of the dyke on the west side of the 88 m level reflects a transition from dyke-like to sill-like form at the western edge of the dyke (modified after Clement, 1982).

Intrusion Number	Textural-genetic Classification	Mineral Classification	Xenolith Content	Comments
F1	TKB	phlogopite–serpentine kimberlite	dolerite, shale, basalt (mm to floating reefs)	occupies about 90% of the pipe. Contains all the floating reefs
F2	macroporphyritic segregationary texture	phlogopite–diopside kimberlite	dolerite and small carbonated inclusions	Radial dyke/sill complex. Locally globular segregations up to 150 mm are common
F3	hypabyssal facies macroporphyritic segregationary texture	phlogopite kimberlite		Limited exposure on 348 m level. Similar to F6 and may be part of it
F4	hypabyssal facies macroporphyritic uniform texture	phlogopite kimberlite		Part of the F2 dyke/sill complex No longer considered a separate intrusion
F5	TKB with segregationary texture	phlogopite–serpentine kimberlite	dolerite (abundant)	Originally thought to be a TKB but, fresher exposures suggest it is hypabyssal similar to F6
F6	hypabyssal facies macroporphyritic segregationary texture	phlogopite kimberlite	dolomite, banded iron formation, dolerite	
F7	TKB with segregationary texture	phlogopite kimberlite	peridotites, granite, gneiss, dolerite	Abundant globular segregations implying a pelletal texture
F8	TKB – segregationary textured hypabyssal facies		dolerite, fragments of chert	May be same as F1, but is less contaminated by extraneous material

Table 2.1 The geology of the Finsch kimberlite intrusions.

diopside-phlogopite kimberlite (sample Finsch B, Smith, 1983a, b). Smith (op. cit.) believed the U-Pb zircon age of 94 Ma reported by Davis (1977a, b) to be erroneous as the zircons used may have been contaminants from the Kimberley area pipes. The conflicting Rb-Sr phlogopite ages of 130 Ma and 170 Ma reported by Allsopp and Kramers (1977) were obtained from altered and contaminated tuffisitic and hypabyssal kimberlites.

Recent isotope studies on the kimberlite matrix (Smith, 1983a, b) and autoliths (Kramers, 1977) have shown that the Finsch kimberlites have more radiogenic $(^{87}Sr/^{86}Sr)_i = 0.7099$ to 0.7103 and less radiogenic $(^{143}Nd/^{144}Nd)_i = 0.51234$, contents than bulk earth, while the unradiogenic Pb contents $(^{207}Pb/^{204}Pb)_i = 15.49$ to 15.54, plot below the Stacey and Kramers (1975) growth curve. Both authors attributed these features to ancient, predominantly mantle processes rather than crustal contamination.

Mineralogy, age and whole rock isotopic data on sample Finsch B led Smith (1983a, b) to place the Finsch kimberlites within his Group 2 division of South African Cretaceous kimberlites and hence derive them from old, enriched sub-continental mantle.

2.2.2 Xenoliths and xenocrysts

Crustal xenoliths, present in all the intrusions, consist mainly of rounded dolerite with lesser shale and basalt. There are also occasional inclusions of dolomite (in F6), banded iron formation (in F6), granitic gneiss (in F7) and fragments of chert (in F8). The xenolith size is highly variable, ranging from fragments ($\simeq$ 1 mm) up to floating reef bodies of Karoo sedimentary rocks and Drakensburg lava (100's m accross; De Beers Internal Report; Clement, 1982). The latter are restricted to the F1 intrusion close to the margins of the pipe. The Finsch pipe lies outside of the present day extent of the Karoo sedimentary basin, so the Karoo inclusions must have been downrafted during emplacement of the kimberlites, from material which has since been eroded. In contrast to the xenoliths within the diatreme facies, those in hypabyssal kimberlite are highly altered. This is consistent with the emplacement of the diatreme kimberlite by a cold gas-fluidisation process and the hypabyssal kimberlite as hot magma.

In November 1979 a large number of peridotite xenoliths (predominantly garnet lherzolites) were found in the F7 intrusion. Prior to this only a few eclogites, possible garnet harzburgites and a garnet websterite had been recovered from Finsch (Gurney et al., 1979b).

A study of eighty peridotites from the F7 intrusion revealed they had a texture, mode and mineralogy entirely typical of the low temperature ($<$1100°C), coarse garnet lherzolites which are the most abundant upper mantle xenoliths in kimberlites (Shee et al., 1982). The Finsch xenoliths are

distinguished only in that the Al_2O_3 content of the orthopyroxenes (0.43 to 0.66 wt%) tends to the lower part of the range observed worldwide, which in turn results in a higher than average equilibration pressure as shown by Shee et al. (1982), where calculations were made on the basis of the work by MacGregor (1974). Two of these eighty peridotites are notable for the occurrence of diamonds. Calculated equilibration conditions for both diamondiferous and nondiamondiferous xenoliths reveal comparatively low temperatures (1200°C) for the high pressures (46.4 to 63.1 Kb) inferred (Shee et al., 1982). The data lie on a steady state geotherm of $\simeq$ 40 mW m^{-2} and indicate depths of origin of $\simeq$ 160 to 200 km. Shee et al. (op. cit.) considered that a detailed comparison of the P/T calculations was unjustified owing to inaccuracies within the various geothermobarometers, although the diamond-bearing lherzolites appear to have originated at slightly deeper depths than the non-diamondiferous xenoliths.

More than 90% of the heavy mineral concentrate produced during the diamond extraction process at Finsch is garnet. This predominance of garnet can only be partly explained by differential weathering of the surface kimberlite, as ilmenite and diopside which normally resist weathering are extremely rare, and there has been no obvious change in concentrate character as mining has progressed to fresher material (Gurney et al., 1979b). Unlike the Kimberley mines, where the concentrate garnets are usually red, those retrieved from Finsch show a wide range in colour from pale yellow through yellow, brown, orange-red, lilac to purple (Gurney and Switzer, 1973). Much of the garnet is believed to have been derived from disaggregated peridotite (and occasionally eclogite). A small proportion (< 1%) of the garnet population consists of the lilac coloured garnets, pyrope in composition, which are more refractory than is usually found in xenolith garnets i.e. higher Mg, Cr, Mg/Fe ratios and lower Ca, Al and Ti contents. These subcalcic garnets have been compared in terms of their distribution (Boyd and Finnerty, 1980), mineral chemistry (Gurney et al., 1979b) and isotopes (Richardson et al., 1984) with subcalcic garnet inclusions within diamonds. Although the latter exhibit lower Ca contents, higher Cr_2O_3 contents and $(^{143}Nd/^{144}Nd)_i$ ratios, similarities between the two garnet populations suggest they are genetically linked (Gurney et al., 1979b; Richardson et al., 1984).

Diamonds from the Finsch pipe have been classified in terms of physical features as a function of size (Harris et al., 1975) and variations with depth of the pipe (Harris et al., 1979). The diamondiferous garnet lherzolites from Finsch are up to 300 × as rich in diamonds, which are less resorbed and corroded, than those found in the kimberlites. Carbon isotopic compositions of diamonds from both the xenoliths and the kimberlites ($\delta^{13}C$ = −2.62 to −8.57 ‰) are reported in Deines et al. (1984), and are within the range

considered typical for mantle carbon ($\delta^{13}C$ = -2 to -9 ‰; Gallimov, 1984).

About 7% of diamonds from Finsch contain microscopic inclusions, 50% of which are silicate minerals (Gurney et al., 1979b). More than 98% of these silicates belong to the peridotite paragenesis; pyrope garnet, chromite, olivine and orthopyroxene, while the remainder have eclogitic assemblages; pyrope-almandine garnet, omphacitic clinopyroxene ± phlogopite (Tsai and Meyer, 1979; Gurney et al., 1979b; Hervig et al., 1980; Boyd and Finnerty, 1980).

The peridotite association exhibits a residual major element chemistry (low Ca, high Mg/Fe and Cr/Al ratios and absence of clinopyroxene), but their trace elements and isotope ratios require derivation from an old, enriched source (Richardson et al., 1984; Shimizu and Richardson, 1987). Sm-Nd and Rb-Sr studies on these garnet inclusions reveal model ages of 3200–3300 Ma, which suggested to Richardson et al. (op cit.) that the diamonds formed subsequent to enrichment of residual subcratonic mantle, such as that remaining after widespread extraction of the 3500 Ma Onverwacht komatiitic lavas. Other Finsch diamond inclusion studies give a Pb model age of > 2 Ga for a sulphide of unknown paragenesis (Kramers, 1979) and a Nd model age of 1670 ± 40 Ma from an eclogitic garnet (Smith et al., 1986). All these ages are significantly older than the emplacement age of the Finsch kimberlite pipe (118 Ma) and therefore, strongly suggest that at least some diamonds are xenocrystic to the kimberlites. Variation in ages indicates that diamond formation does not occur as a single event.

2.3 Sample localities

Twenty-three samples from the Finsch mine kimberlite pipe have been analysed in this study. Samples were collected from the various intrusions within the pipe, as outlined in Appendix A1. The majority are hypabyssal kimberlite, with the exception of CRC 4 which is a tuffisitic kimberlite breccia (TKB) i.e. diatreme facies kimberlite. CRC 5 which was initially reported by Clement (1982) as an opaque oxide-rich calcite kimberlite from a Finsch dyke, is now believed to have come from one of the Kimberley pipes (errata, Clement, 1982). Two country-rock samples; a Karoo lava (F760) and a Precambrian dolomite (F769) have also been analysed as potential crustal contaminants of the Finsch kimberlites during ascent.

2.4 Petrography

Eight sections of hypabyssal kimberlite from a variety of the Finsch intrusions were made available for petrographic examination. Modal analyses are

Sample	Mineral classification
CRC1	Diopside phlogopite kimberlite[1]
CRC6	Phlogopite kimberlite[1]
CRC7	Diopside phlogopite kimberlite[1]
Finsch B	Diopside phlogopite kimberlite[2]
F287	Phlogopite kimberlite[1]
	Phlogopite diopside kimberlite[3]
F340	Phlogopite kimberlite[3]
F652	Serpentine phlogopite kimberlite[3]
F653	Phlogopite kimberlite[3]
F656	Phlogopite kimberlite[3]
F659	Phlogopite kimberlite[3]
F660	Phlogopite kimberlite[3]
F661	Phlogopite serpentine kimberlite[3]

Table 2.2 Mineral classification of Finsch kimberlites using the scheme proposed by Skinner and Clement (1979). 1 = Clement (1982), 2 = Harper (1981) and 3 = this study.

given in Appendix C.1. Mineral classification was made using the scheme proposed by Skinner and Clement (1979). These results are shown in Table 2.2 which reveals that the Finsch kimberlites are characterised by abundant phlogopite ± serpentine ± diopside (note that the latter minerals are in some cases more abundant than phlogopite).

The Finsch kimberlites are generally macroporphyritic in texture and consist of three main components:

1. Large anhedral macrocrysts of possible xenocrystic origin (olivine, spinel and garnet).
2. Subhedral to euhedral phenocrysts (olivine, phlogopite, spinels, perovskite and clinopyroxene).
3. Matrix components (phlogopite, clinopyroxene, calcite, serpentine and apatite).

Altered country rock xenoliths, if present, are invariably insignificant in abundance and size.

In F287 some of the olivines have a rim, sometimes discontinuous, of hypabyssal diopside-rich kimberlite distinct from the main groundmass (Plate 2.1) and in F656 an ovoid area of "distinct" (i.e. consisting of finer grained phlogopite) kimberlite is present. These are both similar to pelletal lapilli often found in diatreme facies tuffisitic kimberlite breccias (TKB). Their origin is unclear, but they may represent some degree of crystallisation prior to physical disruption of the magmas (Clement, 1982).

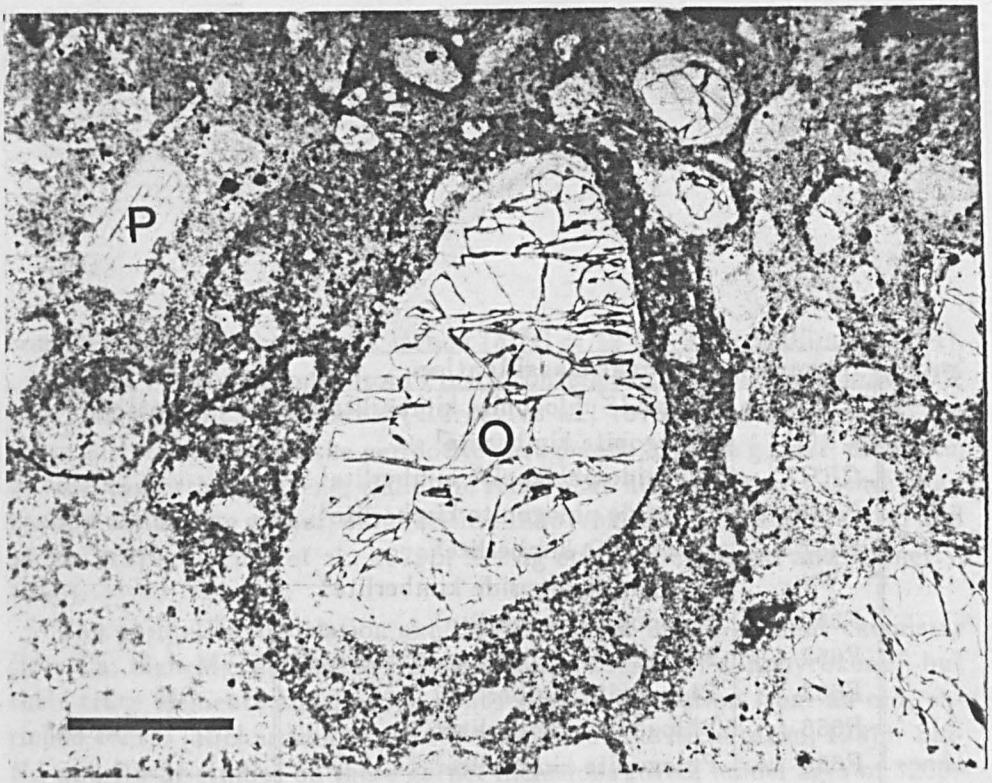

Plate 2.1 F287; Phlogopite diopside kimberlite with olivine surrounded by rim of petrographically distinct hypabyssal diopside-rich kimberlite (PPL). O = olivine P = phlogopite. Scale bar = 0.5 mm.

The general features of mineralogy and order of crystallisation are dealt with below:

Olivine: Two olivine populations are always present. Abundant (8 to 45 vol%) macrocrysts form the larger (0.5 mm to > 1.5 cm) group. They are rounded, elongate or irregular in shape and are frequently characterised by features indicative of strain such as undulose extinction and partial recrystallisation. Inclusions are usually absent, although within one olivine macrocryst (F340) a large (1 mm), red-brown anhedral spinel was observed. It is generally believed (e.g. Dawson, 1980; Clement, 1982 and references therein) that the majority of these macrocrysts are derived through disaggregation of mantle peridotite within the ascending kimberlite magma. On the other hand, the smaller ($\leq$ 0.5 mm) olivines are subhedral to euhedral. These are relatively abundant (8 to 23 vol%) in all sections and are believed to be true phenocrysts from the kimberlite magma.

Both populations are altered to some extent and in some slides no fresh olivine was found (F652, F660, F661, all from the F4 intrusion). Owing to their smaller size, the olivine phenocrysts are usually more altered than the large macrocrysts e.g. 59–100 vol% and 27–100 vol% serpentinisation respectively, in the slides studied. Alteration is predominantly to serpentine and much of this is believed to be deuteric, reflecting the reactive volatile-rich nature of post-olivine, residual kimberlite liquids. Other alteration products include calcite and phlogopite which may be the result of interaction between serpentine and evolving kimberlite liquids (Clement, 1982). Groundmass phlogopite was observed, in some cases, growing from the kimberlite ma-

trix along serpentinised olivine fractures and groundmass opaques may be concentrated around the periphery of the olivine phenocrysts. Secondary blue/black to green coloured, chloritic alteration was occasionally evident (e.g. F659).

Opaques: Two populations of red-brown to black spinels are present. Several large (1.25 to 3 mm) anhedral to euhedral macrocrysts were observed (F653, F652, F340). These spinels are predominantly red-brown in colour, but often exhibit a very thin rim of black material. One of these macrocrysts occurs as an inclusion within an olivine macrocryst (F340). The majority of spinels, however, form small ($\leq$ 0.15mm) subhedral to euhedral grains scattered throughout the groundmass of all sections studied making up to 2–9 vol% of the rocks.

Garnet: Garnet was found only once in the sections studied (F287), as a large ($\simeq$ 5mm accross) rounded pink macrocryst with a thick zoned kelyphitic rim up to 2 mm thick along unbroken edges, in close association with an olivine grain. The garnet is highly fractured, the fractures being infilled with serpentine and phlogopite (possibly from the host kimberlite) and small euhedral to embayed spinels, similar to those observed in the kelyphitic rim. The kelyphitic rim occurs on both broken and unbroken surfaces, but is thicker on the latter, suggesting it started to form prior to the breakup of the garnet.

Phlogopite: The phlogopites can be divided into pre-intrusion macrocrysts and post-intrusion overgrowths on these macrocrysts and groundmass constituents. Euhedral to subhedral macrocryst laths (0.25 mm to 1.5 mm) were observed in F656 and F287. They may be kinked and/or exhibit undulose extinction. They are very pale orange in colour and show only faint pleochroism; normal pleochroism in F287 and reverse pleochroism in F656. In both sections the macrocrysts have overgrowths of a deeper orange, reverse pleochroic phlogopite up to 0.25 mm thick (F656) and this overgrowth phlogopite also differs from the macrocryst cores by poikilitically enclosing abundant groundmass constituents e.g. opaques and microlitic diopside (Plates 2.1 and 2.2). Groundmass phlogopite usually occurs as relatively large (0.2 to 0.75 mm long) anhedral to subhedral interlocking laths. They are reverse pleochroic from pale to dark orange. The rim of the laths tend to be a darker colour than the core (Plate 2.3). The laths poikilitically enclose, or in some instances, are partly moulded around earlier crystallising phases such as olivine, perovskite, opaques, diopside and apatite. In F287 and F656, however, the groundmass phlogopite are generally cryptocrystalline and appear to consist of tiny anhedral interlocking laths and in F656 this groundmass has undergone pronounced deuteric alteration to serpentine. Phlogopite grainsize sometimes increases when adjacent to late stage calcite/serpentine pools. This feature is present in many of the sec-

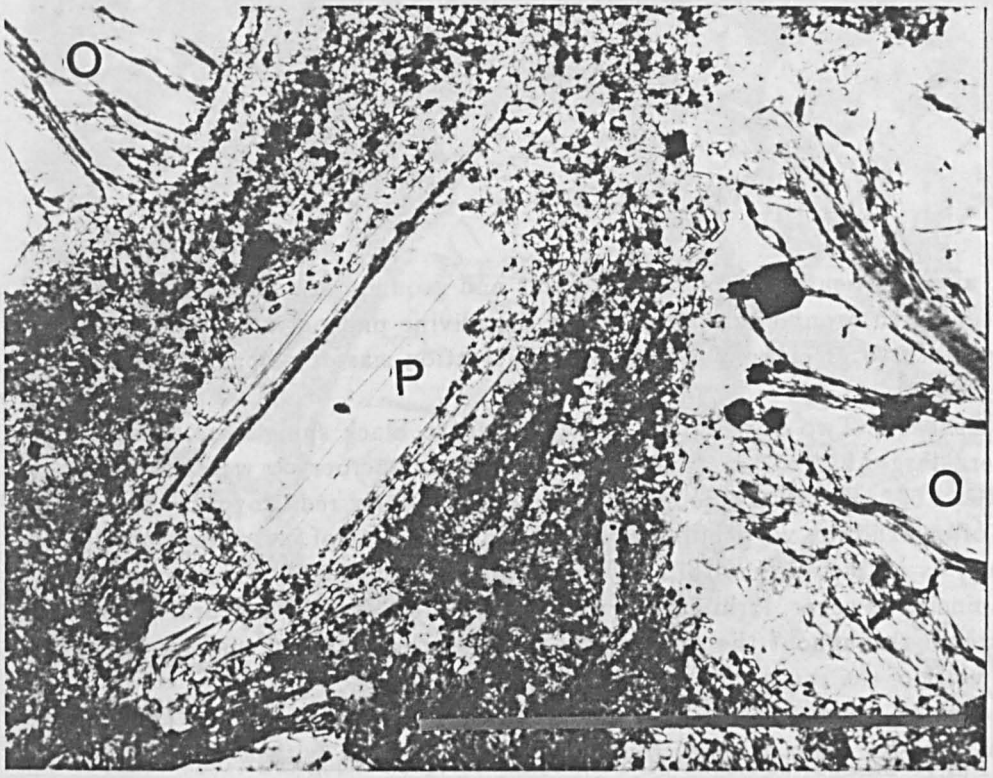

Plate 2.2 F656; Phlogopite kimberlite showing phlogopite lath with poikilitic rim (PPL). P = phlogopite, O = olivine. Scale bar = 0.5 mm.

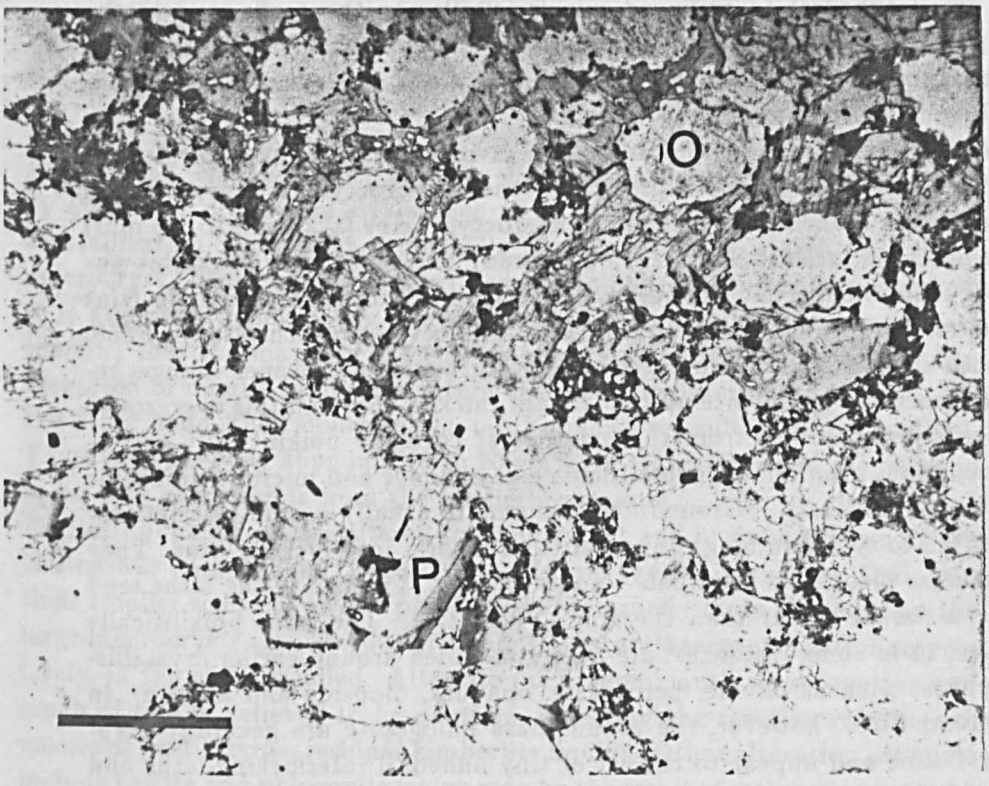

Plate 2.3 F660; Phlogopite kimberlite with zoned groundmass phlogopite laths (PPL). P = phlogopite, O = serpentinised olivine. Scale bar = 0.5 mm.

tions (Plates 2.4 and 2.5). Phlogopites are generally randomly orientated, indicating crystallisation from stationary kimberlite after emplacement.

Diopside: This is found in all the sections except for F340 and F661 and occurs from subhedral phenocrysts (0.1 to 0.6 mm long) down to abundant microlites in the phlogopitic groundmass. Those proximal to calcite/serpentine rich areas may, like phlogopite, be larger in size than those in the general groundmass. The larger phenocrysts are often prone to secondary alteration. They also occasionally contain inclusions of opaque minerals. Thin sections from sample F287 are described in both Clement (1982) and in this study. However, contrary to Clement (op. cit.), no evidence was seen for more than one phase of diopside crystallisation suggesting mineralogical (and hence chemical) heterogeneity on handspecimen scale.

Perovskite: Yellowish-brown to dark brown perovskite is present in all sections studied ($\simeq$ 0.1 to 1.2 vol%), within the groundmass, although owing to their small size ($\ll$ 0.05 mm) in F287 they were difficult to distinguish from groundmass opaques. In general, they are $\leq$ 0.1 mm in size, but in F653 and F660 they can be up to 0.20 to 0.25 mm. They tend to form angular, irregular or equant square euhedra and sometimes enclose diopside. Angular reentrants within some of the grains are indicative of complex twinning (Clement, 1982).

Serpentine: In addition to being a deuteric alteration product of olivine, serpentine is also found as a primary groundmass phase forming irregular shaped pools/patches up to 1 mm in size (Plate 2.6). These may be isolated areas, but where serpentine is abundant, it can be interconnected throughout the rock e.g. F661. The serpentine forms fine-grained felted or microlitic aggregates and occasionally structureless isotropic pools which may represent late-stage serpentinous colloidal deposits (Clement, 1982).

Calcite: Calcite is present in all sections from 0.8 to 10.1 vol%. It often occurs as late-stage anhedral crystals or irregular segregations ($\leq$ 0.1 mm to 0.5 mm), frequently in association with serpentine where it can form small irregular patches with crenulated margins within serpentine, or it can grow from the margins of segregations towards a centre of serpentine. Minor calcite also occurs as deuteric alteration of diopside and phlogopite and as the main alteration product of the rare country rock xenoliths.

Textural evidence (Dawson and Hawthorne, 1973), stable isotope studies (Deines and Gold, 1973; Sheppard and Dawson, 1975) and Sr isotope ratios of kimberlite carbonates (Exley and Jones, 1983) reveal that calcite within kimberlites is often a late crystallising primary mineral, rather than the product of weathering. This conclusion is supported by experimental work on the system CaO–MgO–SiO_2–CO_2–H_2O (Franz and Wyllie, 1967) and Skinner and Clement (1979) consider calcite one of the five primary minerals

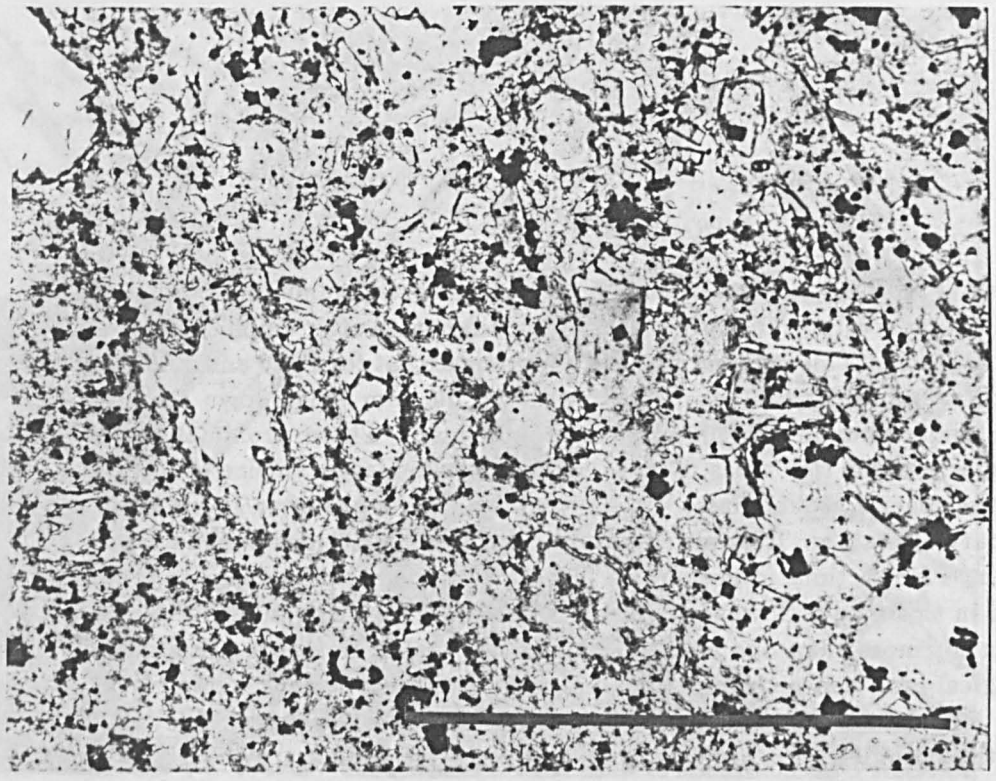

Plate 2.4 F340: Phlogopite kimberlite with groundmass phlogopite and calcite of variable grainsize (PPL). Scale bar = 0.5 mm.

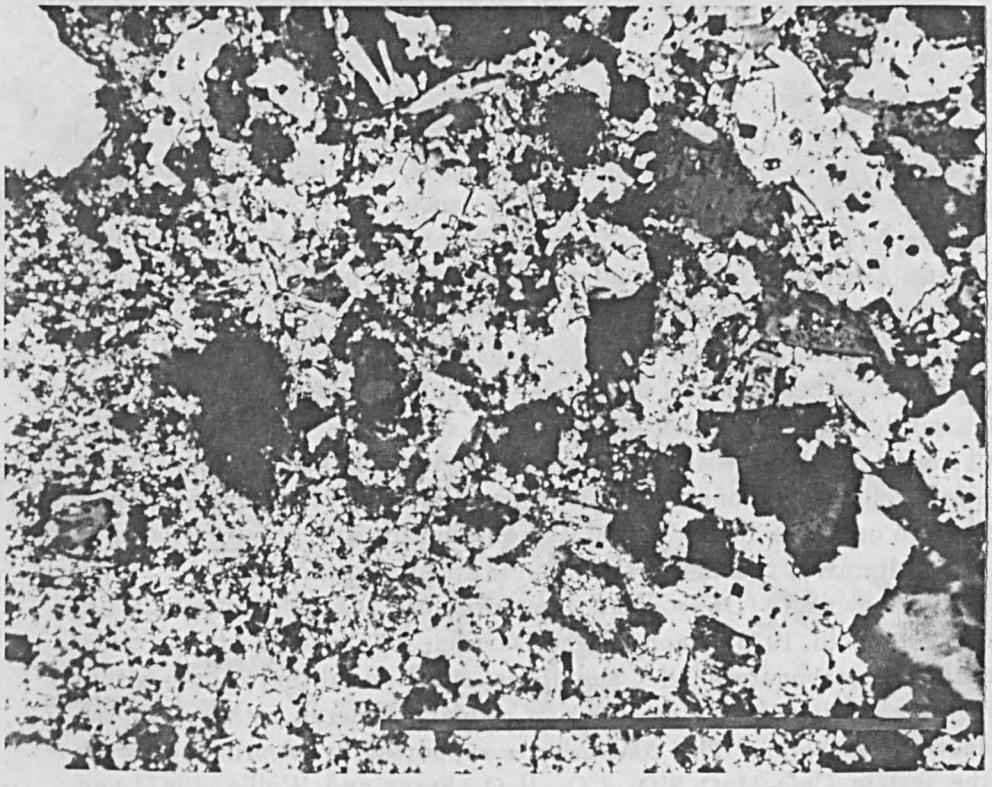

Plate 2.5 F340; Field of view as in Plate 2.4 (XPL).

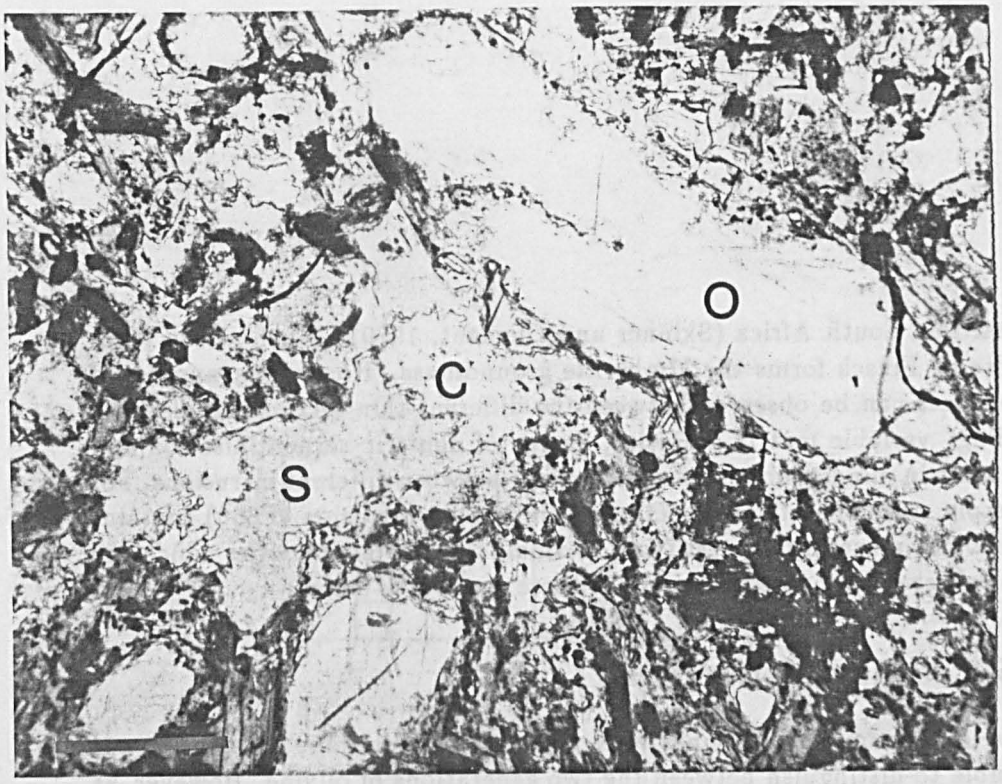

Plate 2.6 F652; Serpentine phlogopite kimberlite with late-crystallising pools of serpentine (S) and calcite (C). O = serpentinised olivine. Scale bar = 0.5 mm.

in their mineralogical classification scheme for kimberlites.

Apatite: Apatite is an accessory mineral in all sections ranging in abundance from trace amounts up to 1.5 vol%. It usually forms small microlitic inclusions within groundmass phlogopite or calcite/serpentine segregations. In F661, in addition to small microlites, apatite forms sub- to euhedral laths up to 0.05 mm wide and 0.3 mm long.

Olivine, spinel and garnet macrocrysts are considered to be xenocrysts and hence, only accidently incorporated into the kimberlite magma as it crystallised olivine, spinels, perovskite ± phlogopite ± diopside en route to the surface. The presence of two distinct phlogopite populations indicates either, a hiatus in phlogopite crystallisation or, the incorporation of xenocrystic phlogopite at some stage. Phlogopite, together with diopside (and apatite), forms the bulk of the groundmass. At a very late stage there is segregation and crystallisation of an essentially volatile component to form pools of calcite and serpentine. To some extent this last stage must overlap with crystallisation of the other groundmass minerals. For example, when proximal to large calcite/serpentine rich areas, the groundmass phlogopite, diopside and apatite may be found growing to larger sizes than in the surrounding groundmass, though without disruption of the interlocking lath texture. The complexity of serpentine alteration (noted in detail by Clement, 1982) suggests, perhaps several stages of alteration.

The hypabyssal Finsch kimberlites are all very similar in their mineral assemblages; olivine, phlogopite, spinel, perovskite, calcite, serpentine, apatite ± diopside ± garnet. They are all phlogopite-rich (14.8 to 36.4 vol%) compared with < 1 to 16 vol%, observed for the Group 1 kimberlites at

Wesselton, South Africa (Skinner and Clement, 1979). Much of the phlogopite at Finsch forms the kimberlite groundmass. However, a number of differences can be observed between the different thin sections studied, including: variable matrix grainsize, degree of deuteric serpentinisation and variation in mineral abundance within and between different intrusions. For example, only one of three sections from the F2 intrusion (F656) contains phlogopite macrocrysts, testifying to small scale heterogeneities which are also reflected in the geochemistry of these rocks (see below).

2.5 Mineral chemistry

Olivine: A number of olivines were analysed to determine whether it was possible to distinguish between the two generations of olivine. However, as found elsewhere (e.g. Boyd and Clement, 1977; Clement, 1982) the compositions from both populations overlap considerably (Figure 2.2). All tend to be homogeneous on the scale of individual grains, but chemical variations exist between grains. This variation in olivine phenocryst composition, on such a small scale, has been interpreted (Boyd and Clement, 1977) as being due to olivine phenocrysts crystallising from heterogeneous batches of magma of differing *mg* number [Mg/(Mg + Fe)], or differing temperatures or both, which were mixed during eruption. Also shown on Figure 2.2 are the data from Clement (1982 and references therein) for olivine phenocrysts and macrocrysts for the Kimberley area pipes and for xenolithic olivines including Finsch data from Shee et al. (1982) and Gurney et al. (1979b). The Finsch phenocrysts and macrocrysts (from this study) fall within the ranges quoted by Clement (1982), although the Finsch phenocrysts with Fo 90–92 and macrocrysts with Fo 89–94 fall at the high end of the Kimberley area range (Fo 85–94 and Fo 85–95 for phenocrysts and macrocrysts respectively). The macrocrysts from both Finsch and the Kimberley area, together with the xenolithic olivines, show a peak at Fo 92–93; this may be consistent with a xenocrystic origin for the kimberlite olivine macrocrysts.

Spinels: The presence of a spinel within an olivine macrocryst implies that they come from the same source, probably through disaggregation of peridotite material. However, both the xenocrystic and groundmass spinels at Finsch are compositionally similar; high Cr_2O_3 (60.6 to 61.1 and 54.1 to 63.8 wt% respectively), moderate to low Al_2O_3 (5.3 to 8.5 and 6.5 to 8.4 wt% respectively) and low TiO_2 (0.67 to 1.5 and 0.17 to 1.05 wt% respectively).

As crystallisation of a magma proceeds, Cr and Mg contents decrease while Ti and total Fe increase. For the groundmass spinels, variations are greater between different intrusions rather than within a single intrusion, perhaps reflecting slightly differing compositions and/or physical conditions

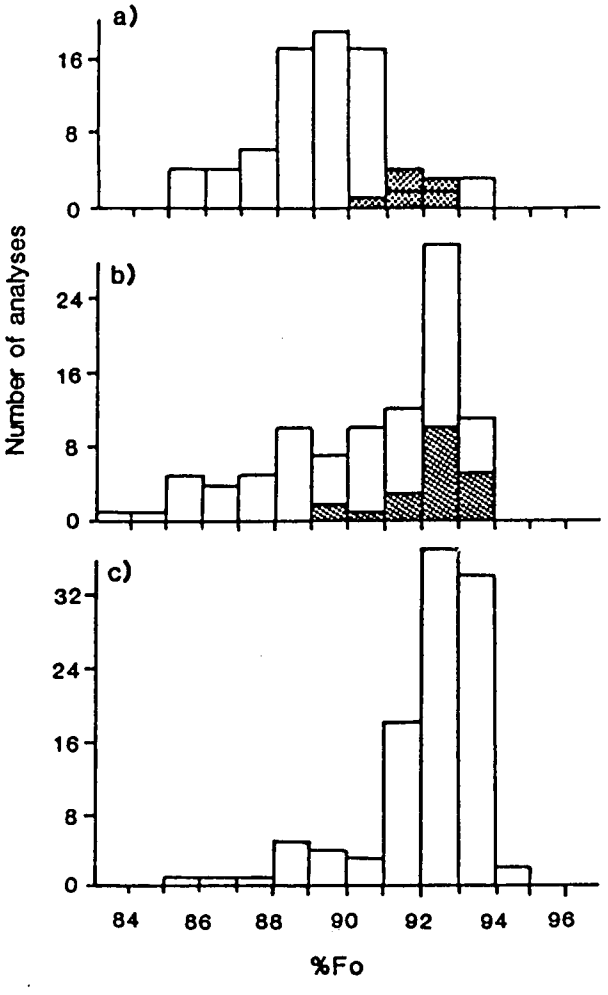

Figure 2.2 Histograms showing distribution of Fo in olivines from Finsch kimberlites (shaded region = this study) compared with olivines from the Kimberley pipes: a) phenocrysts, b) macrocrysts and c) peridotites, pyroxenites and dunites (modified after Clement, 1982).

of the kimberlite magmas during spinel crystallisation.

Shee (1984) noted that xenocrystic and groundmass chrome spinels in the Wesselton mine kimberlite are compositionally distinct, in particular the groundmass spinels have high TiO_2 contents (5.32 to 7.61 wt%) relative to the TiO_2 poor peridotite spinels (< 3 wt%). The Finsch xenocrystic spinels are similar to those from Wesselton. However, comparing groundmass spinels, those from Finsch have similar MgO contents, but higher Cr_2O_3 and much lower TiO_2 contents to those from Wesselton. Lower TiO_2 contents may result from crystallisation of a less fractionated magma. However, the Fo content of olivine phenocrysts from Finsch and Wesselton (Clement, 1982 and see previous section) are comparable and do not indicate large differences in degree of magma evolution. An alternative is that the variation in TiO_2 content of the primary magmas (i.e. Finsch kimberlites have TiO_2 = 0.6 to 1.03 wt%, excluding EPD and the Wesselton mine kimberlites have TiO_2 = 1.07 to 4.04 wt%; Clement, 1982) reflects differences in source composition.

Garnet: The pyrope garnet macrocryst found in F287 is similar in composition to the majority of garnets from both the Finsch concentrate (Gurney and Switzer, 1973) and garnet lherzolites (Gurney et al., 1979b, Shee et al., 1982), which are believed to originate from disaggregated mantle peridotite. Refractory subcalcic garnets from Finsch diamond inclusions (Gurney et al., 1979b) can be distinguished from the so-called 'lherzolitic' garnets by their low Ca and generally higher Cr_2O_3 contents (Figure 2.3). Also shown on Figure 2.3 are the rare subcalcic garnets retrieved from the Finsch concentrate (Gurney and Switzer, 1973) which, although not as extreme in composition as the diamond inclusions, still have significantly lower CaO contents than the main lherzolite trend garnets. The garnet from section F287 plots very close to the main lherzolite trend with a relatively high CaO content of 5.20 wt%.

Phlogopite: The two generations of phlogopite (macrocrysts and groundmass) which can texturally be identified, can also be differentiated in terms of their mineral chemistry. Macrocrysts of phlogopite were observed in sections F287 and F656. Each suite of macrocrysts is distinct in composition, although in F656 there may be two separate populations. One is more similar to those in F287 i.e. they exhibit lower Fe_2O_3 contents, but higher Na_2O contents and *mg* numbers compared to the other F656 macrocrysts. The F656 macrocrysts exhibit a wide range in Cr_2O_3 content in contrast to the more restricted range observed for the F287 macrocrysts.

The groundmass phlogopites at Finsch are zoned from pale cores to darker rims and this is also reflected in mineral chemistry. Trends from core to rim involve increasing FeO and decreasing TiO_2, Al_2O_3, Cr_2O_3 and *mg* numbers. Except for Cr_2O_3 the trends are similar to those noted for core to

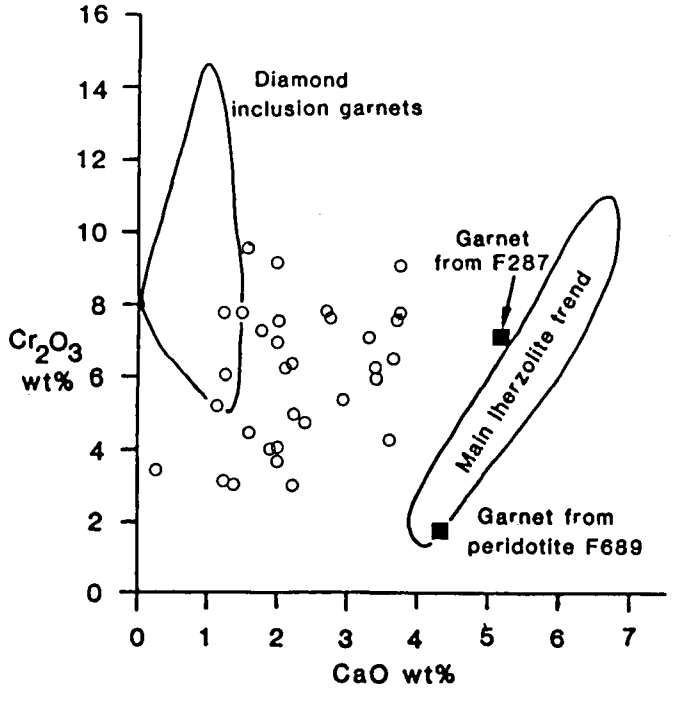

Figure 2.3 Cr_2O_3 wt% vs. CaO wt% in Finsch garnets. o = subcalcic garnets from the Finsch concentrate, ■ = garnets analysed in this study from kimberlite (F287) and peridotite (F689). Also shown are fields enclosing > 95% of subcalcic garnet inclusions in Finsch diamonds (Gurney et al., 1979a) and garnets from Finsch peridotites i.e. the main lherzolite trend (Shee et al., 1982)(modified after Richardson et al., 1984).

rim phlogopites from the Orroroo kimberlites, South Australia (Scott Smith et al., 1984). The dark, reverse pleochroic rims can be termed tetraferriphlogopite, the dark colour resulting from the presence of Fe^{3+} in tetrahedral sites (Scott Smith et al., op. cit.). From macrocryst to groundmass (core) to groundmass (rim) phlogopite there is a general trend of increasing Fe, but decreasing Cr and Mg contents, consistent with magmatic evolution (e.g. Delaney et al., 1980).

Ti and F (fluorine) which are usually incorporated into the liquid phase during melting or crystallisation should parallel the behaviour of Fe. However, there is a decrease in Ti and F contents from the core to the rim of the groundmass phlogopites. Decrease in Ti may be due to concomitant crystallisation of a Ti-bearing phase such as perovskite. Alternatively, since the effective K_D (= element concentration in phlogopite/element concentration in whole-rock) for Ti in cores to groundmass phlogopite is > 1 (F660, K_D = 3 and in F659, K_D = 1.5), then crystallisation of abundant phlogopite would deplete the residual magmas and result in Ti-poor phlogopite rims. The Ti and F contents of the phlogopite macrocrysts and cores of the groundmass micas are generally comparable, though one groundmass phlogopite analysed from F656 has a distinctly higher Ti and F content compared to the F656 macrocrystic phlogopite micas. In F656, the effective K_D's for titanium in phlogopite macrocrysts (= 1.5 to 2.0) and groundmass phlogopite (= 3.2) indicates that crystallisation of phlogopite should deplete the residual magma in Ti. However, assuming the macrocrysts are in fact phenocrysts, then it would appear that initial crystallisation of phlogopite did not occur in sufficient quantity to reduce the Ti content of the magma; rather the Ti content of the magma increased until the crystallisation of abundant groundmass phlogopite (± perovskite) commenced. This is consistent with the apparent rarity of phlogopite macrocrysts.

The sharp textural distinction between phlogopite macrocrysts and groundmass and the relative rarity of the macrocrysts in the sections studied, might suggest that they are xenocrysts rather than phenocrysts to the kimberlite magmas. Phlogopites in upper mantle rocks have several modes of occurrence and in Figure 2.4 data for the Finsch phlogopites are compared with data for primary and secondary peridotite micas (Delaney et al., 1980), averages for GPP, PP and PKP micas (Erlank et al., 1987), glimmerite and megacryst micas (Dawson and Smith, 1975b) and MARID suite micas (Dawson and Smith, 1977). The MARID and glimmerite micas have much higher FeO contents and the primary textured peridotite micas, relatively low FeO contents, compared with Finsch macrocryst phlogopites. There is much overlap in Fe and Ti content between the Finsch data and both the secondary micas and megacryst micas. However, the most distinctive feature on Figure 2.4 is the extremely low Na contents of the Finsch data

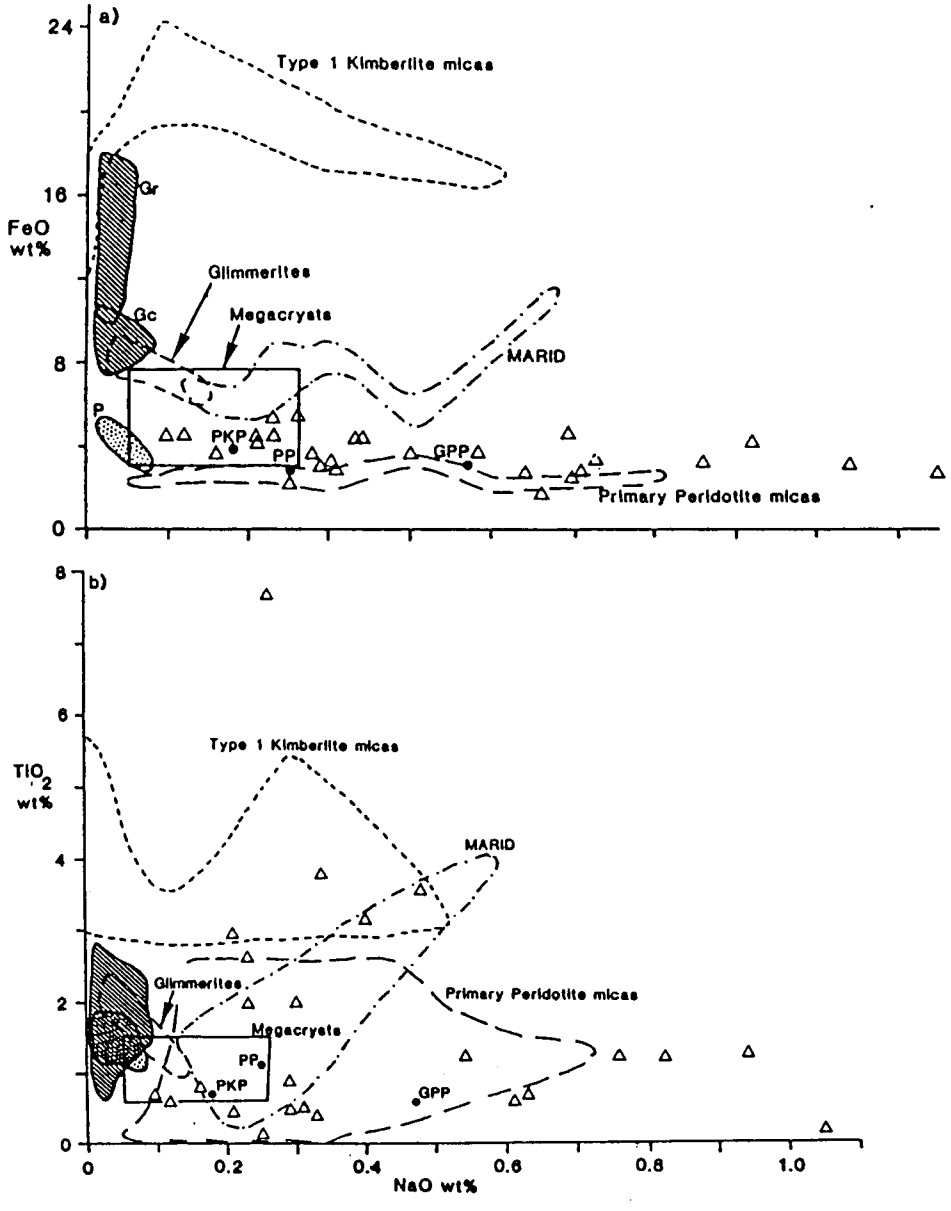

Figure 2.4 a) FeO wt% and b) TiO_2 wt% vs. Na_2O wt% in Finsch and mantle derived micas. P (stippled) = Finsch phlogopite phenocrysts, Gc (core) and Gr (rim) (diagonal hatching) = Finsch phlogopite groundmass. These are compared with mica analyses from megacrysts, glimmerites (Dawson and Smith, 1975b), MARID xenoliths (Dawson and Smith, 1977) and also, Type 1 kimberlite micas (Smith et al., 1978), primary and secondary peridotite micas = (△; Delaney et al., 1980) and average compositions for micas from GPP, PP and PKP xenoliths (Erlank et al., 1987).

relative to the other micas shown. Low Na contents are also a feature of the Finsch whole rocks (Na_2O = 0.03 to 0.49 wt%; Section 2.6). Thus, it is believed that the macrocrystic phlogopites are phenocrysts to the kimberlite magmas, their extremely low Na contents reflecting crystallisation from Na-poor kimberlite magmas.

2.6 Major element geochemistry

The Finsch kimberlites are ultrabasic (SiO_2 < 42 wt%) and ultrapotassic (K_2O/Na_2O > 6.9) igneous rocks, which when compared to basanitic compositions (e.g. basanite 2650, Frey et al., 1978) have lower SiO_2, Fe_2O_3, TiO_2, Al_2O_3, CaO, Na_2O and generally lower P_2O_5 contents, but higher MgO, K_2O and LOI contents.

Kimberlites are prone to contamination by crustal xenoliths and alteration associated with groundwater circulation. Major element geochemistry has previously been used to assess the degree of crustal contamination and alteration of kimberlites. Ilupin and Lutts (1971) used Si/Mg ratios, owing to the higher SiO_2, but lower MgO contents of crustal rocks relative to ultramafic rocks such as kimberlite. Fesq et al. (1975a) suggested that, since olivine (Fo 87 to Fo 93: Si/Mg = 0.6) and phlogopite (Si/Mg $\simeq$ 1.21) normally constitute the bulk of silicate minerals in kimberlite, then a Si/Mg ratio > 1.2 for any kimberlite should indicate excessive crustal contamination. Clement (1982) uses a contamination index;

$$CI = \frac{SiO_2 + Al_2O_3 + Na_2O}{MgO + K_2O}$$

This essentially measures the proportion of clay minerals and tectosilicates relative to olivine and phlogopite (Mitchell, 1986). Contamination indices for fresh kimberlites are usually < 1.3, although they may be as high as 1.5 for phlogopite and/or diopside rich and volatile poor varieties (Clement, 1982).

The majority of samples studied are fresh i.e. Si/Mg < 1.2 and CI < 1.5, though CRC 3 and F766 are borderline and the two external precursor dykes (the EPD; F765 and F758) have extremely high Si/Mg ratios (= 1.99 to 2.36) and CI's (= 2.18 to 2.36). The latter values would apparently suggest that samples F765 and F758 (the EPD) are altered. Furthermore, Clement (1982) and Mitchell (1986) note that alteration leads to an increase in SiO_2, Al_2O_3 and Na_2O contents. However, the EPD exhibit lower SiO_2, but similar Al_2O_3 and Na_2O contents to the rest of the Finsch kimberlites. This would indicate that the EPD samples are also relatively fresh and thus their high Si/Mg ratios and CI's require an alternative explanation. The

major element geochemistry of the EPD is consistent with their being more differentiated than the other Finsch kimberlites analysed (see below). CRC 4 is contaminated (Si/Mg = 1.4, CI =1.95), as are the samples analysed by Ruotsala (1975) from the top 120 m of the Finsch pipe where the kimberlite mineralogy is clay (smectite) dominated (Si/Mg = 1.24 to 5.47, CI = 1.74 to 7.22). The dolomite and Karoo lava country rocks have exceedingly high Si/Mg (> 4.7) and CI (> 7) values.

The Finsch kimberlites show a wide range in major element chemistry (SiO_2 = 27.6 to 41.9 wt%, MgO = 10.4 to 33.4 wt%). The major element oxides are plotted on Harker diagrams in Figure 2.5. It is not possible to discriminate between the samples from the F2, 3 and 4 intrusions, the CRC 1 to 7 (excluding CRC 4 and 5) samples and Finsch B. However, there are major differences between the above samples and the F(5-6) samples and the EPD. The EPD have lower Fe_2O_3, SiO_2 (27.6 and 32.5 wt%) and MgO (10.4 and 12.7 wt%) contents, but higher CaO, TiO_2, MnO, P_2O_5 contents and LOI, while the F(5-6) samples exhibit lower Fe_2O_3, SiO_2 (30.8 to 33.2 wt%), Al_2O_3 and K_2O contents, but higher MnO, CaO contents and LOI. Relative to the F(5-6) intrusion, the EPD have lower MgO and Fe_2O_3 contents, but higher Al_2O_3, CaO, TiO_2 contents and LOI. Taken altogether the Finsch samples show trends of increasing Al_2O_3 and Fe_2O_3 and decreasing CaO and LOI with increasing SiO_2. Much of these trends are defined by the EPD and F(5-6) samples. However, as outlined above, this is probably not due to crustal contamination. Mitchell (1986) suggested that differentiation of a kimberlite magma by olivine fractionation will lead to a residual magma depleted in MgO and SiO_2, but enriched in CaO, TiO_2 and volatiles. Hence the EPD, and to some extent the F(5-6) samples appear to be evolved kimberlites in terms of their major element geochemistry. Anomalous, possibly highly differentiated chemical compositions of precursor or late-stage dykes in kimberlites are well known (Smith et al., 1985).

Figure 2.1b outlines the relative timing of the individual Finsch intrusions i.e. EPD $\rightarrow$ (F(5-6) + F3) $\rightarrow$ F2 and 4. The EPD have the highest LOI, CaO and TiO_2 and the lowest MgO and SiO_2 contents suggesting that, although they are the earliest magmas they are the most 'evolved'. Hence the pipe intrusions were not emplaced in a sequence which can be correlated, at least in major element terms, with single stage crystal fractionation or progressive partial melting. However, the results are compatible with the model proposed by Wyllie (1980) whereby initial, ascending kimberlite magmas establishing a conduit to the surface, are more evolved than the subsequent kimberlite intrusions.

Kimberlite sills and dykes have, on average, higher volatile contents than the main pipe intrusions which tend to be more extensively degassed during emplacement (Clement, 1982). This holds true for the EPD when compared

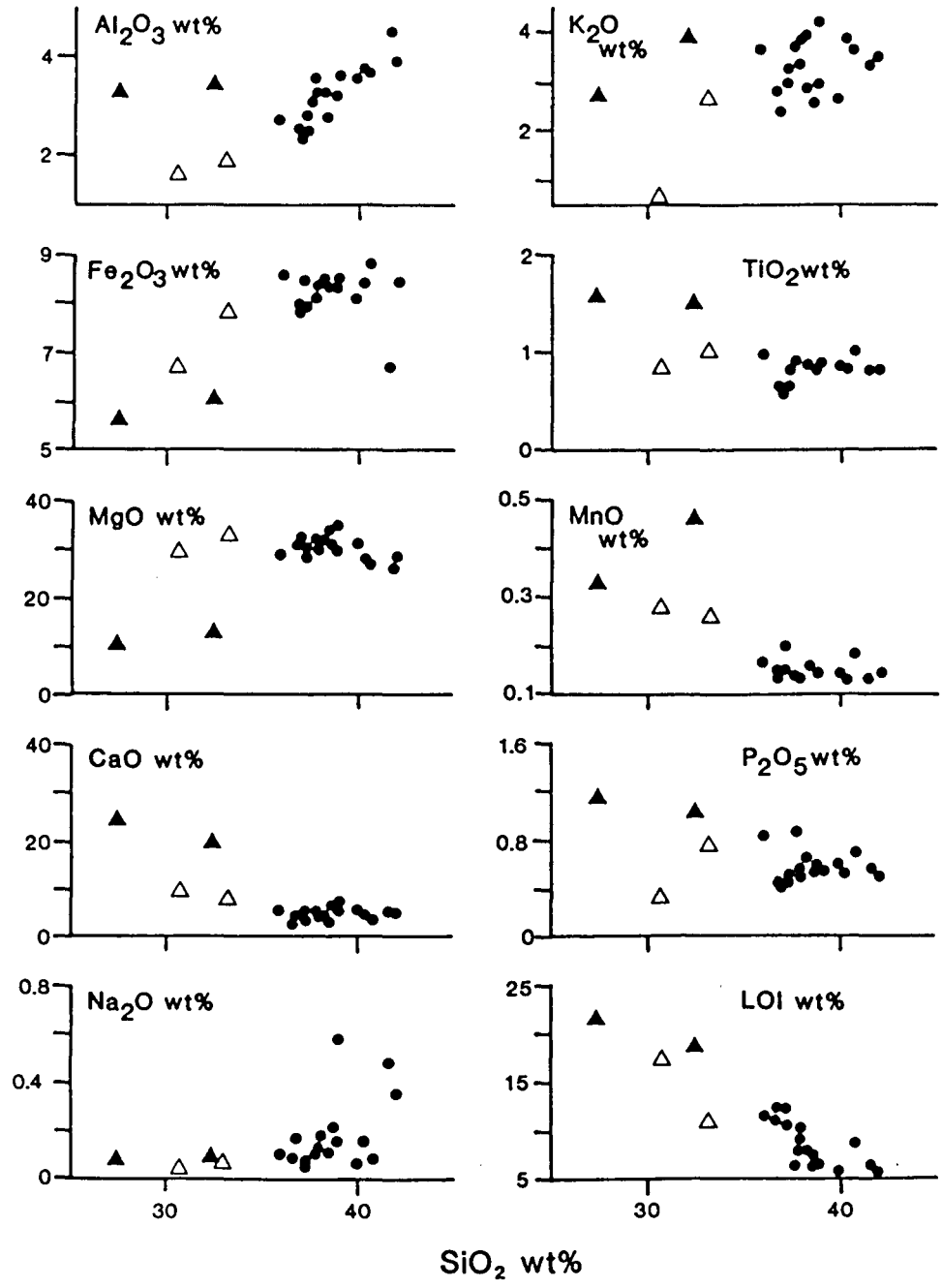

Figure 2.5 Oxide variation with SiO_2 content (wt%) in the Finsch kimberlites. o = F2, 3 and 4 samples and CRC 1, 2, 6 and 7, △ = EPD and △ = F(5-6) samples.

with the Finsch pipe intrusions, but not for the internal F2 and 4 dyke-sill complex.

The F(5-6) samples have low K_2O (and Al_2O_3) contents compared with all the other samples, including the EPD. As the major carrier of K in these rocks is phlogopite, this may indicate low phlogopite contents in the F(5-6) intrusion, and of the thin sections studied, F340 has the lowest phlogopite content, 14.8 vol% compared to 17.8 to 36.4 vol% found for the F2, 3 and 4 intrusions.

Kimberlites are complex heterogeneous rocks which have undergone variable degrees of degassing, crystal differentiation, flow differentiation and can contain a high proportion of xenocrystic material (olivine $\pm$ garnet $\pm$ spinel). Hence, major element variation within an intrusion and overlap between intrusions is not surprising. On the available data and major element chemistry alone, it is not possible to constrain further the importance of the above processes individually.

The South African Cretaceous kimberlites are divisible into two groups; Group 1 kimberlites which tend to be non-micaceous (although differentiated precursor or late-stage dykes may be micaceous; Smith et al., 1985) and Group 2 micaceous kimberlites. In addition to previously outlined isotopic and age differences (Smith, 1983a, b), Group 2 kimberlites are characterised by higher levels of SiO_2 and K_2O, but lower TiO_2, than Group 1 kimberlites (Smith et al., 1985) which may reflect differences in source composition, degree of magma evolution (more 'evolved' rocks contain higher TiO_2 contents; Skinner, 1986) or melting conditions.

Figure 2.6 compares the Finsch data (excluding the EPD and F(5-6) samples; this study and Smith et al., 1985) with fields for South African Group 1 and 2 (minus Finsch B) kimberlites (Nixon et al., 1981; Clement, 1982; Smith et al., 1985). There is a good deal of overlap between the two datasets although, in general, for a given *mg* number, the Group 2 kimberlites tend towards lower TiO_2 and higher SiO_2 and K_2O contents. The bulk of the Finsch kimberlites fall at the high *mg* end of the Group 2 kimberlite field. It is also evident that intrakimberlite variation is less than interkimberlite variation. Also shown in Figure 2.6, are data for micaceous kimberlites from Orroroo, South Australia (Scott Smith et al., 1984) and Holsteinburg, Greenland (Scott, 1979). Both suites show more affinities to the Group 1 kimberlites and have lower K_2O, SiO_2, TiO_2 contents and *mg* numbers than the Finsch kimberlites, although the Holsteinburg kimberlites also have generally low *mg* numbers and high TiO_2 contents relative to the Group 1 kimberlites from the Kimberley area. Kimberlites are volatile-rich (H_2O and CO_2) rocks and Figure 2.7 shows histograms of H_2O and CO_2 contents in Group 1 and 2 kimberlites. Again there is much overlap in the data, although the Group 1 kimberlites appear to extend to higher CO_2 and

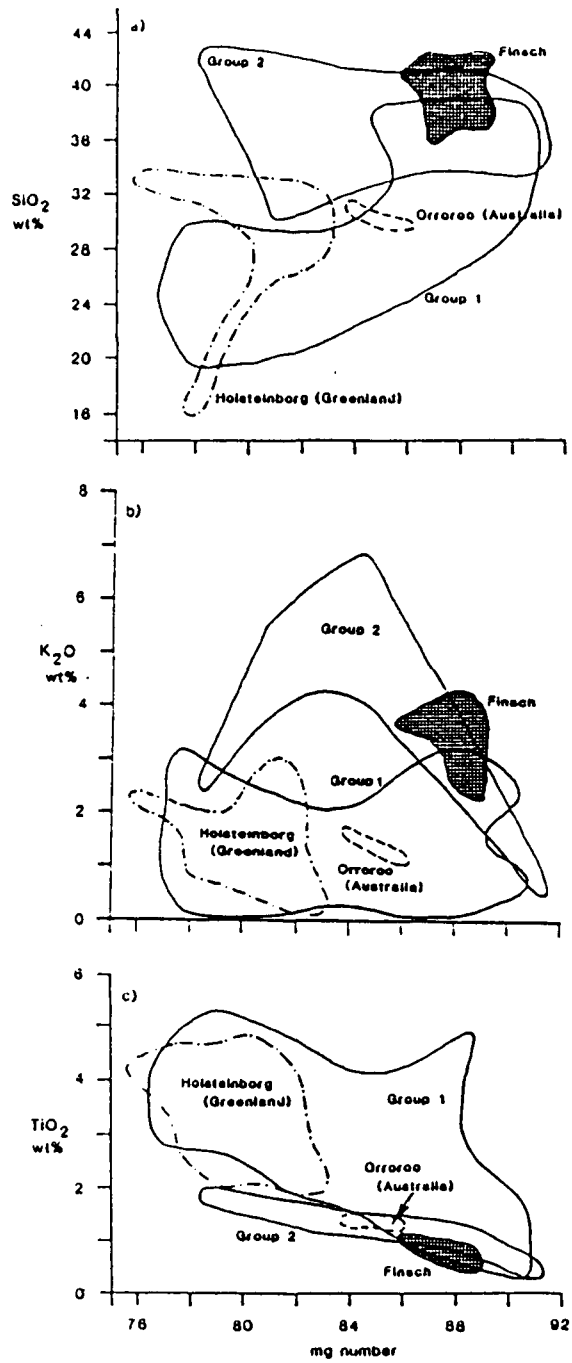

Figure 2.6 a) SiO_2 wt%, b) K_2O wt% and c) TiO_2 wt% vs. *mg* number in kimberlites. Stippled field = Finsch kimberlites, except EPD and F(5-6) samples. Fields are also shown for South African Group 1 and 2 kimberlites (Clement, 1982; Smith et al., 1985) and kimberlites from Orroroo, Australia (Scott Smith et al., 1984) and Holsteinborg, Greenland (Scott, 1979).

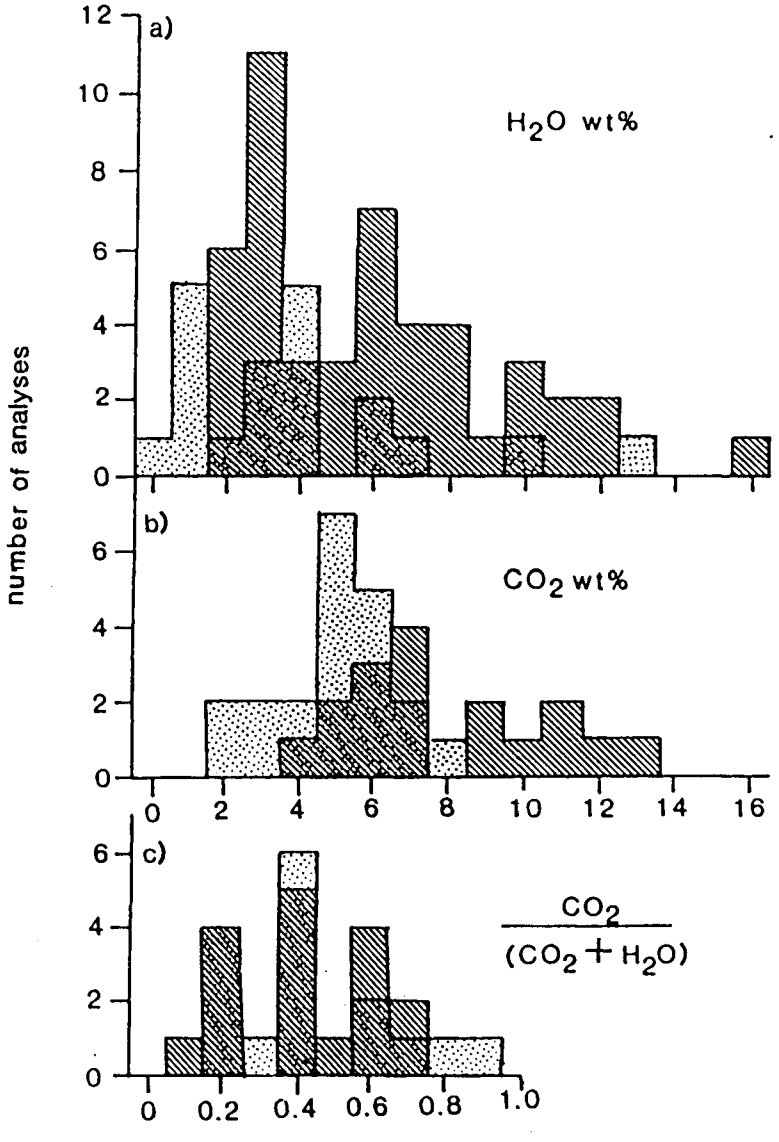

Figure 2.7 Histograms comparing a) H_2O wt%, b) CO_2 wt% and c) $CO_2/(CO_2 + H_2O)$ ratios in Group 1 (diagonal hatching) and 2 (stippled) kimberlites (data from Clement, 1982 and Smith et al., 1985).

H_2O contents than Group 2 kimberlites.

The wide range of data within individual localities and the degree of overlap between localities indicate that major element compositions cannot be used by themselves, to distinguish between different petrographic, geographic and/or isotopic types of kimberlite. It also suggests that extreme care must be taken when comparing individual samples and/or average values from different localities.

2.7 Trace element geochemistry

2.7.1 The compatible trace elements

Partial melting of a peridotite mantle with an *mg* number = 0.92, Ni = 2000 ppm and Cr = 3000 ppm, yields a primary liquid where the *mg* number = 0.68 to 0.74, Ni = 300 to 400 ppm and Cr = 400 to 500 ppm (Kuehner et al., 1981). However, similar to other kimberlites, those from Finsch have Cr and Ni contents significantly higher than those predicted for primary melts (i.e. at Finsch; Cr = 1420 to 2051 ppm and Ni = 1063 to 1544 ppm, excluding the EPD). The EPD have Cr = 1409 and 1429 ppm, Ni = 485 and 719 ppm. CRC 4 has Cr = 759 ppm and Ni = 979 ppm. The Ni and Cr contents of the EPD and CRC 4 while still high, are generally lower than otherwise observed in the Finsch kimberlites.

Mantle peridotite xenoliths from kimberlites exhibit extremely high Ni = 1572 to 2672 ppm and Cr = 1574 to 7116 ppm (Nixon et al., 1981; Erlank et al., 1987). The Finsch data for Ni and Cr reveal they have abundances which are intermediate between those of ordinary melts and mantle derived peridotites.

The Sc contents of the Finsch kimberlites are similar to those exhibited by primary melts such as basanites (e.g. Frey et al., 1978), whereas, V contents fall at the low end of the basanite range.

2.7.2 The incompatible trace elements

The Finsch kimberlites are highly LREE enriched (La = 42.2 to 110 ppm) and exhibit steep chondrite normalised profiles (Ce_N/Yb_N = 28.1 to 62.4) which tend to flatten out at both the LREE and HREE ends (Figure 2.8).

All samples have similar parallel to subparallel trends except for CRC 4, the TKB (Ce_N/Yb_N = 12.6) which is believed to be significantly contaminated. Also shown is CRC 5, the Group 1 kimberlite, which has higher REE contents and a steeper profile (Ce_N/Yb_N = 72) than the Finsch kimberlites.

Within the Finsch data there are variations in REE contents between some of the intrusions. The EPD's have the highest abundances (La = 108 to

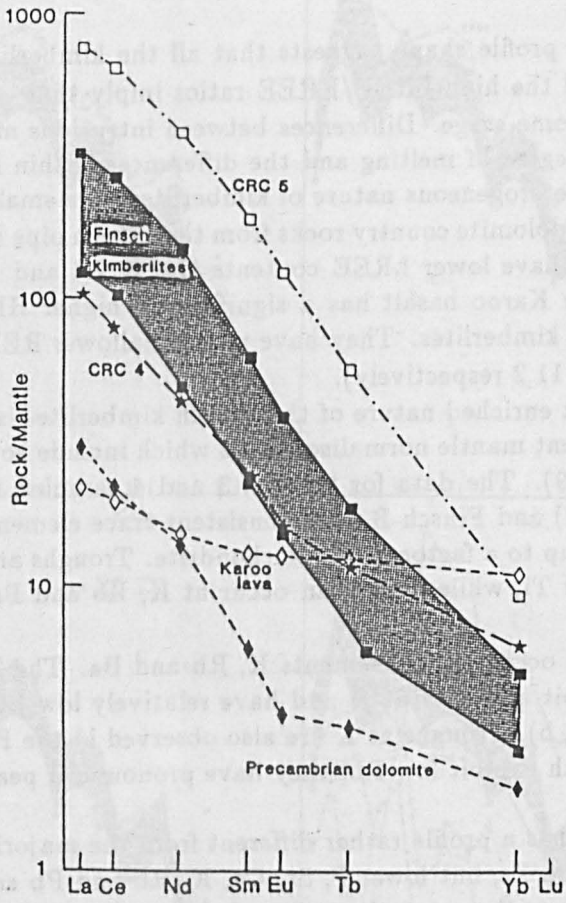

Figure 2.8 Mantle normalised REE patterns showing the range of composition for Finsch kimberlites. REE patterns for CRC 4 (TKB), CRC 5 (Group 1 kimberlite), Karoo lava (F760) and Precambrian dolomite (F769) are also shown.

110 ppm) together with sample F757 (La =105 ppm) from the F4 intrusion. Within the F2 and 4 dyke-sill complex, the F2 samples have higher REE abundances (La =50.9 to 57.5 ppm) than the F4 samples (La = 40.8 to 49.4 ppm). The F(5-6) samples have REE contents which overlap and extend to higher values than the F2 samples (La = 56.3 to 73.3 ppm), while the F3 samples overlap with all the F2 and 4 and F(5-6) samples (La = 42.2 to 77.1 ppm).

The similarity in profile shape suggests that all the kimberlites reflect similar processes and the high LREE/HREE ratios imply that garnet was a residual phase at some stage. Differences between intrusions may reflect slight variations in degree of melting and the differences within intrusions again testify to the heterogeneous nature of kimberlites on a small scale.

Karoo basalt and dolomite country rocks from the Finsch pipe are shown in Figure 2.8. They have lower LREE contents (La = 7.4 and 10.3 ppm respectively) and the Karoo basalt has a significantly higher HREE content than the Finsch kimberlites. They have much shallower REE profiles (Ce_N/Yb_N = 1.83 to 11.2 respectively).

The trace element enriched nature of the Finsch kimberlites is also evident from trace element mantle normalised plots which include some of the REE data (Figure 2.9). The data for the F2, 3 and 4 samples, CRC 1–7 (except CRC 4 and 5) and Finsch B have consistent trace element profiles with Ba enriched by up to a factor of 600 × chondrite. Troughs are present at Pb, Sr, Hf, Zr and Ti, while peaks can occur at K, Rb and Ba (Figure 2.9a).

Variations usually occur in the elements K, Rb and Ba. The EPD and F757 (from F4) exhibit a trough at K and have relatively low Ba and Rb contents (Figure 2.9a, b). Troughs at K are also observed in the F5-6 samples and although both exhibit low Rb, they have pronounced peaks at Ba (Figure 2.9 c).

F667 (from F5-6) has a profile rather different from the majority of the data i.e. higher Ba and Zr, but lower P, Sr, Ce, K, Rb and Pb suggesting it may have a more complex evolution. Sample F287 (F3) also tends to slightly low K and Rb, but exhibits a pronounced peak at Ba. CRC 1–7 and Finsch B have similar profiles to the F2 samples, but variations again occur at Ba and K with peaks and troughs occurring at both elements. Plotted on Figure 2.9d are Karoo lava and dolomite. The dolomite can be discounted as a significant contaminant of the Finsch kimberlites as it has much lower trace element contents and the same applies to the Karoo lava except for the elements Ba and K which are present in amounts similar to those in the kimberlites. However, Rb is almost as abundant as Ba within the Karoo sample, but is significantly lower (by at least a factor of four), than Rb contents in the kimberlites. Thus, again there is little

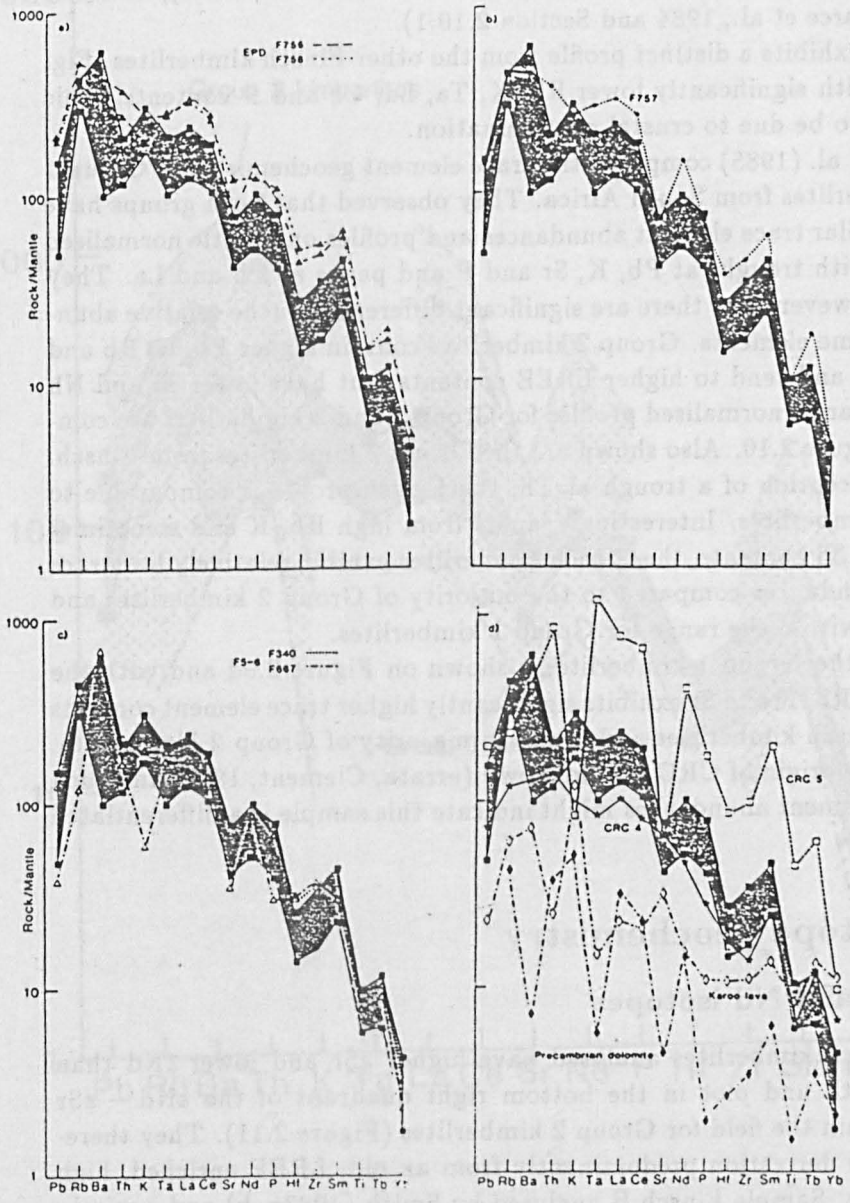

Figure 2.9 Mantle normalised trace element data for the Finsch kimberlites. Stippled field = range of composition for the F2, 3 and 4 samples, CRC 1, 2, 3, 6 and 7, and Finsch B. Also shown; a) the EPD, b) F757, c) F(5-6) samples and d) CRC 4, CRC 5, Karoo lava and Precambrian dolomite.

evidence for significant crustal contamination in the majority of the Finsch kimberlites. Furthermore, the abundances of certain trace elements in the Finsch kimberlites, are up to 15 × higher than in either average continental crust (Weaver and Tarney, 1984; Taylor and McClennan, 1985), or melts thereof (Pearce et al., 1984 and Section 2.10.1).

CRC 4 exhibits a distinct profile from the other Finsch kimberlites (Figure 2.9d) with significantly lower Rb, K, Ta, La, Ce and P contents. This is believed to be due to crustal contamination.

Smith et al. (1985) compared the trace element geochemistry of Group 1 and 2 kimberlites from South Africa. They observed that both groups have broadly similar trace element abundances and profiles on mantle normalised diagrams, with troughs at Pb, K, Sr and P and peaks at Th and La. They did note, however, that there are significant differences in the relative abundances of some elements. Group 2 kimberlites contain higher Pb, K, Rb and Ba contents and tend to higher LREE contents, but have lower Ti and Nb contents. Mantle normalised profiles for Group 1 and 2 kimberlites are compared on Figure 2.10. Also shown are the Group 2 kimberlites from Finsch. With the exception of a trough at Th, the Finsch profile is comparable to the other kimberlites. Interestingly, apart from high Rb, K and sometimes Ba, and low Ti contents, the Finsch kimberlites exhibit relatively low trace element abundances compared to the majority of Group 2 kimberlites and are usually within the range for Group 1 kimberlites.

CRC 5, the Group 1 kimberlite, is shown on Figure 2.9d and with the exception of Rb, K and Sr exhibits significantly higher trace element contents than the Finsch kimberlites and even the majority of Group 2 kimberlites. However, the origin of CRC 5 is unknown (errata, Clement, 1982) and such high trace element abundances might indicate this sample is a differentiated kimberlite.

2.8 Isotope geochemistry

2.8.1 Sr and Nd isotopes

All the Finsch kimberlites analysed have higher εSr and lower εNd than the bulk earth and plot in the bottom right quadrant of the εNd – εSr diagram within the field for Group 2 kimberlites (Figure 2.11). They therefore, indicate derivation predominantly from an old, LREE enriched, high Rb/Sr source. Sample Finsch B analysed by Smith (1983a, b) and again in this study gave slightly different εNd values, although εSr results are very close. $(^{87}Sr/^{86}Sr)_i$ ratios of two autoliths from Finsch, analysed by Kramers (1977), yield initial ratios of 0.7089 and 0.7091 at 118 Ma and are within the range of $(^{87}Sr/^{86}Sr)_i$ = 0.7089 to 0.7106, found in this study for the Finsch

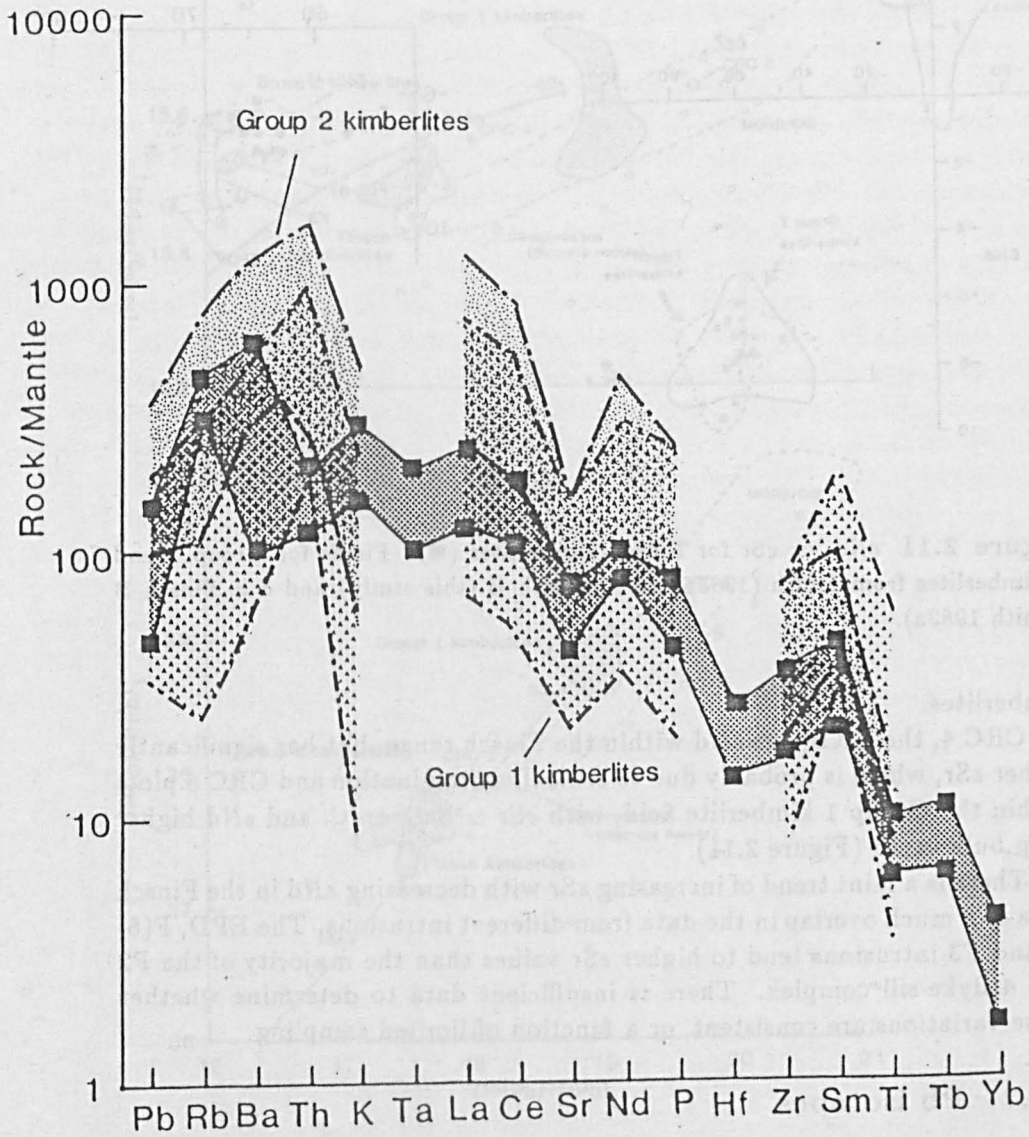

Figure 2.10 Mantle normalised trace element abundance diagram, comparing ranges for Finsch (this study; dark stippled field and ■) and Group 1 and 2 kimberlites (Smith et al., 1985).

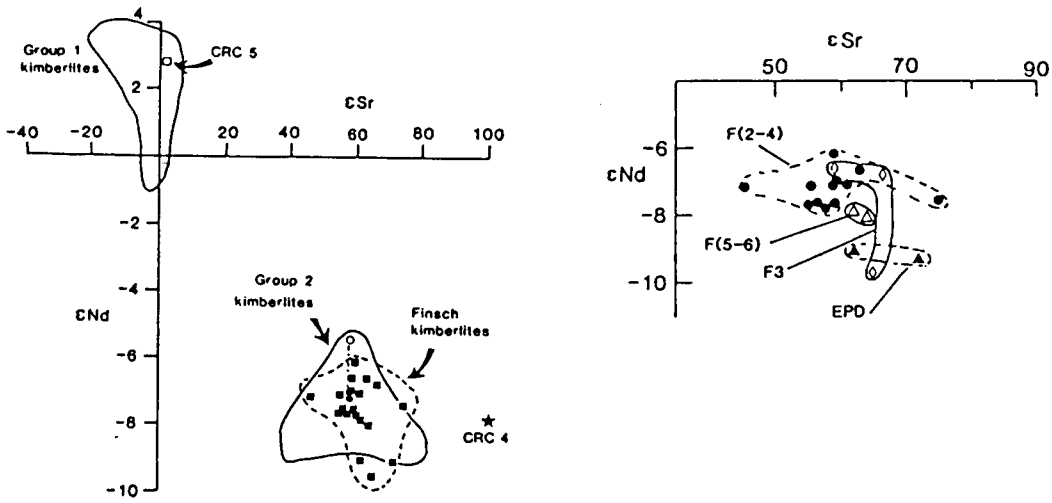

Figure 2.11 ϵNd vs. ϵSr for Finsch kimberlites (■). Fields for Group 1 and 2 kimberlites from Smith (1983a). • = Finsch B (this study) and o = Finsch B (Smith 1983a).

kimberlites.

CRC 4, the TKB, has ϵNd within the Finsch range, but has significantly higher ϵSr, which is probably due to crustal contamination and CRC 5 plots within the Group 1 kimberlite field, with ϵSr $\simeq$ bulk earth and ϵNd higher than bulk earth (Figure 2.11).

There is a faint trend of increasing ϵSr with decreasing ϵNd in the Finsch data and much overlap in the data from different intrusions. The EPD, F(5-6) and F3 intrusions tend to higher ϵSr values than the majority of the F2 and 4 dyke-sill complex. There is insufficient data to determine whether these variations are consistent, or a function of limited sampling.

2.8.2 Pb isotopes

As for ϵSr and ϵNd, the Finsch kimberlites have Pb isotopic signatures similar to the Group 2 kimberlites analysed by Smith (1983a, b). They have unradiogenic $(^{207}Pb/^{204}Pb)_i$ and $(^{206}Pb/^{204}Pb)_i$ contents which plot below the Stacey and Kramers (1975) growth curve (Figure 2.12). Finsch B analyses from this study and those from Smith (1983a, b) are within analytical error and the data for two Finsch autoliths analysed by Kramers (1977) also fall within the Finsch field. The clinopyroxene separate, from a discrete nodule from Finsch, exhibits a higher $(^{206}Pb/^{204}Pb)_i$ ratio (18.21

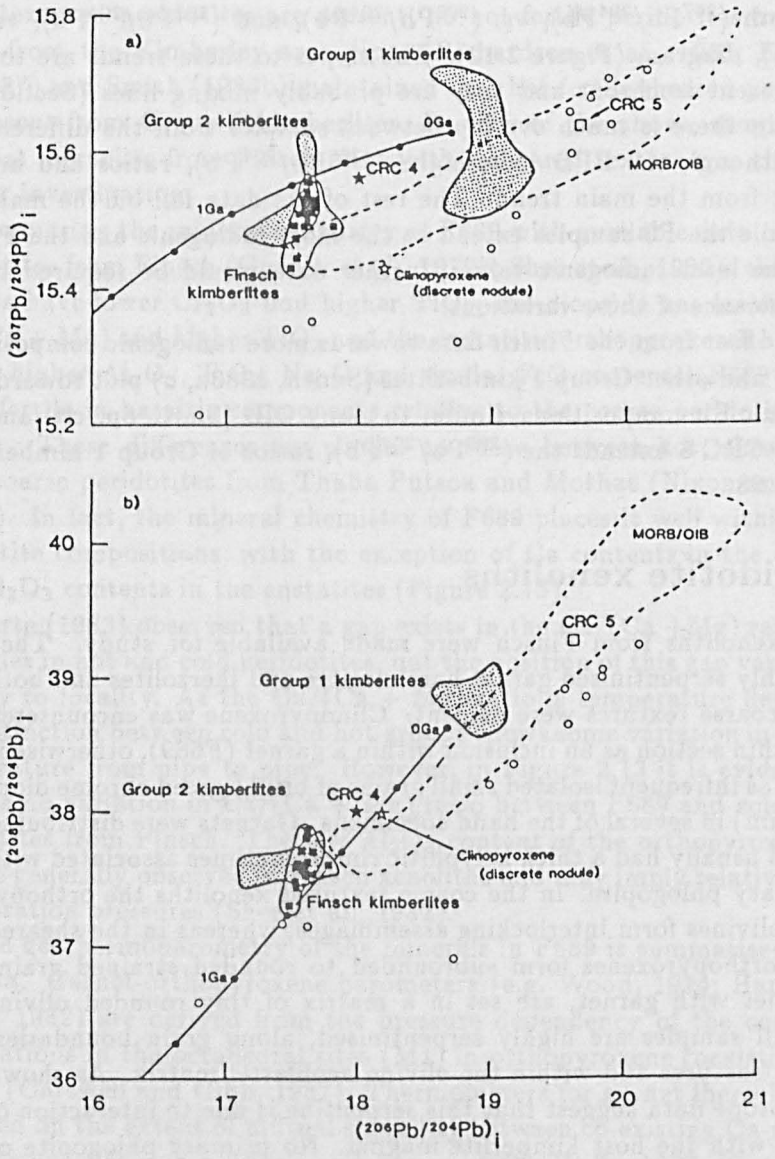

Figure 2.12 Initial Pb isotope ratios for Finsch kimberlites (■)(this study and Kramers, 1977). CRC 4 (⋆) and CRC 5 (□) are also shown. These are compared with fields for selected MORB/OIB (Sun, 1980; Cohen and O'Nions, 1982; Richardson et al., 1982; Stille et al., 1983) and kimberlites (Smith et al., 1983a, b). Th/Pb ratios for the latter are from Smith et al. (1985). Also shown, are data for a clinopyroxene discrete nodule from Finsch (open star) and clinopyroxenes from mantle xenoliths from Southern Africa (open circles; Kramers, 1977, 1979). The Pb-ore growth curve is from Stacey and Kramers (1975).

$\pm$ 0.13; Kramers,1977) than the Finsch data.

The Finsch data (except CRC 4) form well constrained positive correlations on both $(^{207}Pb/^{204}Pb)_i$ vs. $(^{206}Pb/^{204}Pb)_i$ and $(^{208}Pb/^{204}Pb)_i$ vs. $(^{206}Pb/^{204}Pb)_i$ diagram (Figure 2.12). The slopes to these trends are too steep to represent isochrons and they are probably mixing lines (Section 2.10.4). Again there is much overlap between samples from the different intrusions, although the EPD have higher $(^{206}Pb/^{204}Pb)_i$ ratios and are slightly offset from the main trend. The rest of the data fall on the main trend and while the F3 samples extend to the most radiogenic and the F4 samples to the least radiogenic values, further data would be required to test the significance of these variations.

CRC 4 is offset from the Finsch data towards more radiogenic compositions. CRC 5 and other Group 1 kimberlites (Smith, 1983a, b) plot towards more radiogenic Pb compositions, similar to many OIB (Smith op. cit. and Figure 2.12). CRC 5 extends the $(^{206}Pb/^{204}Pb)_i$ ratios of Group 1 kimberlites up to 19.68.

2.9 Peridotite xenoliths

Ten mantle xenoliths from Finsch were made available for study. They consist of highly serpentinised garnet harzburgites and lherzolites and both sheared and coarse textures were evident. Clinopyroxene was encountered only once in thin section as an inclusion within a garnet (F689), otherwise it was observed as infrequent isolated small grains of bright green chrome diopside ($\simeq$ 1–2 mm) in several of the hand specimens. Garnets were distributed randomly and usually had a thick kelyphitic rim, sometimes associated with minor secondary phlogopite. In the coarse textured xenoliths the orthopyroxenes and olivines form interlocking assemblages, whereas in the sheared samples the orthopyroxenes form subrounded to rounded strained grains which, together with garnet, are set in a matrix of tiny rounded olivine neoblasts. All samples are highly serpentinised, along grain boundaries, along olivine fractures and within the olivine neoblastic matrix. As shown below, the isotope data suggest that this serpentine is due to interaction of the xenoliths with the host kimberlite magma. No primary phlogopite or amphibole was observed.

The majority of peridotite xenoliths from kimberlites can be classified in terms of their texture (sheared or coarse), mineral chemistry (whether they are fertile, Fe-Ti-rich, or depleted, Mg-rich, in basaltic components) and temperature (hot or cold i.e. greater, or less than 1100°C, respectively; Nixon and Boyd, 1973a; Harte, 1983 and references therein). Many, but not all, xenoliths fall into one of two broad categories; hot, fertile,

sheared peridotites of probable asthenospheric origin and cold, depleted, coarse peridotites of probable lithospheric origin (Harte, 1983). Although shear-textured peridotites are present, no hot fertile peridotites have been found from the Kimberley area pipes (Richardson et al., 1985; Erlank et al., 1987) and Smith (1983b) maintained that hot fertile sheared peridotites are absent from Group 2 kimberlites. In view of the above, sample F689, a garnet lherzolite from Finsch mine with a sheared texture was chosen for further investigation.

Comparing the mineral chemistry of F689 with available data on coarse peridotites from Finsch (Gurney et al., 1979b; Shee et al., 1982): the pyrope garnets have lower Cr_2O_3 and higher TiO_2, the diopside has lower Cr_2O_3, Ca/(Ca + Mg) and higher TiO_2 and the enstatitic orthopyroxenes have similar to higher Al_2O_3, TiO_2, Na_2O and similar FeO contents. F689 appears to be fertile in basaltic components relative to the coarse peridotites from Finsch. These differences are similar to those between hot, sheared and cold, coarse peridotites from Thaba Putsoa and Mothae (Nixon and Boyd, 1973b). In fact, the mineral chemistry of F689 places it well within fertile peridotite compositions, with the exception of Ca contents in the diopside and Al_2O_3 contents in the enstatites (Figure 2.13).

Harte (1983) observed that a gap exists in the Ca/(Ca +Mg) ratio from diopsides in hot and cold peridotites, but the position of this gap varies from locality to locality. As the Ca/(Ca + Mg) ratio is temperature dependant the distinction between cold and hot groups shows some variation in inferred temperature from pipe to pipe. However, in Figure 2.13 it is evident that there is no variation in Ca/(Ca + Mg) ratio between F689 and cold coarse peridotites from Finsch. The low Al_2O_3 content of the orthopyroxene is a feature generally observed in Finsch xenoliths and may imply relatively high equilibration pressures (Shee et al., 1982).

The geothermobarometry of the minerals in F689 is summarised in Table 2.3a. Garnet-orthopyroxene barometers (e.g. Wood, 1974; Harley and Green, 1982) are derived from the pressure dependency of the content of Al^{3+} cations in the octahedral sites (M1) in orthopyroxene coexisting with garnet (Carswell and Gibb, 1987). Thermometers for garnet lherzolites can be based on the extent of mutual solubility between co-existing Ca-rich and Ca-poor pyroxenes (e.g. Wood and Banno, 1973; Wells, 1977; Kretz, 1982; Nickel et al., 1985) and Fe^{2+}– Mg^{2+} exchange between minerals such as garnet and clinopyroxene (e.g. Ellis and Green, 1979; Saxena, 1979).

Carswell and Gibb (1987) tested the accuracy of a number of different barometer and thermometer formulations, by comparing results against experimentally calibrated mineral composition data for 'natural' multi-component garnet lherzolite assemblages. Table 2.3a also gives $\Delta P = (P_{calculated} - P_{experimental})$, and $\Delta T = (T_{calculated} - T_{experimental})$ from Carswell and Gibb

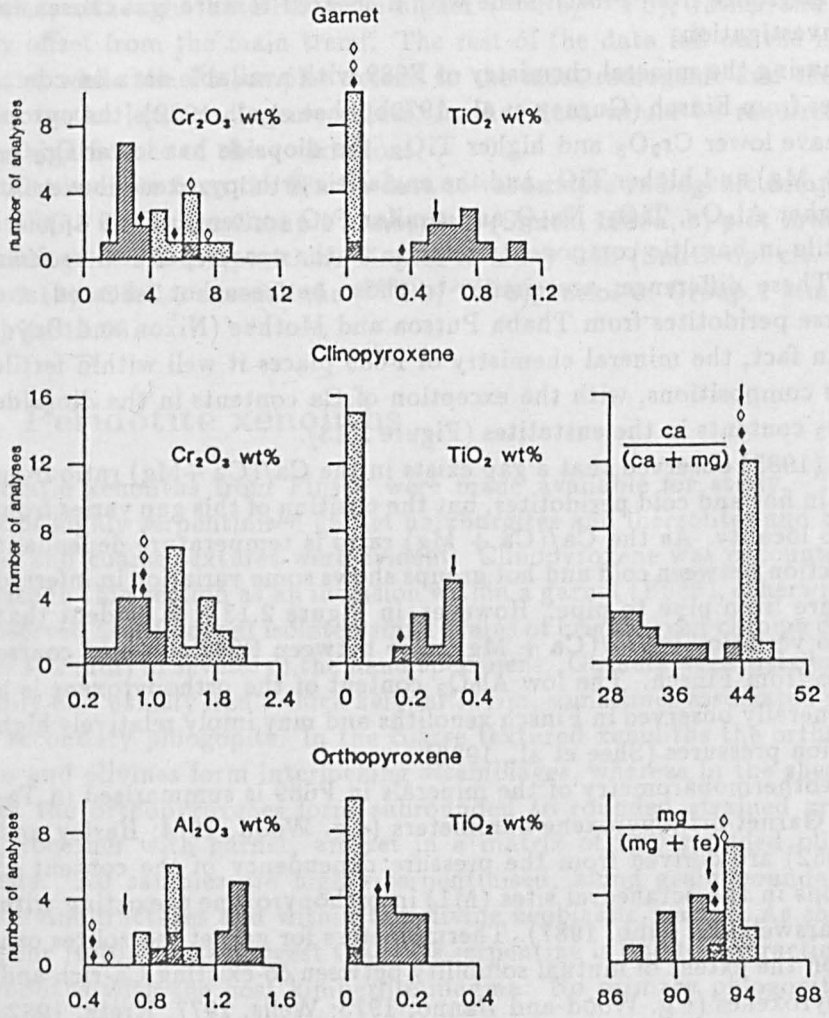

Figure 2.13 Histograms comparing mineral data from the Finsch peridotite (F689) with data on Finsch and Lesotho peridotites. ↓ = F689, ◆ = coarse textured peridotites from Finsch (Gurney et al., 1979b), ◇ = coarse textured, diamondiferous peridotites from Finsch (Shee et al., 1982), shaded field = shear textured peridotites, and stippled field = coarse textured peridotites from Lesotho (Nixon and Boyd, 1973a).

Thermometers	Reference	P (Kb)	T (°C)	ΔT (°C)
Garnet/	Saxena, 1979	20–40	1027–1168	−348 to +41
Clinopyroxene	Ellis & Green, 1979	20–40	881–951	−161 to +91
Orthopyroxene/	Wells, 1977	20–40	1016	−81 to +80
Clinopyroxene	Wood & Banno, 1973	20–40	1116	−18 to +91
	Kretz, 1982	20–40	1113	−1 to +104
	Nickel et al., 1985	20–40	1269–1328	−30 to +156
Barometers	**Reference**	**P (Kb)**	**T (°C)**	**ΔP (°C)**
Garnet/	Wood, 1974	50.6–63.5	1100–1300	−0.3 to −6.5
Orthopyroxene	Harley & Green, 1982	54.0–66.5	1100–1300	−1.0 to −7.3

Sample	Reference	P (Kb)	Reference	T°C
JJG 147[1]	Wood, 1974	39.9	Wells, 1977	1050
JJG 479[1]	Wood, 1974	40.8	Wells, 1977	1030
XM 46[2]	Wood, 1974	49.1	Wells, 1977	1100
	Wood, 1974	55.5	Wood & Banno, 1973	1200
XM 48[2]	Wood, 1974	53.9	Wells, 1977	1047
	Wood, 1974	48.5	Wood & Banno, 1973	1151

Table 2.3 a) Geothermobarometry of F689; $\Delta T = (T_{calculated} - T_{experimental})$ and $\Delta P = (P_{calculated} - P_{experimental})$ from Carswell and Gibb (1987). See text for discussion. b) available geothermobarometry data for Finsch xenoliths. 1 = Gurney et al. (1979b) and 2 = Shee et al. (1982).

(op. cit.) for the thermobarometers used in this study. Both the barometers in Table 2.3a underestimate pressure to some extent. Carswell and Gibb (op. cit.) considered that at P > 37 Kb, the orthopyroxene-clinopyroxene thermometers of Wood and Banno (1973) and Kretz (1982) are more accurate than the Wells (1977) method. Nickel et al. (1985) yields gross overestimates (mostly > 200°C) relative to $T_{experimental}$.

Bearing the above in mind, it is evident that the xenolith F689 had a T = 850 to 1116 °C and P = 50 to 55 Kb. Data available for non-diamondiferous (JJG147 and JJG479; Gurney et al., 1979b) and diamondiferous (XM46 and XM48; Shee et al., 1982) garnet lherzolite xenoliths from Finsch are shown in Table 2.3b. It is evident that all the Finsch xenoliths have similarly low temperatures, but F689 appears to indicate pressures higher than those calculated for the non-diamondiferous lherzolites, yet comparable to those for the diamondiferous lherzolites. Thus, although F689 exhibits a relatively fertile major element chemistry, usually indicative of hot fertile xenoliths, it has a relatively low temperature more characteristic of cold depleted peridotites.

Of the common mantle minerals, clinopyroxene is the major carrier of Sr and hence its Sr isotope composition should be closest to the initial isotope composition of the whole rock xenolith. Diopsides were separated from sample F689 and also, for comparison, from sample F750, a coarse garnet lherzolite from Finsch. These diopsides were analysed for Sr isotopes and the $(^{87}Sr/^{86}Sr)_m$ ratios found were 0.70245 (F689) and 0.70395 (F750). The whole rock analyses of F689 and F750 were 0.70784 and 0.70754 respectively which closely reflects the kimberlite whole rock values (0.70841 to 0.70983). This indicates that by careful selection and preparation, the clinopyroxene Sr analyses probably represent the best estimate of the initial isotope values of the xenoliths and are indicative of long-term trace element depleted sources with low Rb/Sr ratios.

Richardson et al. (1985) noted that hot fertile peridotites in Southern African kimberlites are more frequent in occurrence near the margins of and off the Archaean craton and may well be derived from asthenospheric MORB type sources abutting the shallowing subcontinental lithosphere. Richardson et al. (op. cit.) also observed that the cold coarse peridotites, believed to originate in the lithospheric mantle, have more enriched isotopic signatures than MORB, although they still may have lower $(^{87}Sr/^{86}Sr)_m$ ratios than bulk earth. The degree of isotopic enrichment appears to increase inwards from the craton margin (e.g. Thaba Putsoa, Lesotho) towards the craton interior (e.g. Kimberley). The craton interior is older and has experienced longer time-integrated 'enrichment'. The isotope data for F689 and F750 from Finsch (craton interior) are more comparable with the data from Thaba Putsoa on the craton margin. The low temperature calculated for

F689 indicates that this xenolith was derived from the sub-continental mantle lithosphere. However, the relatively fertile chemistry of the constituent minerals and depleted Sr isotope signature may indicate that F689 is from a portion of the sub-continental mantle 'recently' extracted from the asthenosphere or modified by partial equilibration with an asthenospheric magma intruded into the lithosphere. This would most likely to have occurred near the base of the lithosphere and the high pressure calculated for F689 could be compatible with this model.

2.10 Petrogenesis: The Finsch mine kimberlites

2.10.1 Crust or mantle ?

All the fresh hypabyssal Finsch kimberlites have high *mg* numbers (0.86 to 0.90, EPD: 0.78 and 0.80), high Ni contents (1063 to 1544 ppm, EPD: 485 and 719 ppm) and contain diamonds and other mantle xenoliths and xenocrysts. These observations, together with abundances of certain trace elements preclude the continental crust as a predominant component within these kimberlites. For example, Nd in the Finsch kimberlites = 32.2 to 94.2 ppm, whereas, Nd in average crust = 16 to 23 ppm (Weaver and Tarney, 1984; Taylor and McClennan, 1985) and 22 ppm in average syncollision granites (Pearce et al., 1984) which are regarded as typical upper crustal melts. Unless very specialised selective contamination is invoked the same applies to the Sr contents e.g. Sr in Finsch kimberlites = 426 to 919 ppm, average continental crust = 260 to 503 ppm and average syncollision granite = 158 ppm. Similarly, the Sm/Nd ratios of the kimberlites (except CRC 4) are too low and Ta/Yb ratios too high, to be due simply, to interaction between MORB and/or OIB and the continental crust (Figure 2.14). CRC 4 has a lower Ta/Yb but, higher Sm/Nd ratio and plots away from the main Finsch field on Figure 2.14 towards continental crust compositions.

The above arguments can also be applied to the Karoo lava and Precambrian dolomite country rocks to the Finsch pipe. They have Nd < 10 ppm and Sr < 364 ppm and both have extremely low Ta/Yb ratios < 0.25. Therefore, these compositions have not had any significant influence on the geochemistry of the Finsch kimberlites analysed here.

2.10.2 Fractionation

The only early crystallising phases which could have fractionated from the Finsch kimberlite magmas are olivine (macrocrysts and phenocrysts) and phlogopite (phenocrysts). These are now assessed in turn:

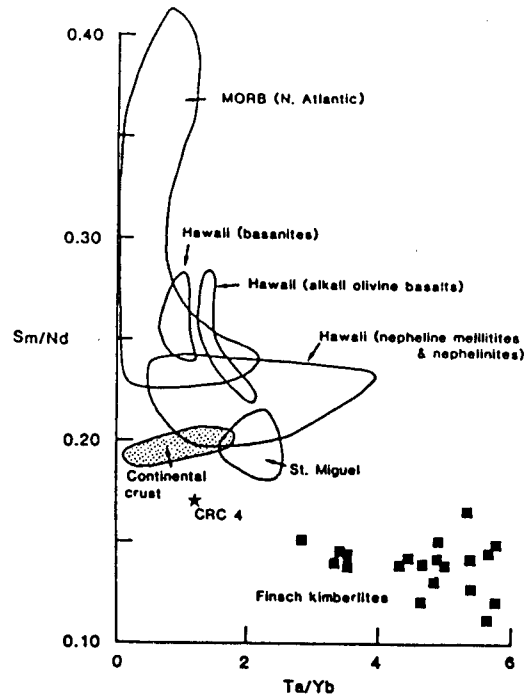

Figure 2.14 Sm/Nd vs. Ta/Yb for Finsch kimberlites (■) including CRC 4 (⋆), compared with those for selected ocean islands (Wood et al., 1979; Clague and Frey, 1982 and Norry, personal communication) and the continental crust (Weaver and Tarney, 1984: Taylor and McClennan, 1985).

Olivine; The extremely high *mg* numbers and Ni and Cr contents argue against significant olivine fractionation. However, it has been suggested above, that the anomalous compositions exhibited by the EPD and F(5-6) samples could be due to differentiation of kimberlite magmas. Mitchell (1986) suggests that differentiation of kimberlite results in depletion of MgO and SiO_2 and the enrichment of CaO, TiO_2 and H_2O in the derivative liquids. The geochemistry of the EPD and F5-6 samples is consistent with these observations. As shown in Figure 2.15, the Finsch data exhibit a positive correlation between Ni ppm and SiO_2 wt%. This trend is predominantly defined by the EPD and F5-6 samples. The majority of the Finsch samples show relatively little variation. The overall positive trend on Figure 2.15 could be due to fractionation of olivine. However, this trend could also, at least in part, result from mixing between peridotite (high Ni and SiO_2 contents) and a melt with low Ni (< 450 ppm and low $SiO_2 < 27$ wt%).

Phlogopite; Phlogopite phenocrysts occur only rarely in the Finsch kimberlites and phlogopite usually occurs as an abundant groundmass phase. This suggests that the late-crystallising kimberlite melt was enriched in K and had not been noticeably depleted by earlier phlogopite fractionation. Furthermore, this is supported by mineral chemistry. As outlined in Section 2.5, abundant crystallisation of phlogopite should deplete the residual kimberlite in Ti and yet Ti contents in cores to groundmass phlogopites

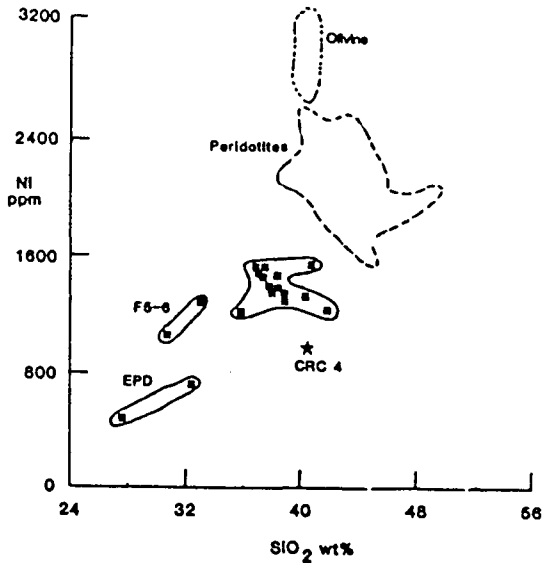

Figure 2.15 Ni ppm vs. SiO_2 wt% for Finsch kimberlites (■), including CRC 4 (⋆) and olivine phenocryst compositions; this study. These are compared with peridotites (Nixon et al., 1981; Erlank et al., 1987).

are significantly higher than Ti contents in phenocryst phlogopites. Abundant crystallisation of groundmass phlogopite ± perovskite has resulted in the Ti-poor rims on groundmass phlogopites. The EPD and F5-6 samples have, with one exception, K_2O contents within the range of other Finsch kimberlites and the EPD have higher Ti contents.

Thus, it would appear that the majority of the Finsch kimberlites are unfractionated mantle derived rocks. The anomalous EPD and F5-6 samples may have fractionated significant olivine, but not phlogopite.

2.10.3 Partial Melting

The high incompatible trace element contents in the Finsch kimberlites could have been generated by small degrees of partial melting. However, the low εNd values obtained from Finsch kimberlites indicate low time-integrated Sm/Nd ratios (LREE enrichment) within the mantle source region caused by an ancient trace element enrichment. Evaluation of the age of this 'event' would indicate the source Sm/Nd ratio and hence, comparison with the observed kimberlite Sm/Nd ratios, would provide an estimate of the amount of Sm/Nd fractionation during melting, assuming the simplest model. It is reasonable to infer that major geological events which are manifest in the

Southern African continental crust relate to the evolution of the associated subcontinental mantle lithosphere. Therefore, the following list of important geological events recorded from Southern Africa have been identified in mantle derived and/or crustal rocks (mainly after Hawkesworth et al., 1983):

1. 3.6 Ga; Age of oldest Archaean rocks identified in the cratonic nucleii.
2. 3.2 – 3.3 Ga; Age of LREE enriched pyrope garnets, which occur as syngenetic inclusions within diamond from the Finsch and Kimberley pipes (Richardson et al., 1984).
3. 2.7 Ga; $(^{143}Nd/^{144}Nd)_m - (^{87}Sr/^{86}Sr)_m$ isochron from Archaean crustal xenoliths and a model age of a mantle diopside.
4. 1.4 – 1.0 Ga; Formation of Namaqua-Natal belt and the generation of considerable volumes of new crust. This is supported by some rather abstruse $(^{143}Nd/^{144}Nd)_m - (^{87}Sr/^{86}Sr)_m$ isochrons for Lesotho granulites, mantle diopsides and the age inferred for the Karoo source region.
5. 190 Ma; Karoo magmatism.
6. 150 Ma; Metasomatism of mantle peridotites e.g. PP and PKP xenoliths (Erlank et al., 1982, 1987).

These events are believed to have influenced the evolution of the subcontinental mantle in this region. Thus, it is appropriate to determine whether the ancient trace element enrichment identified within the Finsch kimberlites could be related to any of the above events. A minimum age of enrichment of $\simeq$ 420 Ma is obtained from T^{Nd}_{CHUR}, which assumes no change in Sm/Nd ratio during magmatism. The trace element enriched source region of the Finsch kimberlites, therefore, appears to have survived unaffected by the mantle upheaval caused by extraction of the Karoo flood basalts.

For a trace element enrichment event in the Finsch source region at 1.4 Ga, the $(^{143}Nd/^{144}Nd)_i$ ratios of the kimberlites imply a source Sm/Nd ratio of $\simeq$ 0.247. The average observed Sm/Nd ratio in the kimberlites is 0.139, which suggests that during magmatism the Sm/Nd ratio decreased by 44%. Assuming a two-stage model, 44% fractionation of the Sm/Nd ratio, implies less than 1% partial melting, even in the presence of residual garnet (Hawkesworth et al., 1979). Older enrichment ages allow higher Sm/Nd ratios in the source regions, which require increased amounts of fractionation during melting. This in turn necessitates even smaller degrees of partial melting e.g. enrichment ages of 2.7 Ga and 3.6 Ga, indicate 52 and

53% fractionation respectively, of the Sm/Nd ratio during melting. Thus, the preferred enrichment age of the Finsch source region is $\simeq$ 1.4 Ga, as it is associated with the least Sm/Nd fractionation. This age is also most consistent with the Pb isotope data (see Section 2.10.4).

The Finsch kimberlites actually exhibit a small variation in Sm/Nd ratio (0.121 to 0.166) and since $D_{Nd} < D_{Sm}$ for basaltic systems (Frey et al., 1978), this ratio may be sensitive to variations in degree of partial melting. In order to assess whether these variations were reflected by other trace element ratios and whether they had any significance in terms of partial melting, the kimberlite Sm/Nd ratios were compared with other X/Nd ratios; X representing a number of incompatible trace elements of varying D values. Positive correlations were found to exist between Sm/Nd and a number of X/Nd ratios, when X = Th, Ta, La, Ce, Sr, Hf, Zr, Sm and Y. By assuming D values for Nd and Sm and using a batch melting equation, it was possible to calculate D values for X. The appropriate calculations are outlined below:

1. $$C_l/C_o = 1/(F + D - FD)$$

   where;

   - C_l = concentration of the element in the liquid.
   - C_o = concentration of the element in the original unmelted source.
   - F = weight proportion of melt formed.
   - D = bulk distribution coefficient for the residual solids at the moment when the melt is removed from the system.

   (Cox et al., 1979)

2. Sm/Nd melt = $[(C_l/C_o)_{Sm}/(C_l/C_o)_{Nd}] \times$ Sm/Nd source.
   Sm/Nd source = 0.25 (see above).

3. X/Nd melt = $[(C_l/C_o)_X/(C_l/C_o)_{Nd}] \times$ X/Nd source.
   X/Nd source = measured from plots of X/Nd vs. Sm/Nd (see above and Figure 2.16).

By varying D and F, partial melting curves were calculated and plotted on diagrams of X/Nd vs. Sm/Nd (e.g. Figure 2.16). Best fit curves were obtained when D_{Nd} = 0.001, D_{Sm} = 0.0035 and D_X = 0.003 to 0.995 (the majority ranging between 0.003 and 0.005). The assumed D values for Sm and Nd are several orders of magnitude lower than clinopyroxene-liquid partition coefficients determined in basaltic systems (e.g. Frey et al., 1978;

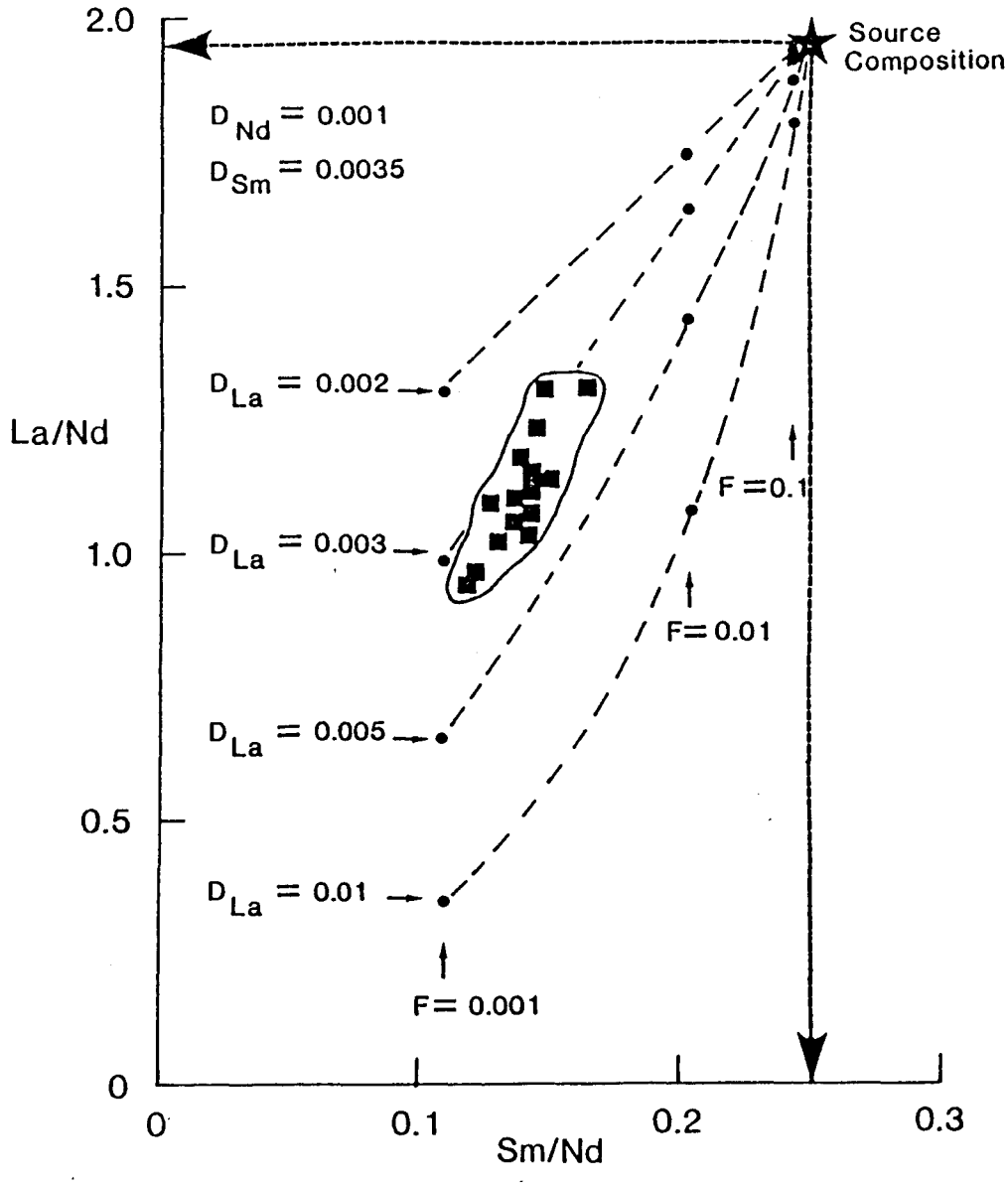

Figure 2.16 La/Nd vs. Sm/Nd for Finsch kimberlites and partial melting curves calculated from an inferred source composition. A linear regression through the Finsch data together with an assumed source Sm/Nd ratio = 0.25, gives a source La/Nd ratio = 1.95. Assuming $D_{Nd} = 0.001$ and $D_{Sm} = 0.0035$, a best-fit melting curve for the Finsch data can be calculated using a batch melting equation and various values for D_{La} and degree of melting (F). See text for discussion.

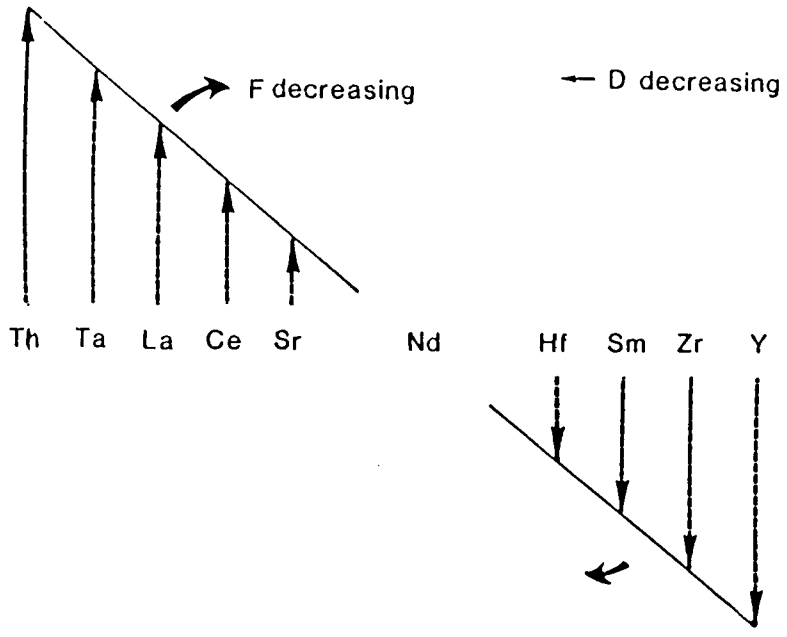

Figure 2.17 Diagram showing how the abundance of various incompatible trace elements changes relative to Nd during partial melting, assuming relative D values pertinent to basaltic systems (Frey et al., 1978; Henderson, 1982). Elements are listed in order of decreasing incompatibility (or increasing D). With small degrees of partial melting, the abundance of all elements increases, but relative to Nd, 1) Th to Sr increases, and 2) Hf to Y decreases. Thus, if a suite of igneous rocks shows a variation in Sm/Nd, then the above would imply that 1) Th/Nd to Sr/Nd vs. Sm/Nd should produce a negative correlation, and 2) Hf/Nd to Y/Nd vs. Sm/Nd should produce a positive correlation.

Henderson, 1982) and an order of magnitude lower than values calculated for clinopyroxene megacryst-kimberlite (Kramers et al., 1981). Furthermore, the calculated D values for the Finsch kimberlites interestingly imply that Nd is the most incompatible element during melting.

This is also evident from consideration of Figure 2.17, where the elements Th, Ta, La, Ce, Sr, Nd, Hf, Zr, Sm and Y are listed in order of decreasing incompatibility (increasing D) as appropriate for basaltic systems. Extraction of a small volume partial melt, from whatever system, will increase the absolute abundance of all these incompatible elements in the liquid relative to the source. However, relative to Nd; Th, Ta, La, Ce and Sr contents will increase as $D_{Th,Ta,La,Ce,Sr} < D_{Nd}$, while Hf, Zr, Sm and Y will decrease relative to Nd contents as $D_{Hf,Zr,Sm,Y} > D_{Nd}$. Thus, if variation in the Sm/Nd ratio is related to differing degrees of partial melting then Th/Nd to Sr/Nd vs. Sm/Nd should correlate negatively, and Hf/Nd to Y/Nd vs. Sm/Nd should correlate positively.

In the case of the Finsch kimberlites, where all the Th/Nd to Y/Nd ratios correlate positively with Sm/Nd, Nd is effectively behaving as the most incompatible element. Thus modelling these correlations as reflecting slight variations in the degree of closed system partial melting is considered unreasonable.

2.10.4 Mixing model

Garnets and ubiquitous macrocrystic olivine found within kimberlites are believed to represent disaggregated mantle peridotite (e.g. Clement, 1982). Up to 45% macrocrystic olivine in the Finsch mine kimberlites and the high garnet content of the heavy mineral concentrate at Finsch (Gurney and Switzer, 1973) all point towards significant entrainment of upper mantle peridotite within these kimberlites.

There is an absence of combined major and trace element data for peridotite xenoliths from the Finsch mine. There are data, however, for peridotites (GP, GPP, PP and PKP) from the Kimberley pipes (South Africa) situated only $\simeq$ 80 km from the Finsch pipe (Nixon et al., 1981; Erlank et al., 1987) which should give a general indication of the composition of the mantle beneath the Finsch pipe. To the author's knowledge, no primary phlogopite and/or amphibole, so indicative of mantle metasomatic processes elsewhere, has been reported from xenoliths recovered from Finsch. This suggests that garnet peridotites (GP's) are the most likely peridotite component within the Finsch pipe. These garnet peridotites tend to have low concentrations of incompatible trace elements e.g. Rb $<$ 38 ppm, Sr $<$ 166 ppm, Zr $<$ 34 ppm and La $<$ 12 ppm, but extremely high concentrations of compatible trace elements e.g. Cr = 1574 to 7116 and Ni = 1572 to 2672 ppm (Nixon et al., 1981 and Erlank et al., 1987). Comparison with the Finsch kimberlite data, where Rb = 43 to 182 ppm, Sr = 416 to 919 ppm, Zr = 110 to 248 ppm, La = 40 to 105 ppm, Cr = 1420 to 2051 ppm and Ni = 1063 to 1544 ppm (excluding the EPD), suggests that if mantle peridotite is a mixing component, then it will most affect the compatible trace element concentrations of the resulting kimberlite composition.

The high compatible trace element contents of the Finsch kimberlites relative to primary mantle melts was discussed in Section 2.7.1. On Figure 2.18, the Ni and Cr contents of the Finsch kimberlites are compared with those of primary mantle melts (as calculated by Kuehner et al., 1981), basanites (Frey et al., 1978; Clague and Frey, 1982) and whole-rock peridotites (Nixon et al., 1981; Erlank et al., 1987). The results show that the Finsch kimberlite data are consistent with their being a mixture between a primary mantle melt and abundant mantle peridotite.

Comparison of the incompatible trace element abundances in the peri-

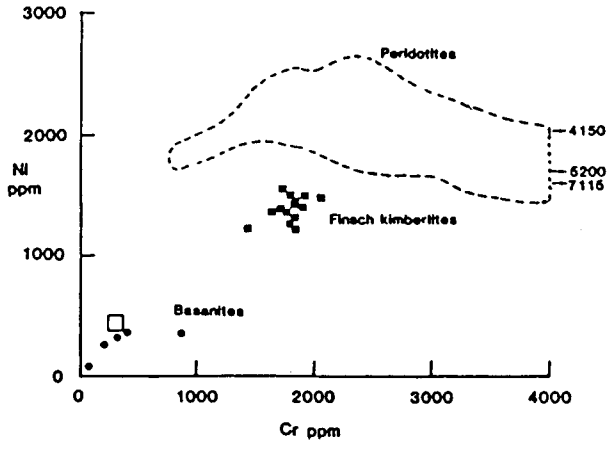

Figure 2.18 Ni ppm vs. Cr ppm for Finsch kimberlites (■) compared with peridotites (Nixon et al., 1981; Erlank et al., 1987), basanites (•; Frey et al., 1978; Clague and Frey, 1982) and calculated primary mantle melt compositions (□; Kuehner et al., 1981).

dotites and Finsch kimberlites reveals that the primary melt component must have been extremely enriched in incompatible trace elements. The addition of peridotite would have diluted the incompatible trace element content of the resultant kimberlite magmas. It was, therefore, instructive to investigate whether the incompatible trace element geochemistry of the Finsch kimberlites bears any evidence of such a mixing relationship.

It was shown in the previous section, that a number of correlations existed between the Sm/Nd and X/Nd (where X = Th, Ta, La, Ce, Sr, Hf, Zr, Sm and Y) ratios of the Finsch kimberlites. These could not readily be explained by simple partial melting models using known K_D values. They may therefore be due to mixing between peridotite and kimberlite melt.

Using La/Nd (X = La) vs. Sm/Nd as an example (Figure 2.19), then one endmember must have Sm/Nd > 0.120 and the other, Sm/Nd < 0.166 as defined by the range of kimberlite data. Whole-rock peridotite data (Nixon et al., 1981; Erlank et al., 1987) are also shown on Figure 2.19. The data show a wide scatter which may, partly, be due to contamination by the host kimberlite (e.g. see Section 2.9), but they generally fall towards high Sm/Nd and La/Nd ratios. In a diagram of Ni vs. Sm/Nd (Figure 2.20) it is clearly demonstrated that peridotite is the high Sm/Nd endmember to mixing.

Assuming an average peridotite Ni content = 2000 ppm and a primary melt component with 300 ppm Ni, then a linear regression through the Finsch data in Figure 2.20 gives Sm/Nd ratios of $\simeq$ 0.20 for the peridotite

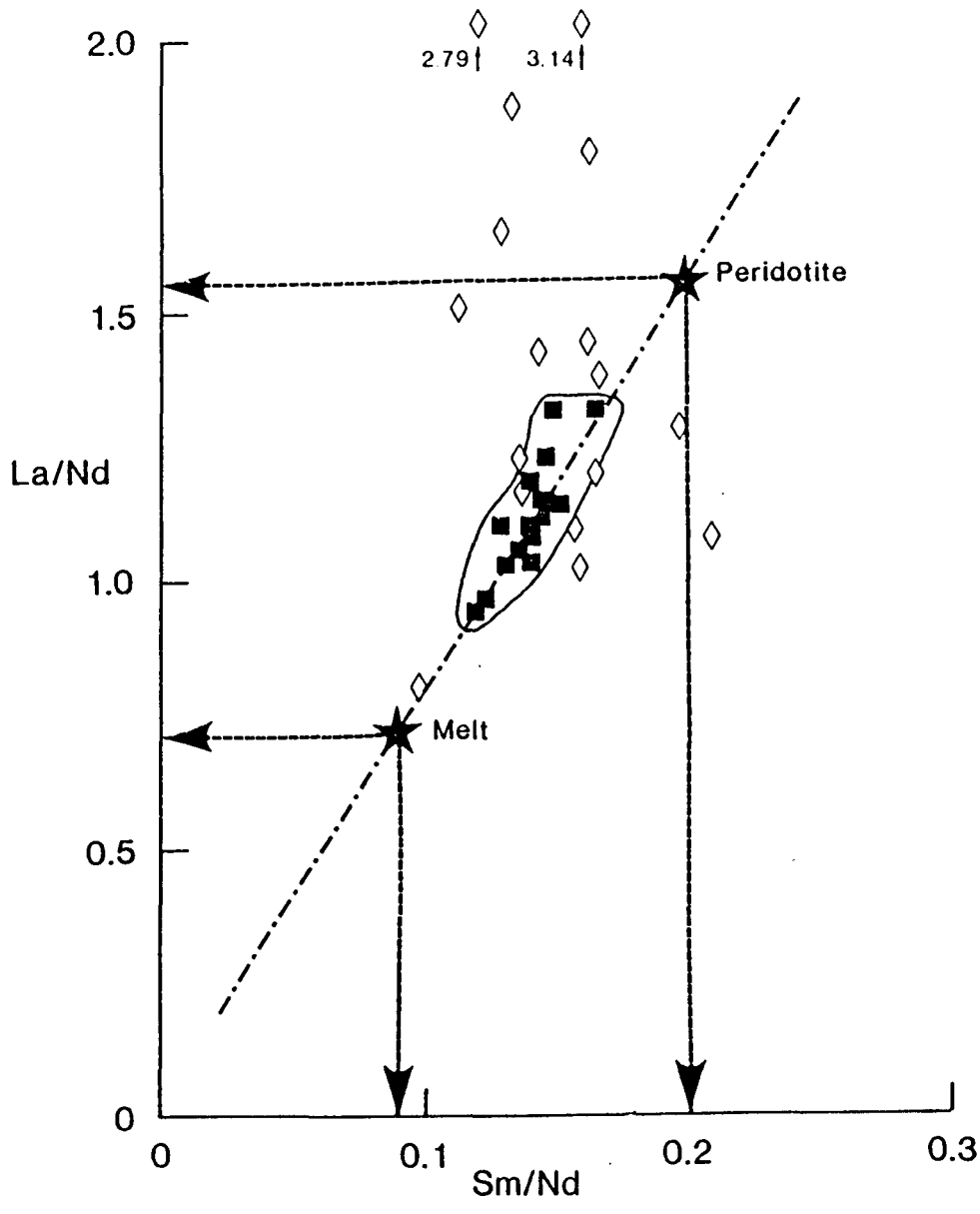

Figure 2.19 La/Nd vs. Sm/Nd for Finsch kimberlites modelled as a mixture between peridotites and primary mantle melts. Peridotite data (◇) from Nixon et al., 1981 and Erlank et al., 1987. See text for discussion.

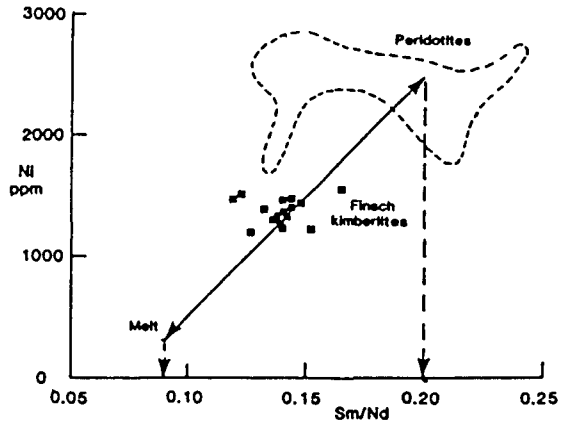

Figure 2.20 Ni ppm vs. Sm/Nd from Finsch kimberlites,which are modelled as mixtures between peridotite and primary mantle melts. Peridotite data from Nixon et al. (1981) and Erlank et al. (1987). See text for discussion.

and $\simeq$ 0.09 for the melt. The latter would have resulted from small degrees of partial melting of a source which has been inferred, in Section 2.10.3, to have a Sm/Nd ratio of $\simeq$ 0.25. Returning to Figure 2.19 and using the above Sm/Nd values for the two endmembers (i.e. melt and peridotite), it is now possible to calculate the La/Nd ratio (and hence other X/Nd ratios) from linear regressions through the data (see also Table 2.4). From Figure 2.19 and Table 2.4, the melt and peridotite have La/Nd = 0.71 and 1.56 respectively.

A typical Nd content for garnet peridotite is $\simeq$ 2.5 ppm (Nixon et al., 1981; Erlank et al.,1987) and the range of possible Nd contents for the melt can be calculated as follows; as the melt dominates the incompatible trace element content of the kimberlites then this component must have higher trace element concentrations than exhibited by the kimberlite whole rock data. From the X/Nd ratios estimated for the melt it can be shown that the Nd content of the melt must be > 200 ppm, for all X concentrations in the melt to be higher than those in the kimberlites. Setting Nd = 2.5 ppm (peridotite) and 200 ppm (melt), the X concentrations (Th, Ta, La, Ce, Sr, Hf, Zr, Sm and Y) of each component can be determined.

The above results, together with Ni and Cr contents of average mantle peridotites and a primary mantle melt (after Kuehner et al., 1981), are shown on Figure 2.21. Also shown in Figure 2.21 is the range of Finsch kimberlite data. Both incompatible and compatible trace element abundances are consistent with these kimberlites representing mixtures of $\geq$ 25% and $\leq$ 75% peridotite. Even with such a high peridotite content, the trace

	1	2	3	4
Ratios	Linear Regression	r	X/Nd perid.	X/Nd melt
Th/Nd	1.39x - 0.041	0.804	0.237	0.084
Ta/Nd	0.58x - 0.021	0.825	0.096	0.032
La/Nd	7.66x + 0.034	0.819	1.56	0.723
Ce/Nd	17.01x + 0.007	0.795	3.41	1.53
Sr/Nd	186x - 12.26	0.806	25.0	4.57
Hf/Nd	0.86x - 0.033	0.783	0.14	0.045
Zr/Nd	32.32x - 1.19	0.861	5.27	1.72
Y/Nd	1.80x - 0.078	0.703	0.28	0.084

	5	6
Elements	Peridotite ppm	Melt ppm
Th	0.06	16.9
Ta	0.08	6.4
La	1.81	145
Ce	3.85	306
Sr	11.4	914
Nd	2.5	200
Hf	0.11	9
Zr	4.30	344
Sm	0.5	18
Y	0.21	16.8

Table 2.4 Calculation of trace element content of melt and peridotite components. Column headings: 1 = equations for linear regressions through X/Nd vs. Sm/Nd (e.g. see Figure 2.19); 2 = r = correlation coefficient; 3 = X/Nd in peridotite, calculated by assuming Sm/Nd ratio of peridotite = 0.20; 4 = X/Nd in melt, calculated by assuming the Sm/Nd ratio of the melt = 0.09; 5 = trace element abundances in peridotite calculated by assuming Nd in peridotite = 2.5 ppm; 6 = Trace element abundances in melt calculated by assuming Nd in melt = 200 ppm.

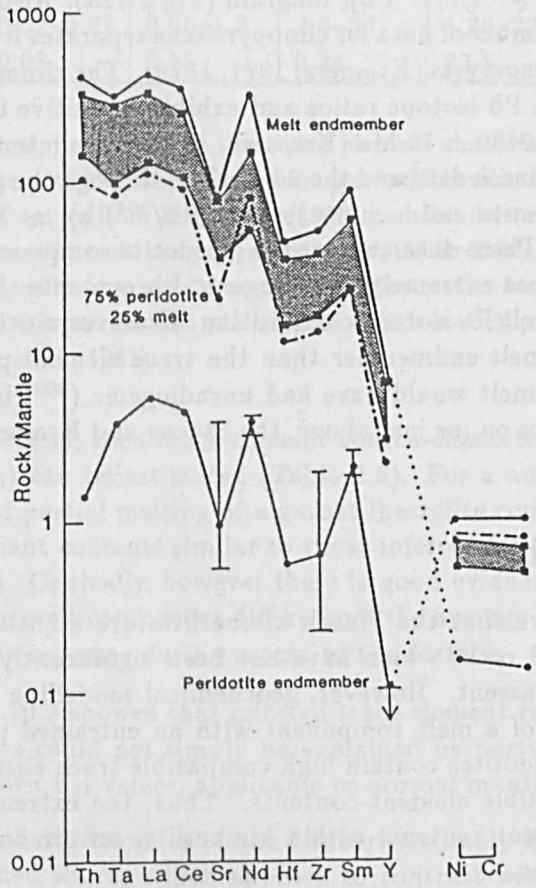

Figure 2.21 Selected mantle normalised trace element data for Finsch kimberlites (shaded area) modelled as a mixture between a peridotite and a melt component. These components were calculated by the method demonstrated in Table 2.4. Also shown are: 1) the composition of a mixture of 75% peridotite and 25% melt, and 2) the range of Sr, Nd, Zr, Sm and Y abundances observed in whole-rock garnet peridotites (Erlank et al., 1987).

element profile (and hence the isotopic systematics) of the kimberlites is dominated by that of the melt endmember, owing to the extremely high trace element content of the melt. Increasing the Nd content of the melt endmember would require larger amounts of peridotite and less melt during mixing. Petrographic estimation of the peridotite content is difficult, as the olivine macrocrysts are rounded and corroded (partially assimilated), while the orthopyroxene fraction is absent (presumably totally assimilated).

As outlined earlier (Section 2.8.2), the Finsch data define a mixing line on a $(^{207}Pb/^{204}Pb)_i$ vs. $(^{206}Pb/^{204}Pb)_i$ diagram (Fig 2.12a). Also included on this diagram are a number of data for clinopyroxene separates from South African xenoliths and xenocrysts (Kramers, 1977, 1979). The clinopyroxenes have variable radiogenic Pb isotope ratios and exhibit a positive trend corresponding to an age of 2480 $\pm$ 70 Ma (Kramers, 1979). The intersection of this trend through the Finsch data and the 2.5 Ga line through the peridotite data indicate the peridotite endmember has $(^{207}Pb/^{204}Pb)_i \simeq 15.25$ and $(^{206}Pb/^{204}Pb)_i \simeq 17.3$. These data suggest the peridotite component within the Finsch kimberlites has extremely unradiogenic Pb contents. There are few constraints on the melt Pb isotope composition. However, since the data will plot closer to the melt endmember than the trace element-poor peridotite endmember, the melt would have had unradiogenic $(^{206}Pb/^{204}Pb)_i$, but $(^{207}Pb/^{204}Pb)_i$ ratios on, or just above, the Stacey and Kramers (1975) growth curve.

2.11 Discussion

It has been shown above that the Finsch kimberlites are mantle derived, generally unfractionated rocks which have not been significantly contaminated by crust during ascent. However, geochemical modelling indicates that they are mixtures of a melt component with an entrained peridotite component. Mantle peridotites contain high compatible trace element contents, but low incompatible element contents. Thus, the extremely high incompatible trace element contents within kimberlites are predominantly from the melt component.

It was suggested in Section 2.10.4 that the entrained peridotite component at Finsch was most likely to be garnet peridotite. Furthermore, the extremely high Fo numbers of the Finsch olivine macrocrysts may indicate a predominance of depleted (by prior melt extraction) peridotites. The incompatible trace element contents can, however, give an indication of the nature of the kimberlite melt composition. For $D = C_o/C_l$, using known K_D values for olivine, orthopyroxene, clinopyroxene and garnet (Frey et al., 1978, Henderson, 1982) and C_l = concentration of the various elements in

Element	Ol	Opx	Cpx	Gnt	Peridotites
	ppm				ppm
Th			0.51–0.85		0.07–0.47
La	0.02	0.07	2.9–11.6	0.14–11.6	0.88–10
Ce	2.45	0.28–12.2	12.2–199	0.92–15.3	2–11
Sr	0.09–18.3	9.14–18.3	64–393	12.8	10–50
Nd	0.26–2	0.38–12	18–260	3.6	0.8–7
Sm	0.02–0.27	0.05–1.8	2.5–32	1.26–22.5	0.2–1.6
Y	0.03	0.15	0.34	23.5	0.02–0.7

Table 2.5 Calculations to show that trace element contents in the Finsch kimberlites could theoretically be derived from garnet lherzolites; D = C_o/C_l (F = 0). D = range of values from Frey et al. (1978) and Henderson (1982), C_l = trace element abundances in melt component as calculated in Table 2.4 and C_o = trace element abundances in source, as shown above. The results for individual minerals are compared with trace element abundances in whole-rock peridotites (Nixon et al., 1981; Erlank et al., 1987).

the melt (Table 2.4), then trace element source characteristics of the melt component (C_o) can be estimated (Table 2.5). For a number of elements, small degrees of partial melting of a garnet lherzolite could generate melts, with trace element contents similar to those inferred for the melt endmember (Table 2.4). Critically, however there is good evidence that the source peridotite of the melt component differs from the average mantle peridotites entrained by the magmas during ascent to the surface:

1. Section 2.10.3 showed that selected trace element ratios of the Finsch kimberlites could not simply be explained by partial melting models using known K_D values, applicable to normal mantle systems.

2. The Sr and Nd isotopes of the kimberlites imply derivation from an old enriched source which appears to contrast with the preliminary 'depleted' Sr isotope data for diopsides separated from garnet lherzolite nodules from Finsch mine. However, as the melt component dominates the incompatible trace element content of the kimberlites (Figure 2. 21) the isotopes are also a reflection of this component and hence, the melt source had an old enriched Sr and Nd isotope signature.

3. Comparison of the Finsch kimberlite data with average depleted/fertile peridotites suggests the melt must have lower SiO_2 and MgO, but higher Al_2O_3, CaO, K_2O, TiO_2, P_2O_5 and volatile contents, consistent with derivation from a phlogopite-magnesite peridotite which experimental petrology has shown to be a promising source rock for kimber-

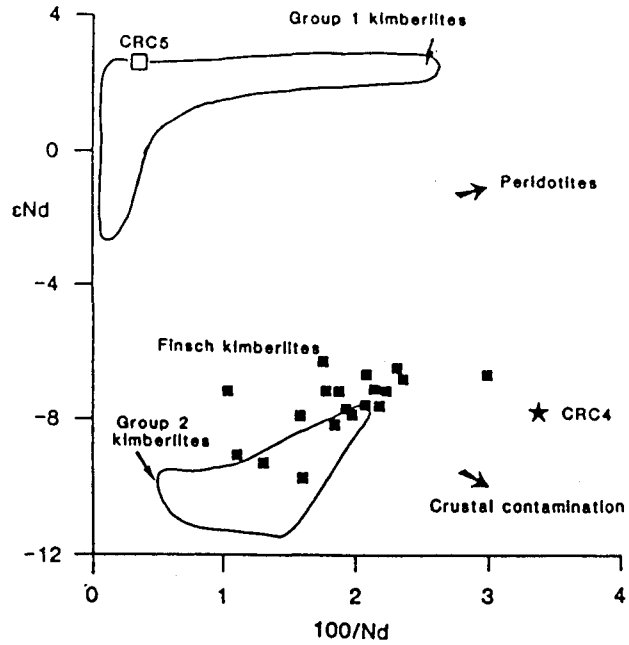

Figure 2.22 ϵNd vs. 100/Nd for Finsch mine and Group 1 and 2 kimberlites (this study and Smith et al., 1983a, b).

lites (see review in Mitchell, 1986). The high HFSE abundances within the Finsch kimberlites (e.g. Figure 2.14), indicates that, although they are volatile-rich rocks, the processes involved in their petrogenesis were melt dominated.

It is mineralogically difficult to estimate the amount of peridotite in each sample, as the enstatite fraction has perhaps, melted incongruently to olivine (?phenocrysts) and SiO_2, while the olivine macrocrysts are rounded and corroded. Thus, correlations between trace elements such as Zr and Nb, La and Th, may represent variations either in the amount of entrained peridotite and/or in degree of partial melting of the melt source region.

Similarities exist between the Finsch kimberlites and other kimberlites. For example, the presence of two olivine populations, high compatible and incompatible trace element abundances and the presence of mantle xenoliths and xenocrysts (e.g. diamond). These appear to require similarities in processes operating during generation and extraction of all kimberlite magmas.

On a diagram of ϵNd vs. 100/Nd (Figure 2.22), trends exhibited by both Group 1 and 2 kimberlites could be explained by mixing between a peridotite component and melts with low 100/Nd. However, the melt components of Group 1 and 2 kimberlites differ significantly in their isotope ratios. For example, on Figure 2.22, ϵNd $\simeq$ 0 for Group 1 kimberlites and ϵNd $\simeq$ -11.3 for the Group 2 kimberlites. Correlated isotopic, mineralogical and age differences indicate distinct mantle source regions, for Group 1 and 2

kimberlites.

The enriched isotope compositions of the Group 2 kimberlite melt components, are features of their mantle source regions and they record evidence of ancient trace element enrichment events. This indicates these source regions were most probably situated in the subcontinental mantle lithosphere isolated from the hot convecting asthenosphere. Group 1 kimberlites, as they have isotopic signatures similar to many OIB, could represent melts from the asthenosphere. Alternatively, the similarities might suggest that, like the Group 2 kimberlites, Group 1 kimberlites could be small partial melts from trace element enriched mantle lithosphere, but in this case from 'young' mantle lithosphere. A small volume partial, perhaps 'basanitic' melt may be introduced and stabilised within the mantle lithosphere and then, shortly afterwards remelted, under volatile-rich conditions, to form a kimberlite magma, which retains an OIB isotopic signature. The presence of hot, deformed peridotites and the Cr-poor megacryst suite in Group 1 kimberlites only (Smith, 1983b) might indicate they are derived from the base of the lithosphere in close proximity to the asthenosphere.

The compositional differences between Group 1 and 2 kimberlites may be due to some combination of a number of factors such as; age of source region, source composition, volatiles present during melting, depth and degree of melting and cause of inferred source enrichment processes. These are discussed in more detail in Chapter 5.

Chapter 3

Lamproites: Western Australia

3.1 Introduction

Lamproite bodies, of two distinct ages, occur near to the Kimberley craton (Western Australia), on both the southwest and southeast margins. The Precambrian Argyle pipe is situated within the East Kimberley Province and the West Kimberley Province comprises over 100 separate lamproite intrusions of Miocene age, which cover an area of 100 km^2. They are believed to form a consanguineous series, from ultrabasic olivine lamproites to basic leucite lamproites. Recent geochemical studies have shown these rocks to be characterised by high trace element contents (Jaques et al., 1984a, 1986a; Atkinson et al., 1984; Nixon et al., 1984) and 'enriched' Nd and Sr isotope signatures (McCulloch et al., 1983). It is the opinion of most authors that these characteristics are not due to crustal contamination. Rather, they reflect primary features of the mantle source regions and/or processes occurring during magma formation and evolution. These mantle source regions are believed to be situated within the cold rigid lithospheric portion of the subcontinental mantle. They were initially depleted by magma extraction, but subsequently affected by an ancient trace element enrichment event (Jaques et al., 1984a, 1986a; McCulloch et al., 1983; Fraser et al., 1985). Recent interest in the Western Australian lamproites has been generated by the discovery that some olivine lamproites (Ellendale, Argyle) contain diamonds.

This chapter considers the combined petrography, major element, trace element and isotope geochemistry of a number of selected West Kimberley lamproites. Results corroborate the above observations and it is argued that the West Kimberley lamproites are small volume partial melts from ancient trace element enriched subcontinental mantle sources. The geochemistry of these rocks indicates a melt related enrichment event, accompanied by the stabilisation of phlogopite. The Pb isotope data indicate a more complex (three-stage) history than has previously been suggested.

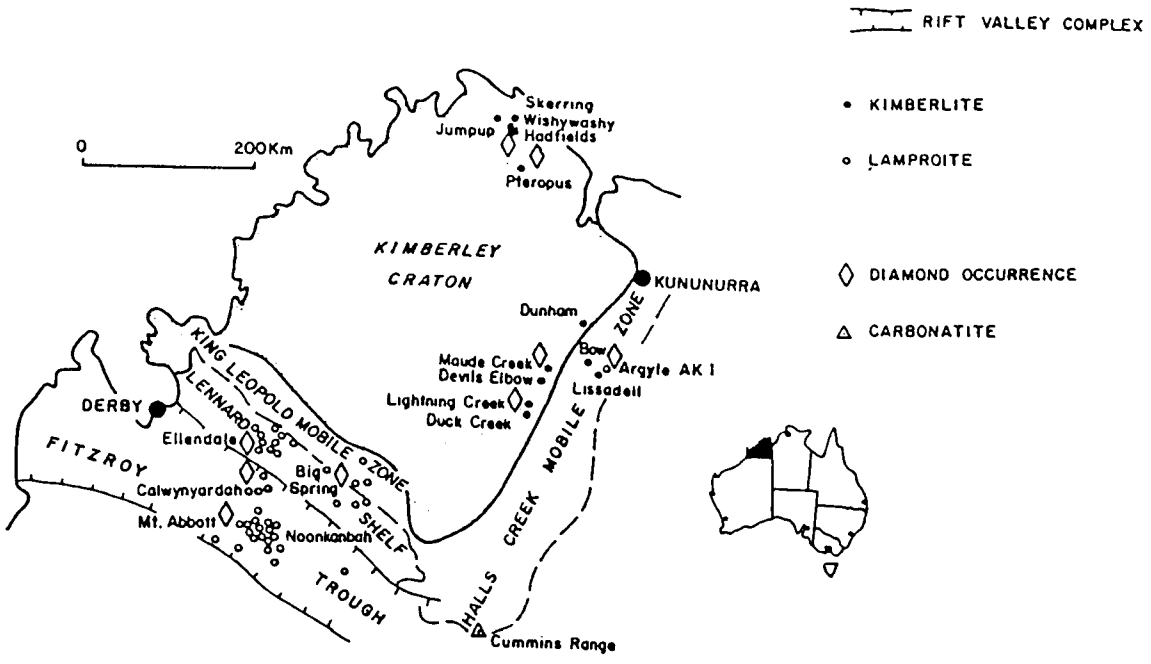

Figure 3.1 Location of kimberlites and lamproites associated with the Kimberley craton, Western Australia (modified after Atkinson et al., 1984)

Small regional variations in lamproite geochemistry are identified within the West Kimberley Province, although the main compositional differences exist between the olivine and leucite lamproite suites. Olivine lamproites appear to originate from deeper sources than leucite lamproites and undergo distinct extraction processes. The leucite lamproites exhibit fractionation trends from primitive lamproite melts, whereas olivine lamproites are believed, like kimberlites, to have entrained bulk peridotite en route to the surface.

3.2 Background geology

Jaques et al. (1986a) considered the structure and evolution of the Kimberley craton in Western Australia, and the adjacent area in detail. Much of what follows, in this section, is from their work. The Kimberley craton (Figure 3.1) is presumed to include an unexposed Archean crystalline basement predating the adjacent mobile zones (i.e. > 2150 Ma). However, this is concealed beneath up to 5 km of very gently folded Proterozoic sedimentary rocks and basalts of the Kimberley Basin succession ($\simeq$ 1830–1750 Ma). Deformation of these sedimentary rocks increases towards the mobile zones. The craton is bordered on the southwest margin by the King Leopold mobile zone (KLMZ) and on the southeast margin by the Halls Creek mobile

zone (HCMZ). These narrow fault-bounded belts are thought to be of similar age. They consist of early Proterozoic sedimentary rocks, the oldest of which are those of the Halls Creek group ($\simeq$ 2150 Ma). These were subsequently metamorphosed and intruded by gabbros and granites during cratonisation (1940–1800 Ma). Much of the HCMZ is not exposed in the KLMZ, but it probably exists concealed beneath the Phanerozoic sedimentary rocks of the Fitzroy Trough and North Canning basin (Figure 3.1). The Fitzroy Trough may be a failed Triassic rift trending east-southeast from a triple point on the northern arm of the Australian continental shelf. The trough, however, has a considerable pre-Triassic history with the main period of subsidence along the marginal faults taking place during Devonian times.

Lamproite bodies occur near to the Kimberley craton on both the southwest and southeast margins. The diamondiferous Argyle pipe, which has yielded emplacement ages of $\simeq$ 1045 to 1253 Ma (Skinner et al., 1985; Pidgeon et al., 1986), intrudes unconsolidated sediments of the Carr Boyd group between the Halls Creek and Glenhill faults in the HCMZ (Figure 3.1). The Miocene lamproite intrusions, of the West Kimberley Province, occur immediately to the south of the southwest margin of the Kimberley block (Figures 3.1, 3.2). Three main fields have been identified, which together form a broad north-south trending belt. The Ellendale field to the north intrudes rocks of the Lennard shelf, the small Calwynyardah field occurs on the northern edge of the Fitzroy Trough and the southerly Noonkanbah field is found within the Fitzroy Trough.

Recent K-Ar and Rb-Sr age studies by Jaques et al. (1984b) and Allsopp et al. (1985) suggested that there is a small age difference between the northernmost intrusions of the Ellendale area (20 to 22 Ma) and those further south on the Noonkanbah field (18 to 20 Ma). A small cluster of bodies intrudes the KLMZ and Lennard Shelf north of the Fitzroy Crossing (Figure 3.2), which Jaques et al. (1986a) loosely termed the Eastern Lennard Shelf field. A number of isolated intrusions also occur within the Fitzroy trough (Figure 3.2).

The distribution of the clusters of lamproites appears to be structurally related to ancient (west-northwest trending) faults within the basement. However, the shape of many individual intrusions is elongated east-west, parallel to the axes of shallow folds in the Palaeozoic sedimentary rocks. These folds may have developed in response to dextral strike-slip movement on the boundary faults of the Fitzroy Trough in late Triassic to early Jurassic times, during continental breakup.

The intrusions form pipes, plugs, sills and rare dykes, but no lava flows. Exploratory drilling has revealed the lamproite pipes have a shallow champagne-glass shape (Scott Smith and Skinner, 1984b; Atkinson at al., 1984). Most commonly, an early explosive phase is followed by the (quiet) intrusion

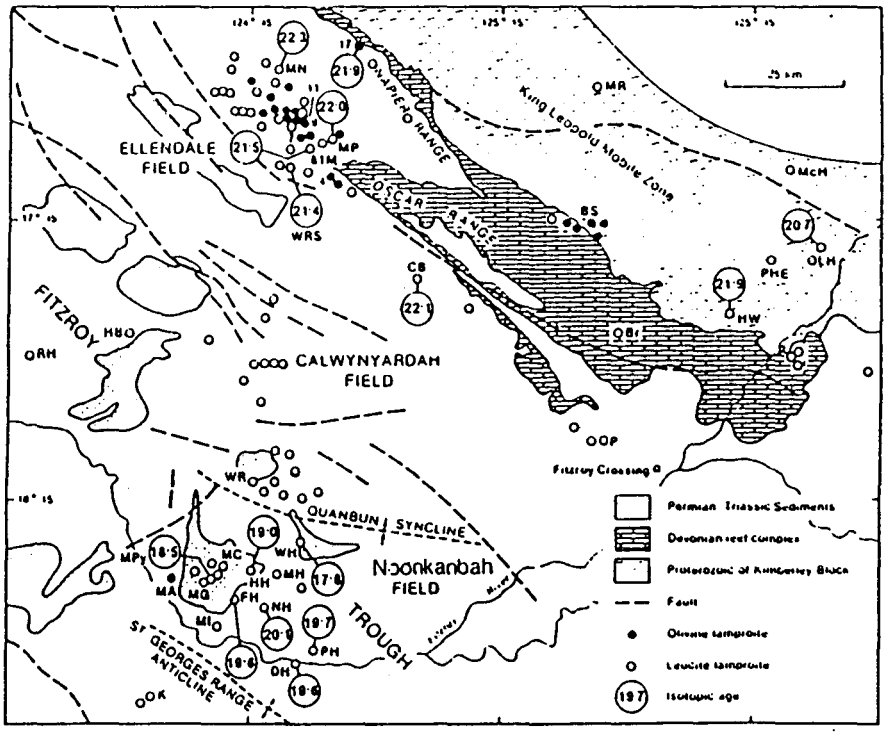

Figure 3.2 Distribution of lamproites in the West Kimberley Province, showing Ellendale, Calwynyardah and Noonkanbah fields, and a summary of K–Ar isotopic ages. Main lamproite bodies from north to south are: MN = Mount North; MR = Mount Rose; 4 = Ellendale 4; 7 = Ellendale 7; 9 = Ellendale 9; 11 = Ellendale 11; 17 = Ellendale 17; MP = Mount Percy; 81–M = 81 Mile Vent; WRS = Water reserve Sill "A"; CB = Camarotoechia Creek; McH = McKinrick Hill; BS = Big Spring; OLH = Old Leopold Hill; PHE = Prairie Hill East; HW = Hooper West; BR = Brooking Creek; RH = Rice Hill; HB = Hansons Bore; OP = Oscar Plug; WR = White Rocks; WH = Walgidee Hills; MC = Mount Cedric; HH = Howes Hill; MH = Mamilu Hill; MA = Mount Abbott; MG = Mount Gytha; MPy = Machells Pyramid; FH = Fishery Hill; NH = Noonkanbah Hill; MI = Mount Ibis; PH = "P" Hill; DH = Djada Hill; K = The Sisters. (Modified after Jaques et al., 1984b, 1986a).

of a central hypabyssal stock or a complex of stocks and sills. Many pipes may be more complex because of multiphase pyroclastic and/or magmatic activity (Scott Smith and Skinner, 1984b). Most bodies appear isolated from one another and appear to have risen from one point source of weakness in the underlying basement. The alignment and close proximity of other vents, however, suggest a dyke-like source at no great depth (Jaques et al., 1986a).

Many of the intrusions of the Noonkanbah field form positive topographic features (Wade and Prider, 1940; Prider, 1960). Erosion of the pyroclastic material has left the magmatic stocks as prominent features. In contrast, many of the recently discovered lamproites including the diamondiferous lamproites of the Ellendale field have no relief (Scott Smith and Skinner, 1984b; Jaques et al., 1986a; Atkinson et al., 1984).

3.3 Review of previous literature

3.3.1 The West Kimberley lamproites

Wade and Prider (1940) established a locality-based system of nomenclature for the leucite lamproites of the West Kimberley:

- Fitzroyite; phlogopite leucite lamproite.
- Cedricite; diopside leucite lamproite.
- Wyomingite; phlogopite diopside leucite lamproite.
- Mamilite; K-richterite leucite lamproite.
- Wolgidite; phlogopite diopside K-richterite leucite lamproite.

It was also noted that each may carry olivine (commonly altered to nontronite). Priderite (termed rutile by Wade and Prider, 1940) is the most common accessory, but others include wadeite, perovskite and apatite. This system, however, depends on the presence or absence of one or more of a suite of typical minerals, but ignores the proportion of an individual mineral present. Thus, rocks of very similar chemistry might be given different names depending upon the degree of crystallisation (Jaques et al., 1986a).

Diamond bearing bodies were recently discovered in the Ellendale area (1976) and at Argyle (1979)(Jaques et al., op. cit.). These bodies were initially termed kimberlites (Atkinson et al., 1982; Jaques et al., 1982; McCulloch et al., 1983). However, subsequent examination revealed that in addition to differences in the geology of the intrusions, they were petrographically distinct from kimberlites (e.g. they contain amphibole, wadeite, leucite and glass) and were in fact related to the Western Australia leucite

lamproites (Scott Smith and Skinner, 1984b). Study of the whole lamproite suite of the West Kimberley led Scott Smith and Skinner (1984a, b) to suggest a mineralogical classification based on the modal proportions of major primary minerals. This has been modified by Mitchell (1985; see Section 1.3). On the basis of this classification the lamproites of the West Kimberley can be subdivided into three broad groups:

1. Leucite lamproites.
2. Olivine bearing leucite lamproites (olivine is a phenocryst).
3. Olivine lamproites (two generations of olivine present; macrocrysts and phenocrysts)

The macrocryst olivine population within the lamproites tend to have a complex shaped margin in contrast to the rounded shape of kimberlite olivine macrocrysts (Scott Smith and Skinner, 1984a, b).

Groups one and two above, are equivalent to the lamproites of previous authors such as Wade and Prider (1940) and Prider (1960), whereas group three includes the so-called 'kimberlites' of this area (Scott Smith and Skinner (1984b). The Argyle pipe also falls into Group three.

The West Kimberley lamproites form a consanguineous group of rocks which belong to the ultrapotassic rock series. They are characterised by high contents of K_2O, TiO_2, Zr, Ba, H_2O and F, but low levels of Na_2O, CaO, CO_2 and Al_2O_3 (Wade and Prider, 1940; Prider, 1960; Jaques et al. 1984a, 1986a). These features are generally believed to reflect the primary nature of the magmas. For, although many of the West Kimberley lamproites are highly weathered, Prider (1982) has shown that weathered lamproites are of similar composition to fresh samples.

Chemical variations exist within the series (Jaques et al., 1984a, 1986a). Ultrabasic, silica-saturated olivine lamproites (MgO up to 29 wt%) grade to basic, silica-oversaturated leucite lamproites (MgO $<$ 5 wt%). The majority have MgO $\geq$ 10 wt%, SiO_2 $<$ 50 wt% and *mg* numbers $>$ 0.65 (range 0.43 to 0.87). Trends within the suite suggest that some fractionation of olivine, diopside and Cr-spinel has occurred (Jaques et al. 1984a).

The West Kimberley lamproites have high trace element contents which either exceed, or fall at the high end of, the range established for kimberlites e.g. Ba is typically $>$ 5000 ppm (Jaques et al., 1984a). They have strongly fractionated REE profiles with high LREE contents (360 to 2000 $\times$ chondrite), but low HREE (3 to 6 $\times$ chondrite; Jaques et al.,1984a; Nixon et al., 1984). Ni and Cr contents are progressively depleted, from high values ($>$ 1000 ppm) in the olivine lamproites to very low values ($<$ 50 ppm) in the leucite lamproites. Most, however, contain more than 200 ppm Ni and Cr,

and many more than 300 ppm Ni, in accord with their comparatively high *mg* numbers and consistent with derivation from a mantle source (Jaques et al., 1984a).

A number of authors have published Sr with or without Nd isotope data on these rocks (Powell and Bell, 1970; McCulloch et al., 1983; Nixon et al., 1984; Allsopp et al., 1985; Fraser et al., 1985). Most now believe that the high εSr and low εNd values are not due to crustal assimilation, rather they indicate that the lamproite magmas were derived from ancient trace element enriched subcontinental lithospheric mantle source regions. Pb isotopic data reported in Fraser et al. (1985 and see Sections 3.8.2, 3.9.3) and Nelson et al. (1986a), showed that the West Kimberley lamproites are characterised by high initial $(^{207}Pb/^{204}Pb)_i$ ratios, but low $(^{206}Pb/^{204}Pb)_i$ ratios requiring a complex three-stage growth model.

Petrogenetic models for these lamproites propose that their source regions were initially depleted by melt extraction (hence the low CaO and Al_2O_3 contents) which was followed by a later, but still ancient, trace element enrichment event. Subsequently, small degrees of partial melting of these sources under H_2O- and F-rich conditions resulted in the formation of silica-saturated, highly trace element enriched, olivine lamproitic melts which, in some cases, fractionated to silica-oversaturated leucite lamproites (McCulloch et al., 1983; Jaques et al., 1984a; Atkinson et al., 1984). Evidence from spinel compositions (Foley, 1986) indicate that the West Kimberley lamproites were derived under reducing conditions. The high pressure (10–40 Kb) experimental study on an Mg-rich (*mg* number = 0.77) and high Ni (= 251 ppm) leucite lamproite from Mount North, carried out by Arima and Edgar (1983), suggested that the lamproite could have been derived from partial melting of a highly metasomatised mantle containing phlogopite + rutile $\pm$ orthopyroxene $\pm$ olivine, but not clinopyroxene.

McCulloch et al. (1983) suggested that the Sr and Nd isotope data of the West Kimberley lamproites could be explained by the mixing of an enriched lithospheric mantle component and a depleted mantle component such as MORB. Nelson et al., (1986a) included Pb isotope data and proposed a similar model, but implied that the mixing was an ancient event between a high $(^{207}Pb/^{204}Pb)_i$ enriched source and a depleted MORB source with $(^{206}Pb/^{204}Pb)_i < 17.00$. On the basis of selected trace element and isotope arguments, Nelson et al. (1986b) proposed that the enriched mantle component was generated by recycling of sediments into the mantle lithosphere via a subduction zone. They did point out that the model was compromised by the lack of obvious association with any known past or modern subduction zones. Hancock and Rutland (1984) suggested that the KLMZ and HCMZ represent a distinctive type of linear Proterozoic ensialic orogeny, and the compression involved during cratonisation (1920–1830 Ma) was accompa-

nied by only limited subduction of the lithosphere beneath the margin of the Kimberley block.

3.3.2 Xenoliths and xenocrysts

Dunites and rare mantle peridotites (harzburgites and lherzolites) occur in both the West Kimberley olivine lamproites and at Argyle. Most are highly altered, but relics of primary phases are commonly preserved and primary textures can generally be discerned. Garnet is completely replaced by symplectic intergrowth of Al-rich spinel and chrome diopside and a number contain diamond at high grades (Jaques et al., 1986a; O'Neill et al., 1986). Most have a coarse texture, while both bulk rock and mineral chemistry of diamondiferous peridotite xenoliths from Argyle reveal they are refractory e.g. whole rock *mg* numbers = 0.92, Al_2O_3 and CaO $\simeq$ 1 wt% and $Na_2O \leq$ 0.03 wt% (O'Neill et al., op. cit.).

P–T calculations have shown that the lherzolites and harzburgites from Argyle originally equilibrated (P_1 assemblage = olivine, orthopyroxene, former garnet $\pm$ clinopyroxene $\pm$ Cr spinel) well within the diamond stability field, under a low geothermal gradient and reducing conditions in which microdiamonds could have formed (O'Neill et al., op. cit.). These peridotites are believed to have originated from highly depleted, relatively cold ($T < 1100°C$) mantle, most probably situated in the subcontinental lithosphere (Jaques et al., 1984a, 1986a; Lucas et al., 1986; O'Neill et al., 1986). Subsequent entrainment in hot lamproite magma and ascent to the spinel stability field near the dry peridotite solidus, resulted in interaction between garnet and olivine ($\pm$ metasomatic fluid from host magma) and the incongruent melting of garnet. This was then quenched to Al-pyroxene and spinel (O'Neill et al., op. cit.).

A number of xenocrysts have been collected from heavy mineral concentrates e.g. olivine, Cr-rich spinel and smaller amounts of garnet, Cr-diopside and enstatite which may have been derived from disaggregated mantle peridotite (Jaques et al., 1986a). Olivine is the most abundant and garnet is rare except in the case of certain olivine lamproites.

In a study of garnets from selected kimberlites and diamondiferous lamproites from Western Australia, Lucas et al. (1986) recovered Cr-pyrope and rare subcalcic pyrope garnets. These are similar in composition to those from non-Australian kimberlites and hence, similar P–T conditions appear to prevail under stable cratons in Western Australia and elsewhere. Variations in garnet composition within and between the studied occurrences indicates vertical and horizontal heterogeneity under northwest Australia.

Exploration for diamonds in the Kimberley area since 1967, culminated in the discovery of diamondiferous olivine lamproite pipes at Ellendale (1976)

and Argyle (1979). Although the latter is economic and is presently being exploited, the former is only subeconomic (Jaques et al., 1986a). Further studies (Jaques et al., op. cit.) have identified diamonds within intrusions in the other fields (East Lennard Shelf, Calwynyardah and Noonkanbah) and have shown that, on the whole, diamonds are restricted to the olivine-rich, leucite-poor lamproites. In any given pipe the early pyroclastic phase is more diamondiferous than the later magmatic phase.

The West Kimberley diamonds tend to be small, the majority are yellow and the remainder colourless. Unresorbed octahedron to resorbed rounded dodecahedral forms have been identified. The majority of the Argyle stones are industrial, although about 5% are gem quality. The dominant colour is brown, while yellow and colourless stones constitute < 20%. Green and pink stones occur rarely. Most are strongly resorbed dodecahedra or octahedra/dodecahedra combination forms (Jaques et al., 1986a). Cubic diamonds have never been recovered from the Western Australia lamproite pipes (Jaques et al., op. cit.).

Both the Argyle and Ellendale diamonds contain syngenetic inclusions. In the latter, the eclogitic and peridotite parageneses are present on equivalent amounts, whereas at Argyle the eclogite paragenesis predominates (Harris and Collins, 1985; Jaques et al., 1986a, b; Richardson, 1986a, b). It is of interest to note, however, that of 130,000 stones examined by Harris and Collins (1985), only 0.16% of these actually contain inclusions. Richardson (1986a, b) reported an Sm-Nd isochron age of 1580 $\pm$ 60 Ma from eclogitic inclusion mineral pairs (garnet and clinopyroxene) in Argyle diamonds which is a few 100 Ma greater than the age of the host lamproite (1045 to 1253 Ma, Section 3.2.). Jaques et al. (1986b) reported that most of the Ellendale stones (both peridotite and eclogite) and the Argyle diamonds with peridotitic inclusions have small negative $\delta^{13}C$ values (–4 to –6 ‰) similar to the bulk of inclusion bearing diamonds elsewhere (e.g. reviews by Meyer, 1985; Mattey, 1987). The majority of the Argyle stones with eclogitic inclusions have significantly lower carbon isotope compositions, lying mostly in the range –9 to –12 ‰. Jaques et al. (1986b) tentatively suggested that these diamonds are derived from recycled crustal material. The Argyle diamonds are unusual in they exhibit extremely high degrees of nitrogen aggregation, implying either high equilibration temperatures, or anomalously old ages i.e. older than the age of the earth (Harris and Collins, 1985). With the exception of the latter feature, none of the characteristics noted in the lamproite diamonds differentiate them from diamonds in kimberlites (Harris and Collins, op. cit.).

3.4 Sample localities

A number of the freshest magmatic lamproite samples from the West Kimberley were chosen from the De Beers collection for this study. Samples were selected from the Ellendale field (Ellendale pipe A, Seltrust pipes 2 and 3 and Mount North), the Noonkanbah field (Mount Gytha, Machells pyramid, Mount Cedric, Noonkanbah Hill, Walgidee Hills and the Sisters West), the Eastern Lennard Shelf field (Mount Rose and Old Leopold Hill), Oscar Plug (an isolated intrusion in the Fitzroy Valley) and Seltrust pipe 1 (of unknown location, but probably in the Ellendale field or an isolated intrusion in the Fitzroy Valley). Details of the sample localities are given in Appendix A.2 and Figure 3.2).

3.5 Petrography

Modal analyses of the samples are given in Appendix C.1. Mineral classification was made using the scheme proposed by Scott Smith and Skinner (1984) with the revisions made by Mitchell (1985). The results are shown in Table 3.1.

The Ellendale pipe A sample is the only olivine lamproite studied. It contains two olivine populations (phenocrysts and macrocrysts) set in a relatively coarse grained groundmass of K-richterite, clinopyroxene, phlogopite with accessory perovskite, spinel, leucite and probable priderite (Robey, 1982). All other samples studied are leucite lamproites which consist of phenocrysts of olivine and/or phlogopite set in a matrix made up of some combinations of leucite (15 to 75 vol%), diopside, K-richterite, phlogopite, glass and priderite (Plates 3.1 and 3.2). Accessory minerals include apatite, opaques, wadeite, rutile and perovskite. The groundmass is often altered to greenish-brown clays which in some cases, may constitute $>$ 60 vol% (WA A12/31, WA A12/50, WA B3/8, WA B3/9). Vesicles are present in a number of samples and are sometimes infilled with zeolite material (WA A12/72, WA B3/8, WA B3/9). Samples WA B3/8 and WA B3/9, from Walgidee Hills, appear highly altered and contain abundant carbonate material (Skinner, 1982). In some samples thin veins of altered material were observed (WA A3/2, WA A3/8, WA A3/16a, WA A12/26). A small (1.5 mm) thermally altered xenolith was observed in sample WA A12/31.

3.6 Major element geochemistry

Major element analyses of the leucite lamproites in this study have similar characteristics to West Kimberley leucite lamproites analysed elsewhere

Field	Intrusion	Sample Number	Mineral Classification
Ellendale	Ellendale Pipe A	WA A1/2	olivine lamproite
	Mount North	WA A3/2	leucite lamproite
		WA A3/3	leucite lamproite
		WA A3/8	leucite lamproite
		WA A3/16a	leucite lamproite
		WA A3/16b	leucite lamproite
	Seltrust Pipe 2	WA A12/1	glassy leucite lamproite
		WA A12/2	leucite lamproite
		WA A12/26	leucite lamproite
		WA A12/30	leucite lamproite
		WA A12/31	leucite lamproite
		WA A12/49	leucite lamproite
		WA A12/72	leucite lamproite
	Seltrust Pipe 3	WA A13/1	leucite lamproite
		WA A13/2	leucite lamproite
Noonkanbah	Walgidee Hills	WA B3/8	altered
		WA B3/9	altered
	Noonkanbah Hill	WA B5/5	leucite lamproite
		WA B5/6	leucite phlogopite lamproite
	Machells Pyramid	WA B8/2	leucite lamproite
	Mount Cedric	WA B9/3	leucite lamproite
		WA B9/4	leucite lamproite
	Mount Gytha	WA B12/1	diopside leucite lamproite
	The Sisters West	WA B20/1	leucite lamproite
Eastern Lennard Shelf	Mount Rose	WA A7/1	leucite lamproite
		WA A7/2	leucite phlogopite lamproite
	Old Leopold Hill	WA A9/1	leucite lamproite
Isolated Intrusion (Fitzroy Trough)	Oscar Plug	WA B9/3	leucite lamproite
	Seltrust Pipe 1	WA A11/1	leucite lamproite

Table 3.1 Mineral classification of the West Kimberley lamproites using the classification scheme of Scott Smith and Skinner, 1984a, b and Mitchell, 1985.

Plate 3.1 WA A13/2; Leucite lamproite with phlogopite laths set in a matrix of clinopyroxene and leucite (PPL). Scale Bar = 0.5 mm.

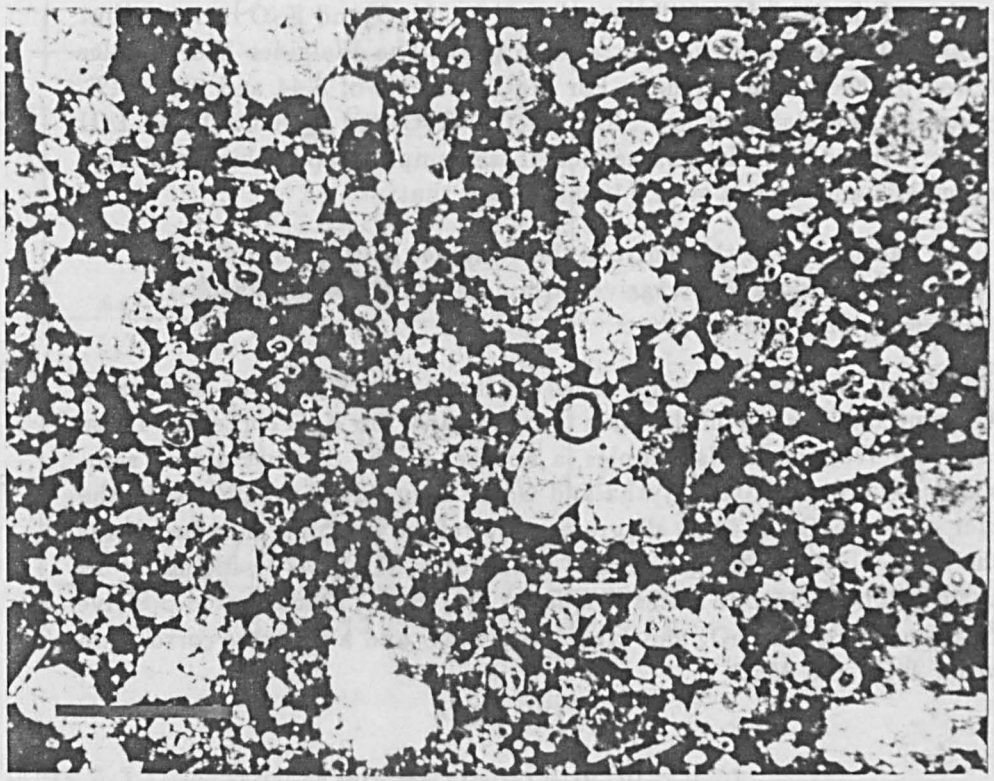

Plate 3.2 WA A19/2; Leucite lamproite with leucite, phlogopite and clinopyroxene phenocrysts set in an altered matrix (PPL). Scale bar = 0.5 mm.

(Wade and Prider, 1940; Prider, 1960; Jaques et al., 1984a, 1986a). They have high K_2O (5.32 to 11.77 wt%), TiO_2 (4.47 to 7.55 wt%), P_2O_5 (0.45 to 4.03 wt%), but very low Na_2O (0.01 to 0.80 wt%) and low CaO and Al_2O_3 contents. Thus, these rocks are all ultrapotassic ($K_2O/Na_2O > 8$). With the exception of WA A12/26, WA A12/30, WA A12/31 and WA A12/49 (which may have been leached of alkalis), they are also peralkaline ($K_2O + Na_2O/Al_2O_3 > 1$) and perpotassic ($K_2O > Al_2O_3$) rocks. MgO contents vary from 2.42 to 14.54 wt%, *mg* numbers are generally high (> 0.65) and vary from 0.43 to 0.81, while SiO_2 contents range from 44.76 to 61.90 wt%. The Walgidee Hills samples (WA B3/8 and WA B3/9) however, have SiO_2 contents of 36.60 and 29.48 wt%, but this may relate to alteration (see below). No olivine lamproites (SiO_2 = 35 to 45 wt%, MgO = 18 to 29 wt%) as reported in Jaques et al. (1984a, 1986a) were analysed for major elements in this study.

Chemical variation within the suite is shown on Harker diagrams where oxides (wt%) are plotted against MgO (Figure 3.3). In general, trends are comparable to those obtained by Jaques et al. (1984a, 1986a). With the exception of the Walgidee Hills samples, SiO_2, $Al_2O_3$and K_2O increase, but CaO and LOI decrease with decreasing MgO. The Walgidee Hill samples plot well off these main trends. For MgO contents of 8.44 and 9.86 wt%, they exhibit anomalously low SiO_2, Al_2O_3, K_2O and high CaO and LOI contents (Figure 3.3). In thin section these samples appear highly altered (Section 3.5) and Jaques et al. (1986a) noted that:

> 'lamproites at the centre of the Walgidee Hills intrusion, with abundant vein and pervasive carbonate material contain up to 20 wt% CaO and CO_2.'

Although there is a general trend of increasing K_2O with decreasing MgO, some samples fall off the main trend towards low K_2O contents. These include the Walgidee Hills samples, a number of the Seltrust pipe 2 samples and some from Mount Gytha and Oscar Plug. This, together with the scatter on a Na_2O vs. MgO diagram, may reflect leaching of some alkalis at the surface. With a larger dataset (number = 250 to 470), including ultrabasic olivine lamproite suites, Jaques et al. (1984a, 1986a) noted positive correlations of Fe (as FeO) and MnO, with MgO and a negative correlation between TiO_2 and MgO.

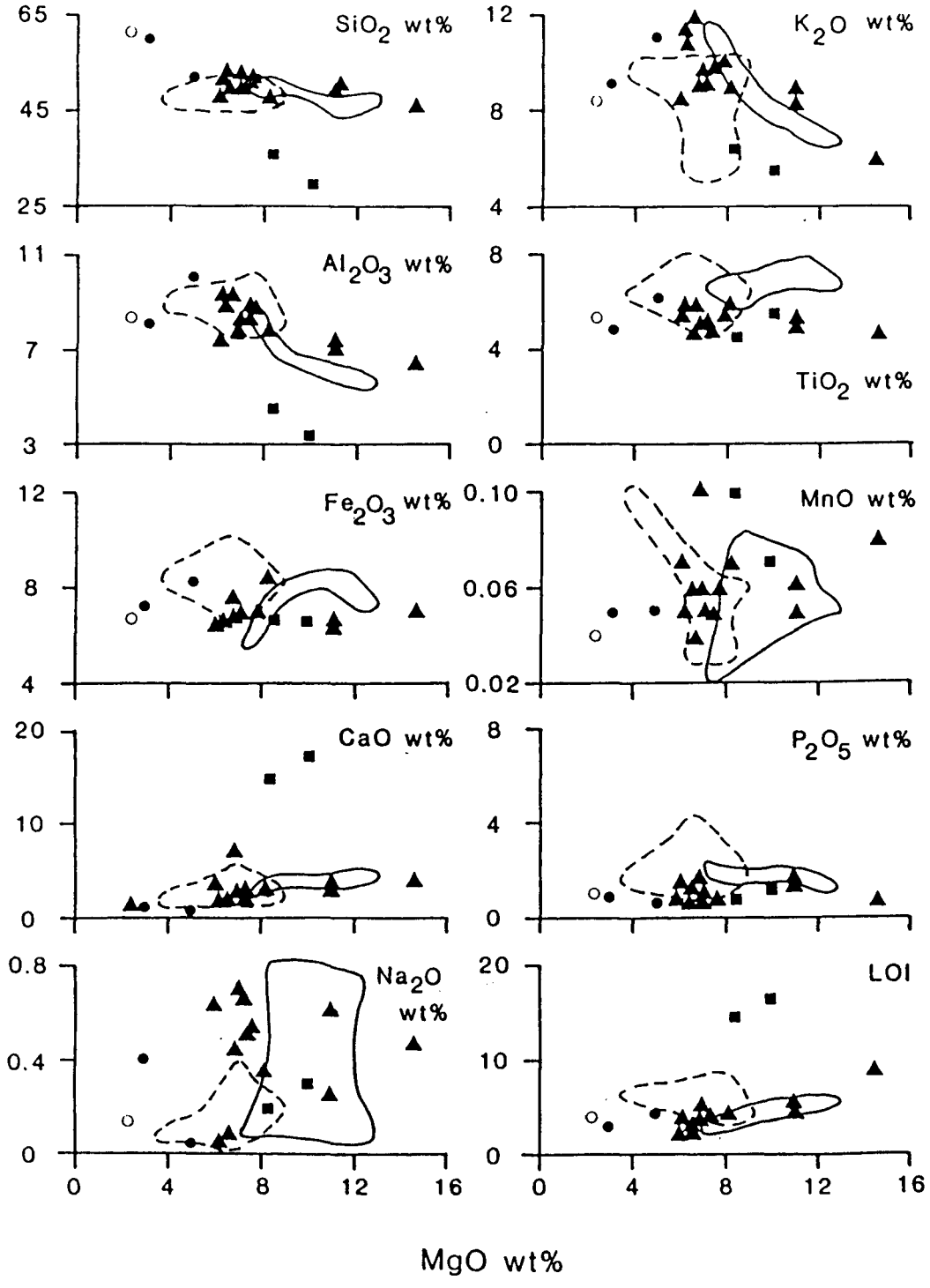

Figure 3.3 Oxide variation with MgO (wt%) in the West Kimberley lamproites. Fields are shown for Seltrust Pipe 2 (dashed line) and Mount North (solid line). ○ = Mount Gytha, • = Oscar Plug, ■ = Walgidee Hills, ▲ = other localities (see Table 3.1).

3.7 Trace element geochemistry

3.7.1 The compatible trace elements

The West Kimberley lamproites analysed in this study, exhibit a range in compatible trace element contents; Ni = 90 to 1090 ppm, Cr = 161 to 593 ppm (two rather anomalous values of 68 and 1931 ppm were also noted), V = 40 to 476 ppm and Sc = 12.7 to 19.9 ppm. When compared with olivine lamproite data, there are general trends of increasing Ni and Cr, but decreasing V, with increasing MgO (Jaques et al., 1984a and 1986a). The olivine lamproites are characterised by very high Ni and Cr contents (1000 ppm up to 1300 ppm Ni and 1600 ppm Cr) and low V (40 to 80 ppm) while Sc contents are low in all lamproites (Jaques et al., op. cit.). Many of the leucite lamproites analysed in this study have Ni and Cr contents comparable with, or even higher, than those predicted for primary mantle melts (e.g. Ni = 300 to 400 ppm, Cr = 400 to 500 ppm; Kuehner et al., 1981).

3.7.2 The incompatible trace elements

The West Kimberley lamproites are highly LREE enriched, e.g. La = 182 to 596 ppm, and they exhibit steep mantle normalised profiles (Ce_N/Yb_N = 50 to 163). The data form subparallel to parallel trends which flatten out at the HREE end (Figure 3.4). The Walgidee Hills samples are shown separately, as these appear to be altered. They have significantly lower La contents (108 and 160 ppm) and shallower profiles (Ce_N/Yb_N = 32.3 and 45.6) than the other samples. Chemical variation is evident both within and between localities. However, as intra-locality variation may be large, care must be taken when interpreting variations existing from one locality to another. For example, eight samples analysed from the Seltrust pipe 2 exhibit La = 232 to 596 ppm and Ce_N/Yb_N = 67.3 to 163.

The olivine lamproite from Ellendale pipe A has La = 290 ppm and Ce_N/Yb_N = 92 and plots well within the data range outlined above for the leucite lamproites. Jaques et al. (1984a, 1986a) observe that typically the leucite lamproites contain greater abundances of REE than the olivine lamproites although there is considerable overlap in the data, and the REE patterns of both rock-types are similar.

Incompatible trace element data for the West Kimberley lamproites are plotted on mantle normalised trace element abundance diagrams which include some of the REE (Figure 3.5). With the exception of the altered Walgidee Hills samples, the data plot on sub-parallel to parallel trends. They are all highly trace element enriched, Rb and Th over 500 × mantle and Ba over 1000 × mantle. Peaks occur at Ba and La, while troughs occur at Pb,

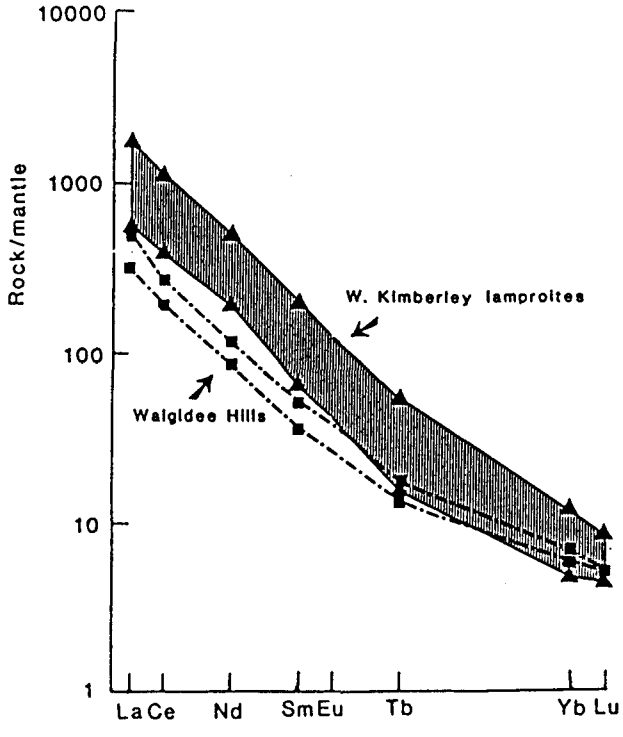

Figure 3.4 Mantle normalised REE patterns showing the range of composition for the West Kimberley lamproites (▲ and vertically lined). REE patterns for the Walgidee Hills samples WA B3/8 and WA B3/9) are shown separately (■ and dot and dashed lines).

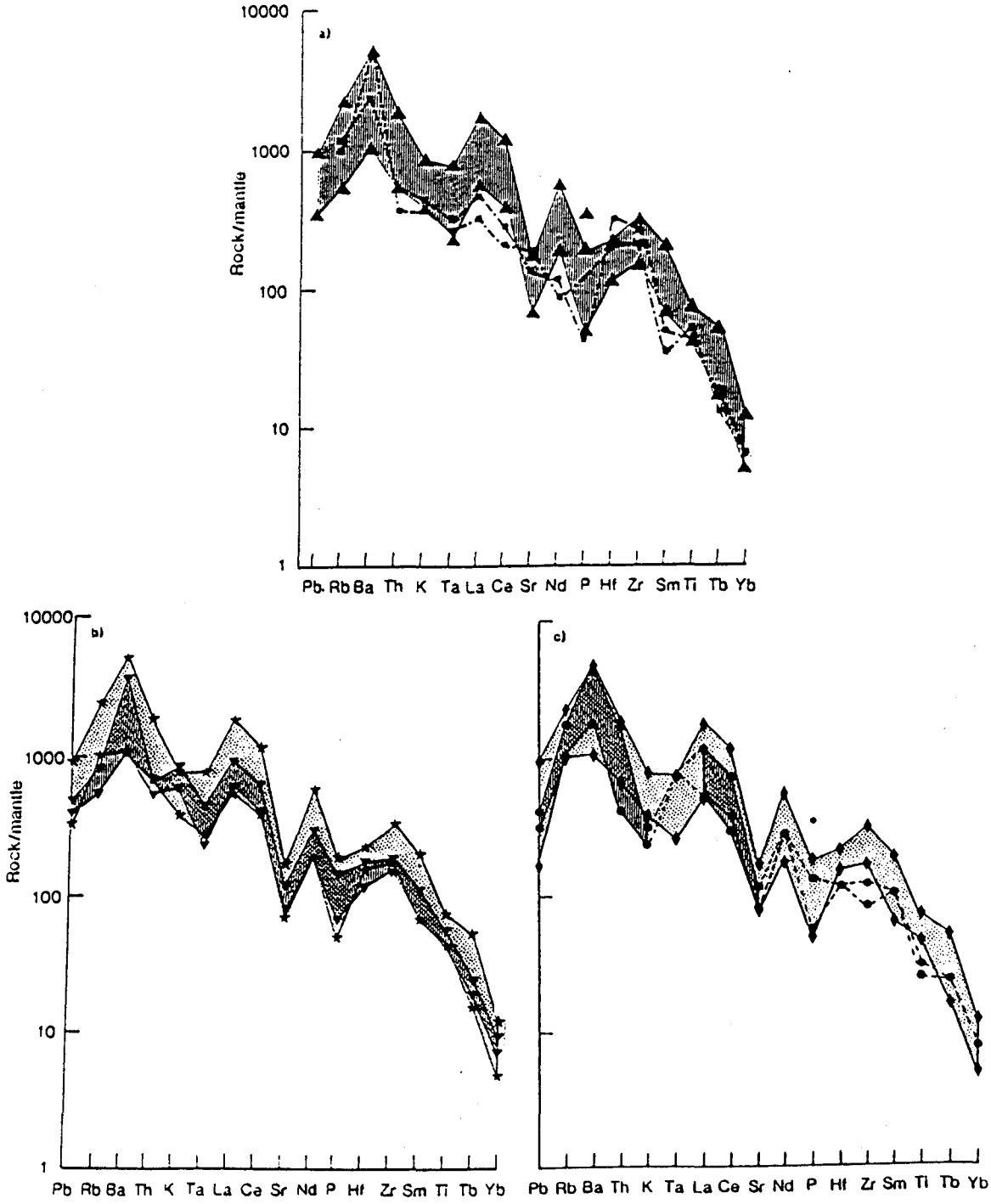

Figure 3.5 Mantle normalised trace element data for the West Kimberley lamproites; a) = range of compositions of the West Kimberley lamproites and the Walgidee Hills samples (symbols as in Figure 3.4), b) = range of compositions for the Ellendale field (▼ and vertically lined) and Noonkanbah field (⋆ and stippled) lamproites, c) = range of compositions of olivine (• and vertically lined) and leucite (◆ and stippled) lamproites from the Ellendale field. Data in c) include those from Jaques et al. (1984a).

Ta, Hf, Sr and P.

Dividing the samples into two geographically determined groups; the Ellendale field and the Noonkanbah field (plus Oscar Plug), trace element profiles for each group are shown on Figure 3.5b. In general, the profiles and trace element contents of both groups are similar, although there are some notable differences. The Noonkanbah field samples, in contrast to the Ellendale field samples, exhibit a peak at K. They also tend to have significantly lower Rb and Th and slightly lower Ta, Hf and Zr contents. The Noonkanbah samples therefore, tend to have higher K/Rb and K/Th ratios (= 213 to 389 and 2042 to 4088 respectively) than the Ellendale samples (= 70 to 227 and 619 to 2298 respectively; Seltrust pipe 3 is anomalous with high K/Rb = 284 and K/Th = 4306).

Comparison of the olivine and leucite lamproites of the Ellendale field (including the data of Jaques et al., 1984a) reveals that both rock-types have very similar mantle normalised trace element profiles (Figure 3.5c), although the olivine lamproites trend towards lower Rb, Th, K, Ti and Zr contents. Interestingly, both the olivine and leucite lamproites of the Ellendale field exhibit low K/Th and K/Rb ratios. Thus variations in K/Th and K/Rb may be a geographically controlled feature and the role of source composition, melting processes and fractionation in generating these variations are considered later (Section 3.9.6)

3.8 Isotope geochemistry

3.8.1 Sr and Nd isotopes

The West Kimberley lamproites have higher εSr and lower εNd than the bulk earth, and plot in the bottom right hand quadrant of the εNd – εSr diagram (Figure 3.6). Therefore, they contain a contribution from old LREE enriched, low Sm/Nd material which most authors would place within the lithosphere, be it subcontinental mantle or crust (McCulloch et al., 1983; Nixon et al., 1984).

The samples analysed in this study show a wide range in εSr = 89.1 to 227 and εNd = –9.95 to –19.1 comparable to values reported elsewhere (McCulloch et al., 1983; Nixon et al., 1984; Powell and Bell, 1970). The data form an overall negative trend on Figure 3.6. With the exception of the Walgidee Hills field, the Noonkanbah data overlap the Ellendale data in εNd, although there is an indication that they extend to slightly higher εSr (Figure 3.6a). However, the most obvious variations on an εNd – εSr diagram exist between the olivine and leucite lamproites (Figure 3.6b). The olivine lamproites from the Ellendale field tend to exhibit lower εSr (= 80.4 to 110) and higher εNd (= –7.8 to –13.8) than the leucite lamproites (= 130

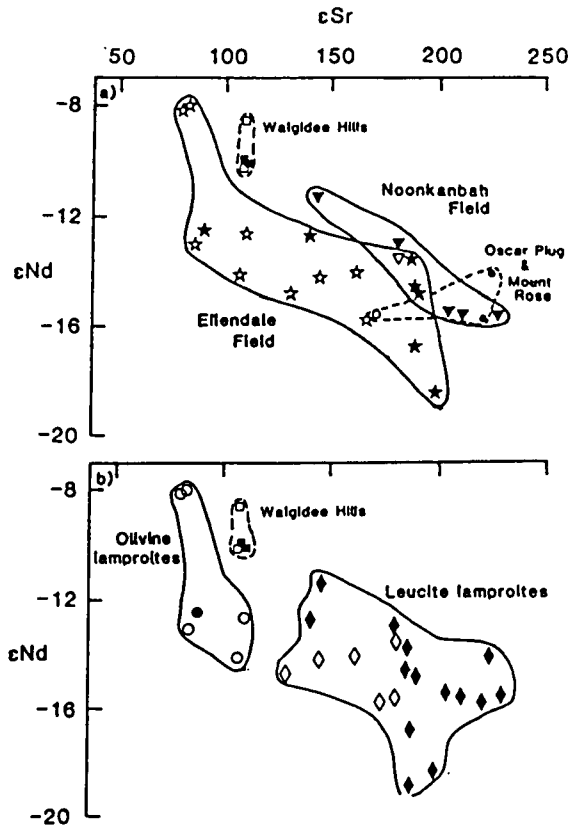

Figure 3.6 εNd vs. εSr for the West Kimberley lamproites; a) shows fields for the Ellendale field (stars), Noonkanbah field (inverted triangles), Walgidee Hills (squares) and the isolated intrusions, Oscar Plug and Mount Rose (circles) and b) shows fields for olivine lamproites (circles), leucite lamproites (diamonds) and Walgidee Hills. Infilled symbols = this study, open symbols = McCulloch et al. (1983).

to 227 and −11.3 to −19.1 respectively). The Walgidee samples from both this study and McCulloch et al. (1983) plot in a separate field closer to the olivine lamproites than the leucite lamproites with εSr = 108 to 110 and εNd = −8.6 to −10.1.

3.8.2 Pb isotopes

The Pb isotope data for the West Kimberley lamproites are shown on Figure 3.7. In contrast to the Group 2 kimberlites from South Africa and North American lamproites (Sections 2.8.2 and 4.7.2 respectively), the West Kimberley lamproites plot above the Stacey and Kramers (1975) growth curve. They have high $(^{207}Pb/^{204}Pb)_i$ ratios = 15.70 to 15.76 and $(^{208}Pb/^{204}Pb)_i$ ratios = 37.86 to 38.30, but low $(^{206}Pb/^{204}Pb)_i$ ratios = 17.22 to 17.57. This requires a complex three-stage evolution involving a high U/Pb (μ), high Th/Pb environment early in earth history, followed by evolution in a low μ environment (see also Section 3.9.3).

The Noonkanbah data overlap with the Ellendale data in $(^{207}Pb/^{204}Pb)_i$ and $(^{206}Pb/^{204}Pb)_i$ ratios. However, for a given $(^{206}Pb/^{204}Pb)_i$ ratio the Noonkanbah samples exhibit relatively low $(^{208}Pb/^{204}Pb)_i$ ratios, although both suites form parallel positive trends on a $(^{208}Pb/^{204}Pb)_i$ vs. $(^{206}Pb/^{204}Pb)_i$ diagram (Figure 3.8). Within the Ellendale field, the olivine lamproites can be distinguished from the leucite lamproites only by the fact they tend towards higher $(^{206}Pb/^{204}Pb)_i$ ratios (= 17.43 to 17.86 and 17.26 to 17.52 respectively; this study and Nelson et al., 1986a).

3.9 Petrogenesis; the West Kimberley lamproites

3.9.1 Crust or mantle?

Similar arguments to those put forward for the Finsch mine Group 2 kimberlites from South Africa (Section 2.10.1) can be used to demonstrate that the West Kimberley lamproites are also predominantly mantle derived with insignificant crustal contamination.

Previous authors (McCulloch et al., 1983; Nixon et al., 1984; Jaques et al., 1984a, 1986a) have suggested that the high *mg* numbers and Ni and Cr contents, together with the presence of mantle xenocrysts (magnesiochromite, chrome diopside, pyrope, diamond) and xenoliths (spinel, originally garnet bearing peridotites), are indicative of a mantle origin. Furthermore, the abundance of certain trace elements are significantly higher than in either average continental crust or melts thereof. For example, Ba = 6976 to 18,281 ppm in olivine lamproites and 3588 to 31,446 in leucite lamproites (this study and Jaques et al., 1984a), is between 5 and 126 ×

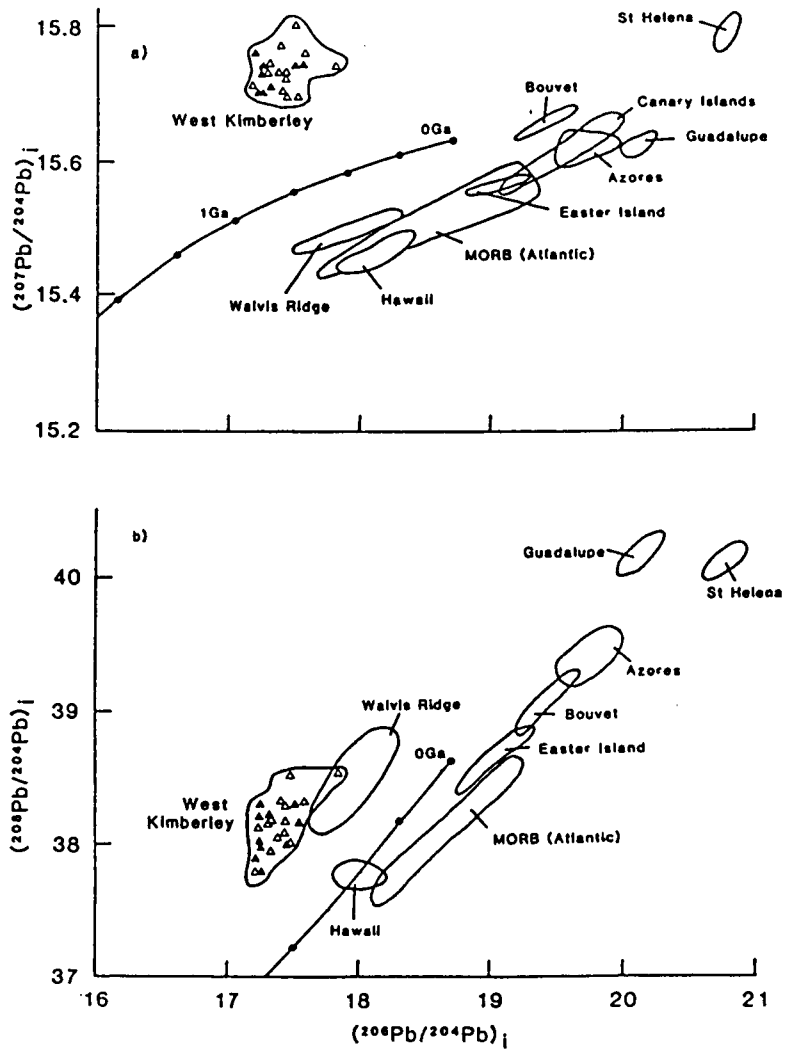

Figure 3.7 Initial Pb isotope ratios for West Kimberley lamproites (▲ = this study, △ = Nelson et al., 1986a) are compared with fields for selected MORB and OIB (Sun, 1980; Richardson et al., 1982; Cohen and O'Nions, 1982; Stille et al., 1983). The Pb-ore growth curve is from Stacey and Kramers (1975).

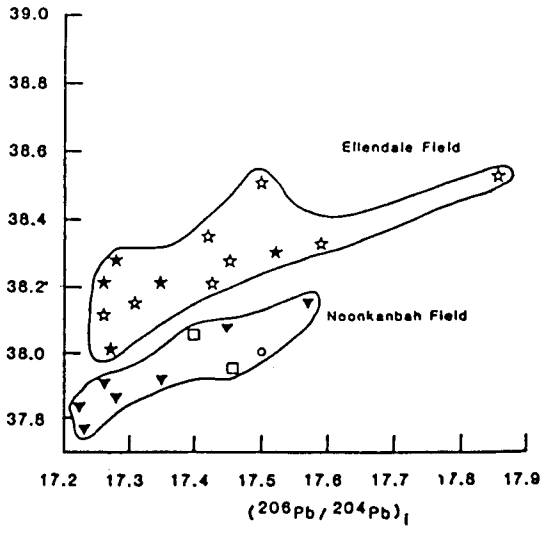

Figure 3.8 $(^{208}Pb/^{204}Pb)_i$ vs. $(^{206}Pb/^{204}Pb)_i$ for the Ellendale and Noonkanbah fields in the West Kimberley. Symbols as in Figure 3.6. o = Oscar Plug.

higher than in average continental crust (Ba = 250 to 707 ppm; Weaver and Tarney, 1984; Taylor and McClennan, 1985). Sr contents in the lamproites range from 801 to 1837 ppm (Oscar Plug: WA B19/2, Sr = 549 ppm) in contrast to 260 to 503 ppm in average continental crust and 158 ppm in average syncollisional granites. Similarly, Nd in the lamproites ranges from 108 to 596 ppm, while in average continental crust Nd = 16 to 23 ppm, and in the syncollisional granites Nd = 22 ppm. Again the continental crust is an extremely unlikely source of such high Sr and Nd contents.

An alternative argument is shown on Figure 3.9, which compares Sm/Nd and Ta/Yb ratios of the lamproites with those for, average continental crust (Weaver and Tarney, 1984; Taylor and McClennan, 1985) and selected ocean islands (Wood et al., 1979; Clague and Frey, 1982 and Norry pers. comm.). It is evident that the lamproites have Sm/Nd ratios which are too low, and Ta/Yb ratios too high, to be due to mixing between MORB and OIB and the continental crust.

If the high Nd contents of the lamproites are too high to be due to crustal contamination then the weak positive correlation between εNd and 100/Nd (Figure 3.10) indicate that neither are the unradiogenic Nd isotopes of crustal origin (see also discussion in McCulloch et al., 1983). Thus, it is concluded that the geochemical characteristics, e.g. the isotope ratios and high trace element contents, of the West Kimberley lamproites were derived from old segments of mantle presumed to be within the lithosphere.

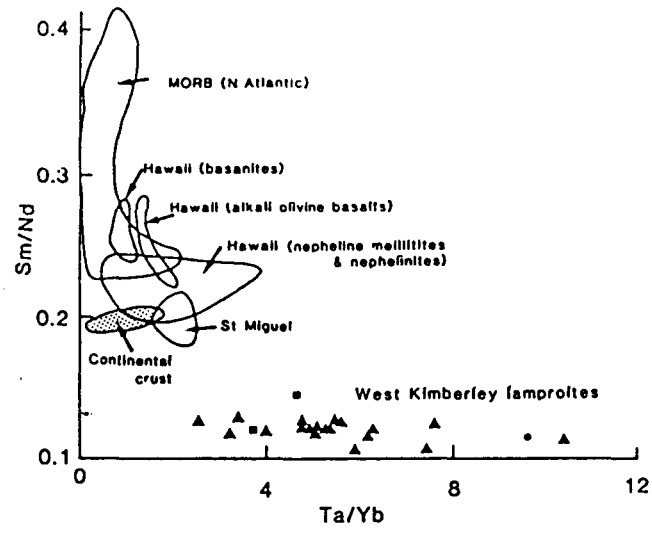

Figure 3.9 Sm/Nd vs. Ta/Yb for West Kimberley lamproites (■ = Walgidee Hills, ▲ = leucite lamproites, •= olivine lamproites). These are compared with fields for selected ocean islands and the continental crust (as in Figure 2.14).

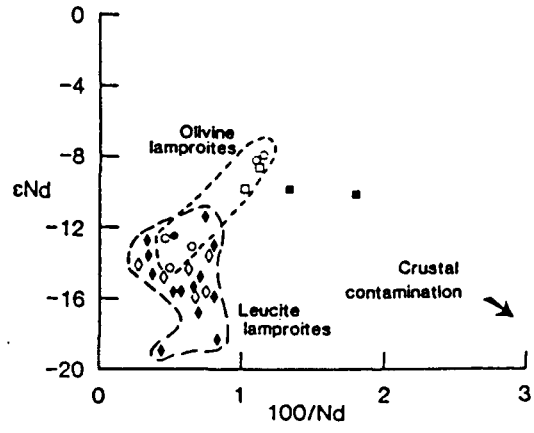

Figure 3.10 εNd vs. 100/Nd for West Kimberley lamproites, showing fields for olivine (circles) and leucite (diamonds) lamproites. Squares = Walgidee Hills. Filled symbols = this study, open symbols = McCulloch et al. (1983).

3.9.2 Fractionation

With a dataset of 470 samples, Jaques et al. (1986a) showed that the West Kimberley lamproites tend to have > 10 wt% MgO (average = 13.9 ± 7.9 wt%), < 50 wt% SiO_2 (average = 49.3 ± 5.8 wt%), *mg* numbers > 0.65 (range = 0.43 to 0.87) and Ni and Cr contents usually > 300 ppm (average = 566 ppm Ni and 600 ppm Cr). These values are consistent with either derivation directly from the mantle, or partial melting followed by limited crystal fractionation.

The fresh leucite lamproites analysed in this study (excluding Walgidee Hills) exhibit MgO = 2.42 to 14.54 wt% (average = 7.73 wt%), SiO_2 = 44.8 to 61.8 wt% (average = 50.7 wt%), *mg* numbers = 0.43 to 0.81 (average = 0.67), Ni = 90 to 1090 ppm and Cr = 142 to 593 ppm; anomalous Cr values of 68 and 1931 ppm were also noted).

Jaques et al. (1984a, 1986a) observed that the regular depletion of MgO, CaO, Ni and Cr can be explained by fractionation of olivine, diopside and Cr-spinel, while depletion in Fe and Mn implies removal of a Fe-rich phase and the progressive depletion of TiO_2 in the more evolved lamproites probably reflects the removal of priderite. Phlogopite phenocrysts are common in some of the lamproites. However, as K_2O contents increase with decreasing MgO, there is no significant fractionation of a potassic phase.

REE and trace element abundance profiles for olivine and leucite lamproites form parallel to sub-parallel trends for most elements. The leucite lamproites do, however, tend towards higher trace element contents than the olivine lamproites, although there is usually a good deal of overlap in the data (Jaques et al., 1984a; Figure 3.5c). The small differences in trace element abundance could relate to minor fractionation and/or dilution caused by the addition of bulk peridotite to the olivine lamproites (Section 3.9.5).

A number of trace elements, most noticeably Rb and Nb, do appear to have been affected by fractionation e.g. average K/Rb = 70 and K/Nb = 225 in the olivine lamproites, and 250 and 570 respectively, in the leucite lamproites. Rb is probably fractionated in clinopyroxene, while Nb may be incorporated into early separating Nb-rich perovskite (Jaques et al., 1984a, 1986a).

3.9.3 Age implications

The Rb/Sr and Sm/Nd ratios of these lamproites are likely to have been changed relative to those in their source regions, during partial melting and emplacement. Thus, Sr and Nd isotopes cannot readily be used to infer the ages of their source regions. However Pb-Pb model ages are insensitive to changes in parent-daughter ratios during magmatism and so Pb isotopes may preserve useful age information.

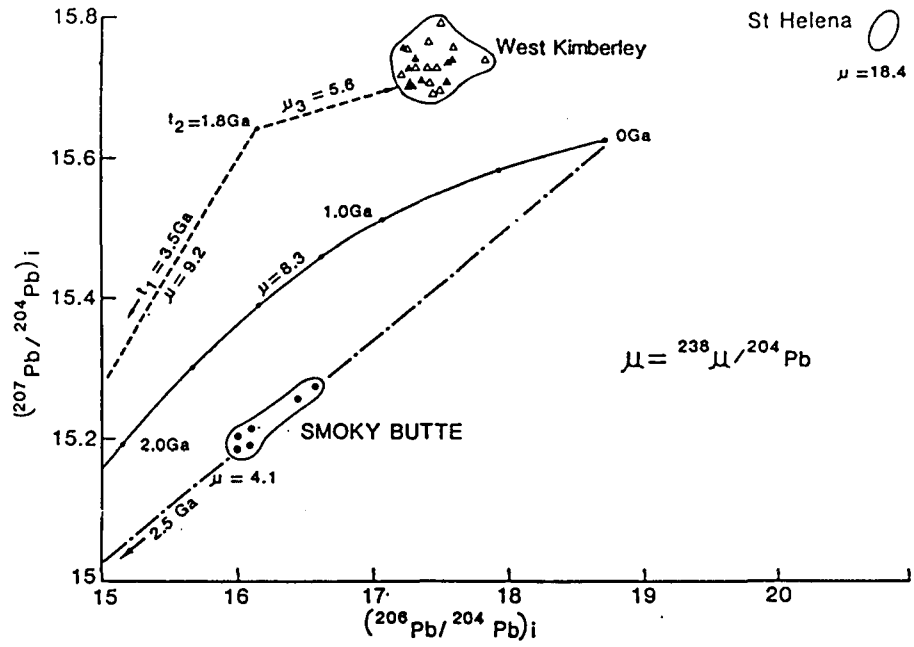

Figure 3.11 Preferred age interpretation of the Pb isotope data for the West Kimberley lamproites illustrating chosen values for μ (for discussion see text).

The data from the West Kimberley lamproites require a more complex history than a simple two-stage model as proposed for the Smoky Butte lamproites (Figure 3.11 and Section 4.8.3). The high $(^{207}Pb/^{204}Pb)_i$, but relatively unradiogenic $(^{206}Pb/^{204}Pb)_i$ ratios indicate they had high U/Pb early and then low U/Pb later in their history. This can be explained by a three-stage model in which $\mu = 8.3$ in stage one, and is then higher in stage two and lower in stage three. The geological constraints on the timing of the start of stage two (t_1) and stage three (t_2) are that the Kimberley craton is thought to be underlain by Archaean basement, which is unlikely to be older than 3.6 Ga, and that the mobile belt in which most of the lamproites occur, yields ages of 1.94 to 1.8 Ga (Atkinson et al., 1984, Section 3.2). The range of μ inferred from mantle derived melts is about 4 to 18. The latter value, is from the high $(^{206}Pb/^{204}Pb)_i$ oceanic basalts from St. Helena (Sun, 1980) and the former, from the unradiogenic Smoky Butte lamproites (Section 4.8.3). The above range provides some constraints on likely mantle source μ values. Returning to the West Kimberley lamproites, then taking t_1 = 3.5 Ga and t_2 = 1.8 Ga yields acceptable μ values of 9.2 and 5.6 for stages two and three (Figure 3.11). Reducing t_1 to, for example, 2.7 Ga increases μ for stage two and results in a slightly lower μ of 4.7 for stage three. Alternatively, reducing t_2 much below 1.8 Ga requires an improbably low μ for stage three (see also discussion in Nelson et al., 1986a).

3.9.4 Rb/Sr, Sm/Nd fractionation

The ages estimated from the Pb isotopic data can be used to calculate the Rb/Sr and Sm/Nd ratios necessary to generate the observed $(^{87}Sr/^{86}Sr)_i$ and $(^{143}Nd/^{144}Nd)_i$ ratios. These can then be compared to the Rb/Sr and Sm/Nd ratios measured in the rocks, in order to estimate the extent of Rb/Sr and Sm/Nd fractionation during melting assuming the simplest two-stage model. Using an enrichment age of 1.8 Ga for the West Kimberley lamproite source regions reveals that Rb/Sr fractionation is highly variable. Inferred source Rb/Sr ratios for the olivine lamproites = 0.31 to 0.38, and leucite lamproites = 0.38 to 0.78, compared to the observed Rb/Sr ratios of 0.35 to 0.57 and 0.17 to 3.41, respectively. On average, the observed Rb/Sr ratios are 100% higher (range = −26 to +1600%). On the other hand, observed Sm/Nd ratios (= 0.09 to 0.14) are all around 45% less (range = 35 to 58% less) than inferred source Sm/Nd ratios (= 0.18 to 0.26).

Variations in the amount of trace element fractionation cannot be correlated with either rock-type or locality. Minor fractionation of clinopyroxene and/or near surface alteration processes may have contributed to the highly variable Rb/Sr ratios. The fractionation of the Sm/Nd ratios in all the West Kimberley lamproites analysed are relatively consistent, and in the simplest model a 45% reduction in Sm/Nd would imply < 1% partial melting even in the presence of residual garnet (Hawkesworth et al., 1979). These data imply that the West Kimberley lamproites were predominantly derived from material that was old, LREE enriched and exhibited high time-integrated Rb/Sr ratios.

3.9.5 Contrasting the olivine and leucite lamproites

Like kimberlites in general (Dawson 1980) and the diamondiferous Prairie Creek lamproites (Scott Smith and Skinner, 1984a; Section 4.4.3), the West Kimberley olivine lamproites contain two olivine populations; macrocrysts and phenocrysts. It has been argued that the Finsch mine Group 2 kimberlites from South Africa, are the result of an isotope and trace element enriched melt from the subcontinental lithosphere entraining mantle peridotite during ascent to the surface (Section 2.10.4, 2.11). The olivine macrocryst population in this model, was derived through disaggregation of the entrained mantle peridotite.

The West Kimberley olivine lamproites also contain mantle xenocrysts, other than olivine such as garnet, chrome diopside, enstatite, chrome spinel and diamond and mantle xenoliths (dunites, harzburgites and lherzolites). These all provide further evidence of a peridotite component within the olivine lamproites.

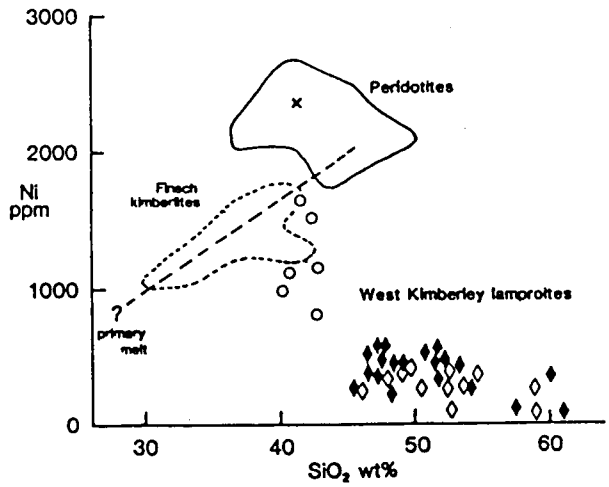

Figure 3.12 Ni vs. SiO_2 wt% for West Kimberley lamproites (symbols as in Figure 3.6b). These are compared with fields for Finsch kimberlites (Chapter 2), garnet peridotites (Nixon et al., 1981; Erlank et al., 1987) and a spinel lherzolite from Ellendale 7 (×; Jaques et al., 1986a). Also shown is a mixing line between a hypothetical kimberlite melt and peridotite. See text for discussion.

The geochemistry of the olivine lamproites is also consistent with their containing a high peridotite component. The spinel lherzolite from Ellendale 7, like other refractory peridotites reported from elsewhere (e.g. Nixon et al., 1981), has extremely high concentrations of Ni = 2316 ppm and Cr = 2801 ppm, but very low concentrations of the incompatible trace elements, Ba = 93 ppm, Rb = 16 ppm, Nd = 3 ppm, Pb < 2 ppm (Jaques et al., 1986a). By analogy with the Finsch kimberlites and from consideration of the high incompatible trace element content of these lamproites (Figure 3.5), entrainment of substantial quantities of peridotite will only affect the compatible trace element abundances (i.e. Ni and Cr; Section 2.10.4 and 2.11). The olivine lamproites of the West Kimberley Province, usually contain > 1000 ppm Ni and Cr, which are significantly higher than those predicted for primary mantle melts (e.g. 300 to 400 ppm Ni, and 400 to 500 ppm Cr; Kuehner et al., 1981).

Figure 3.12 compares the Ni ppm and SiO_2 wt% contents of the West Kimberley olivine and leucite lamproites, with fields for; Finsch kimberlites (Chapter 2) and garnet peridotites (Nixon et al., 1981; Erlank et al., 1987), plus a spinel lherzolite composition from Ellendale 7 (Jaques et al., 1986a). Also shown is a mixing line between a hypothetical kimberlite melt and peridotite. The olivine lamproite data plot on a subvertical trend, and

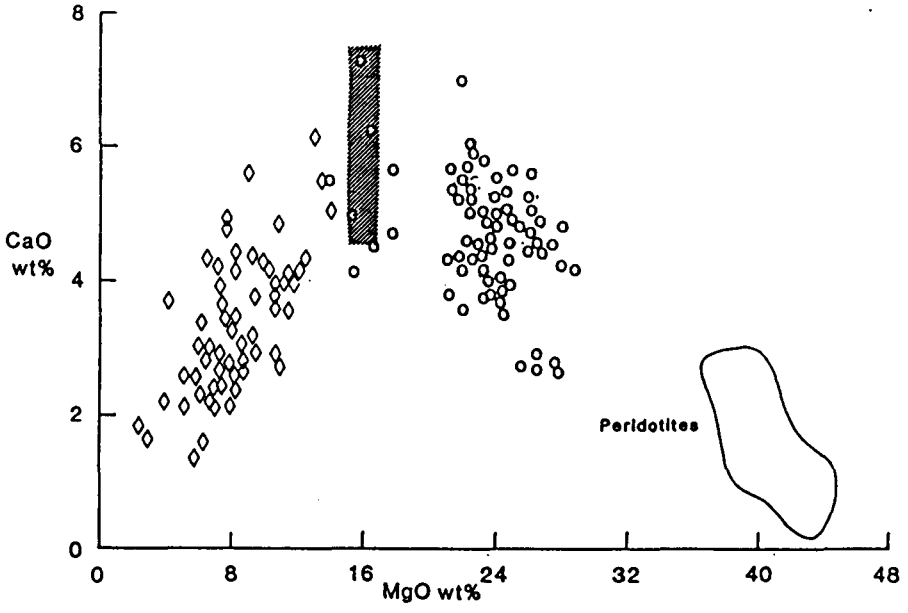

Figure 3.13 CaO wt% vs. MgO wt% for Ellendale lamproites (data from Jaques et al., 1986a). Shaded area = compositions of hypothetical primary lamproite magmas. Symbols as in Figure 3.12. See text for discussion.

hence it is evident that the primitive melt component to these rocks must have had a SiO_2 content $\simeq$ 40 wt%, which is significantly higher than that predicted for kimberlite melts. This is probably due to different volatile compositions during melting (see below and Section 5.1.1). The above melt composition could also represent a primitive leucite lamproite melt, which via fractionation processes (i.e. decreasing Ni, with increasing SiO_2) could generate the leucite lamproite suite. This would suggest that olivine and leucite lamproites followed different evolutionary paths, subsequent to melt formation, i.e. primitive lamproite melts could either fractionate to form leucite lamproite compositions, or they could entrain bulk peridotite to generate olivine lamproite compositions. However, alternatively, a primitive melt could first entrain bulk peridotite and then subsequently fractionate to leucite lamproite compositions. Figure 3.13 helps determine between these two models. Figure 3.13 compares the CaO and MgO contents of the Ellendale field lamproites. The data form a kinked trend, with CaO contents up to $\simeq$ 7.5 wt% at MgO $\simeq$ 16 wt%. This could represent simple crystal fractionation. Starting with a primitive olivine lamproite magma with CaO $\simeq$ 3 wt% and MgO $\geq$ 30 wt%, fractionation of first olivine (MgO $\simeq$ 50 wt%

and CaO $\simeq$ 0 wt%) moves magma compositions towards high CaO and low MgO. This is then superceded by clinopyroxene (MgO $\simeq$ 17 wt% and CaO $\simeq$ 25 wt%; Jaques et al., 1986a) fractionation, and the residual melt moves towards lower MgO and CaO contents. However, this model is considered unlikely, since the inferred primitive magma has MgO $\geq$ 30 wt% and Ni contents would be > 1000 ppm. Such high MgO contents in a primary melt would require very large degrees of melting, yet it has already been deduced that the lamproites were derived by very small degrees (< 1%) of partial melting (Section 3.9.4). Furthermore, to achieve up to 1300 ppm Ni (Jaques et al., 1986a) in a primary melt, produced by low degrees of partial melting, requires unreasonably low D_{Ni} values, compared to those considered typical for basaltic systems (Frey et al., 1978; Henderson, 1982). For example, if a peridotite with a typical Ni content of 2200 ppm, undergoes 1% partial melting, then a $D_{Ni} = 1.7$ is required to produce a melt containing 1300 ppm Ni. Thus, any model invoking simple melt forming processes to generate olivine lamproite compositions encounters problems in how to achieve such high Ni and MgO contents.

As outlined above, primitive olivine lamproite melts probably have $\simeq$ 40 wt% SiO_2. This is very similar to values observed in primary basanitic melts (e.g. 38 to 42 wt%; Frey et al., 1978). These basanites contain 12 to 16 wt% MgO, which is close to the MgO contents of lamproites with the highest CaO contents i.e. the peak on Figure 3.13. However, the basanites and these lamproites differ in their CaO content; basanites contain around 8 to 14 wt% CaO, whereas those lamproites with MgO $\simeq$ 16 wt% only have $\simeq$ 4.5 to 7.5 wt% CaO. Low CaO is often a characteristic feature of lamproites. This is believed to reflect the clinopyroxene-poor nature of the lamproite source regions, which were apparently depleted by melt extraction prior to trace element enrichment (e.g. Jaques et al., 1984a, 1986a; Bergman 1987). Thus, primary lamproite melts could have had CaO $\simeq$ 4.5 to 7.5 wt% and MgO contents around 16 wt% (Figure 3.13). West Kimberley lamproites with MgO $\simeq$ 16 wt% tend to contain around 600 to 700 ppm Ni, which is rather higher than values predicted for primary mantle melts (300 to 400 ppm; Kuehner et al., 1981) and those observed in primitive basanitic melts (300 to 450 ppm Ni; Frey et al., 1978). However, primary peridotite micas can contain up to $\simeq$ 2000 ppm Ni (Delaney et al., 1980) and in the Leucite Hills lamproites, Ni partitions readily into phlogopite i.e. $K_D^{Ni} = 5.2$ to 8.9; Kuehner et al., 1981). The high K_2O contents in all the West Kimberley lamproites, have been attributed to melting of a phlogopite-bearing source. Thus, it seems reasonable to deduce that the "excess" of Ni in primitive lamproite melts can be imputed to melting of phlogopite.

Also shown on Figure 3.13 is a field for garnet peridotites. In the simplest model, the olivine lamproites can be interpreted as being mixtures of

primitive melts and bulk peridotite. This is also compatible with the data on Figure 3.12.

The lamproite trend on Figure 3.13, therefore, reveals that the leucite lamproites cannot have fractionated from primitive melts which had entrained significant quantities of peridotite, and they require a different interpretation. They form a positive trend on Figure 3.13, which could be due either to residual clinopyroxene during melting, or to fractionation of clinopyroxene during crystallisation. There are a number of factors, which argue that the former is unlikely. If the trend is completely generated by residual clinopyroxene during melting, then the lower the CaO content, the more the residual clinopyroxene in the source. Clinopyroxene is the first phase consumed when a garnet lherzolite is melted, hence increasing amounts of residual clinopyroxene indicates decreasing degrees of partial melting. If this were the case, then inspection of Figure 3.13, reveals that the leucite lamproites, in general, would have been derived by smaller degrees of partial melting than the primitive olivine lamproite melts. This is inconsistent, with the greater depth of origin inferred for the latter, because they contain diamond. Moreover, the above model assumes all the leucite lamproites are primitive mantle melts, and this is incompatible with the low Ni ($<$ 100 ppm) contents in the most Mg-poor leucite lamproites (Jaques et al., 1986a). Rather, the data is more consistent with fractionation of clinopyroxene. This interpretation is supported by the presence of diopside phenocrysts and a number of diopside-bearing cognate xenoliths within the leucite lamproites (Jaques et al., 1986a). The data on Figure 3.13, therefore, suggest that primitive leucite lamproite melts could have had similar compositions to the inferred primitive olivine lamproite melts.

It would appear that olivine and leucite lamproites may originally be of similar composition, but are extracted from the mantle and ascend to the surface by different processes. This may be depth related, since the olivine lamproites are more diamondiferous than the leucite lamproites, and diamondiferous kimberlites are also modelled as entraining abundant bulk peridotite, during ascent to the surface.

The isotopes are also compatible with the above evidence. The olivine lamproites tend to have higher ϵNd and lower ϵSr values than the leucite lamproites (McCulloch et al., 1983; Section 3.8.1; Figure 3.6b). There are no Sr and Nd isotope analyses (known to the author) of the Kimberley block peridotites. However, these peridotites have a similar chemistry to depleted mantle xenoliths in kimberlites and Richardson et al. (1985) have shown that many mantle peridotites from South Africa exhibit low ϵSr and high ϵNd. Hence, entrained peridotite could be the isotopically depleted component within the West Kimberley olivine lamproites rather than MORB as suggested by McCulloch et al. (1983) and Nelson et al. (1986a).

Furthermore, leucite and olivine lamproites erupted within the same pipe can exhibit quite distinct εNd and εSr values. For example, an olivine lamproite from Ellendale 7 (WAK 16) has εNd = -8.19 and εSr = 80.4, whereas an olivine-diopside-leucite lamproite (WAK 17) from the same pipe has εNd = -15.80 and εSr = 171 (McCulloch et al., 1983). Addition of a depleted peridotite to a lamproite melt would result in a reduction of εSr and increase εNd values and subsequent fractionation should not alter these values. Assuming the olivine lamproite, WAK 16 (MgO = 26.90 wt%) and the olivine-diopside-leucite lamproite, WAK 17 (MgO = 8.29 wt%)(Jaques et al., 1984a), from the Ellendale 7 pipe, are from the same source, it is possible to calculate how much peridotite is required to change the εSr and εNd values of the leucite lamproite to those of the olivine lamproite. Assuming a hypothetical peridotite component which has εSr = -10 and εNd = 4, and Sr and Nd contents similar to the peridotite from Ellendale 7 (23 and 3 ppm respectively; Jaques et al., 1986a), then entrainment of > 95% peridotite is required. This is considered unreasonable and it seems likely that, in addition to different extraction and ascent processes, the olivine and leucite lamproites, at least in this case, are derived from slightly different source compositions.

3.9.6 Contrasting the Ellendale and Noonkanbah fields.

Lower Rb and Th contents in the Noonkanbah field data result in their having higher K/Th and K/Rb ratios compared to the more northerly situated Ellendale field intrusions (Section 3.7.2). The majority of the Noonkanbah field data have $(K/Th)_N > 1$ whereas the Ellendale field samples tend to exhibit $(K/Th)_N < 1$. There is more overlap in the K/Rb data, but the Noonkanbah field samples have K/Rb ratios from 130 to 450 and the Ellendale field samples have K/Rb = 10 to 345. These features are either source or extraction phenomena and these possibilities are evaluated below.

The $(K/Th)_N$ and K/Rb ratios of the lamproites are plotted against MgO in Figure 3.14. Olivine lamproites (MgO > 21 wt%) appear to be restricted to the Ellendale field. MgO has previously been used as a fractionation index (Section 3.6; Jaques et al., 1984a, 1986a) and comparison of the leucite lamproites from the two fields shows that for a given MgO content, the Noonkanbah field has higher $(K/Th)_N$ and K/Rb ratios. Hence, these variations are not attributable to fractionation. They could have been generated by small differences in degree of partial melting. However, in a simple two-stage model, it appears that the Sm/Nd ratio fractionated by $\simeq$ 45% during melting for all the West Kimberley lamproites (Section 3.9.4).

In Figure 3.6a there is a good deal of overlap in εSr values between the Ellendale and Noonkanbah fields. The latter, however, appear to extend to

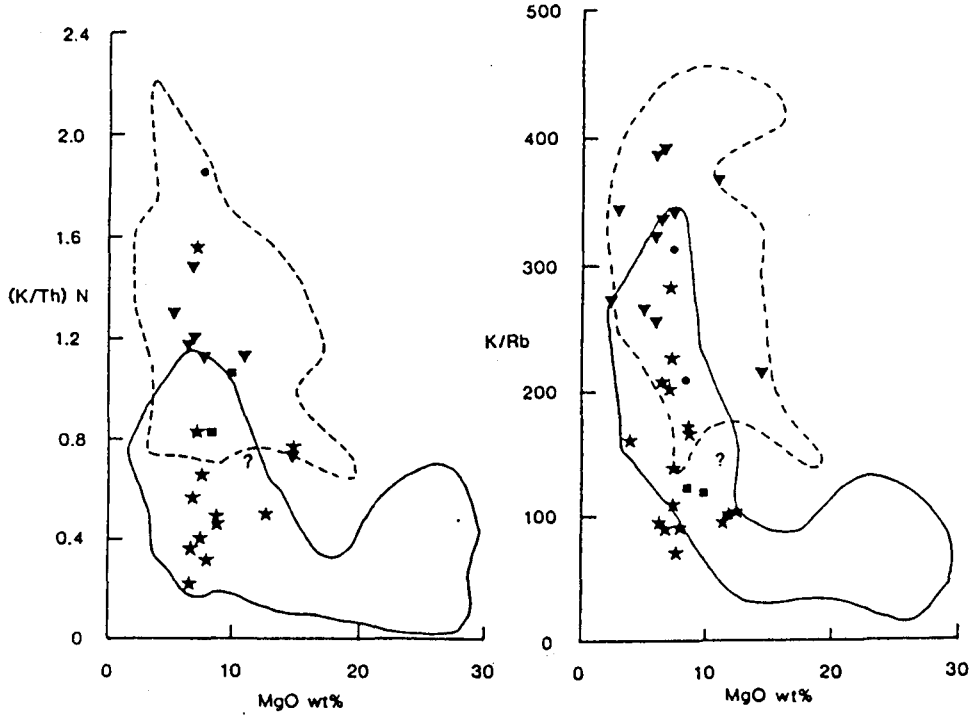

Figure 3.14 a) $(K/Th)_N$ and b) K/Rb vs. MgO wt% for the West Kimberley lamproites. Symbols as in Figure 3.6. (?) = Seltrust Pipe 1, • = East Lennard shelf. These are compared with fields for Noonkanbah (dashed line) and Ellendale (solid line) lamproites from Jaques et al. (1986a).

slightly higher values. Assuming a simple two-stage model (Section 3.9.4), inferred Rb/Sr ratios for the Noonkanbah field data (= 0.13 to 0.25) are slightly higher than those for the Ellendale field data (= 0.11 to 0.22). This contrasts with the observed Rb/Sr ratios of 0.17 to 0.37 and 0.19 to 1.17, for the Noonkanbah and Ellendale fields respectively. The lower observed Rb/Sr ratios in the Noonkanbah field data are due to their relatively low Rb contents, which therefore, appear to have been generated during melting and extraction processes. CaO and MgO contents of leucite lamproites from both fields overlap totally (not shown) and fractionation (as shown above) of clinopyroxene, cannot account for this variation. The West Kimberley lamproites have high K_2O contents (= 2 to 12 wt%; Jaques et al., 1986a) and a K-bearing phase such as phlogopite, has been inferred to be present within their source regions. The relationship between K and Rb is obscure, since no K-bearing phase appears to be fractionating, but Rb is affected by fractionation (Section 3.9.2). Again the Noonkanbah and Ellendale fields cannot be differentiated on the basis of their K contents. Thus, the reason for the lower Rb in the Noonkanbah samples during melting is unclear.

On the other hand, it has been observed that the Noonkanbah samples exhibit lower $(^{208}Pb/^{204}Pb)_i$ ratios than the Ellendale field data (Section 3.8.2, Figure 3.8). This is consistent with small, but old time-integrated variations in Th/Pb ratio within the lamproite source regions.

3.10 Discussion

The West Kimberley lamproites form a consanguineous series from olivine to leucite lamproites. These are highly trace element and isotopically enriched rocks. Their unusual geochemistry cannot be attributed to crustal contamination and they have been shown to originate by very small degrees of partial melting (< 1%) of ancient trace element source regions. These are believed to be situated in the mantle portion of the subcontinental lithosphere. Olivine lamproites appear to be derived from greater depth than the leucite lamproites, since they contain diamond.

Previous petrogenetic models for the West Kimberley lamproites have proposed mantle source regions which were originally depleted by magma extraction, and then subsequently enriched in trace elements. The trace element (Figures 3.4, 3.5) and isotope (Figures 3.6, 3.7) similarities, between all the West Kimberley lamproites, suggests their source regions were affected by the same enrichment event. A predominantly melt related enrichment event is indicated by the high Ta/Yb ratios (Figure 3.9) and Ti contents (= 2.64 to 8.12 wt%; this study and Jaques et al., 1984a). This melt had high K, Ti, Ta, Zr, Nd, LREE, Rb, Sr and Ba contents and is believed to have

stabilised phlogopite and rutile (Arima and Edgar, 1983) within the source regions. The Pb isotope data suggest that these melts, were derived from sources which had high time-integrated μ i.e. high $(^{207}Pb/^{204}Pb)_i$. During melting and emplacement in the lamproite source region, this component obtained a low μ (see Section 3.9.3) in order to generate the observed low $(^{206}Pb/^{204}Pb)_i$. The nature and origin of this trace element enrichment event, are discussed further in Chapter 5.

Small geochemical differences, however, exist between olivine and leucite lamproites, and between the Noonkanbah and Ellendale field samples. These are source features and/or reflect processes occurring during melt formation and ascent. Olivine and leucite lamproites from the same pipe (Ellendale 7) have distinct isotope signatures (McCulloch et al., 1983). The olivine lamproites bear petrographic (two olivine populations) and geochemical (high incompatible and compatible trace element contents) similarities to kimberlites, which can be attributed to mixing models. By analogy to the Finsch kimberlites (Section 2.10.4), a primitive olivine lamproite melt entrains and disaggregates bulk peridotite en route to the surface. The leucite lamproites, on the other hand, appear to represent primitive lamproite melts which have fractionated to varying degrees, en route to the surface, but without significantly entraining bulk peridotite. Mass balance considerations indicated that bulk entrainment of peridotite was unlikely to account for the observed differences in isotope ratio within the Ellendale 7 pipe. Thus, it is believed that small depth-related variations in parent/daughter ratios, existed within the source regions of the West Kimberley lamproites.

Relative to the Noonkanbah field, those in the Ellendale field exhibit higher Th and Rb contents, which cannot be imputed to variable degrees of fractionation. The reasons for the differences in Rb are not clear, though they may relate to extraction processes. However, higher Th contents in the Ellendale lamproites, are accompanied by higher $(^{208}Pb/^{204}Pb)_i$ ratios, which indicate higher source Th/Pb ratios.

The diamondiferous olivine lamproites from the West Kimberley, bear similarities to kimberlites owing to the bulk entrainment of peridotite, which appears to be a feature of both rock suites. However, the kimberlite and lamproite melt components differ in composition. For example, the West Kimberley lamproites have higher SiO_2 contents = 38 to 60 wt% compared to kimberlites from South Africa, SiO_2 = 19.9 to 41.9 wt% (this study and Smith et al., 1985). Figure 3.13 indicates that the lamproite primary melts had higher SiO_2 contents $\simeq$ 40 wt%, than the Finsch kimberlite primary melts ($SiO_2 \simeq$ 30 wt%). This may relate to differences in volatile composition (Eggler, 1974); kimberlites are H_2O and CO_2-rich rocks, whereas the West Kimberley lamproites are H_2O-rich (> 1.4 wt%) and CO_2-poor rocks (< 0.75 wt%)(Jaques et al., 1984a). The nature and origin of composi-

tional differences between kimberlites and lamproites are discussed further in Chapter 5.

Finally, there is no regional tectonic event which obviously created suitable conditions for the emplacement of the West Kimberley lamproites. However, the Ellendale, Calwynyardah and Noonkanbah fields form a north-south trend, where the intrusions in the north (Ellendale) are older (21.4 to 22.3 Ma) than in the southerly Noonkanbah field (17.8 to 20.1 Ma), and this may be consistent with the northerly progression of the Australian continent over a hotspot (Jaques et al., 1984b and 1986a).

Chapter 4

Lamproites: North America

4.1 Introduction

This chapter considers lamproites from three localities in North America; Leucite Hills (Wyoming), Smoky Butte (Montana) and Prairie Creek (Arkansas). Bergman (1987) observed that lamproite occurrences in North America, are generally found near the craton margin, where the estimated age of the basement varies from 1.5 to 2.5 Ga. Integrated petrographic and geochemical study, of the above three lamproite suites, demonstrates that they are primitive, uncontaminated mantle melts. They were derived from portions of the subcontinental lithosphere depleted in major elements, but characterised by variable ancient trace element enrichment events which appear to have stabilised K-bearing phases. Within this framework, the petrogenesis of each locality is discussed using a combination of mineralogy, major element, trace element and isotope geochemistry and where relevant, the results of previous studies.

A number of authors have considered the origin of the Leucite Hills lamproites, in particular the relationship between madupites and wyomingite/orendites from studies of mineralogy, geochemistry and experimental petrology. There are fewer studies, however, dealing with the petrogenesis of the Smoky Butte and Prairie Creek intrusions. There are sufficient similarities between the Prairie Creek lamproites, the West Australian olivine lamproites and the South African Group 2 kimberlites to warrant comparison. It is believed that these diamondiferous rocks have all entrained and disaggregated mantle peridotite en route to the surface. The geochemical evidence at Smoky Butte, unlike the other localities, appears to require the presence of amphibole, in addition to phlogopite within the source. The presence of diamond in the Prairie Creek rocks and amphibole inferred in the source region of the Smoky Butte rocks indicates that lamproite melts are derived from a range of mantle depths ($>$ 150 km to $<$ 100 km).

The North American lamproites, together with other continental vol-

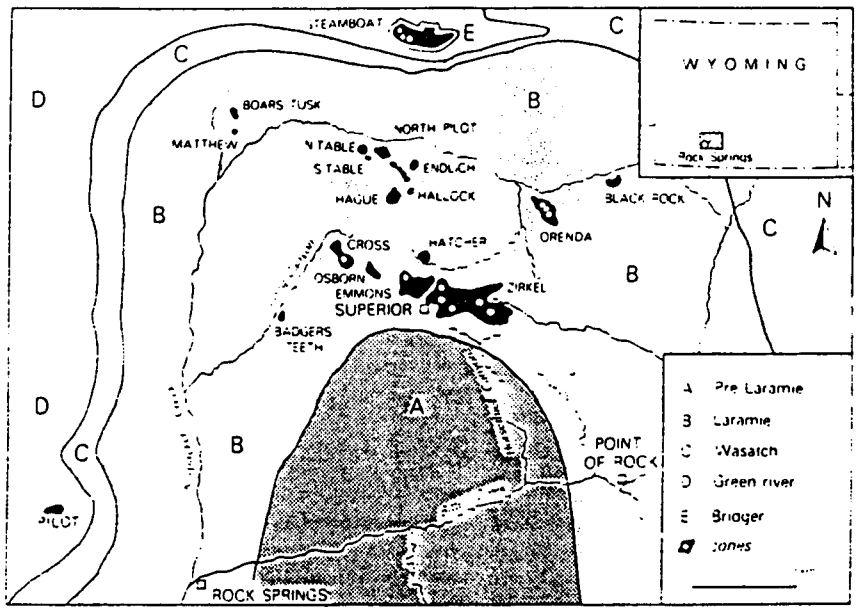

Figure 4.1 Location of the Leucite Hills lamproites (after Barton and van Bergen, 1981 and De Beers Internal Report).

canics from the North American craton, are characterised by low εSr, εNd and unradiogenic Pb isotopes, which contrasts with the high εSr, low εNd Finsch kimberlites and Western Australia lamproites. These appear to be a feature of this region and reflect a certain style of trace element enrichment occurring within the subcontinental mantle lithosphere. Pb-Pb model ages for the North American lamproites range from 1.9 to 2.5 Ga, indicating that such trace element enrichment events have occurred during the Late Archaean to Early Proterozoic times.

4.2 Review of previous literature

4.2.1 Leucite Hills

The Leucite Hills lamproites occur in Sweetwater County, southwestern Wyoming. There are 22 major exposures consisting of cinder cones, lava flows, volcanic necks, dykes, intrusive sheets and pyroclastics. These, with the exception of Pilot Butte, lie within an area of $\simeq$ 250 km^2, centred 45 km northeast of Rock Springs (Ogden, 1979; Figure 4.1).

The age of the volcanism is 1.1 Ma (K-Ar age on micas; MacDowell, 1966). The rocks overlie and are intrusive into Palaeozoic and Eocene sedimentary rocks on the northeast flank of the Rock Springs uplift. The vent

Orendite	Wyomingite	Madupite
(apatite)	(hercynite)	DIOPSIDE MP-G
-resorbed grains	*-resorbed grains*	*-twinning very*
(dark phlogopite cores)	apatite MP	*-common*
-resorbed grains	*-subhedral grains*	apatite
PHLOGOPITE MP	(dark phlogopite cores)	(leucite)
-microphenocrysts	*-resorbed grains*	perovskite G
-strongly resorbed	(pale green diopside cores)	wadeite
olivine G	*-resorbed grains*	phlogopite G
-may form reaction rim	PHLOGOPITE MP	*-ragged poikilitic*
-around phlogopite	DIOPSIDE MP	*- masses*
DIOPSIDE MP	*-twinning not rare*	(euhedral opaques)
-twinning rare	apatite	*-found only in*
apatite	LEUCITE G	*-phlogopite*
SANIDINE G	(priderite)	(skeletal opaques)
priderite	*-dark brown in colour*	GLASS
-amber colour	(phlogopite)	*-dirty green colour*
(wadeite)	*-narrow rims on the*	
LEUCITE G	*-phlogopite phenocrysts*	
RICHTERITE G	richterite G	
	(sanidine)	

Table 4.1 Mineralogy and paragenesis of rock-types at Leucite Hills. Minerals are listed in order of crystallisation sequence, rare minerals are in brackets, common minerals unbracketed and major minerals in capitals. P = phenocryst, MP = microphenocryst and G = groundmass. (modified after Kuehner et al., 1981).

alignment is controlled by northwest-trending structures related to this uplift (Ogden, 1979), which is one of the Late Cretaceous-Palaeocene Laramide uplifts (Vollmer et al., 1984). The basement is believed to be part of the Archaean Wyoming Craton, which seems to have formed and stabilised in the period 3200 to 2500 Ma (Peterman, 1979; cited by Vollmer et al., 1984).

There have been a number of studies on the petrology, geology and geochemistry of these occurrences; Cross (1897), Kemp (1897), Kemp and Knight (1903), Carmichael (1967), Powell and Bell (1970), Kay and Gast (1973), Ogden (1979), Barton and Hamilton (1978, 1979, 1982), Barton (1979), Barton and van Bergen (1981), Kuehner et al. (1981), Vollmer et al. (1984) and references therein. The Leucite Hills are also discussed in lamproite review papers by Bergman (1987) and Mitchell (1985).

Three major rock-types have been identified petrographically: orendite, wyomingite and madupite (Cross, 1897; Carmichael, 1967). Table 4.1 outlines the petrography of these groups after Kuehner et al. (1981). Im-

portant differences lie in the nature of the phlogopite and the groundmass constituents. Madupites contain poikilitic groundmass phlogopite, whereas in the wyomingite/orendites phlogopite usually occurs as nonpoikilitic phenocrysts. Glass and leucite constitute the main portion of the wyomingite groundmass, which contrasts with the leucite and sanidine-rich, glass-poor groundmass of the orendites.

The Leucite Hills rocks are ultrapotassic and sometimes peralkaline rocks, but while the madupites are silica-undersaturated, the wyomingites and orendites are silica-saturated to oversaturated (Kuehner et al., 1981). The madupites have higher MgO, FeO and CaO contents, but lower SiO_2, Al_2O_3 and K_2O contents (Vollmer et al., 1984).

In common with other ultrapotassic rocks, the Leucite Hills lamproites have high incompatible trace element contents (e.g. Rb, Sr, Ba, Zr and LREE) and also high compatible trace element contents (e.g. Ni and Cr: Kuehner et al., 1981; Vollmer et al., 1984). The latter may be present in amounts comparable to primary mantle melts (Kuehner et al., 1981). High *mg* numbers and Cr contents in both rock series precludes fractional crystallisation as a major mechanism in their genesis (Kuehner et al., 1981).

Orendites and wyomingites are chemically indistinguishable, which together with their close association in the field, has led to suggestions that the differences in mineralogy probably relate to cooling rates, P_{H_2O} (Ogden, 1979) or depth of crystallisation (Kuehner et al., 1981). The close geological association of the madupite and wyomingite/orendite rock-types intimate at a genetic relationship (Ogden, 1979; Kuehner et al., 1981).

A number of models have been proposed which have attempted to relate the madupite and wyomingite/orendite series to the same source material, but generated under different melting conditions. On the basis of REE data alone, Kay and Gast (1973) suggested very small ($< 1\%$), but slightly different degrees of partial melting of a garnet lherzolite source. Ogden (1979) proposed progressive melting of a phlogopite lherzolite source involving the incongruent melting of phlogopite. Initial melting at the eutectic, in the system $KAlSiO_4$-SiO_2-Mg_2SiO_4-$CaMgSi_2O_6$, results in madupitic compositions and subsequent melting at the clinopyroxene-free peritectic results in wyomingite/orendite compositions. Kuehner et al. (1981) proposed that high pressure phase relations in the systems Mg_2SiO_4-$KAlSiO_4$-SiO_2 and $KAlSiO_4$-MgO-SiO_2-H_2O-CO_2 are consistent with the madupites being generated at pressures of 24–34 Kb and then the wyomingite/orendites at pressures of 14–19.5 Kb, from the same K-enriched peridotite source. However, experimental studies have shown that only the wyomingite/orendites could equilibrate with a garnet lherzolite assemblage at $P > 26$ Kb and $P_{H_2O} = P_{total}$ (Barton and Hamilton, 1978, 1979, 1982). The melting relations of a madupite indicates that it could *not* originate by partial melting of mantle

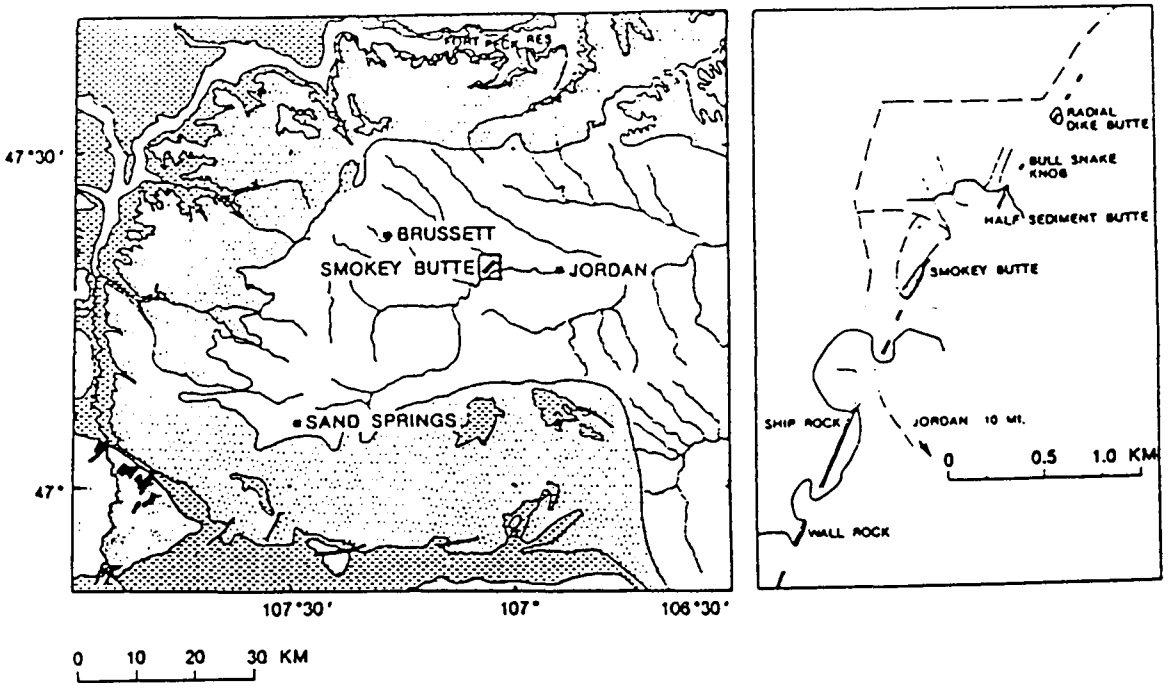

Figure 4.2 Location of the Smoky Butte lamproites after Matson, 1960.

peridotite in the presence of H_2O and CO_2. Rather, it may represent the partial melting product of mica-pyroxenite or mica-olivine-pyroxenite in the upper mantle (Barton and Hamilton, 1979).

Isotopic studies have also shown that, although the madupites and wyomingite/orendites have overlapping ϵSr values (= 9.79 to 12.77 and 10.64 to 18.73 respectively), they can be distinguished by their ϵNd values (= −10.5 to −12.3 and −13.7 to −17.0 respectively; Vollmer et al., 1984).

Significant crustal contamination is considered unlikely on the basis of both major element (Ogden, 1979) and trace element (Vollmer et al., 1984) arguments.

4.2.2 Smoky Butte

The lamproites from Smoky Butte are situated $\simeq$ 13 km due west of Jordan, Garfield County, Montana (approximately 47°20′ N, 107°04′ W). They form a small ($\simeq$ 3 km long) north-northeast trending outcrop of thin dykes and plugs which have intruded the Tullock member of the Palaeocene Fort Union formation, along the axis of a very broad, gently dipping regional syncline (Matson, 1960; Figure 4.2). Matson (1960) claimed extrusive rocks were absent at Smoky Butte and that the lamproites were entirely hypabyssal. However, Marvin et al. (1980), Bergman (1987) and Mitchell et al. (1987) have recognised extrusives such as bedded pyroclastics composed of welded autolithic lamproite lapilli in a clay rich matrix, which overlie and are marginal to the intrusions (Bergman, 1987). Hypabyssal rocks occur as fine grained to glassy dykes which often contain zeolite or carbonate filled

vesicles, while massive, coarse grained lamproite occurs at the Smoky Butte plug (Bergman, op. cit.). Velde (1975) identified three major rock-types at Smoky Butte consisting of:

1. Sanidine, armalcolite, K-richterite and K-riebeckite.
2. Armalcolite, Ti-phlogopite, diopside, olivine (altered) and sanidine.
3. Armalcolite, Ti-phlogopite, diopside, olivine (altered), analcite and glass.

The Smoky Butte rocks are Si-saturated to oversaturated, peralkaline and have low Al_2O_3, high TiO_2 and K_2O contents (Velde, 1975). The lack of variation in major element compositions suggest that mineralogical and textural differences can be attributed to different cooling histories (Velde, 1975; Mitchell et al., 1987). Mitchell and Hawkesworth (1984) demonstrated that these rocks are highly trace element enriched, e.g. Ta, Hf, Th and LREE (La/Yb = 189 to 281). They also showed that the Smoky Butte lamproites are characterised by relatively low $(^{87}Sr/^{86}Sr)_i$ and $(^{143}Nd/^{144}Nd)_i$ ratios (0.70587 to 0.70633 and 0.51128 to 0.51151 respectively) and suggested that they were derived from old low Rb/Sr, Nd/Sm (i.e. LREE enriched) mantle sources.

4.2.3 Prairie Creek

The Prairie Creek intrusion or Crater of Diamonds State Park, as it is currently known, is situated 4 km SSE of Murfreesboro, Pike County, Arkansas (34°2′ N, 93°40′ W). It is in close proximity to three smaller lamproitic intrusions: American mine, Kimberlite mine and Black Lick.

There have been a number of studies on the intrusion including; Miser and Ross (1923), Meyer (1976), Goginini et al. (1978), Bolivar and Brookins (1979), Scott Smith and Skinner (1984a), Bergman (1987), Mitchell (1985) and references therein.

The Prairie Creek lamproites intrude Carboniferous and Cretaceous sedimentary rocks which dip gently to the South. Field relations suggest it is mid-Cretaceous in age (Miser and Purdue, 1929; cited in Bergman, 1987). More recently, K-Ar isotopic analyses on phlogopite reveal an age of around 106 ± 3 Ma (Goginini et al., 1978).

The main Prairie Creek diatreme is roughly triangular in cross-section and occupies an area of 29.5 Ha. Three main lithological units have been identified (Miser and Ross, 1923; Figure 4.3 after Meyer, 1976):

1. Grey blue tuffs and fine-grained breccias.

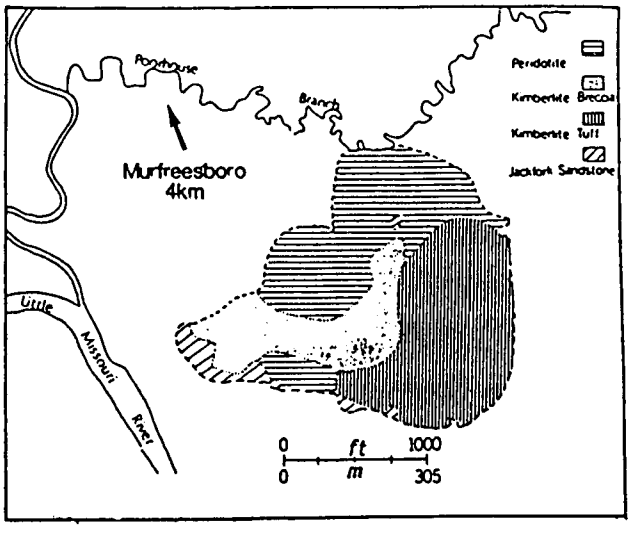

Figure 4.3 Location of the Prairie creek lamproites, after Meyer (1976).

2. Greenish brown volcanic breccias.

3. Hypabyssal intrusive peridotite.

Only the breccia phase is presently believed to contain an economic concentration of diamonds (Bergman, 1987). Two of the other associated intrusions (American mine and Kimberlite mine) are also diamondiferous (Bergman, op. cit.).

The first two groups have been interpreted as pyroclastic and epiclastic deposits respectively (Scott Smith and Skinner, 1984a). They are intruded by hypabyssal material which until recently was considered to be micaceous kimberlite, albeit an anomalous kimberlite owing to the rarity of garnet and lack of Mg-ilmenite and enstatite (Bolivar and Brookins, 1979).

These magmatic rocks consist of two generations of olivine set in a predominantly fine-grained groundmass of phlogopite, diopside, K-richterite, perovskite, spinel, apatite, serpentine and glass. Many of the features at Prairie Creek are more typical of lamproites than kimberlites, such as the shallow champagne-glass shape of the diatreme, the presence of amphibole and glass and the absence of primary serpentine and calcite (Scott Smith and Skinner, 1984a).

Although the high olivine content is comparable to kimberlites, the groundmass phlogopite and bulk-rock compositions are intermediate between known lamproites and kimberlites and Scott Smith and Skinner (op. cit.) believe the Prairie Creek intrusion forms an extension of the lamproite field. The hypabyssal rocks have been classified as olivine lamproites (Scott

Smith and Skinner, op. cit.) or olivine-phlogopite lamproites (Bergman, 1987).

Sr isotope analyses have been reported for all rock units by Bolivar and Brookins (1979; $(^{87}Sr/^{86}Sr)_i$ = 0.7066 to 0.7132) and for the hypabyssal unit by Smith (1983) and Scott Smith and Skinner (1984a) where $(^{87}Sr/^{86}Sr)_m$ = 0.7072. The latter authors believe the high ratios quoted by Bolivar and Brookins (1979) to result from analyses of altered samples.

Cognate xenoliths consisting of phlogopite, K-Ti-richterite, diopside and priderite from the hypabyssal facies have been described by Mitchell and Lewis (1983).

4.3 Sample localities

Twenty-six magmatic samples of Leucite Hills lamproites were selected for study, from the De Beers collection. Location of the samples within the Rock Springs area can be determined from Appendix A.3 and Figure 4.1. Information regarding the geological form of individual intrusions can be found in Ogden (1979).

Six samples of Smoky Butte lamproites (SB11, SB35, SB45, SB59, SB66 and SB70) were provided by R.H. Mitchell. Their location can be found on Figure 4.2. They are all magmatic, with the exception of SB35, which is a pyroclastic rock.

Three samples of Prairie Creek lamproites (PK1/4, PK1/18 and PK1/20) were selected from the De Beers collection. They are all from the hypabyssal intrusive at Prairie Creek (Figure 4.3).

4.4 Petrography

4.4.1 Leucite Hills

A number of magmatic madupites, wyomingites and orendites from several of the intrusions were studied and modal analyses are given in Appendix C.1. The petrographic observations made here, are in close agreement with findings elsewhere (e.g. Carmichael, 1967; Ogden, 1979; Kuehner et al., 1981). Mineral classification after Scott Smith and Skinner (1984a, b) and Mitchell (1985), is shown in Table 4.2, together with the rock-type names after Ogden (1979).

Phlogopite is ubiquitous and tends to occur as non-poikilitic phenocryst laths in the wyomingite/orendites (Plates 4.1 and 4.2). These phenocrysts are pleochroic yellow to orange and may show faint polysynthetic twinning. They may also be kinked, strained and/or may have ragged or corroded edges, indicative of some resorption. In the madupites from Pilot Butte,

Locality	Sample Number	Mineral Classification	Rock Types
Boars Tusk	LH2/9		w
North Table Mountain	LH4/7		w/o
Middle Table Mountain	LH5/7	phlog. lc lamproite (g)	m/w
	LH5/9	lc. lamproite	w
South Table Mountain	LH6/12	lc. lamproite	ol-o/ol-w
	LH6/15	lc. sanid. lamproite	
Iddings Butte	LH7/1		w
Endlich Hill	LH8/3	lc. lamproite	ol-o
	LH8/8	lc. sanid. phlog lamproite	
Hague Hill	LH9/1	sanid. lc lamproite	o
Spring Butte	LH11/1	lc. sanid. lamproite	o/w
Black Rock	LH12/1		o
	LH12/16	lc.lamproite	
Deer Butte	LH13/18	phlog. di. lamproite	o/w
Hatcher Mesa	LH15/1	lc. lamp	o/w
Emmons Mesa	LH16/8		o
Zirkel mesa	LH17/3		o/w
	LH17/19	(altered base)	
	LH17/26	(very fine-grained)	
	LH17/28	(very fine-grained)	
	LH17/34	lc.lamproite	
	LH17/48	sanid.lamproite	
Pilot Butte	LH19/25	lc. sanid. lamproite	m

Table 4.2 Mineral classification of the Leucite Hills samples. lc. = leucite, sanid. = sanidine, di. = diopside, phlog. = phlogopite, o = orendite, w = wyomingite, m = madupite, ol = olivine (xenocrysts) and g = glassy. Rock-types after Ogden (1979).

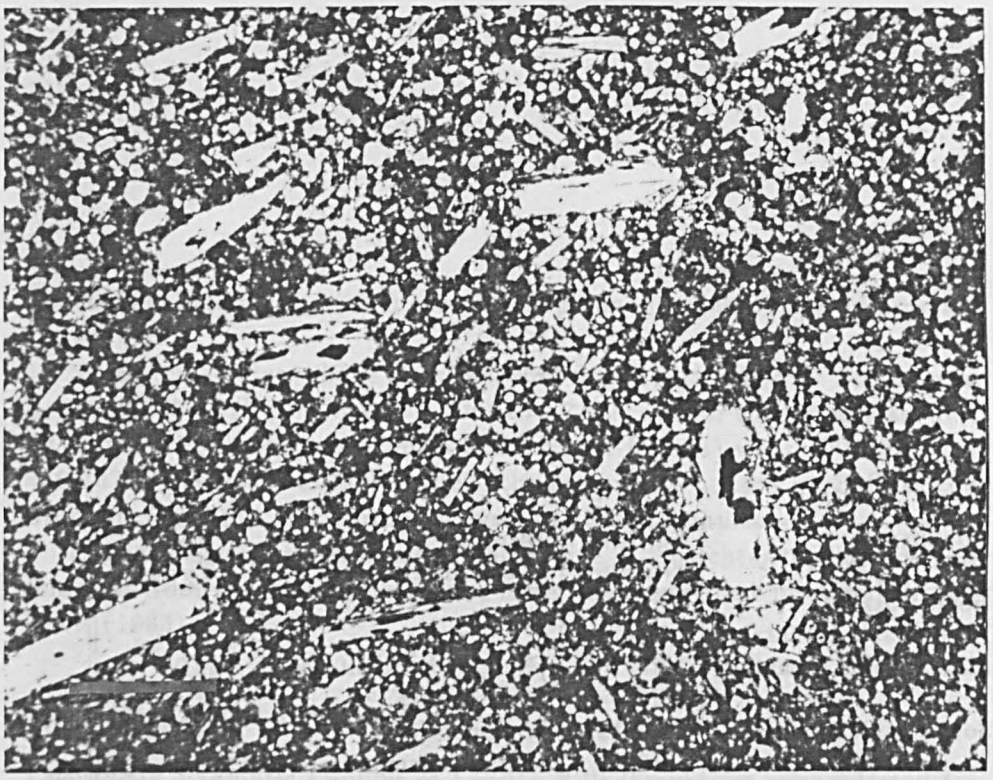

Plate 4.1 LH5/9; Wyomingite from Leucite Hills; phlogopite and clinopyroxene phenocrysts set in a groundmass of mainly leucite, clinopyroxene and glass (PPL). Scale bar = 0.5 mm.

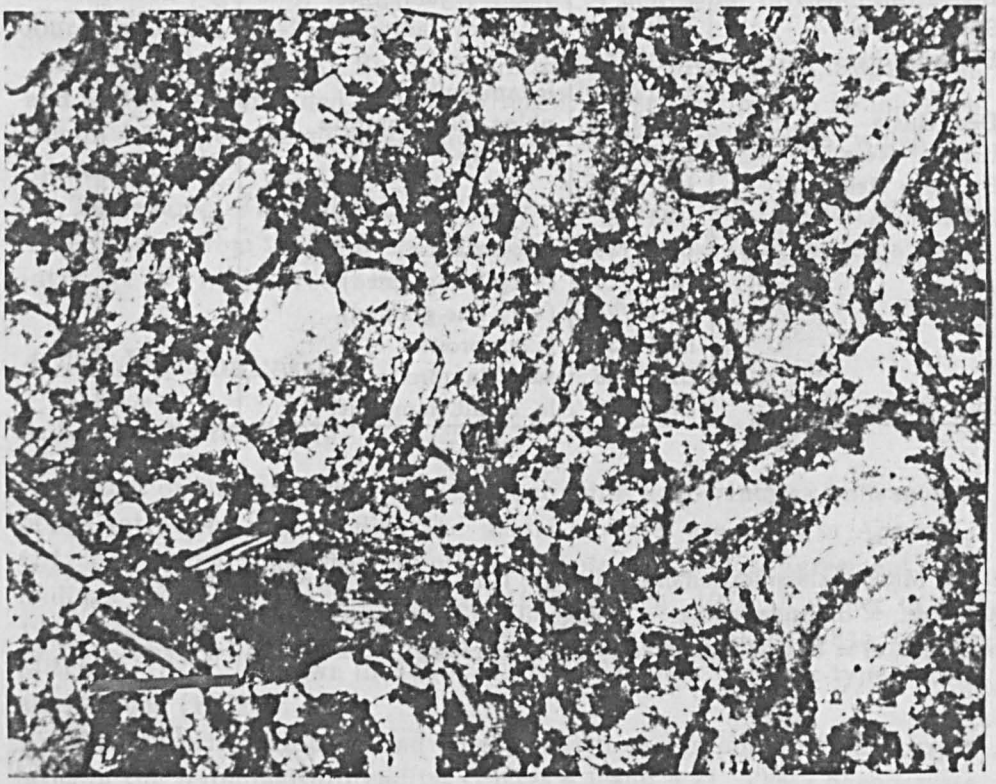

Plate 4.2 LH8/8; Orendite from Leucite Hills; phlogopite and clinopyroxene phenocrysts are set in a groundmass of mainly sanidine and leucite (PPL). Scale bar = 0.5 mm.

Plate 4.3 LH5/7; Madupite from Leucite Hills; poikilitic phlogopite, and clinopyroxene phenocrysts set in a groundmass of mainly leucite, clinopyroxene and glass (PPL). Scale bar = 0.5 mm.

phlogopite occurs as anhedral to subhedral poikilitic plates enclosing groundmass phases (leucite, clinopyroxene and apatite). Phlogopites from the Middle Table Mountain madupites are texturally intermediate between those in the wyomingite/orendites and those in the Pilot Butte madupites. They have pale orange non-poikilitic cores, but very uneven ragged, darker orange, poikilitic rims (Plate 4.3). Phlogopite analyses by Carmichael (1967), Kuehner et al. (1981) and Mitchell (1985) demonstrate that madupitic micas are richer in TiO_2, FeO_T and Ba contents, but poorer in Al_2O_3, MgO, Cr_2O_3 and K_2O contents, than the latter.

Colourless clinopyroxene, shown to be diopside in composition (Carmichael, 1967; Kuehner et al., 1981; Mitchell, 1985), forms abundant phenocrysts in the madupites. A few phenocrysts are also observed in wyomingite/orendite sections from Endlich Hill, Hague Hill, Hatcher Mesa and Zirkel Mesa. In the wyomingite/orendites, clinopyroxene usually forms abundant groundmass microphenocrysts or microlites.

Olivine phenocrysts as observed by Carmichael (1967) in the olivine orendites at South Table Mountain were not found in this study.

The groundmass of the wyomingites is composed mainly of abundant, small ($\leq$ 0.1 mm) rounded leucites and microlitic to microphenocrystal diopside set in a dirty grey-brown to brownish -green isotropic altered glass. The groundmass of the orendites consists of patchy distributions of 'sanidine-rich' and 'leucite-rich' areas. Sanidine usually forms areas of interlocking subhedral to euhedral laths, although isolated laths were also observed.

Sanidine may poikilitically enclose diopside, apatite and sometimes leucite. The leucite-rich areas contain abundant, usually small ($\leq$ 0.1 mm) rounded isotropic leucites and microlitic-microphenocrystal diopside. These phases are poikilitically enclosed in a matrix of pleochroic yellow to pink K-richterite. As well as forming late crystallising anhedral poikilitic plates, the K-richterite may also occur as poikilitic euhedral laths ($<$ 1 mm long; LH8/3 and LH15/1), relatively inclusion-free plates interstitial to sanidine laths within the sanidine-rich areas and rarely as small ($<$ 0.25 mm long; LH15/1 and LH17/48) non-poikilitic euhedral laths proximal to vesicles. Within these orendites, sometimes sanidine and sometimes leucite predominates and crystallises earlier (Carmichael, 1967). The groundmass of the madupites consists of phlogopite and dirty grey-brown altered glass.

Accessory minerals may include apatite, priderite and opaques (spinels?). Small anhedral perovskite grains are quite abundant in the madupites, but they were not found in the wyomingite/orendites, which is consistent with the observations of Carmichael (1967). Wadeite may be present (Carmichael, 1967; Kuehner et al., 1981), but was not observed in this study. Some of the samples are vesicular, however, only in the madupite from Pilot Butte were the vesicles infilled with zeolitic material.

A number of xenocrysts and xenoliths were also identified in some sections. Anhedral olivines (0.5 to 3 mm), which are either polycrystalline or exhibit strained extinction and which are always surrounded by a reaction rim of phlogopite laths, were observed in a number of samples (LH6/12, LH6/15, LH12/16). Analyses of similar olivines suggest that they were not in equilibrium with the host magma (Kuehner et al., 1981) and that they are similar in composition to olivines within a harzburgite xenolith from Hatcher Mesa (Barton and van Bergen, 1981). Hence, they are probably xenocrysts rather than high pressure phenocrysts as was suggested by Carmichael (1967).

A number of different clinopyroxene xenocrysts were observed. Large (0.5 to 2 mm; LH6/15, LH9/1, LH12/16, LH13/18, LH17/19) anhedral colourless clinopyroxenes, often surrounded by a phlogopite reaction rim, may be similar to the augites described by Carmichael (1967) and Kemp (1897, cited by Kuehner et al., 1981). Bright green, isotropic anhedral crystals, which are again surrounded by a reaction rim of phlogopite (LH5/9 and LH13/18) and slightly pleochroic pale to mid-green clinopyroxenes with colourless possibly diopsidic rims (LH15/1) may represent the salitic pyroxenes from Hatcher Mesa described by Barton and van Bergen (1981) who believed they are xenocrysts from disaggregated ultramafic xenoliths.

The dark green to black pleochroic cores of some phlogopites from LH17/19 differ from the near colourless to red-brown pleochroic megacryst phlogopites reported by Barton and van Bergen (1981), but may still be xenocrysts of

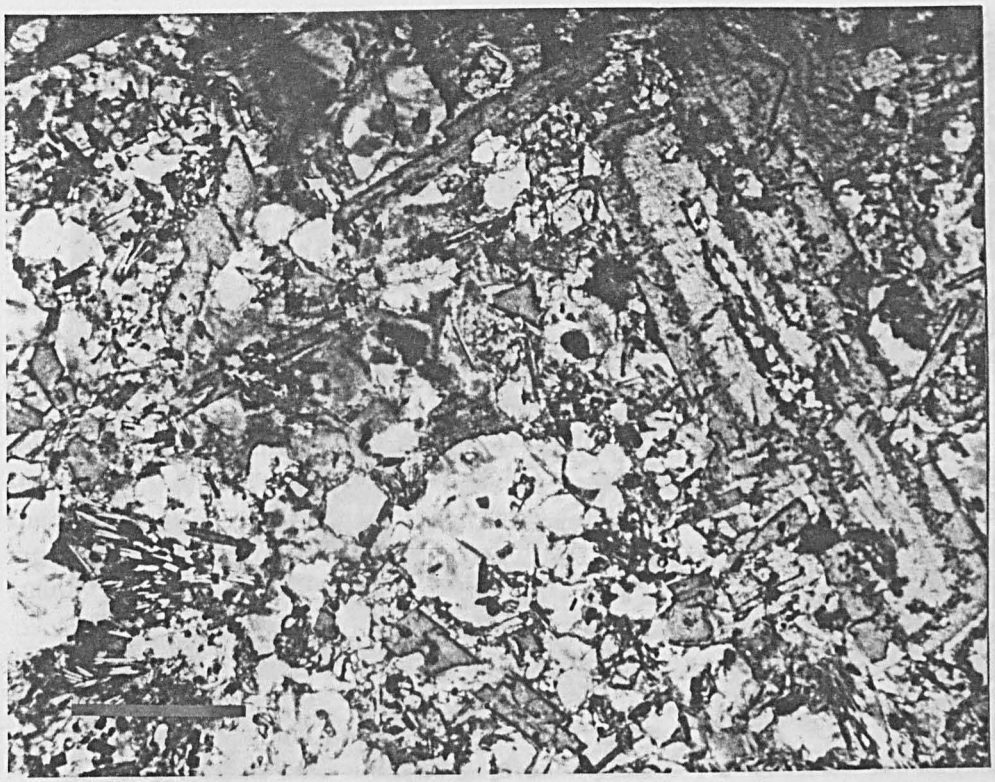

Plate 4.4 SB59; Vitrophyric analcite olivine phlogopite lamproite from Smoky Butte (PPL). Scale bar = 0.5 mm

unknown origin.

There is also a large (1 mm) xenocryst in LH17/19, which is dirty grey in colour. It has low birefringence colours and a thin secondary overgrowth of ragged material which is similar in colour to the core, but not in optical continuity with the core. The xenocryst may be a feldspar with overgrowth of sanidine. (Carmichael, 1967). A few small (< 1.5 mm), often partially assimilated, country rock xenoliths were also observed.

4.4.2 Smoky Butte

The mineralogy and mineral chemistry of the Smoky Butte rocks has previously been described by Matson (1960), Velde (1975) and Mitchell et al. (1987) who show that these rocks consist of various combinations of olivine, phlogopite, clinopyroxene (diopside), opaque oxides (armalcolite), analcite (?pseudomorphs after leucite), sanidine, glass, amphibole (K-richterite), priderite and apatite. Mineral assemblages which clearly demonstrate they belong to the lamproite suite of rocks.

Modal analyses of the six samples studied (five of which are also discussed in Mitchell et al., in prep.) can be found in Appendix C.1. Apart from SB35, which appears to be of pyroclastic origin, the samples are magmatic rocks (e.g. Plates 4.4 and 4.5). In the coarser grained rocks (SB11, SB59 and SB66) phenocrysts of olivine and phlogopite are present. The phlogopites form subhedral laths and are strongly pleochroic in shades of yellow-orange to deep orange. Velde (1975) showed that phlogopites at Smoky Butte are highly titaniferous (TiO_2 = 9.36 wt%). Olivines form euhedral crystals

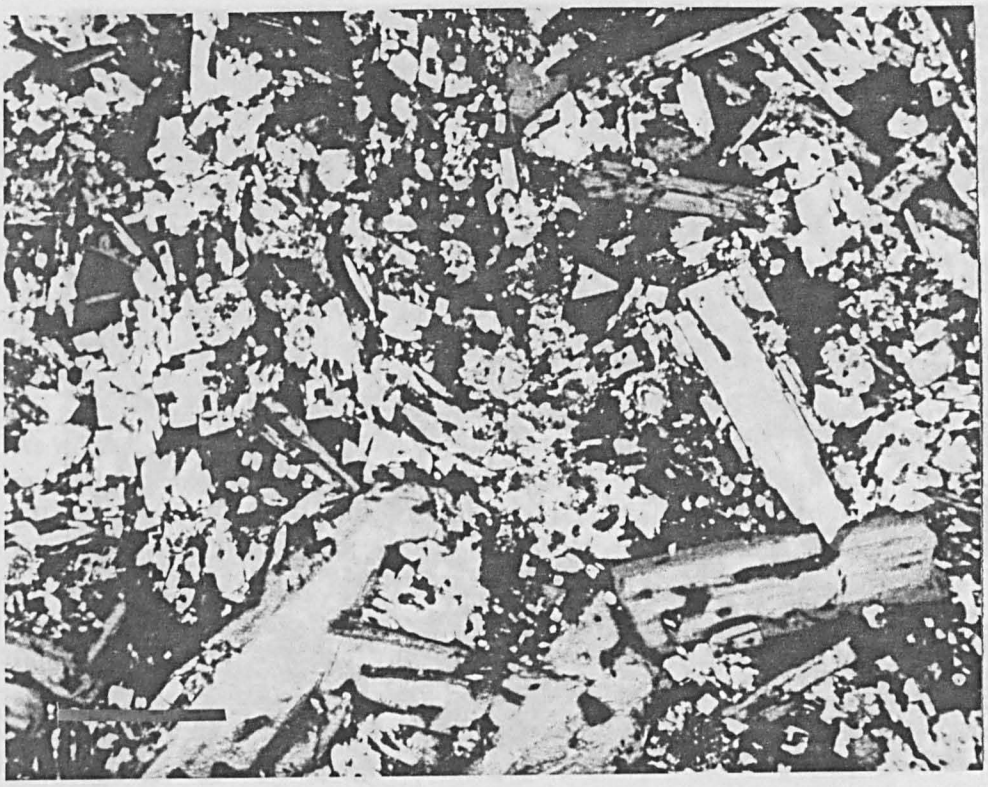

Plate 4.5 SB66; Sanidine lamproite from Smoky Butte (PPL). Scale bar = 0.5 mm

which are often serpentinised. Both the phlogopite and olivine phenocrysts generally show signs of extensive resorption, indicating that at the time of groundmass crystallisation, they were no longer in equilibrium with the melt. Phlogopite occurs only once as a groundmass phase (SB45), where it forms small anhedral poikilitic plates.

Clinopyroxene and purplish, near opaque oxides are present as ubiquitous, sub-euhedral microphenocrysts in all the magmatic samples. The clinopyroxenes are diopsidic in composition and the opaque oxides have the general composition $(Ti_{0.80}Si_{0.03})\,(Al_{0.04}Cr_{0.02}Fe^{3+}_{0.02})\,(Fe^{2+}_{0.38}MgO_{0.57})O_5$, corresponding to that reported for lunar armalcolite, except for the presence of trivalent iron, in the Smoky Butte samples (Velde, 1975). Armalcolite is a pseudobrookite-like mineral, which has also been noted as a primary phase in lamproites from Cancarix (Spain) and Moon Canyon (Utah) (Wagner and Velde, 1986). In the glass-rich section SB59, colourless isotropic euhedral microphenocrysts, with the morphology of leucite, are abundant. Microprobe analyses of such grains have shown they have the composition of Si-rich analcite (Velde, 1975). Velde (op. cit.) suggested that the analcite may be a low temperature replacement of earlier crystallising, higher temperature leucite.

The groundmass of these rocks mainly consists of yellow-brown isotropic glass (SB11, SB70), sanidine (SB45) or both (SB59, SB66). Sanidine may occur as anhedral patches (SB45), interlocking subhedral, long blocky laths with square cross-sections (SB66), or as thin laths in radial clusters (SB45, SB59). K-richterite, pleochroic from pale yellow to pale pink, forms late-

stage euhedral microphenocrysts and anhedral plates in thin-section SB66. Priderite, present in some Smoky Butte rocks (Velde, 1975) was not found in the thin-sections studied here.

The presence of glass, radial clusters of sanidine and acicular clinopyroxene and armalcolite are indicative of rapid quenching. A crystallisation temperature of 965°C, has been calculated for the Smoky Butte rocks, using the relationship established by Helz (1979), which is based on the partitioning of Na and K between amphibole and liquid, i.e. glass (Wagner and Velde, 1986).

According to the lamproite nomenclature proposed by Scott Smith and Skinner (1984a, b) and modified by Mitchell (1985), the five magmatic lamproites can be classified as follows;

SB11 Vitrophyric armalcolite-phlogopite lamproite.

SB45 Armalcolite-phlogopite-sanidine lamproite.

SB59 Vitrophyric analcite-olivine-phlogopite lamproite.

SB66 Sanidine lamproite.

SB70 Vitrophyric armalcolite lamproite.

SB35 is a pyroclastic rock with a very fine-grained altered groundmass and contains clasts of country rock quartz and rare euhedral olivine crystals.

4.4.3 Prairie Creek

Three sections were studied from the Prairie Creek intrusion. They are mineralogically all very similar and correspond closely to the petrographic descriptions of hypabyssal Prairie Creek material given by Scott Smith and Skinner (1984a). Modal analyses can be found in Appendix C.1. All three samples are olivine lamproites. Thin section PK1/18 is discussed both in this study and by Scott Smith and Skinner (op. cit.).

The rocks have a porphyritic texture owing to the presence of two generations of olivine (Plate 4.6). The larger (1.5 to 4 mm) of the populations are generally anhedral in shape and many show signs of resorption. Some, however, are subhedral in shape, often with parts of the crystal margin having a complex but euhedral shape (Figure 1 in Scott Smith and Skinner, 1984a). They are often serpentinised, although some of the larger grains may have fresh cores which tend to show evidence of strain, such as undulose extinction, while some grains were obviously polycrystalline prior to serpentinisation. These features suggest that these olivines, like the macrocrystic olivines in kimberlites, may be xenocrystic in origin. The second of

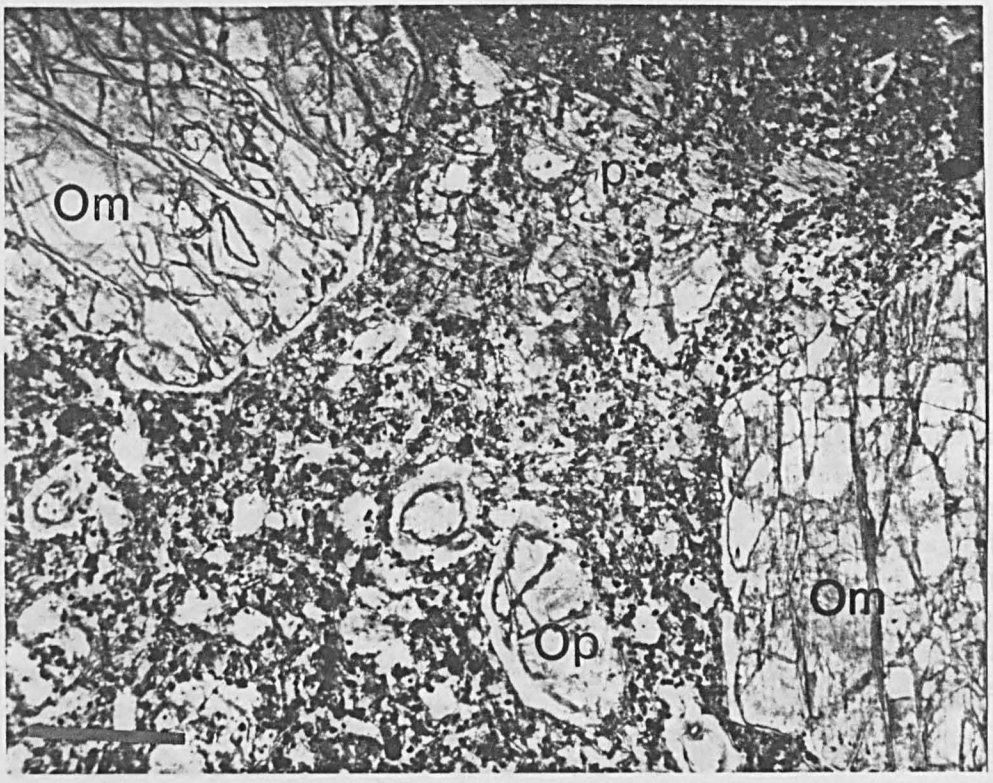

Plate 4.6 PK1/4; Olivine lamproite from Prairie Creek; Om = olivine macrocryst, Op = olivine phenocryst, P = phlogopite (PPL). Scale bar = 0.5 mm.

the two populations are smaller in size (< 2 mm), subhedral in shape and are invariably serpentinised. In general, olivine serpentinisation is zoned with a very thin rim (0.1 mm) of optically distinct serpentine around both the phenocryst and macrocrystic olivines.

Clinopyroxene (diopside) forms small (≤ 0.5 mm) euhedral phenocryst laths. Subhedral to euhedral perovskite (< 0.1 mm) and red-brown to opaque spinels (< 0.2 mm) are found scattered throughout the groundmass.

The above minerals are set in a groundmass consisting of phlogopite, amphibole and glass. Differences between the sections studied are usually due to the groundmass grainsize. The phlogopite is poikilitic and occurs as individual laths or forms areas of interlocking laths. They are pleochroic in shades of yellow and orange and simple twinning is sometimes evident. The amphibole (K-richterite; Scott Smith and Skinner, 1984a) is pleochroic pale yellow to pale pink, contains fewer inclusions than the phlogopite and forms irregular late-stage plates unevenly distributed throughout the groundmass.

4.5 Major element geochemistry

The lamproites from Smoky Butte, Prairie Creek and Leucite Hills exhibit a wide range in SiO_2 contents (SiO_2 = 38 to 54 wt%). The madupites from Leucite Hills are Si-undersaturated, the Prairie Creek lamproites are Si-saturated, while the wyomingite/orendites from Leucite Hills and the Smoky Butte lamproites are Si-saturated to oversaturated (Carmichael, 1967; Kuehner et al., 1981; Velde, 1975; Bergman, 1987; Bolivar and Brookins, 1979).

These lamproites also, in general, have high MgO (= 3.64 to 27.92 wt%; SB70 = 0.98 wt%; average = 9.57 wt%) and K_2O (= 2.34 to 12.34 wt%; average = 9.03 wt%) contents combined with low Al_2O_3 (= 3.85 to 11.06 wt%; average = 8.95 wt%) and Na_2O (= 0.13 to 2.34 wt%; average = 1.09 wt%) contents. Thus, they have high *mg* numbers (= 0.62 to 0.87; SB70 = 0.30; average = 0.76) and they are ultrapotassic rocks (K_2O/Na_2O = 5 to 78 with the exception of SB11, where $K_2O/Na_2O = 1$) rocks. Furthermore, they exhibit high (K + Na)/Al ratios (= 0.75 to 1.58; average = 1.26). The Smoky Butte and Leucite Hills rocks, with the exception of SB11 and LH19/25, are all peralkaline i.e. (K + Na)/Al > 1. The majority of the Leucite Hills rocks are also perpotassic ($K_2O/Al_2O_3 > 1$). The major element analyses for these rocks are compared, using Harker diagrams, in Figure 4.4 where major element oxides are plotted against SiO_2.

The Leucite Hills data are divided, on the basis of mineralogy, into the wyomingite/orendite and madupite groups. In general, the data corroborate those of Ogden (1979). Taking both groups together, Al_2O_3 and K_2O vary proportionally with SiO_2, while MgO, CaO, P_2O_5, MnO, LOI and Fe_2O_3 vary inversely with SiO_2. However, the madupites tend to have lower SiO_2, Al_2O_3, K_2O and higher Fe_2O_3, MnO, LOI and CaO contents. Madupites from Pilot Butte exhibit the lowest Al_2O_3, K_2O and SiO_2 contents, but the highest CaO, MnO and LOI contents, while the data for the Middle Table Mountain madupites are intermediate between the Pilot Butte madupites and the wyomingite/orendite field. Most samples also confirm that chemical variation in the Leucite Hills rocks is predominantly between localities rather than within each locality, although individual data points from this study may extend the fields of Ogden (1979). The Pilot Butte, madupite samples reported here have lower SiO_2 contents than those published by Ogden (1979) and Kuehner et al. (1981). However, they are consistent with the major element trends as outlined above, except for rather low Fe_2O_3 contents and in one case (LH 19/25) a low MgO content. LH 19/25 also has a high volatile content, but low alkali content, which suggests that it is rather altered. Ogden (1979) remarked that the Black Rock locality is at the lowest elevation of all the Leucite Hills occurrences and samples may be contaminated by groundwater i.e. lower K_2O, but higher Na_2O contents. Although the Black Rock samples studied here show petrographic evidence of some groundmass alteration, they plot in major element terms within the main wyomingite/orendite field i.e. they have high K_2O, but low Na_2O contents, albeit they may extend to slightly high volatile contents. Within the wyomingite/orendite data, samples from Hatcher Mesa are generally poor in SiO_2 and rich in CaO and Na_2O, which Barton and van Bergen (1981) suggested may be either a primary geochemical characteristic of the lavas or reflects the abundance of megacrysts in these lavas.

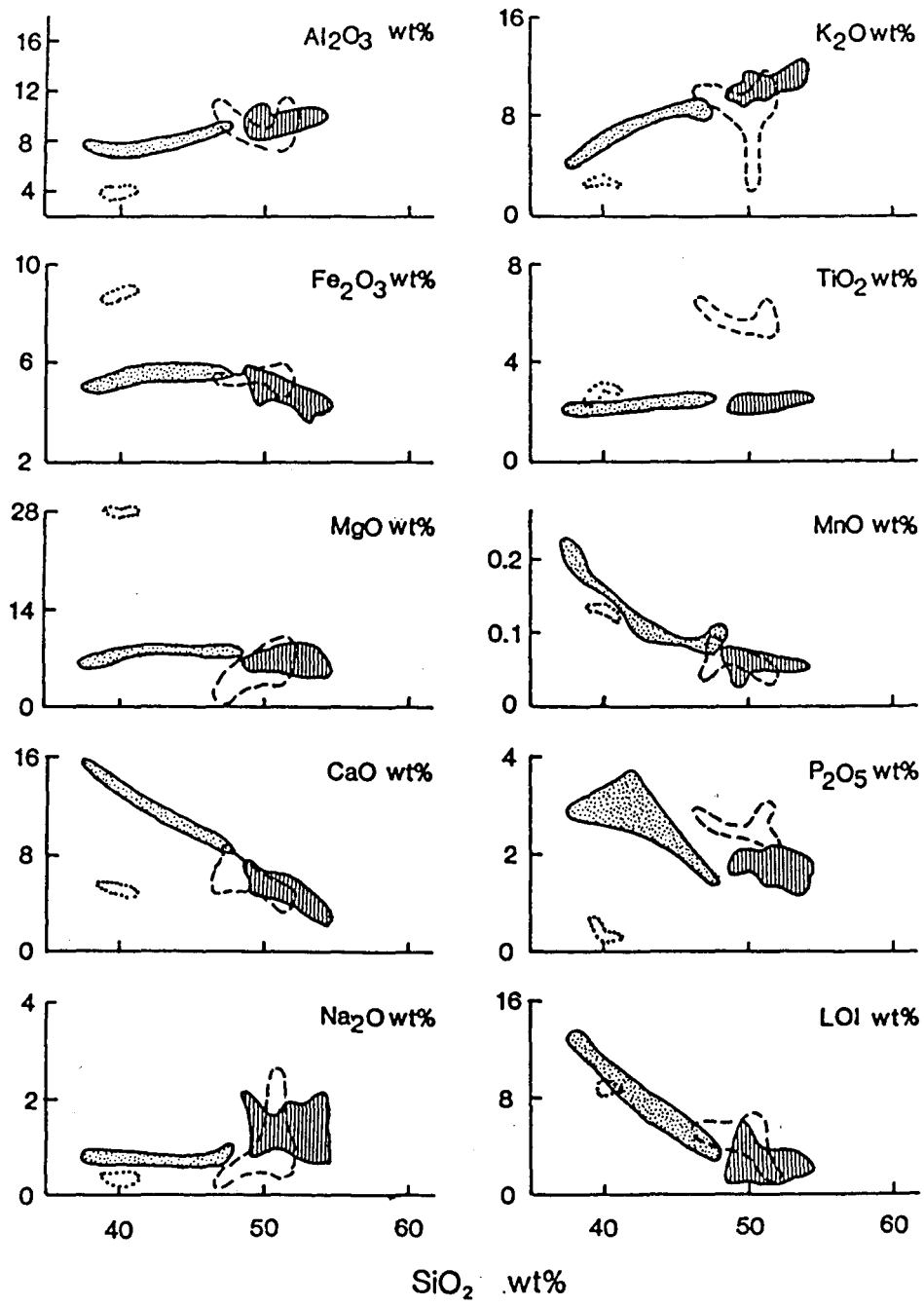

Figure 4.4 Oxide variation with SiO_2 content (wt%) in North American lamproites. Leucite Hills; madupites = stippled field, wyomingite/orendites = vertically lined field, Smoky Butte = dashed line and Prairie Creek = dotted line.

The majority of the Smoky Butte samples have SiO_2 contents that fall in the range of the wyomingite/orendite field. SB45 (SiO_2 = 47.8 wt%) is intermediate between the two Leucite Hills fields and SB70 (SiO_2 = 46.8 wt%) falls in the madupite field. In general, the major element contents of the Smoky Butte rocks overlap with the Leucite Hills data, but there are a few differences which may relate to either alteration, or source differences. SB11 and SB59 have low K_2O (2.34 and 6.38 wt%) and high Na_2O (2.34 and 1.30 wt%) contents relative to the other Smoky Butte samples (8.31 to 10.69 wt% and 0.13 to 0.80 wt% respectively). Both these samples are glass-rich and the differences may relate to groundwater alteration (Mitchell et al., 1987), although sample SB70 has a high glass content, it still has high K_2O (10.08 wt%) and low Na_2O (0.13 wt%) contents. However, SB70 is unusual in having an extremely low MgO content (0.98 wt%) relative to the others (3.64 to 9.19 wt%). Compared to the other samples, no olivine was noted in SB70. P_2O_5 = 2.23 to 2.87 wt% reported in this study (and Mitchell et al., in prep.) are significantly higher than those reported in Velde (1975) where P_2O_5 = 0.22 to 0.25 wt% and at the high end of the range quoted by Bergman (1987) where $P_2O_5 = 1.7 \pm 0.9$ wt% (n = 13). It is of interest to note that SB35, the pyroclastic sample from Smoky Butte, has a major element composition indistinguishable from the magmatic samples.

Compared to the Leucite Hills lamproites, the Smoky Butte samples have high P_2O_5 contents for a given SiO_2 content. They also have much higher TiO_2 contents (= 5.32 to 638 wt%) than the Leucite Hills rocks (TiO_2 = 2.05 to 2.62 wt%). These features may reflect source differences between the two localities.

The three Prairie Creek hypabyssal lamproites analysed here show little chemical variation and are comparable with whole rock data reported by Scott Smith and Skinner (1984a). They are generally quite distinct in major element contents from both the Leucite Hills and Smoky Butte lamproites (Figure 4.4). They have relatively low SiO_2 contents (39.3 to 41.1 wt%) which fall at the low SiO_2 end of the madupite field, but much higher MgO and Fe_2O_3 and lower Al_2O_3, K_2O and P_2O_5 contents. Na_2O and CaO contents overlap with the Smoky Butte data, while the TiO_2, MnO and LOI contents are comparable with the madupite data. Scott Smith and Skinner (1984) demonstrated that the Prairie Creek major element data is intermediate between the Holsteinberg (Greenland) lamproite and kimberlite fields. The high MgO and Fe_2O_3 contents at Prairie Creek can be attributed to the high modal % of olivine.

4.6 Trace element geochemistry

4.6.1 The compatible trace elements

Partial melting of a peridotite mantle with an *mg* number = 0.92, Ni = 2000 ppm and Cr = 3000 ppm yields a primary liquid where the *mg* number = 68 to 74, Ni = 300 to 400 ppm and Cr = 400 to 500 ppm (Kuehner et al., 1981). As outlined above (Section 4.5), all the North American lamproites analysed within this study (except the low Mg sample from Smoky Butte) have high *mg* numbers (= 0.62 to 0.87). The Ni and Cr contents of these rocks are also high and in some cases may be consistent with their being primary mantle melts e.g. Leucite Hills wyomingite/orendites; Ni = 135 to 429 ppm and Cr = 262 to 532 ppm and the Smoky Butte lamproites; Ni = 115 to 341 ppm and Cr = 365 to 520 ppm.

Within the Leucite Hills data, the madupite rocks have lower Ni (120 to 171 ppm), but comparable Cr (305 to 405 ppm) contents to the wyomingite/orendites. Kuehner et al. (1981) suggested that the lower Ni contents in the madupites may be attributable to olivine fractionation, although they considered that the absence of olivine and the high *mg* numbers of the madupites might preclude this model. In the Smoky Butte lamproites, the Ni contents are correlated with MgO and may relate to the relative abundance of olivine. On the other hand, the Prairie Creek lamproites have much higher Ni (1285 to 1443 ppm) and Cr (1440 to 1500 ppm) contents than in either the aforementioned lamproites, or predicted values for primary mantle melts. These values are, however, comparable to those found in kimberlites e.g. the Finsch mine Group 2 kimberlites from South Africa have Ni = 1063 to 1544 ppm and Cr = 1420 to 2051 ppm. In the Finsch mine kimberlites these high Ni and Cr contents were attributed to the presence of disaggregated mantle peridotite which had been entrained by the kimberlite primary melts en route to the surface (Section 2.10.4). Like kimberlites, the Prairie Creek lamproites contain two discrete olivine populations, one of which may be xenocrystic, an interpretation also favoured by Scott Smith and Skinner (1984a).

4.6.2 The incompatible trace elements

All three lamproite suites are highly LREE enriched (La = 112 to 437 pm) and exhibit steep chondrite normalised profiles (Ce_N/Yb_N = 42 to 123) which may flatten out at the LREE and HREE ends (Figure 4.5). Within individual suites or groups, the data forms parallel to sub-parallel trends.

Considering the Leucite Hills data (Figure 4.5a), the madupites are more LREE enriched (La = 260 to 357 ppm) and exhibit steeper profiles (Ce_N/Yb_N = 97 to 123) than the wyomingite/orendites (La = 112 to 182

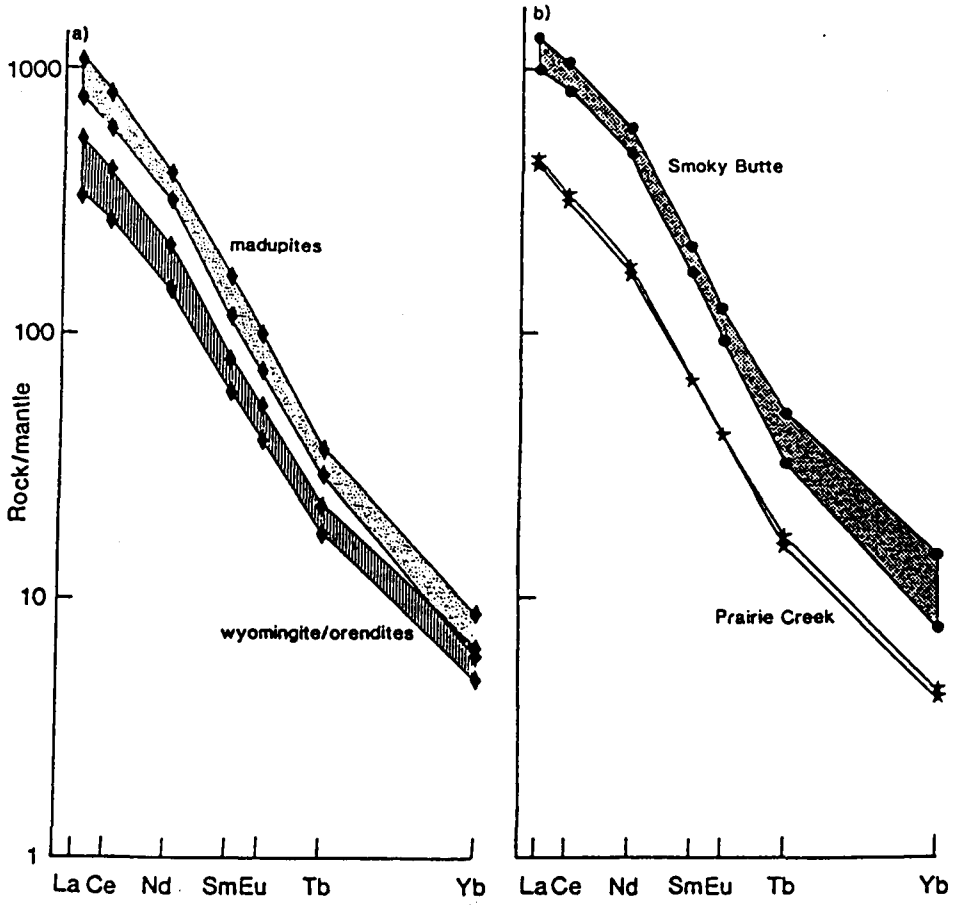

Figure 4.5 Mantle normalised REE patterns for North American lamproites, showing the range for a) Leucite Hills (◆); madupites = stippled and wyomingite/orendites = vertically lined and b) Smoky Butte = • and stippled field and Prairie Creek = ⋆.

ppm, Ce_N/Yb_N = 42 to 80). The two rock-types overlap in their HREE abundances (madupites Yb = 1.3 to 1.49 ppm; wyomingite/orendites Yb = 1.00 to 1.45 ppm). Within the madupite data, the sample from Pilot Butte is more LREE enriched than the Middle Table Mountain samples (La = 357 ppm and 260 to 273 ppm respectively). The wyomingite/orendite data again show that variation between localities is greater than intralocality variation.

The La content of the Smoky Butte samples (La = 332 to 437 ppm) overlaps with, and extends to higher values than the madupites. However, due to generally higher Yb abundances (= 1.69 to 3.19 ppm relative to 1.45 to 1.91 ppm in the madupites) the Smoky Butte lamproites have Ce_N/Yb_N ratios = 101 to 112, within the madupite range (Figure 4.5b).

The Prairie Creek samples (Figure 4.5b) have La contents (= 142 to 147 ppm) in the middle of the wyomingite/orendite range, but they exhibit slightly steeper profiles . The Ce_N/Yb_N values (= 72 to 80) are at the high end of the wyomingite/orendite range owing to the lower Yb contents at Prairie Creek (= 0.90 to 0.96 ppm). Although the Prairie Creek lamproites and Finsch mine Group 2 kimberlites from South Africa have comparable compatible trace element contents (Section 4.6.1) the Prairie Creek samples have higher La contents and steeper profiles than the Finsch kimberlites where La = 42 to 110 ppm and Ce_N/Yb_N = 33.5 to 56.9 (Section 2.7.2).

Incompatible trace element data for the three lamproite suites are plotted on trace element abundance diagrams (Figure 4.6) which include some of the REE data.

The madupite and wyomingite/orendite groups from the Leucite Hills plot on two distinct profiles (Figure 4.6a). Generally, both groups exhibit quite similar shaped profiles and show high degrees of enrichment in the incompatible trace elements. Ba and La are enriched by a factor of > 750 × mantle. Both suites show peaks at Ba, La, Hf and Zr, but troughs at Pb, Ta, Ti, P and Sr, although the Sr trough is more pronounced in the madupites. However, a number of differences between the two groups are also evident. In addition to LREE and the MREE, the madupites exhibit high Pb, Th and Ta contents and generally higher, but overlapping, Rb, Ba, Sr and P contents. There is a peak at K within the wyomingite/orendite samples which is not evident in the madupite profile. The madupites, in general, have lower K contents. Zr and Ti contents of the madupites are either lower, or plot within the lower part of the wyomingite/orendite trend.

The Smoky Butte and Prairie Creek suites are shown on Figure 4.6b. The Smoky Butte samples are highly trace element enriched with Ba and La enriched by a factor of over 1000 × mantle. Pronounced peaks are evident at Ba, K, La and Zr and troughs occur at Pb, Th, Ta, Sr and P. The Prairie Creek samples are less trace element enriched than the Smoky Butte rocks, although Rb and La are still enriched by a factor of > 400 × mantle. Peaks

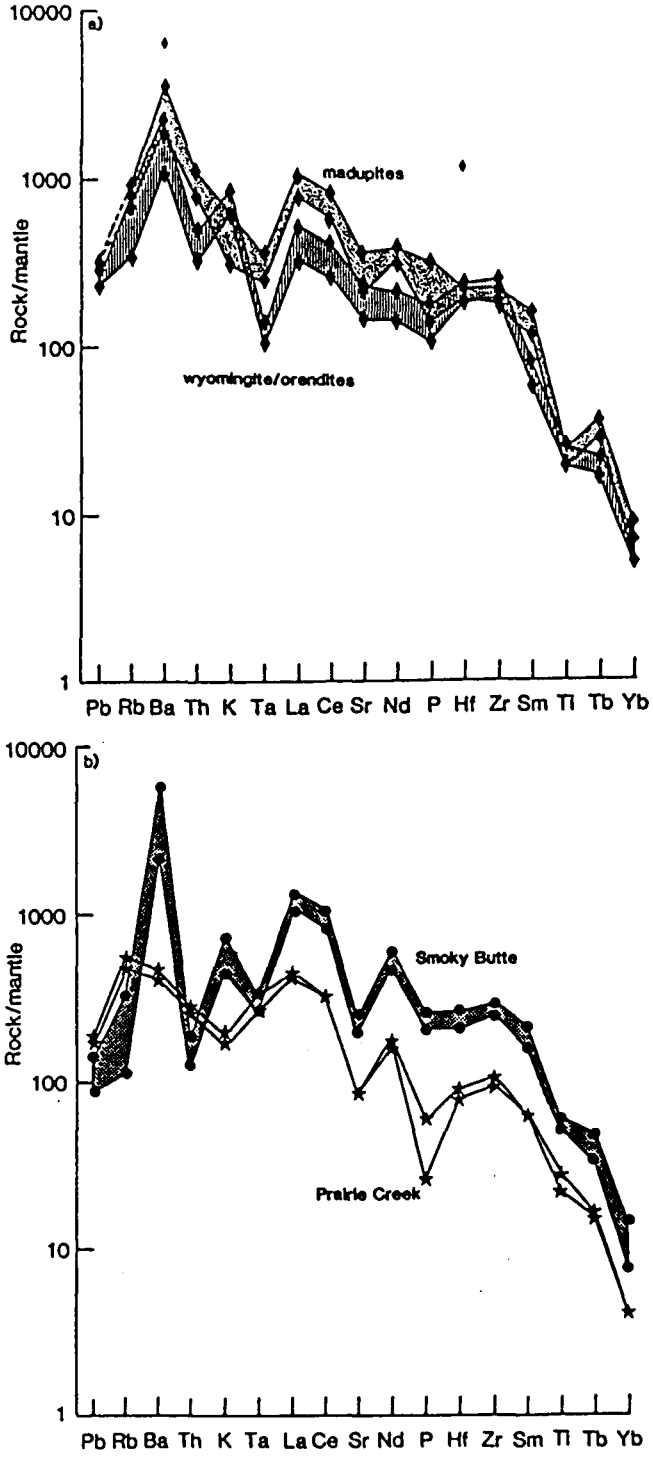

Figure 4.6 Mantle normalised trace element data for North American lamproites. Symbols as in Figure 4.5.

are evident at Rb, La and Zr and troughs at Pb, K, Sr and P. On Figure 4.6b both the Smoky Butte and Prairie Creek rocks have similar shaped profiles in the elements from La to Yb, although the Prairie Creek samples have a more pronounced trough at P. From Pb to Ta, however, the profiles are quite distinct. The Prairie Creek samples have higher Pb, Rb and Th, but similar Ta contents. The Smoky Butte samples exhibit peaks at Ba and K, whereas the Prairie Creek rocks have no peak at Ba and a trough at K.

Both Smoky Butte and Prairie Creek lamproites exhibit different shaped profiles to the Leucite Hills lamproites. The latter have pronounced troughs at Ti, Sr and P, but the most obvious differences again lie in the elements from Pb to Ta. Like Smoky Butte, both the Leucite Hills suites exhibit peaks at Ba, although only the wyomingite/orendites have a trough at Th and peak at K. The madupites have the highest Th contents and relatively low K contents. Smoky Butte has extremely low Pb and Rb contents relative to the other localities. The madupites, Smoky Butte and Prairie Creek lamproites have virtually identical Ta contents, whereas the wyomingite/orendites exhibit significantly lower Ta.

4.7 Isotope geochemistry

4.7.1 Sr and Nd isotopes

All three lamproite suites have higher εSr and lower εNd than the bulk earth and plot in the bottom right quadrant of the εNd – εSr diagram (Figure 4.7). Thus, they contain a contribution from old LREE enriched (low Sm/Nd) material which most observers would place within the lithosphere, be it subcontinental mantle or continental crust.

The Leucite Hills and Smoky Butte data plot on a steep sub-vertical trend with low εSr which shows little variation (εSr: Leucite Hills = 9.8 to 18.7, Smoky Butte = 16.4 to 23.2), but an extreme range in εNd extending down to -26 in the Smoky Butte samples. The Leucite Hills data from this study confirm those of Vollmer et al. (1984) which showed that the madupites and wyomingite/orendites plot in two distinct fields. Both groups have overlapping and relatively low εSr values (εSr: madupites = 9.8 to 12.8 and wyomingite/orendites = 10.6 to 18.7). But the madupites have higher εNd (= -10.5 to -12.3) than the wyomingite/orendites (= -13.7 to -17.9). Vollmer et al. (1984) suggested this was due, either to slightly different source regions, or mixing.

The Prairie Creek rocks have similar εNd values (= -10.6 to -11.2) to the Leucite Hills madupites, but have slightly higher εSr values (= 29.4 to 34.5) such that they plot to the right of the steep trend defined by the Leucite Hills and Smoky Butte lamproites (Figure 4.7).

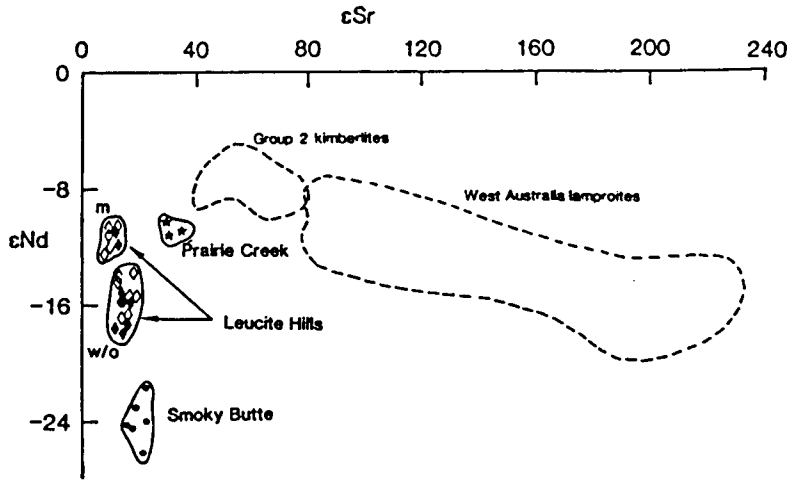

Figure 4.7 εNd vs. εSr for the North American lamproites. Symbols as in Figure 4.5. Filled symbols = this study, open symbols = Vollmer et al. (1984). m = madupites and w/o = wyomingite/orendites. These are compared with fields for Group 2 kimberlites (this study and Smith, 1983a) and West Kimberley lamproites (this study and McCulloch et al., 1983).

4.7.2 Pb isotopes

The Pb isotopes for the three lamproite suites are shown on Figure 4.8. They exhibit a wide range in $(^{206}Pb/^{204}Pb)_i$ = 16.01 to 17.54, $(^{207}Pb/^{204}Pb)_i$ = 15.19 to 15.50 and $(^{208}Pb/^{204}Pb)_i$ = 36.17 to 37.55. All three suites plot below the Stacey and Kramers (1975) growth curve, implying long-term evolution in a low μ environment.

The Leucite Hills lamproites exhibit more radiogenic Pb contents than either of the other suites. The madupite (from Middle Table Mountain) has a more radiogenic Pb content i.e. $(^{206}Pb/^{204}Pb)_i$ = 17.54, $(^{207}Pb/^{204}Pb)_i$ = 15.50, $(^{208}Pb/^{204}Pb)_i$ = 37.55, than the wyomingite/orendites, where $(^{206}Pb/^{204}Pb)_i$ = 17.15 to 17.28, $(^{207}Pb/^{204}Pb)_i$ = 15.43 to 15.47, $(^{208}Pb/^{204}Pb)_i$ = 37.18 to 37.34. These data are insufficient to establish whether this is a consistent pattern.

The low εNd Smoky Butte rocks have extremely unradiogenic Pb contents e.g. $(^{206}Pb/^{204}Pb)_i$ = 16.01 to 16.57, $(^{207}Pb/^{204}Pb)_i$ = 15.19 to 15.27. The Prairie Creek rocks have similarly low $(^{206}Pb/^{204}Pb)_i$ ratios = 16.58 to 16.64, but higher $(^{207}Pb/^{204}Pb)_i$ ratios = 15.30 to 15.36.

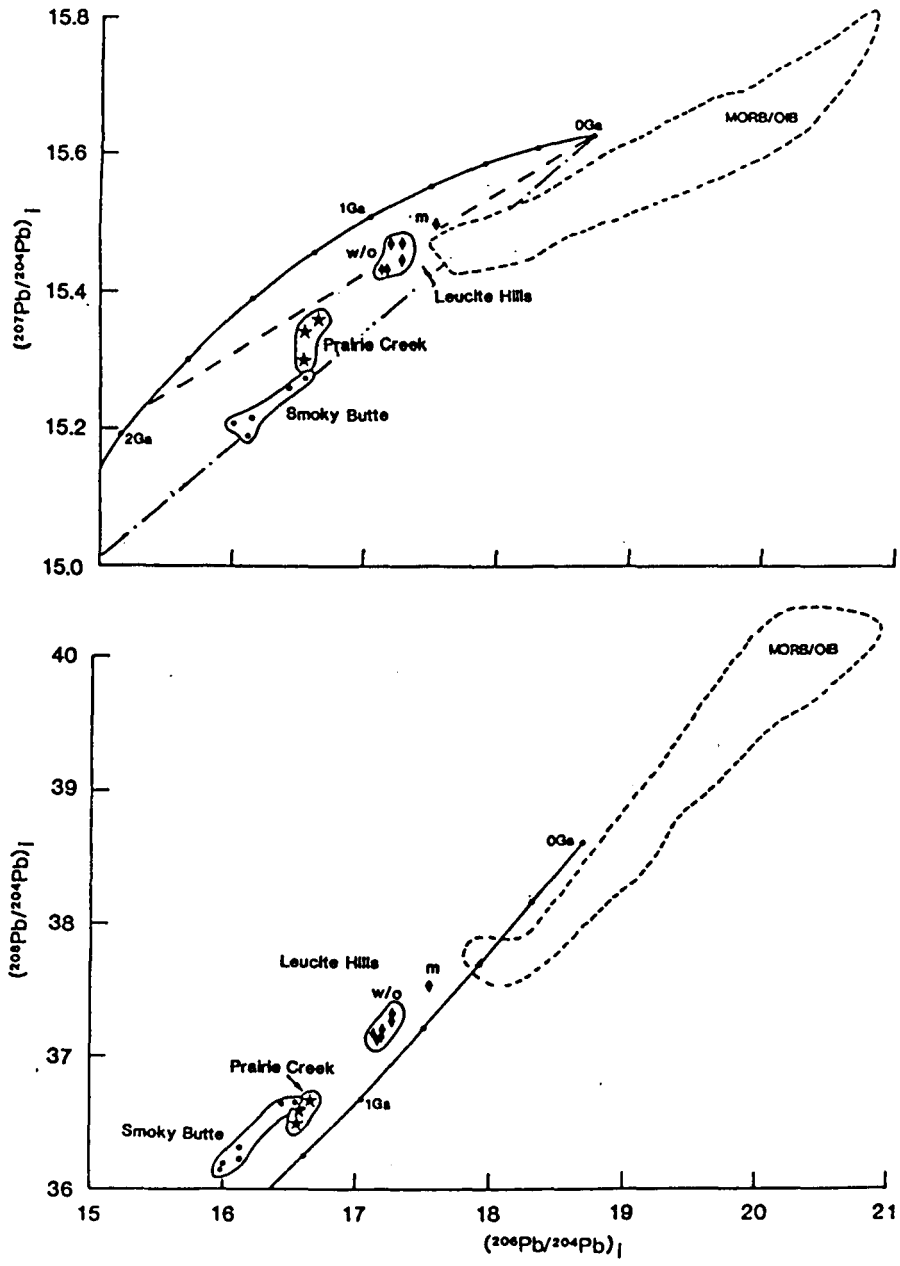

Figure 4.8 Initial Pb isotope ratios for the North American lamproites. Symbols as in Figure 4.7. These are compared with a field for selected MORB and OIB (as in Figure 2.12). The Pb-ore curve is from Stacey and Kramers (1975).

4.8 Petrogenesis

4.8.1 Crust or mantle?

Low εSr and low εNd, as observed in these lamproites, have often been regarded as indicative of a lower crustal origin (Moorbath and Taylor, 1985). Similarly, unradiogenic Pb isotopes have also been taken to be diagnostic of old granulite facies lower crustal material. And yet the present consensus is that fresh lamproites are primitive mantle melts and their trace element and radiogenic isotope compositions reflect mantle rather than crustal processes.

All the rocks studied here have high *mg* numbers, Ni and Cr contents, often similar to those regarded as typical for primary melts (Section 4.6.1). This is further reinforced by the high forsterite content of the olivine phenocrysts within these rocks, Fo = 87 to 93 (Scott Smith and Skinner, 1984a; Mitchell, 1985; Kuehner et al., 1981).

Ultramafic xenoliths are rare, although a phlogopite-chromite-harzburgite has been observed in a lava from a Leucite Hills lamproite (Barton and van Bergen, 1981) and diamonds have been retrieved from the Prairie Creek lamproite. Experimental studies from atmospheric conditions up to 5 Kb P_{H_2O}, showed that both the wyomingite/orendites and madupites from Leucite Hills have extremely high liquidus temperatures (> 1200°C; Carmichael, 1967; Sobolev et al., 1975; Barton and Hamilton, 1979, 1982), comparable with those of the most common basaltic magmas and higher than those of average crustal material. At Smoky Butte, a high crystallisation temperature of 965°C was obtained from coexisting late-stage amphibole and glass (Wagner and Velde, 1986). Thus, these K-rich, highly trace element enriched lamproites represent high temperature primitive mantle melts.

This can also be argued from a trace element perspective. The abundances of certain trace elements are over 20 × higher than in either average continental crust, lower crust or melts thereof. Sr contents in the lamproites range from 972 to 4420 ppm in contrast to 260 to 503 ppm in average continental crust (Weaver and Tarney, 1984; Taylor and McClennan, 1985), 569 ppm in Archaean lower crust (Weaver and Tarney, 1984) and $\simeq$ 160 ppm in average syncollision granites (Pearce et al., 1984) which are regarded as typical upper crustal melts. Likewise, Nd in the lamproites = 91 to 379 ppm, while in average crust Nd = 16 to 23 ppm, in lower Archaean crust = 18.5 ppm and in the syncollision granites = 22 ppm. Clearly the continental crust is an unlikely source of such high Sr and Nd contents in the lamproites.

A comparable argument is illustrated in Figure 4.9 which shows that the Sm/Nd ratios of the lamproites are too low and Ta/Yb ratios generally too high to be due to interaction between MORB and OIB and the continental crust. However, this does not preclude mixing between OIB,

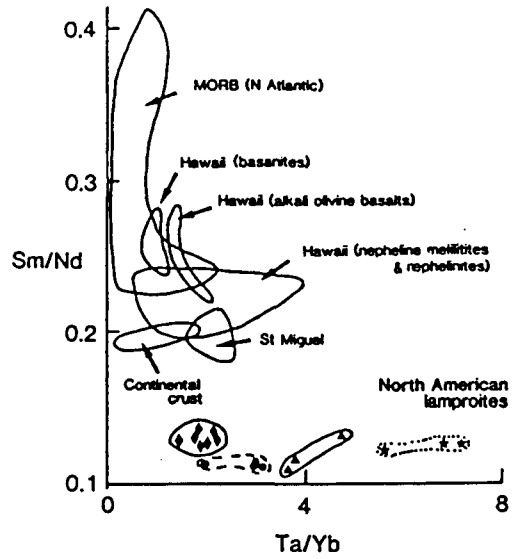

Figure 4.9 Sm/Nd vs. Ta/Yb for North American lamproites. • = Smoky Butte, ⋆ = Prairie Creek, ▲ = madupites, ◆ = wyomingite/orendites. These are compared with fields for selected ocean islands and the continental crust (as in Figure 2.14).

MORB or continental crust with a Leucite Hills madupite to generate the wyomingite/orendite compositions. The wyomingite/orendites are intermediate in composition between these potential endmembers, in terms of the REE, however, they have higher K, Hf, Zr and Ti contents than the trace element enriched madupites which appear to rule out mixing in this context. Vollmer et al. (1984) modelled Nd isotopes assuming bulk contamination of a madupite magma with crustal material. Using $\epsilon Nd = -30$ (after DePaolo and Wasserburg, 1979) and 26 ppm Nd for a crustal component of the Archaean Wyoming craton, the average Nd composition ($\epsilon Nd = -11$) and concentration (290 ppm) of madupite would require up to 85% assimilation of crust to change the Nd isotopic composition of the magma to that of a wyomingite/orendite magma with $\epsilon Nd = -17$. Such a mixture would have only half the Nd concentration actually observed in wyomingite/orendites. Therefore, if the high trace element contents are not due to crustal contamination, then neither are the unradiogenic Nd isotope ratios. Similar arguments can be applied to Sr and Pb isotopes and thus it is concluded that the isotope ratios and high trace element contents of these North American lamproites were derived from old segments of the subcontinental lithosphere.

4.8.2 Fractionation

As shown in the previous section, these North American lamproites are predominantly derived from mantle sources. Having ruled out crustal contamination as a process for generating high incompatible trace element contents from low incompatible trace element melts, an alternative and conventional method of achieving this is via fractionation processes.

The high Ni and Cr contents and *mg* numbers in these rocks argues against significant fractionation. At Leucite Hills, although both madupites and wyomingite/orendites have similar Cr contents, the latter have higher Ni contents. On diagrams of Ni vs. Cr and Ni vs. MgO (Figure 4.10) the wyomingite/orendites and madupites form distinct trends. Comparison with observed phenocryst phases suggest that these individual trends could originate by some fractionation of diopside in the madupites and phlogopite in the wyomingite/orendites. A peak at K in the wyomingite/orendites (Figure 4.6) and the clinopyroxene-rich nature of the madupites suggests only very minor fractionation. At Smoky Butte a positive correlation between the elements La and Cr preclude significant fractionation of phlogopite, spinel or garnet (Mitchell et al., 1987). Extremely high Ni and Cr abundances, and *mg* numbers at Prairie Creek may, partly, be due to the presence of abundant xenocrystic olivine. The presence of diamond, however, does require very rapid ascent from mantle depths.

Hence, the incompatible trace element contents observed in these North American lamproites are primary features of the magmas and reflect trace element enriched source characteristics and/or conditions of melt formation and extraction. The low εNd values of all these rocks indicate their source regions had long term low Sm/Nd ratios (LREE enriched) while the low degrees of partial melting inferred for magma genesis suggests that trace elements with $D < 1$ will be highly enriched in the resultant melt under batch melting conditions.

4.8.3 Age implications

The Rb/Sr and Sm/Nd ratios of these lamproites are likely to have been changed, relative to those in their source regions, during partial melting and emplacement. Thus, Sr and Nd isotopes cannot be used readily to infer the age of their source regions. However, Pb-Pb model ages are insensitive to changes in parent/daughter ratios during magmatism and so Pb isotopes may preserve useful age information. One interpretation of the lamproite data is shown in Figure 4.8, where two-stage Pb evolution models are illustrated. The Smoky Butte data are consistent with the development of relatively low U/Pb ratios ($\mu = 4.5$) at 2.5 Ga. The Leucite Hills data are not so well constrained. As outlined above, there are insufficient data to

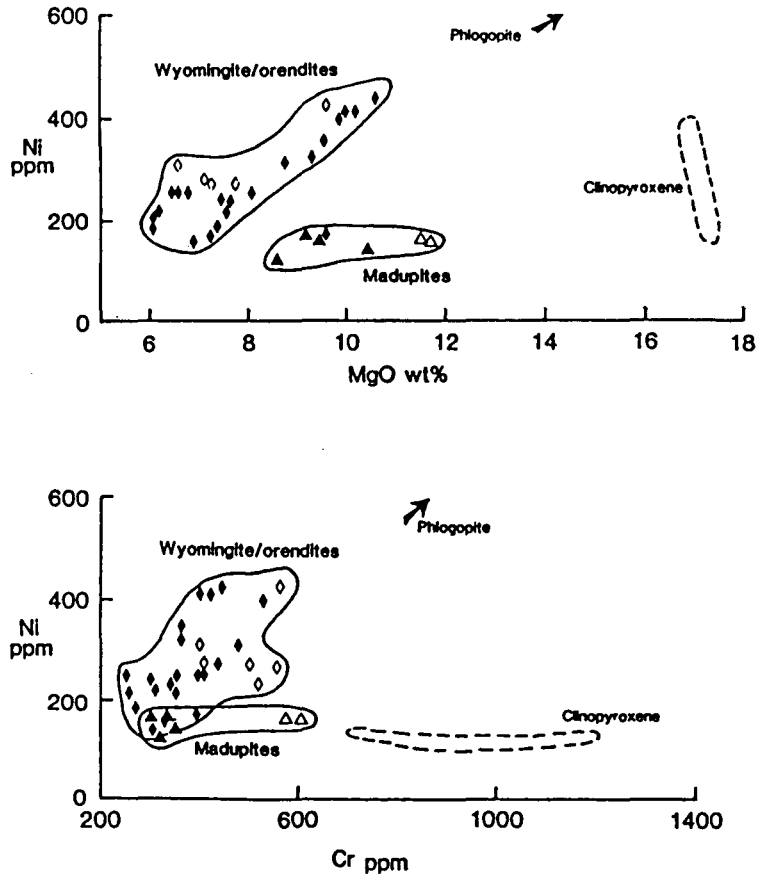

Figure 4.10 Ni vs. a) MgO wt%, and b) Cr ppm for the Leucite Hills lamproites. Filled symbols = this study and open symbols = Vollmer et al. (1984). Mineral compositions (phlogopites have Ni = 1021 to 3615 ppm, and MgO = 18.3 to 26.0 wt%) from Carmichael (1967), Kuehner et al. (1981) and Mitchell (1985).

determine whether there are significant differences between the madupites and wyomingite/orendites, while major and trace element variations have revealed small-scale (1 to 10 km) source heterogeneities which may well have affected the isotopic ratios. However, geographical, mineralogical and geochemical similarities between the Leucite Hills lamproites indicate that it is probable that their source regions formed at similar times. Slopes to individual points give model ages ranging from 1.7 to 2.1 Ga. Thus, low U/Pb ratios developed in the Leucite Hills source regions at approximately 1.9 Ga.

When considering the Prairie Creek data, it should be recalled that they have a high macrocrystic olivine content, together with high Ni and Cr comparable to kimberlites such as the Finsch mine Group 2 kimberlites from South Africa (Section 4.6.1). In the latter case, these features were believed to be representative of entrained and disaggregated peridotite (Section 2.10.4) and on a $(^{207}Pb/^{204}Pb)_i$ vs. $(^{206}Pb/^{204}Pb)_i$ diagram (Figure 2.12a) the Finsch data define a steep mixing trend. There are insufficient data on the Prairie Creek samples to determine if a similar situation applies. Moreover, there are no available data for mantle peridotites locally. However, inspection of the Pb isotope data for clinopyroxene separates from South African mantle xenoliths and xenocrysts (Kramers, 1977, 1979) suggest peridotite would represent an extremely unradiogenic endmember (Section 2.10.4 and Figure 2.12a). The 'melt' endmember would thus have a more radiogenic Pb isotopic composition, than the observed whole-rock ages. This would imply younger ages than those obtained from the slopes to individual data points, which range from just over 2.0 to 2.4 Ga. However, the Pb content of the Prairie Creek lamproites is over 170 × mantle compared to less than 14 × mantle in clinopyroxenes in peridotites (Kramers, 1977, 1979). Thus, the melt endmember must dominate both the Pb content and presumably the Pb isotopic composition. Hence, whatever the Pb isotope composition of the entrained peridotite, it is likely that the Prairie Creek data plot reasonably close to the trace element enriched melt endmember.

4.8.4 Rb/Sr and Sm/Nd fractionation

Pb-Pb model ages can be used to calculate the Rb/Sr and Sm/Nd ratios necessary to generate the observed εSr and εNd and these can be compared to the Rb/Sr and Sm/Nd ratios measured in the rocks.

Using Pb-Pb model ages of 2.5 Ga for Smoky Butte, 1.9 Ga for Leucite Hills and 2.0 Ga for Prairie Creek and taking into account the emplacement ages of these lamproites, inferred Rb/Sr and Sm/Nd ratios were calculated. In all three areas, the average measured Sm/Nd ratios (i.e. Leucite Hills: wyomingite/orendites = 0.12 to 0.14 and madupites = 0.11 to 0.12; Smoky

Butte $\simeq$ 0.11; Prairie Creek $\simeq$ 0.12) are less than those inferred for their source regions (i.e. Leucite Hills: wyomingite/orendites = 0.20 to 0.22 and madupites $\simeq$ 0.25; Smoky Butte = 0.19 to 0.21; Prairie Creek $\simeq$ 0.26). On average, measured Sm/Nd is 44% less than inferred source values. Rb/Sr is much more variable. Observed Rb/Sr ratios at Leucite Hills (= 0.08 to 0.16) and Prairie Creek (= 0.17 to 0.18) are higher than inferred source values (= 0.04 and 0.06, respectively). In contrast, at Smoky Butte observed Rb/Sr ratios (= 0.01 to 0.04) are similar, or lower than inferred source ratios (= 0.04).

Such calculations indicate the possible scale of Rb/Sr and Sm/Nd fractionation during magma genesis. In the simplest model, a 44% reduction in Sm/Nd would imply < 1% partial melting even in the presence of residual garnet (Hawkesworth et al., 1979). Assuming a garnet lherzolite source, Kay and Gast (1973) modelled the Leucite Hills REE data, and concluded they were derived by very small (< 1%) degrees of partial melting. They also suggested that the madupites were generated by smaller degrees of partial melting than the wyomingite/orendites, which is consistent with the variation in inferred Sm/Nd fractionation ($\simeq$ 54% in the madupites and $\simeq$ 40% in the wyomingite/orendites). The wide range in observed Rb/Sr ratios may reflect differences in the processes operating during melt formation, extraction and ascent of the magmas. Whatever the details of such processes, most of the Nd, Sr and Pb in these lamproites (and by implication, the rest of the incompatible elements) were derived from mantle material that was old and LREE enriched, with Rb/Sr ratios generally only slightly higher than bulk earth.

4.8.5 Leucite Hills

The close spatial and mineralogical association and a number of major element trends have previously been taken to imply that there is a genetic relationship between the madupite and wyomingite/orendites (Carmichael, 1967; Ogden, 1979; Kuehner et al., 1981).

Attempts to relate these rock-types by fractionation processes have been unsuccessful:

1. Both rock-types have high Ni and Cr contents and high *mg* numbers and are thus believed to be primitive unfractionated mantle melts.

2. Fractionation of observed phases (diopside in the madupites and phlogopite in the wyomingite/orendites) cannot relate the two rock-types. Figure 4.10 demonstrates that the wyomingite/orendites form trends consistent with phlogopite control, whereas the madupites form distinct trends compatible with clinopyroxene control. Fractionation can-

not relate the two rock-types trends, although the trends do explain why the two rock-types have similar Cr contents, but the madupites have lower Ni contents.

3. Consideration of the relative proportions and probable compositions of near liquidus phases at P < 5 Kb in the system $CaMgSi_2O_6$-Mg_2SiO_4-$KAlSi_2O_6$-SiO_2 reveals that madupites would fractionate to less silicic compositions, whereas the wyomingite/orendites would fractionate to more siliceous compositions (Carmichael, 1967).

4. Although madupites contain higher REE contents, their more mafic character indicates they are unlikely to be related to the wyomingite/orendites by high pressure fractionation (Barton and Hamilton, 1978).

Subsequent models have endeavoured to relate the two rock-types by melting of a single source, usually considered to be a mica-bearing peridotite. Ogden (1979) modelled the data in terms of phase relations in the system $KAlSiO_4$-SiO_2-$CaMgSi_2O_6$-Mg_2SiO_4 and progressive melting. Initial non-equilibrium melting of an olivine-clinopyroxene-orthopyroxene-phlogopite source at the eutectic forms madupitic compositions. After diopside is completely consumed, melting would occur at the peritectic, resulting in wyomingite/orendite compositions. During magma genesis, phlogopite melts incongruently to forsterite and liquid.

Kuehner et al. (1981) based their model on the phase relations in the systems $KAlSiO_4$-Mg_2SiO_4-SiO_2-CO_2 and $KAlSiO_4$-MgO-SiO_2-CO_2-H_2O under mantle conditions. They considered that initial melting of a K-enriched peridotite at pressures of 24 to 34 Kb generated madupite compositions, subsequent melting of the same source at pressures of 14 to 19.5 Kb resulted in wyomingite/orendite compositions.

Recent work has shown that the madupites have slightly more radiogenic Nd than the wyomingite/orendites (Vollmer et al., 1984 and this study), which suggests that the geochemical differences between the two groups may, at least in part, result from their being derived from slightly different mantle sources. However, Pb-Pb model ages for both the madupites and wyomingite/orendites are similar, and this implies that source regions for both rock-types were probably formed during the same event. Differences in composition observed between the madupites and wyomingite/orendites are believed to result from; variation in source composition and depth and degree of melting. These are now discussed further.

CIPW norm calculations show that the madupites are clinopyroxene-rich relative to the wyomingite/orendites, and the latter may originate from clinopyroxene-free source regions (Ogden, 1979). Since the pre-enrichment

source region of lamproites is generally believed to be peridotite, depleted by prior melt extraction, it may be that the madupite source region was less depleted (i.e. residual clinopyroxene) than the wyomingite/orendite source region. Alternatively, both source regions were poor in, or devoid of, clinopyroxene and during the trace element enrichment event, clinopyroxene was stabilised only within the madupite source region. However, Ca abundances in lamproites generally, are typically low, which implies that clinopyroxene was not a predominant phase crystallised during inferred enrichment events. Yet, the madupites exhibit extremely low Na and Al contents comparable with, or lower than, those observed within the wyomingite/orendites, which may be difficult to explain if these elements provide any indication of the depleted nature of the source regions prior to trace element enrichment.

High pressure experimental studies have demonstrated that the degree of si-saturation decreases, and the phase volume of phlogopite increases with the depth of melting (Foley et al., 1986a, b, and references therein). The madupites are characterised by lower K_2O contents and are si-undersaturated relative to the high K_2O, si-saturated to oversaturated wyomingite/orendites. These observations are consistent with madupites being derived from greater depth. The K_2O content of the wyomingite/orendites is extremely high and, in many cases, higher than values observed in peridotite micas. Ogden (1979) suggested that incongruent melting of phlogopite at upper mantle conditions could result in such K-rich liquids.

Smaller degrees of partial melting, inferred from trace element and isotopic considerations, are also compatible with greater depth of melting for the madupites. Inferred versus observed Sm/Nd ratios indicate that the Leucite Hills rocks could be generated by very small degrees of partial melting ($< 1\%$). The madupites exhibit steeper REE profiles (i.e. lower observed Sm/Nd ratios), but more radiogenic $(^{143}Nd/^{144}Nd)_i$ ratios (higher source Sm/Nd) ratios. During partial melting within the mantle, the Sm/Nd ratio will tend to decrease in the melt. Hence, during extraction of the wyomingite/orendite and madupite magmas, the Sm/Nd ratio of the madupites decreased the most, indicating smaller degrees of partial melting.

4.8.6 Smoky Butte

A distinctive feature of the Smoky Butte lamproites (with the exception of the altered glassy SB11) is their K/Rb ratios = 707 to 932, which exceed those exhibited by primary peridotite micas (K/Rb = 200 to 620; Smith et al., 1979; Delaney et al., 1980), but fall at the low end of the range for K-richterite amphiboles from MARID suite nodules and PKP xenoliths (K/Rb = 678 to 1283; Kramers et al., 1983; Hawkesworth, unpublished data). The K_2O content of the Smoky Butte rocks (= 6.38 to 10.69 wt%) is higher than

those found in the K-richterite amphiboles (= 3 to 7 wt%). The highly potassic lamproites have contents comparable with those found within peridotite micas (K_2O = 9 to 11%). Thus, these lamproites have K_2O contents and K/Rb ratios, generally, intermediate between those observed for mantle derived micas and amphiboles. As recent studies have shown that the alkali content of many mantle derived rocks may be controlled by either phlogopite or amphibole (Beswick, 1976; Smith et al., 1979; Matson et al., 1986), the Smoky Butte rocks could be derived from a source containing both phlogopite and amphibole. Melting of this source could result in the intermediate K/Rb ratios and if phlogopite melts incongruently, then relatively high K_2O contents could also be generated. The Leucite Hills and Prairie Creek lamproites, typically, have K/Rb ratios < 400 and it is probable they derived their alkali content from phlogopite-bearing sources.

As amphibole is stable to shallower depths than phlogopite, the presence of amphibole in the source region of the Smoky Butte lamproites suggests these lamproites are derived from shallower depths in the mantle compared to the other lamproite localities. K-richterites from MARID suite nodules have very low U/Pb ratios (< 0.048, Kramers et al., 1983) which may, further explain, the extremely unradiogenic Pb content of the Smoky Butte samples.

The question of whether low εSr and extremely unradiogenic Pb contents at Smoky Butte reflects the nature of the ancient trace element enrichment event or whether it is related to the stabilisation of a phase such as amphibole, might best be considered by comparison with the Leucite Hills rocks. Isotopically, the Smoky Butte and Leucite Hills lamproites form a steep vertical trend on an εNd – εSr diagram (Figure 4.7), with the Smoky Butte rocks recording the most unradiogenic Nd contents yet found in potassic rocks. Both suites also exhibit unradiogenic Pb isotope ratios (Figure 4.8), although the Leucite Hills lamproites have more radiogenic Pb contents than the Smoky Butte lamproites. The differences in Pb and Nd isotopes may be related to differences in source age, although both rock suites were derived from sources exhibiting low Rb/Sr and low μ values. As the Leucite Hills rocks do not require the presence of amphibole within the source region, it is believed that stabilisation of amphibole in the source region is not a major factor in generating the isotope geochemistry of the Smoky Butte rocks.

4.8.7 The Prairie Creek lamproites

A number of features at Prairie Creek are more akin to kimberlites than to the majority of lamproites. Features such as extremely high *mg* numbers, Ni and Cr contents and the presence of two olivine populations. In kimberlites these features have been attributed to bulk entrainment of peridotite dur-

ing magma ascent (Section 2.10.4). It is reasonable to assume this is also applicable to the Prairie Creek lamproites, although there is insufficient variation in the available data to quantitatively assess this interpretation. Thus there appear to be processes operating during magma genesis and ascent that are common to both kimberlites and at least some lamproites. It has been shown that bulk entrainment of peridotite will have little effect on the incompatible trace element content of the Finsch kimberlites. The Prairie Creek lamproites are even more incompatible trace element enriched than the Finsch kimberlites. Assuming the entrained peridotite is of similar composition to those inferred within the Finsch kimberlite, then the incompatible element geochemistry of the Prairie Creek lamproites reflects that of the melt component. Trace element variations can reflect processes occurring during melting and/or source differences.

Like other lamproite suites, the Prairie Creek lamproites are H_2O-rich, CO_2-poor rocks (Scott Smith and Skinner, 1984a), contrasting with the H_2O and CO_2-rich nature of kimberlites. This can be reflected in the SiO_2 content of the melts (Eggler, 1974). The Prairie Creek rocks have SiO_2 = 39.33 to 41.10 wt%, similar to those reported for olivine lamproites from the West Kimberley region (40.10 to 42.80; Jaques et al., 1984a). The latter are believed to be derived from melts which had significantly higher SiO_2 contents ($\simeq$ 38 wt%) than the Finsch kimberlites ($<$ 30 wt%)(Section 3.9.5).

Comparison of Nd and Sr isotopes reveal that geochemical differences do not relate only to melting conditions. The Finsch kimberlites and the Prairie Creek and West Kimberley lamproites are believed to be derived from ancient, trace element enriched sources situated within the subcontinental lithosphere. However, the Prairie Creek lamproites exhibit lower εNd than the Finsch kimberlites, and lower εSr than the Finsch kimberlites and the West Kimberley lamproites. These variations cannot be attributed solely to differences in age, but must reflect different Rb/Sr and Sm/Nd ratios within the sources which in turn may reflect different styles of trace element enrichment.

The Prairie Creek lamproites are not the only North American lamproites to contain such extremely high Cr contents. The lamproite sills from Woodson County, Kansas: the Silver City and Rose Dome lamproites have Cr contents of 1040 to 2600 ppm and 1150 to 1700 ppm respectively (Cullers et al., 1985). The Rose Dome lamproites are highly altered and although olivine is identified in the Silver City lamproites, there is no mention of whether or not there are two populations.

4.9 Discussion

The lamproites from Smoky Butte, Prairie Creek and Leucite Hills represent primary unfractionated mantle melts. They were derived by very small degrees of partial melting of old, variably trace element enriched, low Rb/Sr, Sm/Nd, U/Pb sources, which were most probably situated within the subcontinental lithosphere. Furthermore, the high TiO_2 contents (= 2.05 to 6.38 wt%) and Ta/Yb ratios (= 1.45 to 7.15) argue that the trace element enrichment processes were melt dominated rather than fluid dominated.

The geochemical characteristics of these lamproites results from a number of factors including; the nature and degree of trace element enrichment within the source regions, conditions of melt formation and extraction and volatile composition during both the aforementioned processes.

The high K_2O contents (= 2.27 to 12.34 wt%) of the North American lamproites analysed in this study, seem to indicate they originate from sources containing a K-bearing phase, such as phlogopite and/or amphibole. Only the Smoky Butte lamproites (Section 4.8.6) require the stabilisation of amphibole in addition to phlogopite within the source region. The above has important implications on the depth of origin of lamproite magmas. Amphibole implies depths of < 100 km for the Smoky Butte lamproite sources. On the other hand, the presence of diamond in the Prairie Creek lamproites means they were derived from depths > 150 km. Furthermore, the olivine lamproites from Prairie Creek are characterised by two olivine populations and extremely high MgO, Ni and Cr contents. These characteristics in kimberlites and the olivine lamproites from the West Kimberley, were attributed to the entrainment and disaggregation of bulk peridotite. On the above evidence, these features appear to occur in rocks (kimberlites and lamproites) derived from deep within the subcontinental mantle.

At Leucite Hills, it has been postulated that the madupites are derived from greater depth than the wyomingite/orendites. There is no diamond within these rocks, nor is there evidence for amphibole within their source regions. Arguably, the depth of origin of the Leucite Hills lamproites is intermediate to the other two localities.

Although each locality exhibits its own geochemical characteristics, reflecting heterogeneities in the processes operating, there are geochemical trends which indicate close affinities between those processes operating in the subcontinental lithosphere in North America, during the Late Archaean and Early Proterozoic. Compared to the high εSr, low εNd Finsch kimberlites and West Kimberley lamproites, the North American lamproites plot on steep $\varepsilon Nd - \varepsilon Sr$ isotopic trends with low εNd and εSr. These isotopic trends are also recorded in other mantle derived igneous rocks from this region e.g. alkalic and subalkalic igneous rocks from the Crazy moun-

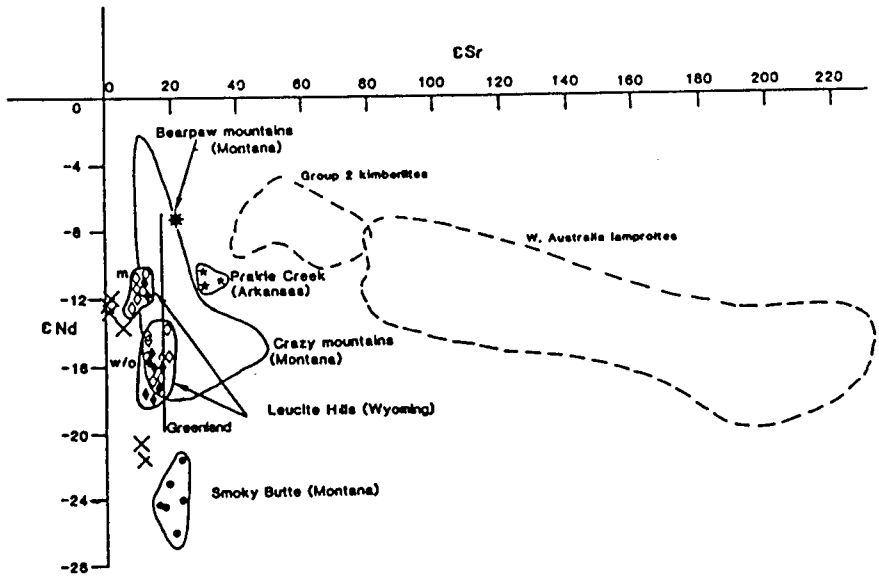

Figure 4.11 εNd vs. εSr for selected mantle derived rocks from the North American Craton. Symbols and fields as in Figure 4.7. Also shown are subalkalic and alkalic rocks from the Crazy Mountains, a carbonatite from the Bearpaw Mountains (Dudás et al., 1987), rocks (×) from the Independance volcano (Meen, 1983) and the range of data for lamproites from Greenland (Stecher et al. 1987).

tains, a carbonatite from the Bearpaw mountains (Dudás et al., 1987), the tholeiite-shoshonite and andesite-banakite series from the Independance volcano (Meen, 1983)(Figure 4.11). This implies that the mantle source regions to these rocks were subjected to similar styles of trace element enrichment. Lamproites from Greenland (Stecher et al., 1987), also appear to belong to this province, since they plot on the same vertical trend on an εNd – εSr diagram (Figure 4.11).

Dudás et al. (1987) also observed that the Pb isotope data for a variety of young mafic igneous rocks from the northwest United States including the Crazy mountains, the Saddle member of the Columbia River basalts (Carlson, 1984), Yellowstone (Doe et al., 1982), Independance (J.K. Meen and D.H. Eggler, in preparation), Smoky Butte (Fraser et al., 1985) and Leucite Hills (Salters and Barton, 1985), plot close to the 2.6 Ga trend found by Leeman (1982) for Snake River Plain basalts. In detail, the individual

units do not give identical Pb-Pb model ages (e.g. Leucite Hills = 1.9 Ga, Prairie Creek = 2.0 Ga and Smoky Butte = 2.5 Ga). However, this data does suggest that the subcontinental mantle underlying this region was affected, at least in parts, by a certain style (low Sm/Nd, Rb/Sr, U/Pb) of trace element enrichment in Late Archaean, Early Proterozoic times.

Chapter 5

Melt formation, extraction processes and source evolution

5.1 Introduction

In the previous three chapters, it was shown that Group 2 kimberlites from South Africa and lamproites from Western Australia and North America (Smoky Butte, Montana; Leucite Hills, Wyoming; Prairie Creek, Arkansas) were small volume partial melts (< 1%) of ancient trace element enriched sources situated within the subcontinental lithosphere. It was also argued that with careful selection of whole-rock samples, the effects of crustal contamination and alteration could be ignored.

The petrogenesis of these rocks involves processes occurring during magma generation and ascent to the surface, and processes which participated in the evolution of the source regions. Thus, this chapter is divided into essentially three main parts. The first considers melting and extraction processes. Kimberlites and lamproites are volatile-rich rocks and the effects of melting at mantle depths, under high volatile pressures, are investigated. The presence of abundant, entrained and disaggregated peridotite within kimberlites and some lamproites may have a bearing on melt extraction models and this is examined in the light of recent studies. The possible triggers to magmatism are also considered. In the second part, the geochemistry of the individual localities in question, are compared and contrasted, in the context of variations in mantle enrichment styles recorded. Finally, the present debate on the origin of mantle enrichment events (recycled continental crust or mantle processes) is detailed and investigated with available data.

5.1.1 Volatiles

Kimberlites are CO_2- and H_2O-rich rocks and these volatiles are believed to play an instrumental role in melting and ascent processes. Kimberlites

are found on ancient cratonic areas, characterised by low geothermal gradients. In such regions, the solidus for anhydrous peridotite (Wyllie, 1977) lies at several hundred °C higher than representative shield geotherms (Gurney and Harte, 1980). However, the presence of volatiles such as CO_2 and H_2O, considerably reduces the peridotite solidus temperature (Wyllie, 1980; Olafsson and Eggler, 1983; Brey et al., 1983) such that it may intersect the shield geotherm and result in melting. A number of authors have proposed that the presence of volatiles is essential for kimberlite melt formation, and also for their rapid ascent from great depth to the surface (e.g. Anderson, 1979; Wyllie, 1980; Bailey, 1984, 1985).

Since mantle which could represent kimberlite source material does not appear to have been sampled as xenoliths, it has been necessary to estimate a kimberlite source composition by alternative means. The stability field of diamond, equilibration pressures and temperatures of mantle xenoliths, and experimental studies in the system peridotite-CO_2-H_2O suggest that kimberlite magmas probably formed at P $\simeq$ 40 to 50 Kb, T $\simeq$ 1000 to 1300°C and from phlogopite-magnesite-garnet lherzolite sources (e.g. Wyllie, 1980 and discussion in Mitchell, 1986). From here, recent partial melting models diverge into two main groups; diapirism (Green and Gueguen, 1974; Wyllie 1980) versus volatile fluxing (Bailey 1984, 1985).

With regard to kimberlite magmatism, the diapir model originally evolved from textural examination of the various xenolith suites found within kimberlites (Green and Gueguen, 1974). Wyllie (1980) modified this earlier model of Green and Gueguen (1974), by taking into account interpretations of peridotite-CO_2-H_2O melting relationships (Figure 5.1). He proposed that a minor thermal perturbation within the deep mantle (presumably the convecting asthenosphere) might trigger release of vapours with major components C-H-O. Where these volatile components cross the estimated solidus boundary near 260 km, partial melting occurs. The density inversion causes diapiric uprise along adiabats. These partially melted diapirs begin to crystallise at 80–100 km depth where they reach a temperature maximum (thermal barrier) on the solidus. Crystallisation of the volatile-rich melt results in solid plus vapours. Released vapour, at this stage, enhances the prospects for crack propagation through the overlying lithosphere when stress tension in the vicinity of the crack balances out hydrostatic pressure (Anderson, 1979). This could produce a channel to the surface. Clement (1982) has observed that most kimberlite pipes are composite intrusions and that the kimberlite magma forming an embryonic pipe is differentiated. Wyllie (1980) suggested that the initial intrusion establishes the conduit, which subsequently permits magma separation from progressively greater depths. This would release CO_2-undersaturated kimberlite magmas, which would rise through the established conduit, quite unaffected by the thermal bar-

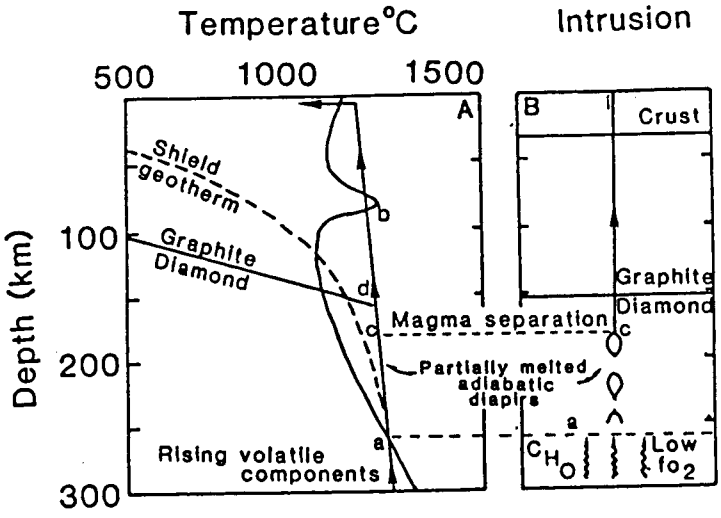

Figure 5.1 A diapiric model for the origin and eruption of kimberlite magmas, triggered by volatile components rising from deep within the mantle. Partial melting initiated at the intersection of the shield geotherm and the peridotite solidus at a produces a density inversion, which is followed by the uprise of partially melted adiabatic diapirs along the path a to b. At level b the magma crystallises. Crystallisation is accompanied evolution of CO_2-rich vapour, which may initiate crack propagation through the overlying lithosphere, followed by explosive eruption of the magma rising from a depth of about 90 km. Once a conduit is established to the surface, then magma separation may occur from partially molten adiabatic diapirs at progressively deeper levels, extending down through a region which may contain diamonds e.g. c at depths > d. After Wyllie (1980).

rier on the solidus of peridotite-CO_2-H_2O (Figure 5.1). This would permit preservation of diamonds and dense mantle xenoliths within the magmas.

Bailey (1984, 1985) preferred models for alkaline magmatism, whereby a mantle disturbance results in influx of asthenospheric volatiles into the vapour-free lithosphere, at temperatures above the vapour-saturated solidus. Bailey (1985) believed that kimberlite is the limiting case of cratonic magmatism and occurs when the ambient solidus and geotherm are within 'grazing incidence'. The incoming 'volatile flux', accompanied by various major elements (i.e. K, Al, Ca, P, Ti, Fe) and presumably incompatible trace elements, interacts with the common lithospheric peridotite minerals. The reaction products are either fixed in the mantle as metasomatically introduced solids, or become ingredients of any flux induced melt. The latter percolate through the mantle maintaining thermal and chemical equilibrium along their paths. Such melts may accumulate where the solidus recrosses the geotherm. Any sudden upward movement of the melt results in depressurisation and potentially catastrophic degassing. Ascent of the kimberlite melt to the surface is believed to occur as a fluidised and/or gas-solid system.

In detail, each of the two models suffers from problems. These are outlined in the following discourse, where pertinent, and some discussion can be found in Bailey (1984) and Mitchell (1986). Mitchell (1986) considered that;

> 'the differences between the models may be simply ones of perspective ... 'volatile fluxers' look down into the lithosphere, while 'diapiricists' work upward from the asthenosphere'

The geochemistry of the Cretaceous Group 2 kimberlites from South Africa, can place important constraints on kimberlite magmatism. The isotope compositions of these rocks favour an origin from ancient trace element enriched source regions, situated within the subcontinental lithospheric mantle (Section 2.11; Smith, 1983a, b). The subcontinental mantle lithosphere isolated from the hot, convecting asthenosphere will be relatively cold and rigid, hence it may preserve the effects of enrichment events over long periods of time. Only the model proposed by Bailey (1984, 1985) makes provision for source enrichment prior to magmatism. Although evidence from many continental alkaline volcanics suggest source enrichment events and magmatism were closely associated in time (Bailey, 1985), the enriched (high εSr, low εNd) isotope signatures of the Group 2 kimberlites require a time gap of at least 1 Ga (Section 2.10.3) between the two events. Thus, models invoking magmatism via ascending asthenospheric diapirs appear untenable for Group 2 kimberlites.

Cretaceous Group 1 kimberlites from South Africa, could potentially be derived from one of two sources:

1. Asthenospheric mantle. Group 1 kimberlites have isotope (Sr, Nd and Pb) signatures similar to those in many OIB (Smith, 1983a, b). Moreover, unlike the Group 2 kimberlites, they frequently contain hot, deformed Fe-Ti-rich peridotites and Cr-poor megacrysts which Harte (1983) has shown could have been in equilibrium with a basanitic melt. As such, they could have originated from ascending diapirs along the lines proposed by Wyllie (1980).

2. Lithospheric mantle. Group 1 kimberlites could represent melts from 'young' trace element enriched lithospheric mantle source regions. In this case, the isotope signature of these kimberlites would then signify a close temporal relationship between source enrichment and magmatism, while the nature of the mantle xenolith and xenocryst content would suggest a close spatial relationship with the asthenosphere.

It is not possible to determine between the two models above. All that can be said is that the composition of Group 1 kimberlites indicates a close association with asthenospheric mantle.

It was suggested above that kimberlites result from melting of phlogopite-magnesite-peridotite sources. If, as indicated by Group 2 kimberlites, portions of the continental lithosphere can exist with this composition for long periods of time, then mantle xenoliths containing phlogopite and a carbonate phase might be expected. Phlogopite has been identified in a number of mantle xenoliths from the sub-continental mantle (e.g. Delaney et al., 1980; Erlank et al., 1982, 1987). The question of mantle carbonate is however enigmatic. CO_2 is a common volatile phase associated with magmatism and a number of experimental studies have demonstrated that carbonation reactions could occur between CO_2 and peridotite in the upper mantle to form dolomite or magnesite (Wyllie and Huang, 1976; Brey et al., 1983; Olafsson and Eggler, 1983). Yet, samples of carbonated mantle are extremely rare. There are only two reported occurrences of mantle carbonate; McGetchin and Besancon (1973) found primary dolomite and calcite inclusions in pyrope garnets from the Cane valley diatreme, Utah, while Berg (1986) noted the presence of primary brucite/calcite intergrowths ($Mg(OH)_2/CaCO_3$) in mantle xenoliths from the Kimberley pipes, South Africa. Wyllie (1978), however, believes that the paucity of samples of carbonated mantle can be explained by their rapid transport from depth.

Radiogenic isotope arguments have also been used to infer ancient trace element enriched source regions situated within the subcontinental lithospheric mantle for the West Kimberley and North American lamproites (Section 3.10 and 4.9). Furthermore, the high K content of these rocks has often been cited as evidence of their derivation from a phlogopite and/or amphibole bearing source (Ogden, 1979; Jaques et al., 1984a; Wagner and Velde,

1986). Hawkesworth et al. (1985) proposed that the extremely high Rb/Sr and Ba/Sr ratios of the West Kimberley lamproites required the stabilisation of phlogopite within the source region. The idea of lamproites being derived from phlogopite-bearing rocks within the mantle has also been supported by a number of experimental studies (e.g. Barton and Hamilton, 1982; Arima and Edgar, 1983). So far, lamproite magmatism could, by analogy, parallel that proposed above for the Group 2 kimberlites. However, kimberlites and lamproites differ significantly in their volatile composition. In contrast to the CO_2- and H_2O-rich nature of kimberlites, lamproites are CO_2-poor, yet H_2O- and F-rich. These differences cannot be due to differences in depth of melting, since some lamproite suites are diamondiferous. There are a number of possibilities however, to be considered. The variation in volatile content between kimberlites and lamproites could be due to different volatile sources (i.e. subduction related versus juvenile), varying tectonic settings or modification of juvenile volatiles within the lithosphere. These are now discussed in turn.

Some authors conjecture that continental crust recycled into the mantle, via subduction, could contribute to lamproite magmatism (e.g. Nelson et al., 1986b). This would provide a ready source of H_2O-rich volatiles. Yet, there are doubts regarding the feasibility of retaining H_2O to great depth (i.e. $>$ 150 km as required by diamondiferous lamproites) during subduction. Moreover, carbonates form a substantial portion of some ocean floor sediments and subduction could also therefore provide a source for significant quantities of CO_2. The role of recycled sediment in lamproite genesis is further discussed in Section 5.3.1.

Kimberlites are generally situated within ancient cratons, whereas the lamproites are positioned on or close to the edge of cratonic regions. It is therefore possible that juvenile volatile composition varies with tectonic setting. However, the gaseous emanations from volcanoes, in both oceanic and continental settings, are dominated by both CO_2 and H_2O. Furthermore, mantle derived igneous rocks e.g. carbonatites, olivine melilitites etc., from a wide range of tectonic settings e.g. continental, oceanic and rifting (Brey and Green, 1975; Brey, 1978; Dawson, 1980; Le Bas 1984) all require the presence of, in some cases, substantial amounts of CO_2.

Alternatively, as indicated by the above observations, juvenile volatiles are essentially of the same composition i.e. CO_2- and H_2O-rich. But, in the case of lamproites, these are modified during ascent through the lithosphere. Thus, lamproite source regions have 'lost' a CO_2 component by some process. They either never saw this component, or it passed through the system without being stabilised. Carbon-bearing volatiles from the convecting asthenosphere or below have been proposed as a possible source of diamond in the lithospheric mantle (Haggerty, 1986; Green et al., 1986). Under rel-

atively reducing conditions within the deep mantle, carbon is stabilised as CH_4, but under oxidising conditions as CO_2. Depending on the nature of the carbon species and the relative oxygen fugacities of lithospheric and asthenospheric mantle, redox reactions could occur, whereby CH_4 is oxidised, or CO_2 reduced to diamond (Haggerty, 1986; Green et al., 1986). This would provide a means of removing the carbon-bearing species near the base of the lithosphere, with the volatile composition evolving to progressively H_2O-rich, CO_2-poor. Alternatively, a CO_2-, H_2O-rich 'volatile flux' interacts with lithospheric mantle, phlogopite is stabilised and retains H_2O and F. However, a late-stage CO_2-bearing phase does not crystallise and passes through and out of the system, and presumably stabilises at shallower mantle depths through carbonation reactions. It is difficult to assess the validity of either model. The diamonds generated in the former model would be situated below the lamproite source region and hence probably not sampled by the lamproite magmatism itself, while the problems of sampling carbonated mantle were mentioned earlier. Modification of the 'volatile flux' composition, within the lithosphere, may therefore relate to the interaction of the geothermal gradient and ambient solidus and/or to the relative oxygen fugacities of the lithosphere and 'volatile flux'.

To determine whether variation of volatile content between kimberlites and lamproites relates either to subduction processes, or modification of juvenile volatiles requires some investigation into the origin of the trace element enrichment events. This is discussed in Section 5.3.

Whatever the cause, it is evident that kimberlite and lamproite source regions were characterised by different volatile compositions. Subsequently, these source regions were remobilised by melting processes. The available data for kimberlites and lamproites are therefore examined in the light of recent experimental studies, which suggest that the volatiles present during melting can influence the composition of the resultant melt. However, depth of melting can also influence melt composition. For example, it has been shown in the Ne-Fo-Qz and Ks-Fo-Qz systems that the degree of si-saturation in a melt will decrease with increasing amounts of CO_2 and F (Eggler, 1974; Foley et al., 1986a, b; Figure 5.2) and increasing pressure, under both dry (Kushiro, 1968, 1980) and H_2O-saturated (Foley, 1986b) conditions; Figure 5.3). Decreasing pressure and the presence of H_2O or HF will result in higher degrees of si-saturation in a melt (Figures 5.2, 5.3).

Similarly, consideration of the phlogopite-enstatite-forsterite peritectic in the water saturated system at 3 and 28 Kb reveals the phlogopite phase field is much larger at higher pressures (Foley et al., 1986b; Figure 5.4). The Ks/Fo ratio of melts must be strongly dependant on pressure, with an increase in pressure resulting in higher MgO, but lower K_2O contents (Foley et al., op. cit.). Inspection of Figure 5.4 shows that in the system

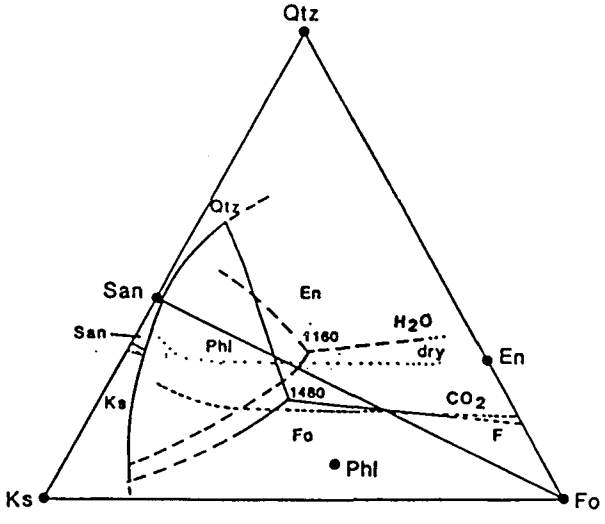

Figure 5.2 Comparison of data for Ks-Fo-Qz at 28 Kb with various volatiles. There is no phlogopite field in dry and CO_2-present systems. Phase fields for H_2O, CO_2 and volatile-free systems are from Gupta and Green (in prep.)(after Foley et al., 1986a).

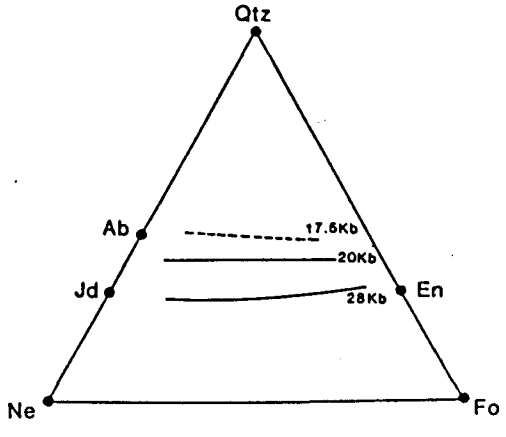

Figure 5.3 The effect of pressure on the Fo-En phase boundary in the water-saturated Ne-Fo-Qz system showing shift to more silica-undersaturated compositions at higher pressures. Positions taken from Kushiro (1972; 17.5 and 20 Kb) and Gupta and Green (in prep.; 28 Kb)(after Foley et al., 1986b).

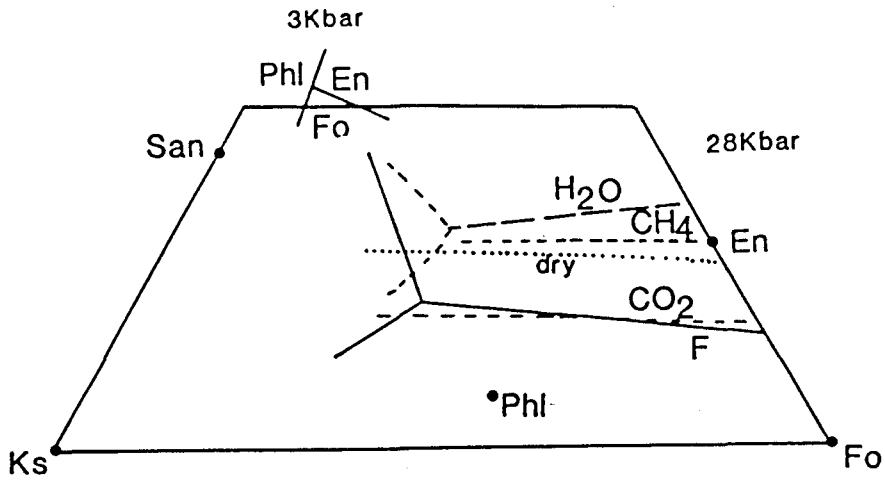

Figure 5.4 Part of the system Ks-Fo-Qz showing the relative positions of the En-Fo phase boundary in the presence of various volatile species. The boundary for CH_4 is estimated from its position in the Ne-Fo-Qz system, taken from Gupta et al. (in prep.). The position with HF is uncertain, but can be expected to be close to the CH_4 position. The data for the water-saturated Ks-Fo-Qz system at 3 kb are taken from Luth (1967)(after Foley et al., 1986b).

Ks-Fo-Qz, the presence of F and H_2O can affect the phlogopite phase field. Fluorphlogopite has a much greater thermal stability (1490° to 1500°C) than hydroxyphlogopite (< 1200°C) at 28 Kb (Foley et al., 1986b). There is no phlogopite phase field in a dry system, or where CO_2 is the only volatile species.

Kimberlites and lamproites are derived from a range of mantle depths, and from source regions believed to contain potassic phases such as phlogopite and/or amphibole. Since both rock-types are H_2O-rich rocks, it is likely the depth of melting was important in determining the range in K_2O contents of the magmas. Figure 5.5 shows the ranges of K_2O content in various kimberlites and lamproites. They are arranged in order of inferred depth of melting. The Group 1 kimberlites are believed to originate at the base of the lithosphere in close proximity to the asthenosphere, whereas Group 2 kimberlite and lamproite source regions were situated within the lithosphere. Of these, the diamondiferous Group 2 kimberlites and olivine lamproites from Prairie Creek and the West Kimberley must have been derived from depths > 150 km. The non-diamondiferous lamproites are believed to have come from shallower depths. The inferred presence of amphibole in the source region of the Smoky Butte lamproites indicates depths of origin < 100 km (Section 4.8.6). The non-diamondiferous Leucite Hills and West Kimberley lamproites which do not appear to have arisen from amphibole bearing sources, may therefore have originated from intermediate depths (> 100 km, but < 150 km).

On Figure 5.5 there is a general increase in K_2O content from field a, through b to c, which corresponds to a decrease in depth of melting. In more

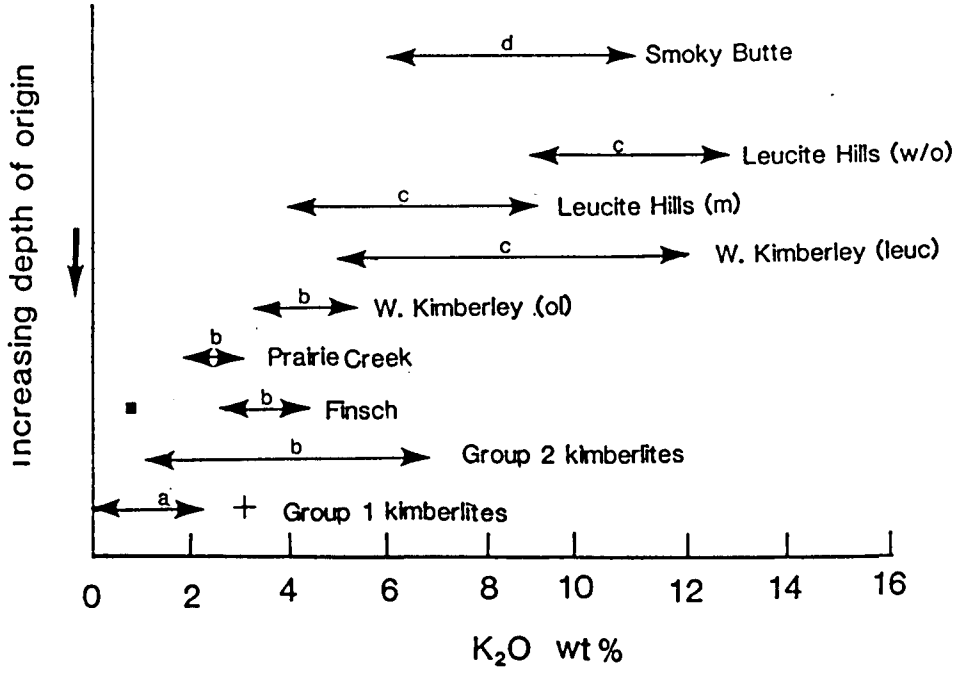

Figure 5.5 The ranges of K_2O wt% in kimberlites and lamproites (source of data: this work; Ogden, 1979; Jaques et al., 1984a; Smith et al., 1985). They are arranged in order of inferred depth of melting: a = Group 1 kimberlites from the base of the subcontinental mantle lithosphere in close association with the asthenosphere (> 150 km). b = Group 2 kimberlites and diamondiferous lamproites from the West Kimberley and Prairie Creek, from within the subcontinental mantle. c = Non-diamondiferous lamproites from the West Kimberley and Leucite Hills derived from phlogopite-bearing, but amphibole absent source regions. d = Non-diamondiferous Smoky Butte lamproites from within the amphibole stability zone (< 100 km). See text for discussion.

detail, at Leucite Hills, the madupites with lower K_2O than the wyomingite/orendites are believed to originate from greater depths than the latter (Kuehner et al., 1981; Section 4.8.5). The Smoky Butte lamproites, however, are displaced towards lower K_2O contents. This may be attributed to melting of source regions that contained amphibole in addition to phlogopite. K-richterite has lower K_2O contents compared to mantle phlogopite (e.g. 4.7 wt% and 9.4–10.0 wt% respectively; Erlank et al., 1987). Thus, the K_2O content of the magmas, appears to have been influenced by the depth of melting. As the phase field of phlogopite increases with depth (Foley et al., 1986b), then the greater the depth of magma generation, the lower the K_2O content of the resultant magma.

When considering the SiO_2 contents of these rocks, the main differences lie between the kimberlite and lamproite rock-types. Comparing those believed to come from similar mantle depths (i.e. from within the diamond stability zone) the kimberlites generally exhibit lower SiO_2 contents and are si-undersaturated rocks compared to the more SiO_2-rich and si-saturated to si-oversaturated olivine lamproites. This probably reflects the high CO_2 contents of the kimberlite magmas (Eggler, 1974). Hence, both the volatile content and the depth of melting appear to influence the composition of the resultant melts.

To recapitulate, Group 2 kimberlites and lamproites are believed to be derived from ancient trace element enriched portions of the subcontinental lithospheric mantle. These lithospheric source regions were generated by some form of 'volatile fluxing' into the lithosphere which stabilised minerals such as phlogopite $\pm$ amphibole $\pm$ magnesite. Subsequently, after a time gap of at least 1 Ga, these regions were remobilised by melting. The volatile composition of kimberlite and lamproite source regions differed. The latter appear to have 'lost' a CO_2 component, probably through some modification of the 'volatile flux' during ascent and/or stabilisation in the lithosphere. The source regions were situated at a wide range of mantle depths ($<$ 100 km to $>$ 150 km) and it appears that both the source volatile content and the depth of melting can account for some of the compositional variation between these rocks.

A word of caution should be made regarding the use of Bailey's (e.g. 1985) term 'volatile flux'. Bailey (1985) envisages this as being composed of a predominant volatile (CO_2 and H_2O) component associated with a subordinate silicate component. However, the high HFSE content of the kimberlites and lamproites argue for principally melt dominated processes and hence the so-called 'volatile fluxes', as used in this work are actually envisaged as being volatile-rich small volume silicate melts.

5.1.2 Melt Migration

Both 'volatile fluxers' and 'diapiricists' are in agreement that kimberlite melt migration is essentially a two-stage process. Initial relatively slow upward movement and/or accumulation of melt within the mantle lithosphere is succeeded by rapid ascent from within the diamond stability field to the surface. There appears to be a general consensus that rapid ascent of kimberlite magmas occurs through deep propagating cracks (Anderson, 1979; Wyllie, 1980; Artyushkov et al., 1984; Bailey, 1984, 1985; Spera, 1987). Rates of 10–30 ms^{-1} have been proposed from consideration of fracture mechanics (Artyushkov et al., 1984). The high volatile content of kimberlite magmas helps promote propagation of the lithospheric cracks and hence ascent of the magmas. However, the nature of the hypabyssal root zones to kimberlite pipes demonstrate that ascent from the upper mantle occurred as a silicate magma and not via a fluidised process as proposed by Bailey (1984, 1985). It is only in near surface conditions that adiabatic expansion of exsolving CO_2, and/or introduction of meteoric water results in explosive breakthrough to the surface and the development of diatreme facies kimberlite (Dawson, 1980; Mitchell, 1986). This section discusses the evidence within the kimberlites for each of the two stages of melt migration. A refined model is then proposed, which explains the bulk entrainment of mantle peridotite observed within kimberlite magmas. The discourse is then extended, by analogy, to assess lamproite magmatism.

The existence of kimberlite melts at depth, comes principally from the presence of euhedral olivine phenocrysts which are believed to have crystallised slowly within the upper mantle (Clement, 1982). Microprobe analyses of individual olivine phenocrysts reveal that the core of each grain has a constant composition, but variations exist between individual grains. This indicates several batches of melt coalesced during kimberlite ascent to form a single magma (Boyd and Clement, 1977). Clement (1982) cogently argues that the olivine phenocryst compositions indicate crystallisation must be essentially complete prior to mixing, and therefore must occur at an early stage, i.e. within the upper mantle. The lack of extensive re-equilibration between the olivine phenocryst populations, and between olivine phenocryst and macrocryst populations was attributed to mixing of melt batches during rapid ascent to the surface. Rapid ascent rates are also required to explain the presence of metastable diamond and dense mantle xenoliths in kimberlites. Furthermore, in a review, Harte (1983) discusses the evidence for rapid eruption of the Cr-poor megacrysts suite, found in Group 1 kimberlites, whilst still at high temperature. For example, their lack of aggregation, lack of exsolution in the microscopic-megascopic range and the presence of submicroscopic exsolution structures. The latter have been shown to be the

result of rapid cooling at low pressures (McCallister et al., 1979 as referenced in Harte, 1983).

A two-stage model of kimberlite melt migration can also explain one of the characteristic features of kimberlite magmatism i.e. the high proportion of xenocrystic olivine believed to originate from disaggregation of mantle peridotite. For example, it was demonstrated in Section 2.10.4 that the composition of the Finsch kimberlites could be modelled as representing mixtures between kimberlitic melts and bulk peridotite. It is therefore envisaged that small degrees of partial melting ($< 1\%$) of trace element enriched subcontinental lithospheric mantle source regions generated kimberlitic melts. Initial, relatively slow ascent of these melts took place along grain boundaries (McKenzie, 1985) into overlying, sometimes diamondiferous, garnet peridotite. In some cases, small batches of melt would accumulate, in which olivine would crystallise. Subsequently, as a result of melting together with some thermal or tectonic trigger (Section 5.1.3) a crack is induced within the overlying lithosphere. The kimberlite melts and associated garnet peridotite 'matrix' are channelled into the crack and rapidly ascend to the surface. Composite intrusions can be explained by the process of stress relaxation in the country rocks (Artyushkov et al., 1984). The geochemical similarities and lack of differentiation sequence between the hypabyssal material from the main intrusions in the Finsch kimberlite pipe (Sections 2.6, 2.7 and 2.8) indicates there is probably very little time interval between intrusions within a single pipe.

Slower ascent rates have been inferred for lamproite magmatism: diamonds from lamproites tend to be highly resorbed (Jaques et al., 1986a) and within individual pipes they are more abundant in the early pyroclastic phase relative to the later magmatic phases (Scott Smith and Skinner, 1984b; Jaques et al., 1984a). Furthermore, peridotite xenoliths are fewer and those that are present have had time to equilibrate within the spinel stability field (O'Neill et al., 1986). Slower ascent of lamproite magmas may be due to lower abundances of volatiles. This has been postulated as a reason for the differences in the geology of the intrusions: the champagne-glass shape of the lamproite pipes versus the carrot shape of the kimberlite pipes (Scott Smith and Skinner, 1984b). Yet, there are sufficient similarities between diamondiferous kimberlites and lamproites to suggest related styles of magma ascent:

1. The presence of metastable diamond.

2. The evidence for disaggregation of bulk peridotite, e.g. a) the presence of mantle xenocrysts, in particular an anhedral olivine macrocryst population. This occurs in addition to a smaller euhedral olivine population, and b) the extremely high MgO, Ni and Cr contents of

these magmas.

Thus, the model outlined above for kimberlite melt migration and ascent to the surface is considered applicable to diamondiferous lamproites derived from deep within the upper mantle lithosphere.

Non-diamondiferous lamproites, believed to be derived from shallower mantle depths, are not characterised by the presence of a macrocrystic olivine population and their geochemistry does not bear evidence of a significant bulk peridotite component. However, their high volatile content, primitive compositions and similarity in geological form to the diamondiferous lamproite pipes (Scott Smith and Skinner, 1984b) still favours rapid ascent rates. The lack of a peridotite component could result from melt segregation from the surrounding matrix prior to ascent, and since crack formation will be more readily achieved at lower pressures, there may have been insufficient time between melt formation and ascent to the surface for the melt to migrate from its source region. Alternatively, initial ascent along cracks is relatively slower at shallower depths and effectively the melt drains from the surrounding matrix into the crack and thence to the surface.

5.1.3 Trigger to magmatism

Kimberlites and lamproites are generally found on or close to ancient cratonic areas and frequently magmatism cannot be readily linked to any tectonic or thermal event. Most opinions on the trigger to magmatism have hence been conjectural. These are usually based on observed tectonic or thermal events, recorded from adjacent regions (e.g. ocean rifting or hotspot activity) and which are believed to have occurred concurrently with the kimberlite/lamproite magmatism. In Section 5.1.1 it was argued that diapiric models for most kimberlite and lamproite magmatism were untenable on the available data. Some form of 'volatile fluxing' into the lithosphere was the preferred model. However, the origin of the 'volatile flux', or rather the volatile-rich melts, was not addressed. Although this is discussed in detail later (Section 5.3), it is important to point out at this stage, that an origin from hotspot activity is not inconceivable, especially since the Nd, Sr and Pb isotope ratios of the Group 1 kimberlites are comparable to those in many OIB. Moreover, hotspots need not necessarily provide mantle material for kimberlite and/or lamproite magmatism. Rather, they may simply provide a thermal input sufficient to cause melting of trace element- and volatile-rich portions of the subcontinental lithospheric mantle and promote their ascent to the surface. Thus, the above does not negate earlier observations and hotspot activity, as a trigger to kimberlite and lamproite magmatism is potentially a viable process that needs to be assessed.

The Cretaceous kimberlite magmatism of South Africa has been variably attributed to tensile stresses within the subcontinental lithosphere, which are related to oceanic rifting and to OIB-type hotspot activity. The proposed models are outlined and discussed below. Smith (1983a, b) argued from Rb-Sr phlogopite ages that the Group 2 kimberlites are older than the Group 1 kimberlites. This has more recently been modified by Skinner (1986) who stated that the majority of Group 1 kimberlites (excluding the Precambrian Premier mine) in South Africa range from 250 to 50 Ma, whereas the Group 2 kimberlites range in age from 110 to 200 Ma. However, where Cretaceous kimberlites occur in the same area, Group 2 kimberlites are always older than the Group 1 kimberlites, with age differences varying from 5 to 55 Ma. Smith (1983b) proposed that Group 2 kimberlites were emplaced in response to the opening of the South Atlantic. Skinner (1986) however, observed that Group 2 kimberlites occur in a broad southwest-northeast trend with ages increasing from 110 Ma in the southwest (Eendekuil) to 200 Ma in the northeast (Dokolwayo). Furthermore, the older ages correspond to the opening of the Indian ocean and the younger to the opening of the South Atlantic. Thus, the extensional regimes germane to these oceanic rifting basins, may have continued into the adjacent continental region. Tensile stresses induced within the subcontinental mantle resulted in small degrees of decompressional melting of ancient trace element enriched portions of the upper mantle and the formation of deep lithospheric cracks. The latter were utilised by these Group 2 kimberlite melts for rapid ascent to the surface (Section 5.1.2).

In South Africa diatremes are lined up along deep-seated fractures which are infilled by kimberlite dykes (Dawson, 1980). The orientation of these kimberlite-filled fractures is highly variable and this may, in part, result from kimberlite intrusions exploiting pre-existing lines of weakness in the upper crust. This hinders identification of a relationship between tectonically induced stresses on the continental lithosphere and Group 2 kimberlite magmatism. Consideration of the stress regimes involved, and the identification of the structures associated with Group 2 kimberlites alone are required to assess this in detail.

Group 1 kimberlite magmatism may have occurred as a result of hotspot activity (Smith, 1983b). However, Bailey (1984) has raised a number of objections to there being a possible relationship between kimberlite magmatism and hotspot activity, suggesting they fail to account, for example, the apparently random distribution of kimberlite diatremes on some cratons and repetition of magmatism at particular sites. However, Smith (1983b) conjectured that perhaps these arguments are not sufficient to completely refute a relationship with hotspot activity, for the following reasons:

1. Deep-seated fault zones could exert important control over the surface manifestations of kimberlite emplacement.

2. Palaeo-reconstructions, showing the relative motion of South Atlantic hotspots and the South African craton, indicate the latter overrode several hotspots during Jurassic and Cretaceous times.

3. A rising mantle plume of the order 100–150 km (Parmentier et al., 1975; Morgan, 1982) will thermally affect a region of the order 100 km accross (Morgan, 1982).

Thus, it is probably simplistic to expect 'hotspot tracks' in old cratonic regions, on the scale of a few hundred kilometres. Furthermore, Smith (1983b) noted that the 60–75 Ma melilite basalts of the Cape Province (Duncan et al., 1978) and kimberlites west of the Kaapvaal craton (ages from Davis 1977a, b, 1978) fit predicted hotspot tracks. This was believed to relate to their being emplaced through thinner crust off the craton and/or to the rate of plate motion.

Le Roex (1986) has extended this hotspot model to include the Group 2 kimberlites. The model is based on trace element (e.g. LILE/HFSE ratios) and isotopic similarities between Group 2 kimberlites and OIB hotspots falling within the Dupal anomaly. Hart (1984 and unpub. data referenced in Le Roex, 1986) delineated a major region in the South Atlantic between Southern Africa and South America, and between $\simeq$ 20°S and $\simeq$ 54°S, in which OIB can bear the isotopically enriched Dupal signature. Although the kimberlites of South Africa have been studied more intensely than any other kimberlite locality, it is important to note that the isotopic characteristics of Group 2 kimberlites have only been recorded, to date, from South Africa. It would appear there is a close correlation between the OIB Dupal anomaly and Group 2 kimberlites on the Kaapvaal craton. Le Roex (op. cit.) proposed that the Group 2 kimberlite and Dupal signature resulted from portions of enriched delaminated lithosphere recycled into the asthenosphere. Palacz and Saunders (1986) also favoured such a model for the Dupal anomaly. The Le Roex (1986) model overcomes the problem of deriving spatially juxaposed kimberlite magmas of relatively similar age from two tectonically different source regions, since both would originate from within the asthenosphere. However, if both kimberlite groups are asthenospheric, then why are hot deformed Fe- Ti-rich peridotite xenoliths and the Cr-poor megacryst suite generally restricted to the Group 1 kimberlites?

The preferred model here, is that Group 2 kimberlites are predominantly derived from ancient trace element enriched source regions from within the subcontinental mantle lithosphere. The trigger to magmatism resulted from tensile stresses induced in the lithosphere during ocean rifting (Smith,

1983a, b; Skinner, 1986). Group 1 kimberlites are essentially asthenospheric, though it is possible they could be derived from 'young' trace element enriched lithospheric material near the base of the lithosphere. The trigger to Group 1 kimberlite magmatism was hot-spot activity (Smith, 1983a, b), which potentially also provided the magmatic material. From the spatial proximity of these kimberlites in the field, it is possible to infer that, even though both kimberlite groups are derived from within the diamond stability field (> 150 km) Group 1 kimberlites are from the greatest depths.

The North American lamproite suites are not obviously related to any magmatic trigger. For example, in northcentral Montana, the Smoky Butte lamproites are a spatially and temporally isolated phase of magmatism at 27 Ma. In this region, igneous activity was concentrated in an area to the west of Smoky Butte, and took place between 69–46 Ma (Marvin et al., 1980).

Jaques et al. (1984b and 1986a) note that the West Kimberley (Australia) lamproites occur on a N-S trend, with ages decreasing southwards. They attributed this to the northward migration of the Australian continent over a hotspot, during Miocene times. Since these lamproites are believed to be derived from ancient lithospheric mantle source regions, this indicates that hotspots could thermally induce magmatism, without contributing a significant amount of, presumably, OIB-type material.

5.2 Trace element enrichment styles

Attention is now given to the nature and origin of the ancient trace element enrichment events within the subcontinental lithosphere as recorded by kimberlites and lamproites. The major element composition of these rocks is characterised by low Ca, Al, Fe and Na, suggesting that their sources were depleted in basaltic components. They are therefore believed to be derived from source regions depleted by melt extraction prior to trace element enrichment (Jaques et al., 1984a, 1986a; Bergman, 1987). The latter processes significantly modified the composition of portions of the subcontinental mantle, as evinced by the wide range in trace element and isotope geochemistry of the kimberlites and lamproites studied in this work. This section outlines the similarities and disparities in the observed compositions of these rocks, while the subsequent section considers the possible origin of the inferred trace element enrichment events.

The lamproites analysed here, in general, have higher REE contents and steeper REE profiles than the kimberlites (Table 5.1). The greater variation in the West Kimberley and Leucite Hills analyses is probably because samples were collected over large areas which have numerous composite intrusions. Overall, trace element features are illustrated on mantle normalised

Locality	Ce_N/Yb_N	La ppm
Kimberlites		
Finsch mine	33.2–62.4	40–110
Group 1 kimberlites[1]		23–294
Group 2 kimberlites[1]		43–400
Lamproites		
West Australia	50–163	108–596
Smoky Butte	101–112	332–437
Leucite Hills	42–123	112–357
Prairie Creek	72–80	142–147

Table 5.1 Ce_N/Yb_N ratios and La contents in kimberlites and lamproites. 1 – data source is Smith et al. (1985).

diagrams on Figure 5.6. On Figure 5.6a, the West Kimberley lamproites have higher trace element contents, but similar shaped profiles to the Finsch kimberlites. The Smoky Butte rocks, in contrast, are depleted in Rb, Pb and Th relative to the West Kimberley lamproites, even though they have comparable HFS element abundances. The North American lamproites have been compared in detail in Chapter 4 (Section 4.6.2) and are shown together on Figure 5.6. Furthermore, these trace element differences are accompanied by markedly different isotope-isotope trends. The latter is important, since it demonstrates that trace element variations between the above rocks are not completely due to processes occurring during melt formation and extraction.

All the lamproites and kimberlites analysed here have higher ϵSr and lower ϵNd than the bulk earth (Figure 5.7). Within the data, two main trends are identified. Results on samples from Finsch Mine and West Kimberley lie on an apparently discontinuous trend from Group 1, through Group 2 kimberlites to the West Kimberley lamproites, which have ϵSr = 80 to 228 and ϵNd = -8 to -19. In contrast, the North American lamproite data from Leucite Hills and Smoky Butte, exhibit little variation in ϵSr, but an extreme range in ϵNd extending down to -26 in a sub-vertical ϵNd - ϵSr trend (Figure 5.7). These appear to represent endmembers between which there may be a continuum of isotope trends, as shown by Prairie Creek and the Gaussberg (Collerson and McCulloch, 1983) lamproites, which have ϵSr = 30 to 72, and ϵNd = -10 to -15. The ϵNd values are comparable to those in the Leucite Hills and West Kimberley. However, on a geographical basis, the Prairie Creek lamproites are probably associated with the steep vertical trend of the North American lamproites, whereas the Gaussberg lamproites are more likely to relate to the shallow Finsch and West Kimberley trend

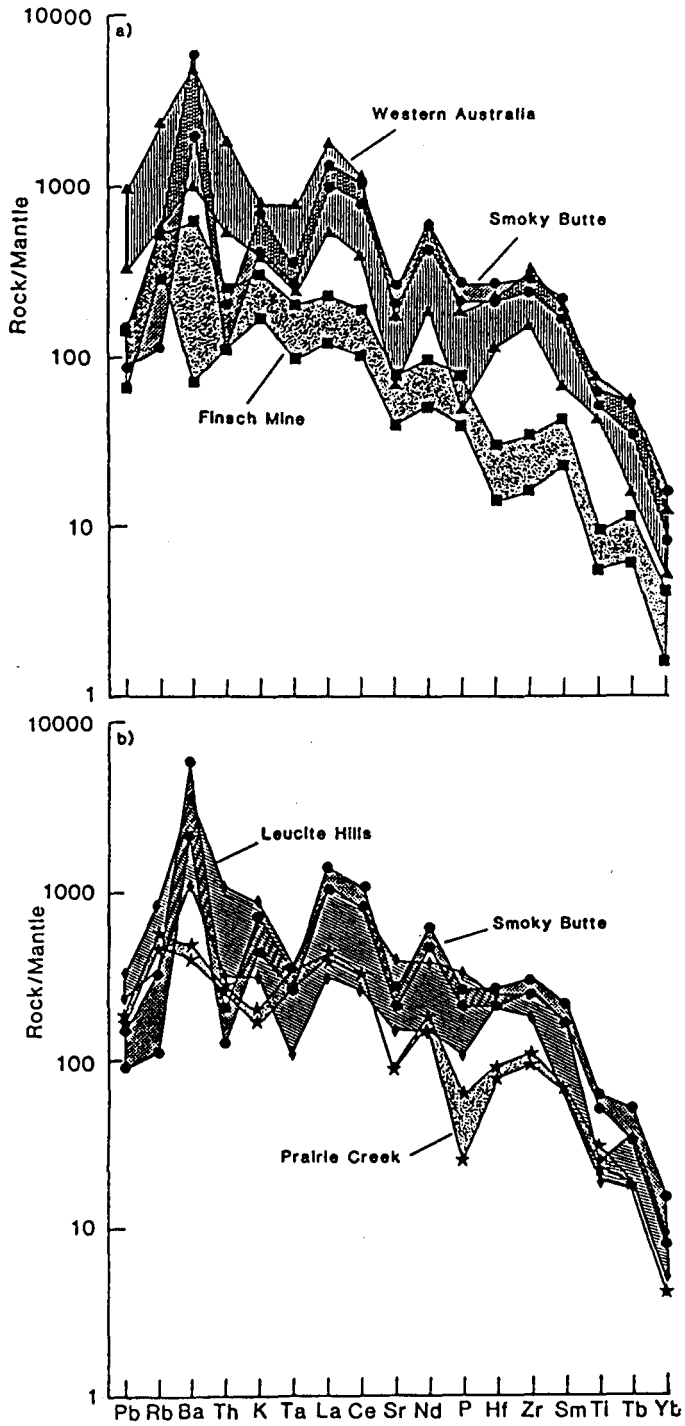

Figure 5.6 Mantle normalised trace element abundance profiles for kimberlites (Finsch mine, South Africa = ■) and lamproites (West Kimberley = ▲ and North America; Smoky Butte = •, Prairie Creek = ⋆ and Leucite Hills = ◆.

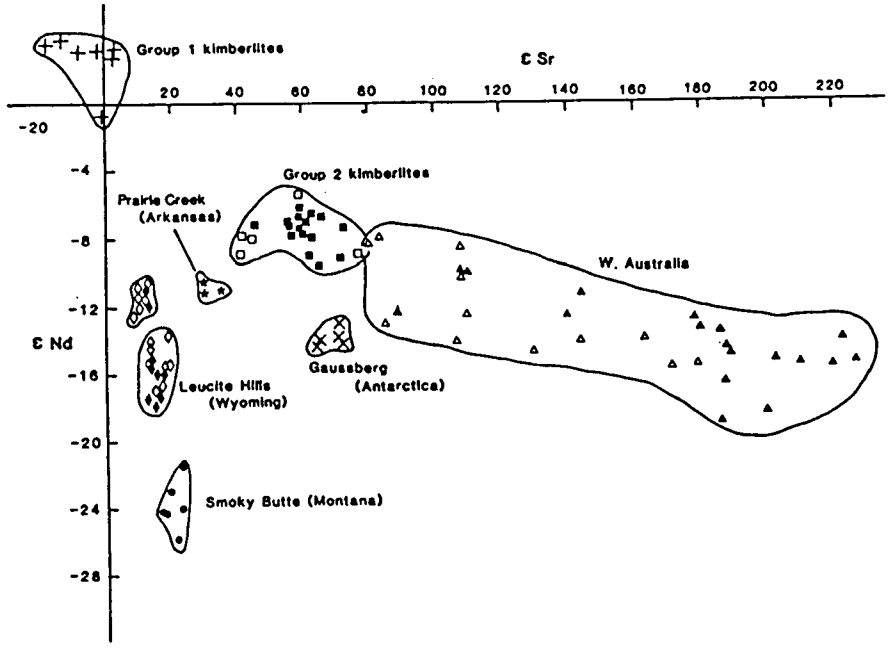

Figure 5.7 ϵNd vs. ϵSr for kimberlites and lamproites. ■ = Finsch kimberlites, □ = Group 2 kimberlites, + = Group 1 kimberlites (Smith 1983) and lamproites from West Kimberley (▲ = this study, △ = McCulloch et al., 1983), North America (⋆ = Prairie Creek, Leucite Hills; ◆ = this study, ◇ = Vollmer et al., 1984 and • = Smoky Butte) and Gaussberg, Antarctica = × (Collerson and McCulloch, 1983).

(Figure 5.7).

Lamproites and Group 2 kimberlites exhibit a wide range in $(^{206}Pb/^{204}Pb)_i$ = 16.02 to 17.99, $(^{207}Pb/^{204}Pb)_i$ = 15.19 to 15.80 and $(^{208}Pb/^{204}Pb)_i$ =36.9 to 38.5, but they are all less radiogenic than the published analyses of Group 1 kimberlites (Smith, 1983; Kramers, 1977; Figure 5.8). The low εSr North American lamproites are characterised by unradiogenic Pb isotope signatures with $(^{206}Pb/^{204}Pb)_i$ extending down to values of 16.02 in the Smoky Butte rocks. The high εSr Group 2 kimberlites also plot below the Pb-ore evolution curve in a similar position to the Leucite Hills lamproites (Figure 5.8). The Pb isotope compositions of the West Kimberley and Gaussberg lamproites require a more complex three-stage growth history requiring early evolution in a high U/Pb, high Th/Pb environment and subsequently in a low U/Pb environment (Fraser et al., 1985; Nelson et al., 1986a; Section 3.9.3). As with εNd and εSr, only the Group 1 kimberlites have Pb isotope ratios within the range of those from oceanic basalts; both lamproites and Group 2 kimberlites are characterised by more extreme compositions.

These findings show that each regional lamproite suite and kimberlite type was derived from an isotopically distinct source. It has been discussed in earlier chapters, that with the exception of the Group 1 kimberlites, these source regions were ancient and situated in the subcontinental lithospheric mantle. Since kimberlite and lamproite melts do not appear to have interacted with crust during their ascent the isotope trends recorded in these rocks represent different styles and/or ages of trace element enrichment within the subcontinental mantle.

Menzies and Wass (1983) proposed that deviation from the mantle array on a εNd – εSr diagram may partly relate to volatile content: high CO_2 maintains low Rb/Sr, but can develop low Sm/Nd. High H_2O, on the other hand, results in high Rb/Sr. With time, these variations would result in two distinct trends on a εNd – εSr diagram. The Group 2 kimberlite and lamproite data are inconsistent with this hypothesis, otherwise the two trends on Figure 5.7 would have been defined by CO_2- and H_2O- rich kimberlites with low εSr and high εSr, H_2O-rich lamproites. Thus, the volatile composition does not appear to have been instrumental in determining the Rb/Sr ratio of source regions.

Figure 5.9 shows the relationship between εNd and $(^{206}Pb/^{204}Pb)_i$ for kimberlites and lamproites. These rocks define a positive correlation between the low εNd, low $(^{206}Pb/^{204}Pb)_i$ Smoky Butte rocks to the relatively high εNd and $(^{206}Pb/^{204}Pb)_i$ Group 1 kimberlites. This correlation raises several points. Firstly, the data demonstrate that during source enrichment a relationship was maintained between U/Pb and Sm/Nd systematics. This implies some affinity between enrichment processes at each locality, despite the wide range in Rb/Sr ratios that were generated. Secondly, this posi-

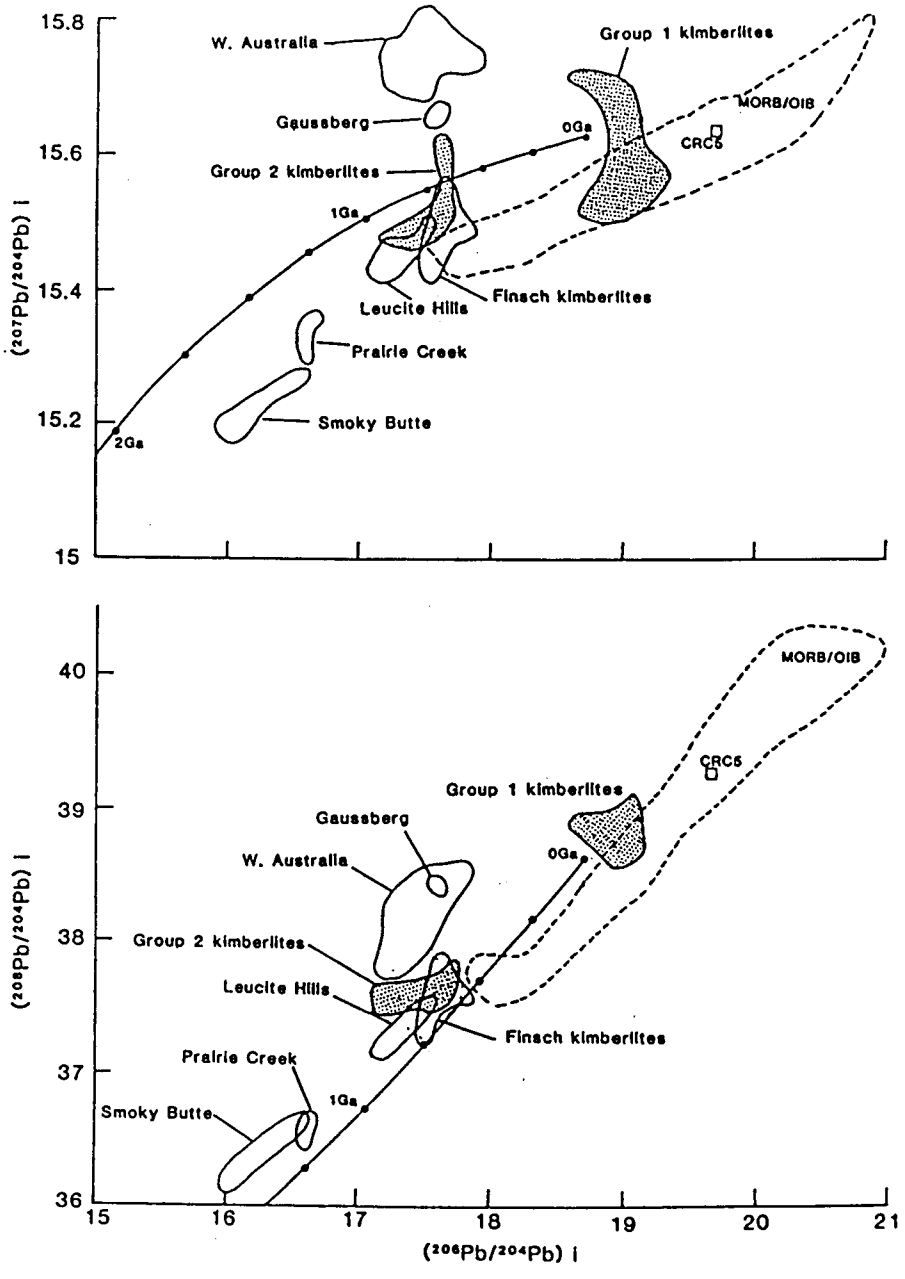

Figure 5.8 Initial Pb isotopes for kimberlites and lamproites. Data sources and symbols as for Figures 2.12 and 5.7, with the exceptions of the Gaussberg and a number of the West Kimberley lamproites, which are from Nelson et al., (1986a).

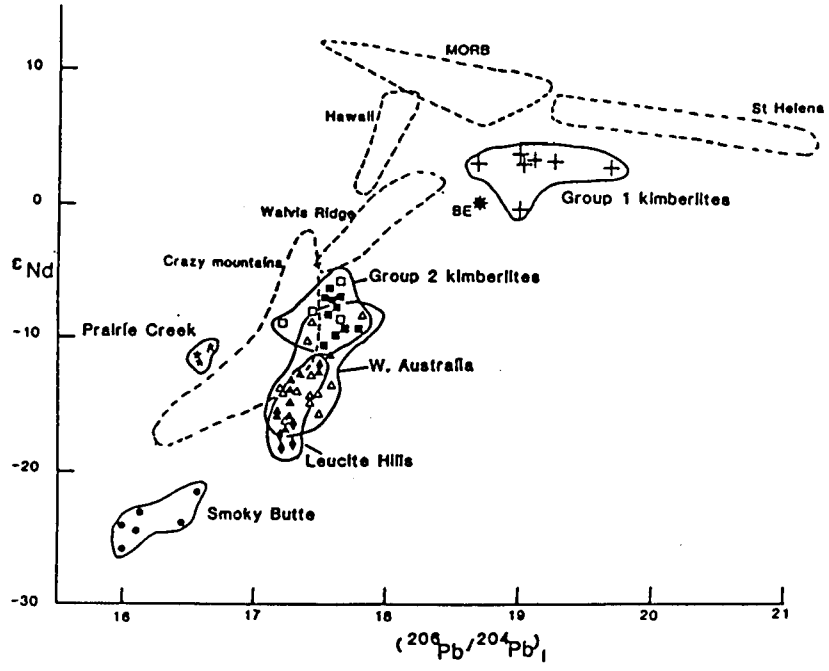

Figure 5.9 εNd vs. $(^{206}Pb/^{204}Pb)_i$ for various mantle derived rocks. Symbols and data sources for kimberlites and lamproites as in Figure 5.7. These are compared with fields for the Walvis Ridge (Richardson et al., 1982), Hawaii (Stille et al., 1983), MORB, St. Helena and the Crazy Mountains alkalic rocks (Dudás et al., 1987).

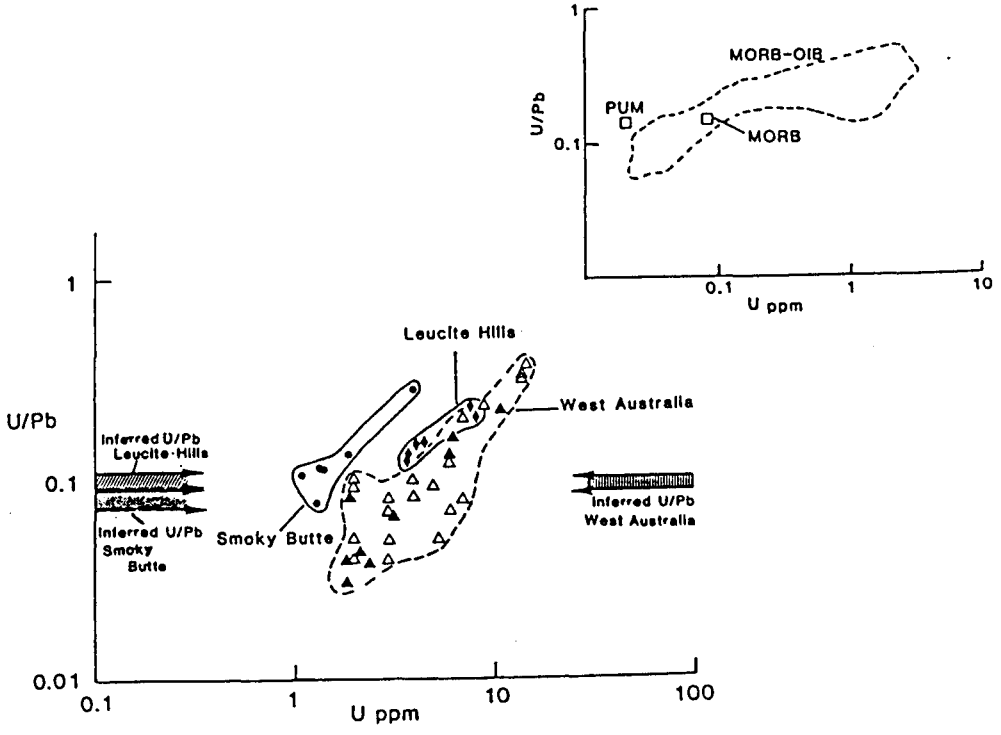

Figure 5.10 U/Pb vs. U ppm for lamproites from Smoky Butte = •, Leucite Hills = ◆ and West Australia ▲ = this study, △ = Jaques et al., 1984a). Also shown are the ranges of source region U/Pb ratios calculated from Pb-Pb model ages. Inset shows U/Pb vs. U ppm for MORB-OIB, average MORB and a value for primitive upper mantle (PUM)(after Newsom et al., 1986).

tive trend is the opposite of the negative trend exhibited by the majority of MORB and OIB (Figure 5.9). The kimberlite/lamproite trend is inconsistent with inferences made for the bulk distribution coefficients of Sm, Nd, U and Pb for melting at mantle depths, where estimates suggest $D_{Nd} < D_{Sm}$ and $D_U < D_{Pb}$ (Frey et al., 1978; Henderson, 1982; Newsom et al., 1986). Thus, unradiogenic Pb isotope ratios should coexist with radiogenic Nd isotope ratios and vice versa. Interestingly, both MORB/OIB (Newsom et al., 1986) and the lamproite data indicate that during magmatism $D_{Nd} < D_{Sm}$ and $D_U < D_{Pb}$. A positive correlation exists between U/Pb ratios and U contents in MORB/OIB and lamproites (Figure 5.10; Hawkesworth, pers. comm.). At Smoky Butte and Leucite Hills, inferred U/Pb ratios are less than observed U/Pb ratios. The observed U/Pb ratios in the West Kimberley lamproites range from 0.03 to 0.36, this study and Jaques et al., 1984a) whereas inferred U/Pb ratios are 0.08 to 0.10. Calculation of inferred ratios

assumes simple two-stage models and the high $(^{207}Pb/^{204}Pb)_i$ ratios of the West Kimberley lamproites requires evolution in a high μ environment prior to the low μ needed to generate the low $(^{206}Pb/^{204}Pb)_i$ ratios. Thus, the inferred μ's for the West Kimberley lamproites are maximum values and Figure 5.10 indicates that the source U/Pb ratio may be as low as 0.03 (μ = 1.8). However, in general, comparison of inferred source and observed U/Pb ratios suggests that melt formation and extraction results in an increase in U/Pb ratio and $D_U < D_{Pb}$. Thus, during melt formation and extraction, relative D values are comparable to those for basaltic systems. Similarly, it was demonstrated earlier, that inferred source Sm/Nd ratios in lamproites were higher than observed Sm/Nd ratios and hence $D_{Nd} < D_{Sm}$ during magmatism.

It is interesting to note that other continental and oceanic volcanics believed to contain a contribution from the subcontinental mantle lithosphere also trend towards low εNd and $(^{206}Pb/^{204}Pb)_i$ ratios (Dudás et al., 1987). Hence, this may be a not uncommon feature of ancient enriched portions of the subcontinental mantle lithosphere. Bearing the above in mind, the origin of these trace element enrichment events is now considered.

5.3 Origin of trace element enrichment processes

The cause of trace element enrichment processes recorded from within the subcontinental mantle is generally disputed. Previously, models for the evolution of the earth have often explained the so-called mantle array on a εNd – εSr isotope diagram as being the result of differentiation events into enriched crust (high εSr, low εNd) and depleted (e.g. MORB and OIB type sources) mantle (low εSr, high εNd). In such a model, any upper mantle derived continental igneous rock with low εNd and high εSr, relative to bulk earth, was believed to contain a significant contribution from a crustal component. More recently, xenoliths from the sub-continental mantle have been shown to preserve a wide range in Sr, Nd and Pb isotope ratios, which are thought to have developed in old mantle material within the continental lithosphere (Kramers et al., 1983; Menzies, 1983; Richardson et al., 1985). Two schools of thought have emerged with regard to the processes responsible for the inferred fractionation in parent/daughter ratios. One proposes that continental crust recycled into the lithosphere via subduction processes, can provide enriched isotope signatures and/or the required fractionation in parent/daughter ratios. Alternatively, they could denote extreme mantle processes. Numerous studies of late have attempted to distinguish between these two options. This section will therefore review the predilections of recent authors with particular emphasis on kimberlites and lamproites, de-

tailing previous work and examining the problem with available data.

5.3.1 Recycled continental crust

In the model of plate tectonics, oceanic lithosphere is consumed at subduction zones and reprocessed back into the mantle. Since continental-derived sediments are deposited on ocean crust, these convergent plate boundaries potentially provide a means for recycling continental crust to mantle depths. To assess whether, to what extent and in what form, sediments are subducted has been the focus of much recent work.

Integrated geochemical studies of island arc volcanics have identified a number of characteristics that are probably due to a subducted sediment component. For example, enrichments in certain incompatible trace elements (in particular, K, Sr, Ba and Pb), radiogenic Sr and Pb isotope ratios, low $^{143}Nd/^{144}Nd$ and $^{176}Hf/^{177}Hf$ ratios and high concentrations of ^{10}Be (Taylor and McClennan, 1985 and references therein). Modelling this in detail has proved difficult. These magmas are H_2O-rich, and H_2O during magmatism will affect the behaviour of a number of trace elements (e.g. Pearce, 1983). Moreover, the arc source appears to be a three component mixture of mantle, hydrothermally altered oceanic crust and sediment (White, 1987). Thus, evaluation of the amount of sediment involved in island arc magmatism is largely conjectural. Most estimates are low, $< 3\%$ (Taylor and McClennan, 1985), but may extend up to $\simeq 10\%$ (White, 1987). Since, there is a large degree of uncertainty regarding the amount of sediment that is initially subducted, it is possible that some may be recycled to even greater depths than that of island arc volcanism, i.e. > 80 to 150 km (Taylor and McClennan, 1985). Trace element and isotope (both radiogenic and stable) geochemistry has been cited as evidence for a contribution of 'recent' subducted sediments in back arc basin volcanism (Mattey et al., 1984; White, 1987 and references therein) and mantle xenoliths from areas affected by recent subduction (Mattey et al., 1987).

If sediments are subducted further, they could be incorporated into very deep levels of the subcontinental lithospheric mantle and/or be recycled, together with oceanic lithosphere, back into the asthenospheric mantle. There are problems in determining if this occurs for several reasons. Apart from there being little conception of how much sediment may be involved at these depths, the composition of the residue after island arc and back arc magmatism is unknown. Furthermore, intraplate magmatism which might contain a sediment component, tends not to be temporally or spatially, associated with active, or recent subduction processes. In which case, any enriched isotope signature would reflect the isotopic composition of the subducted crust and with time any change in inferred parent/daughter ratios gener-

ated during the subduction event. With this in mind, various studies have attempted to assess whether intraplate magmatism bears evidence of a subducted crust component. This is usually by direct comparison with sediment compositions rationalised as being the most likely crustal component during subduction processes.

To explain their high εSr and low εNd, relative to MORB, it has frequently been postulated that OIB contain a contribution from recycled ocean lithosphere and sediments (White and Hofmann, 1982; Hofmann and White, 1982). More recently, attention has focussed in the origin of the Dupal anomaly (anomalous Pb- and Sr-isotope compositions) observed in some southern hemisphere ($\simeq$ 30°S) OIB (Hart, 1984). On Pb-Pb arrays, the Dupal OIB exhibit sub-parallel trends to the main OIB-MORB, but are displaced above it, towards higher $(^{207}Pb/^{204}Pb)_i$ and $(^{208}Pb/^{204}Pb)_i$ ratios. These latter values require high U/Pb early in earth history. This, together with $\varepsilon Sr > -10$, may be considered, in one model, compatible with a contribution from crustally derived sediment. Hart (op. cit.) argued that, if the anomaly is due to recycled crust, it must have been introduced into the mantle a long time ago, to be consistent with the Pb-Pb arrays. Such an interpretation was also favoured by Weaver et al. (1986) who further observed that these OIB contain high Ba/Nb, La/Nb and Th/Nb ratios, which are features characteristic of pelagic sediments. However, there is trace element evidence that recycling of sediment into OIB sources has been very limited. For example, Newsom et al. (1986) brought attention to the constancy of the Pb/Ce ratio in both MORB and OIB $\simeq$ 0.036. Average continental crust exhibits significantly higher Pb/Ce ratios (0.24 to 0.26; Weaver and Tarney, 1984; Taylor and McClennan, 1985). White (1987) considered that observed Pb/Ce ratios in MORB and OIB, together with the high concentrations of Pb in sediment and low Pb concentrations in the mantle, are a strong constraint on sedimentary recycling. He calculated that additions of $< 1\%$ sediment to the mantle would lead to Pb/Ce ratios in the mixture, that are higher than any observed in fresh oceanic basalt. Thus, it is considered that the evidence for recycled sediment in OIB source regions is, as yet, equivocal.

Turning now to evaluate the evidence for recycled oceanic lithosphere and/or sediments in intracontinental mantle derived rocks. Helmstaedt and Gurney (1984) attempted to relate Karoo flood basalt magmatism and metasomatised nodules from South Africa to large scale shallow subduction of oceanic lithosphere under the South African craton. Some eclogitic xenoliths from kimberlites are believed to represent recycled oceanic lithosphere (Ringwood, 1975; MacGregor and Manton, 1986). Diamonds of eclogitic paragenesis exhibit a much wider range in $\delta^{13}C = +0.5$ to -34.5 ‰, than those of peridotite paragenesis where $\delta^{13}C = -2$ to -9 ‰ (Sobolev et al.,

Rock-type	K/Rb	Ba/Nb	La/Nb	Th/Ta
MORB	568, 623	11.4, 5.7	1.7	0.73, 1.1
OIB	370–900	5.9, 6.8	0.65, 0.69	1.0–1.1
Post-Mesozoic sediment		521	8.2	8.9
Pre-Mesozoic sediment		338	5.7	11.1
Upper continental crust	208	22	1.2	4.9
Upper Archaean crust	249	28	1.2	
Lower continental crust	439	25	1.8	1.8
Lower Archaean crust	755	151	4.4	
Kimberlites				1.8
Group 1 kimberlites A	55–279	1.4–8.5	0.28–0.84	
Group 2 kimberlites	107–245	7.8–39.6	1.0–2.0	
Finsch kimberlites	161–230	6.0–59.4	0.99–1.6	2.0–3.0
Lamproites				
West Australia	44-405	21.3–141	0.64–2.3	2.4–6.0
Smoky Butte	498–932	86.3–96.8	3.3–3.6	1.0–1.2
Leucite Hills	128–408	91.4–178	2.3–4.6	5.3–9.2
Prairie Creek	113–117	15.9–20.6	1.4–1.7	1.7–2.2

Table 5.2 Selected trace element ratios of various rock-types. Data are shown for kimberlites and lamproites. Group 1 and 2 kimberlite data from Smith et al. (1985) and includes CRC 5 from this study and the West Kimberley data includes those of Jaques et al. (1984a). These are compared with values for MORB (Pearce, 1983; Taylor and McClennan, 1985), OIB (Morris and Hart, 1983; Weaver et al., 1986 and references therein), post- and pre-Mesozoic sediments (Weaver and Tarney, op. cit. and references therein), averages for upper and lower continental crust (Taylor and McClennan, 1985) and averages for upper and lower Archaean crust (Weaver and Tarney, 1984).

1979; Deines et al., 1984). A number of authors conjectured this may indicate a crustal origin for some eclogitic diamonds (see reviews: Meyer, 1985; Mattey, 1987). Schulz (1986) used major element arguments to suggest that peridotitic diamonds and low Ca harzburgites could be subducted metaserpentine.

Nelson et al. (1986b), Nelson and McCulloch (1987) and McCulloch (1987) proposed a component of recycled continental crust to explain the unusual geochemical characteristics of continental potassic magmatism (e.g. variable oxidation state, high P_2O_5, F, H_2O and enriched isotope signatures). Table 5.2 demonstrates that kimberlites and lamproites exhibit a number of trace element ratios more typical of continental crust than either MORB or OIB. Relative to MORB and OIB, continental crust compositions

have low K/Rb (except lower Archaean crust) and high Ba/Nb, La/Nb and Th/Ta ratios i.e. high LIL/HFSE ratios. Group 2 kimberlites and lamproites from West Kimberley, Leucite Hills and Prairie Creek are comparable with the continental crust and have high Ba/Nb, La/Nb, Th/Ta, but low K/Rb ratios. The Smoky Butte lamproites exhibit high Ba/Nb, La/Nb and K/Rb similar to an Archaean lower crust composition. However, the Smoky Butte rocks have low Th/Ta ratios, similar to values observed in MORB and OIB. Group 1 kimberlites, which have Sr-Nd-Pb isotopes indicative of an OIB source (Smith, 1983a, b, Figure 5.7) exhibit low Ba/Nb and La/Nb ratios similar to those in MORB and OIB. However, they exhibit low K/Rb ratios comparable to continental crust and Group 2 kimberlites. Also the Th/Ta ratio = 1.77 of one Group 1 kimberlite (CRC 5) is higher than typically observed in either MORB or OIB.

Figure 5.11 shows that the kimberlites and lamproites all have high Pb contents and with the exception of Smoky Butte, high Pb/Ce ratios (0.18 to 0.21) generally intermediate between MORB and OIB and the continental crust. The Smoky Butte samples, however, have Pb/Ce ratios (0.015 to 0.023) lower than those in OIB and MORB.

The above discussion illustrates a number of trace element traits in Group 2 kimberlites and lamproites that are more similar to those observed in continental crust, than in either MORB and/or OIB. Interestingly, Group 1 kimberlites, with typical OIB isotope signatures, also exhibit some anomalous trace element ratios.

It has further been suggested that the isotope characteristics of at least the West Kimberley lamproites require a three-stage growth model, with high μ early in earth history and then low μ later in their history (Fraser et al., 1985; Nelson et al., 1986a; Section 3.9.3). Nelson et al. (1986b), Nelson and McCulloch (1987) and McCulloch (1987) have interpreted this as being due to a recycled crustal component, since erosion of continental crust can result in pelagic sediments which have high $(^{207}Pb/^{204}Pb)_i$, but low U/Pb ratios. Subduction of such a component and incorporation into the deep subcontinental lithospheric mantle, without any significant modification of the parent/daughter ratio, would result in retardation of the growth of radiogenic Pb and in time low $(^{206}Pb/^{204}Pb)_i$ ratios. The unradiogenic Nd and radiogenic Sr isotope ratios of the West Kimberley lamproites are also not inconsistent with this model. Moreover, pelagic sediment with low U/Pb and Sm/Nd could explain the positive correlation between εNd vs. $(^{206}Pb/^{204}Pb)_i$ exhibited by Group 2 kimberlites and lamproites (Figure 5.9).

On Figure 5.12 average compositions for upper, lower and bulk crust and recent pelagic clay (Taylor and McClennan, 1985) define a negative trend from low U/Pb, relatively high Sm/Nd lower crust to high U/Pb,

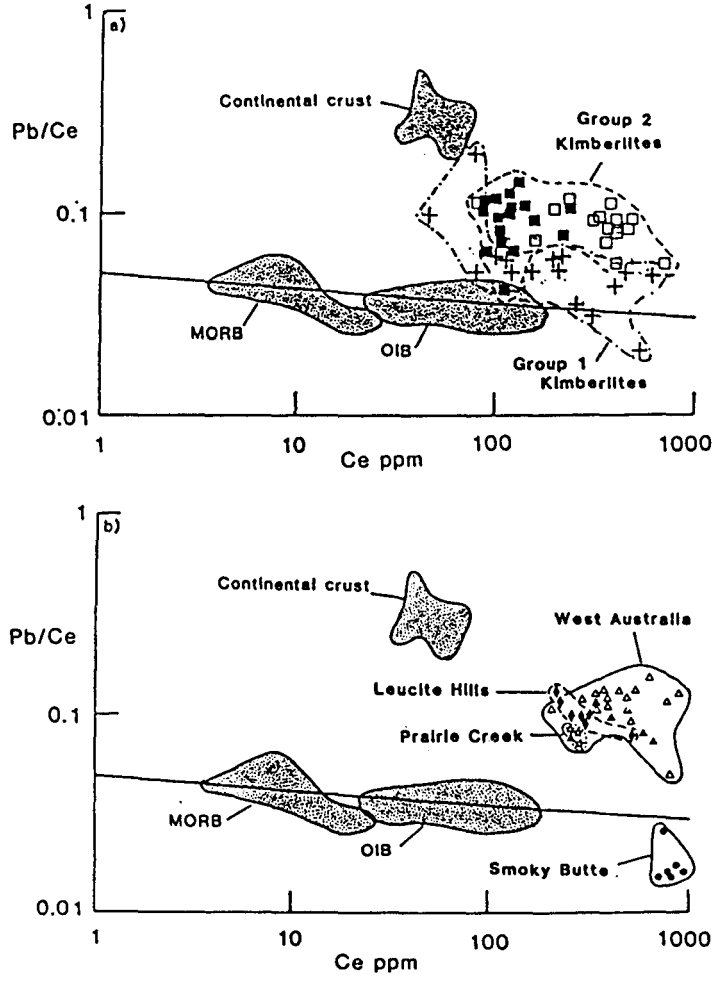

Figure 5.11 Pb/Ce vs. Ce ppm for kimberlites and lamproites. Symbols and data sources as in Figure 5.7, with the exception of the West Kimberley lamproites where ▲ = olivine lamproites and △ = leucite lamproites. These are compared with fields for MORB and OIB (Newsom et al., 1986) and continental crust (Weaver and Tarney, 1984; Taylor and McClennan, 1985).

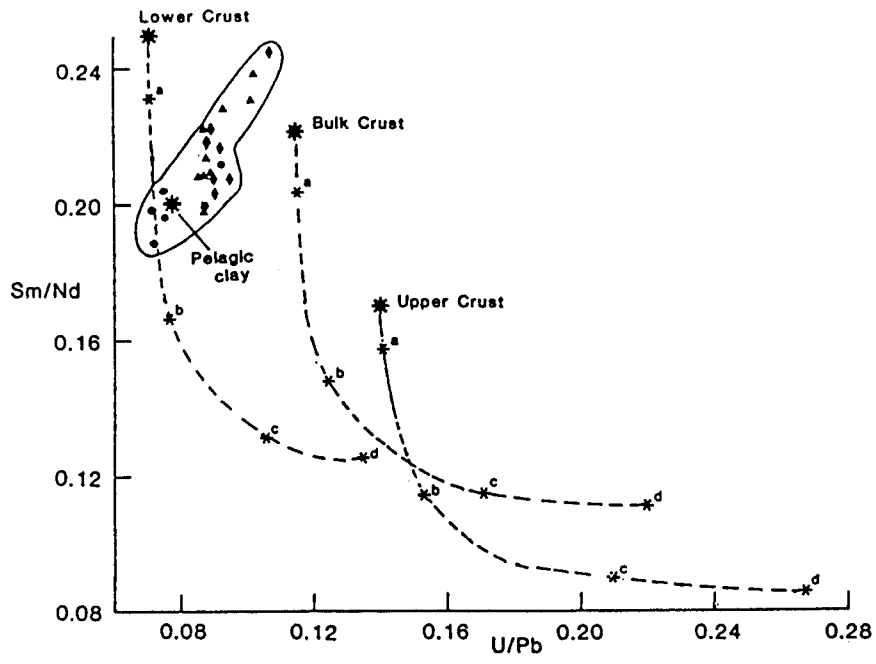

Figure 5.12 Sm/Nd vs. U/Pb for various lamproite source regions (symbols as in Figure 5.7). Ratios are calculated from Pb-Pb model ages. These are compared with average values for lower, bulk and upper crust compositions (Taylor and McClennan, 1985). Also shown are melting curves calculated from simple batch melting equations assuming $D_{Sm} = 0.05$, $D_{Nd} = 0.01$, $D_U = 0.001$ and $D_{Pb} = 0.005$ and F = a) 0.1, b) 0.01, c) 0.001 and d) 0.0001.

low Sm/Nd upper crust. This contrasts with the positive trend shown by the inferred source Sm/Nd, U/Pb ratios for lamproites from Smoky Butte, Leucite Hills and the West Kimberley, which intersects the above correlation between lower and bulk continental crust compositions. The pelagic clay composition however, falls within the lamproite data near the low U/Pb and Sm/Nd end of the trend. If one assumes that pelagic sediment was a component within these lamproite source regions, then the positive trend on Figure 5.12 could reflect either mixing with a high Sm/Nd, high U/Pb component, or variable degrees of melting of a pelagic component during source enrichment.

To generate the positive trend on Figure 5.12, from partial melting of pelagic sediment compositions, would require $D_{Pb} > D_U$ and $D_{Sm} > D_{Nd}$. The latter effectively suggests that partial melting could result in LREE depleted melts, and this is considered unlikely.

Possible mixing endmembers could include a subducted MORB component, OIB or lithospheric mantle. Clinopyroxenes from garnet peridotite xenoliths, believed to represent the composition of the bulk of the lithospheric mantle, give U/Pb ratios generally < 0.1 (Kramers, 1977, 1979). Whole-rock data of cold coarse garnet peridotites give Sm/Nd $\simeq$ 0.14–0.19 (Richardson et al., 1985). Thus, mixing between pelagic sediment and a lithospheric mantle component will not give the required range of Sm/Nd and U/Pb ratios on Figure 5.12. Average oceanic crust has U/Pb = 0.125–0.27 and Sm/Nd = 0.23–0.4 and OIB have high U/Pb $\simeq$ 0.4 and Sm/Nd = 0.17–0.27 (Wood et al., 1979; Sun, 1980; Clague and Frey, 1982; McClennan and Taylor, 1985; Norry, personal communication). Thus, the positive correlation on Figure 5.12 could ostensibly result from pelagic sediment-oceanic crust mixtures, which would with time develop the observed range of isotope ratios (Figure 5.9).

So far, the evidence for an ancient recycled crust component within Group 2 kimberlite and lamproite sources has been favourable. However, these rocks exhibit a number of features which are difficult to explain if the inferred source trace element enrichment events are totally due to sediment:

1. The North American lamproites and the majority of Group 2 kimberlites plot below the Pb-ore curve (Figure 5.8) and do not yield evidence of an earlier, high U/Pb history. The Smoky Butte lamproites, in particular, are most readily explained by a simple two-stage growth model (Section 4.8.3).

2. The North American and Greenland lamproites are characterised by low εSr and are therefore derived from low Rb/Sr source regions. Although oceanic sediments are characterised by variable εSr (McCulloch, 1987), they have high Rb/Sr ratios (e.g. Taylor and McClennan,

1985; Hart and Staudigel, 1987) which with time will result in radiogenic Sr isotope ratios.

3. Both Group 2 kimberlites and lamproites are characterised by HFSE contents significantly higher than those observed in continental crust, MORB and OIB (Figures 2.14, 3.9, 4.9). High HFSE abundances imply predominantly melt related processes in their petrogenesis.

It would appear that to invoke a contribution of sediment within the source regions is most difficult in the case of the North American lamproites. However, in view of the correlation between Nd and Pb isotopes in Figure 5.9 exhibited by all the lamproite suites and the Group 2 kimberlites, it would seem reasonable to infer that source enrichment events were all related to common processes. As outlined above, although a recycled crust component can explain a number of the characteristic features of these rocks, some aspects of their geochemistry are not readily incorporated into this model. Further insight, into the composition of subducted sediments (both recent and ancient), the possible chemical modifications that occur during island arc and back arc magmatism and, if applicable, during incorporation of this component, via melts or fluids, into the deep subcontinental mantle lithosphere, may help resolve these problems.

5.3.2 Mantle enrichment processes

Conversely, it has been argued that trace element events occurring within the subcontinental mantle lithosphere could be the result of intra-mantle enrichment processes. The wide range in Sr, Nd and Pb isotope ratios in xenoliths and mantle-derived magmas, implies that there are portions of the mantle with different parent/daughter trace element ratios that have been kept separate for long periods of time. The subcontinental mantle lithosphere is a region in which this could occur. It is believed to be relatively cold and rigid, and stabilised against convective disruption (Hawkesworth et al., 1983, 1984; Bickle, 1986). Furthermore, at least in some areas, it has existed to the depths of diamond stability since early Archaean times (Richardson et al., 1984). It is therefore possible that, mantle-derived small volume silicate melts and fluids stabilised and preserved in such regions over long periods of time, would develop a wide range in isotope ratios, depending upon the parent/daughter ratios.

Hawkesworth et al. (1984) in a review of the Sr and Nd isotope and selected trace element data of both within-plate basalts and mantle xenoliths tentatively identified the existence of at least two upper mantle enrichment processes. One is consistent with the migration of small volume silicate melts with 'basanitic' trace element distribution patterns (low Rb/Sr, Rb/Ba and

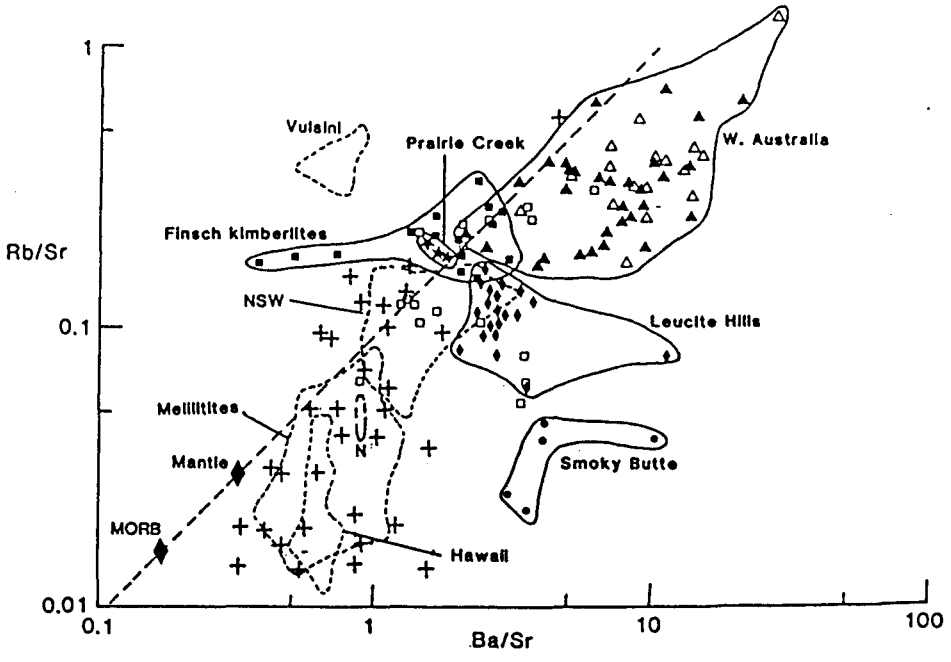

Figure 5.13 Rb/Sr vs. Ba/Sr for various mantle derived rocks. Fields are shown for melilitites (Alibert et al., 1983), Hawaii (Clague and Frey, 1982), New South Wales leucitites (Cundari, 1973), Vulsini rocks (Rogers et al., 1985) and N = Nuanetsi, average picrite basalts (Duncan et al., 1984), typical MORB from Pearce (1983) and primitive upper mantle is from Taylor and McClennan, 1985). Data are also shown for kimberlites and lamproites. symbols and data sources as in Figure 5.7.

K/Ti). The other, as evidenced from K-richterite bearing peridotite nodules (Erlank et al., 1982 and 1987) and the Italian high K rocks from Vulsini (Rogers et al., 1985) may reflect the migration of H_2O-rich and alkali rich fluids (high εSr, Rb/Sr, Rb/Ba and K/Ti).

Hawkesworth et al. (1985) have shown for the majority of rocks (MORB, OIB, continental crust etc.) that although Ba/Sr and Rb/Sr ratios can vary by up to two orders of magnitude, Rb/Ba ratios are restricted between 0.1 and 0.03 (Figure 5.13). Exceptions to this Rb-Sr trend are the Vulsini leucitites and the PP xenoliths (Rb/Sr = 0.16–1.09, Rb/Ba = 0.18–1.18; Rogers et al., 1985; Erlank et al., 1987). These rocks all have high Rb/Sr and Rb/Ba reflecting an enrichment in alkalis (i.e. Rb and K) over both Ba and Sr, which has again been attributed to the migration of H_2O-rich fluids (Hawkesworth et al., 1985).

Normal mantle minerals do not fractionate Rb/Ba ratios (Figure 5.14) and although partition coefficient data indicate that micas have Rb/Ba ratios that are three times higher than those in coexisting basaltic liquids,

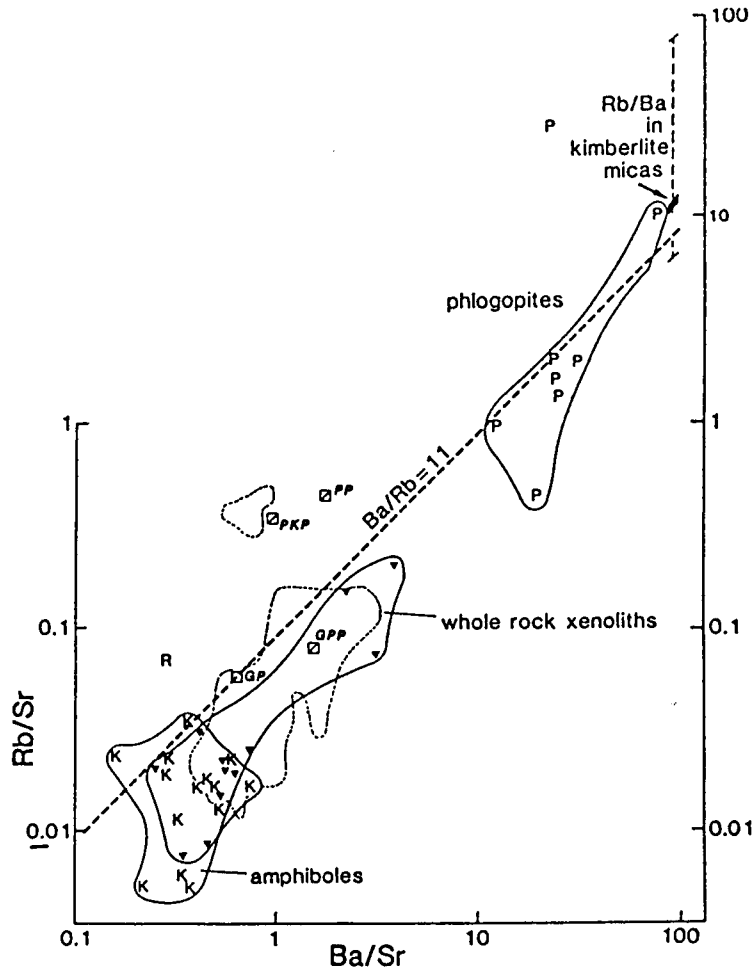

Figure 5.14 Rb/Sr vs. Ba/Sr for various mantle phases. Fields are shown for selected mineral phases and xenolith data. PKP, PP, GP, GPP = average whole-rock analyses of different peridotite xenolith suites (Erlank et al., 1982). P = phlogopites, K = kaersutites, R = K-richterite, ▼ = whole-rock xenoliths from Uganda, Eifel and southeast Australia (Basu, 1978; Wass and Rogers, 1980; Lloyd and Bailey, 1975; Smith et al., 1979; Kuehner et al., 1981; Ridley and Dawson, 1975) (after Hawkesworth et al., 1985).

Hawkesworth et al. (1985) suggest that this is an upper limit since the relative enrichment in Rb/Ba in micas is much lower in lamproites (e.g. at Leucite Hills $K_D^{Rb}/K_D^{Ba} \simeq 1.6$ for phlogopites, Kuehner et al., 1981). Thus, since the average Rb/Ba ratio on the main trend is $\simeq 0.05$, simple mica-liquid fractionation would appear to be inadequate to explain the average Rb/Ba of the PKP whole rocks (0.35) or their phlogopites, which can have Rb/Ba ratios > 2. Hence, on present data such micas crystallised from liquids or fluids which had already developed high Rb/Ba (Hawkesworth et al., 1985).

Hawkesworth et al. (op. cit.) and Fraser et al. (1985) argued that kimberlites and lamproites are among the most extreme products of mantle enrichment processes and that the notions of mantle enrichment processes developed in the study of basalts and xenoliths (Hawkesworth et al., 1984) could be extended to these high K and ultrapotassic rocks.

Figure 5.13 also shows the Rb/Sr and Ba/Sr ratios found in kimberlites and lamproites. The majority of lamproites fall on the main Rb/Ba trend (i.e. Leucite Hills, Prairie Creek and the West Kimberley). The Smoky Butte lamproites have extremely low Rb/Ba ratios due to very high Ba contents (= 8867 to 23,108 ppm; Figure 5.6). The majority of fresh hypabyssal Group 1 and the high εSr Group 2 kimberlites (Smith et al., 1985 and this study) also plot on the main Rb/Ba trend, although some do trend towards higher Rb/Ba values.

Hawkesworth et al. (1985) and Fraser et al. (1985) identified three probably idealised groups:

1. Low Sm/Nd, low Rb/Sr rocks which plot on near vertical εNd – εSr trends e.g. Leucite Hills and Smoky Butte lamproites.

2. Low Sm/Nd, high Rb/Sr which still maintain low Rb/Ba e.g. W. Australia lamproites and the majority of kimberlites.

3. Low Sm/Nd, high Rb/Sr rocks in which Rb/Ba is also high e.g. PP, PKP, Vulsini and some kimberlites.

The majority of the kimberlite and lamproite suites studied fall in the main Rb/Ba trend on Figure 5.13. Thus, despite their volatile-rich nature and high LILE/HFSE ratios, the processes involved in their petrogenesis would appear to have been predominantly melt related. This is, however, consistent with their high HFSE contents. Interestingly, low Rb/Ba is associated with both, low Rb/Sr and high Rb/Sr ratios. Migration of small volume silicate melts like basanites which have low Rb/Sr could, with time, result in low εSr as observed in the North American lamproites. Hawkesworth et al. (1987) argued from batch melting curves for garnet lherzolite (assuming $D_{Rb} = 0.0028$, $D_{Sr} = 0.021$, $D_{Nd} = 0.024$ and $D_{Sm} = 0.040$), that

low Sm/Nd, low Rb/Sr rocks could be generated by melting residues from previous small volume melting events. The West Kimberley lamproites are characterised by low Rb/Ba, but high Rb/Sr and Ba/Sr ratios. Comparison with Ba/Sr and Rb/Sr ratios in phlogopites (Figure 5.14) indicates that West Kimberley lamproites required the stabilisation of a melt related phlogopite within the source (Hawkesworth et al., 1985). Hawkesworth et al. (1987) suggested that very high Rb/Sr ratios in rocks with low Rb/Ba might represent very low degrees of partial melting of mantle which had been previously enriched by small volume melts and/or they could be derived from source regions characterised by phlogopite accumulation from a previous enrichment event. This could be consistent with the three-stage growth model for the West Kimberley lamproites inferred from Pb isotopes (Section 3.9.3).

Diagrams of K/Ba vs. K/Rb (Figures 5.15 and 5.16) illustrates a similar argument to Figures 5.13 and 5.14, since slope on these diagrams records the Rb/Ba ratio.

Smith et al. (1979) noted that data for carbonatites, phonolites, nephelinites, minerals from xenoliths (clinopyroxene, amphibole) and inclusions from diamonds lie on a positive trend with Rb/Ba = 0.1 to 0.01. This correlation is also shown on Figure 5.15 which includes data for Namibian melilitites (Palacz, unpub. data), OIB (Palacz and Saunders, 1986; Clague and Frey, 1982). This is analagous to the main Rb/Ba trend observed on Figure 5.13 where it was attributed to the migration of small volume basanitic melts. Again, the exceptions to this trend (PP and PKP whole-rock xenoliths and the Italian high K rocks from Vulsini) which tend towards high K/Ba and low K/Rb ratios. Figure 5.15 also reveals that MARID micas and mica macrocrysts (termed megacrysts by Smith et al., 1979) fall off the main trend towards high Rb/Ba ratios.

Primary peridotite micas plot on a broad negative trend on Figure 5.15. Smith et al. (1979) interpreted this as being due to mica-liquid fractionation. However, the high K/Ba, low K/Rb end of the peridotite trend overlaps with the PKP's and MARID micas, whereas the low K/Ba, high K/Rb peridotite micas intersect the main Rb/Ba trend. The negative trend might therefore be due to variations in fluid/melt ratio of the transporting medium. All the peridotite and MARID micas have low TiO_2 contents (< 2.34 wt%; Dawson and Smith, 1977; Delaney et al., 1980) and low Ti/K ratios < 0.17. The Ti and K contents of all these micas fall on the low Ti/K trend of Hawkesworth et al. (1984) which was ascribed to movement of H_2O- and alkali-rich fluids. Intuitively, a negative correlation between K/Ba ratios and Ti contents in these micas might be expected, however there is no obvious correlation observed. A negative correlation is observed when K/Ba > 200

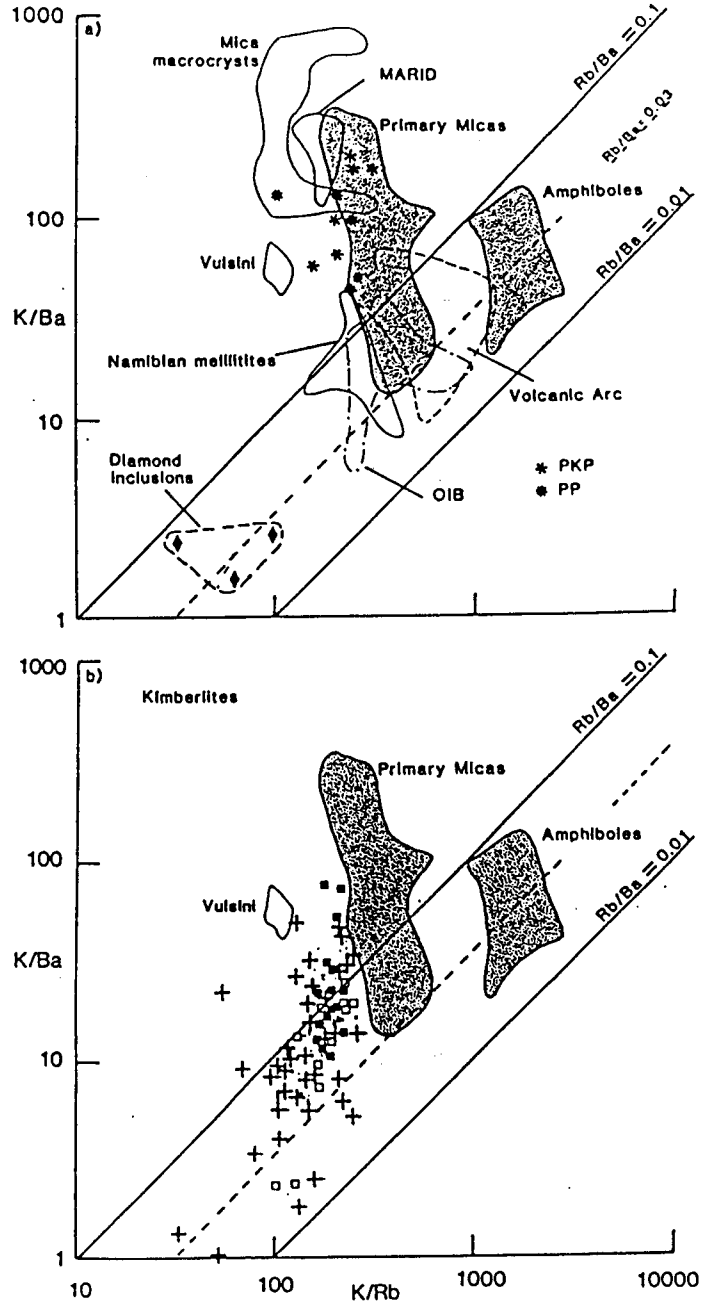

Figure 5.15 K/Ba vs. K/Rb a) for primary peridotite micas, mica macrocrysts from kimberlites, MARID micas (Smith et al., 1979), peridotite amphiboles (kaersutites; Basu and Murthy, 1977), diamond inclusions (Fesq et al., 1975b), Vulsini rocks (Rogers et al., 1985), Namibian melilitites (Palacz unpub. data), OIB (Clague and Frey, 1982; Palacz and Saunders, 1986), volcanic arc rocks (Dupuy et al., 1982), PKP and PP whole-rocks (Erlank et al., 1987) and b) includes kimberlites ■ = Finsch kimberlites, □ = Group 2 kimberlites (Smith et al., 1985) and + = Group 1 kimberlites (Clement, 1982; Smith et al., op. cit.).

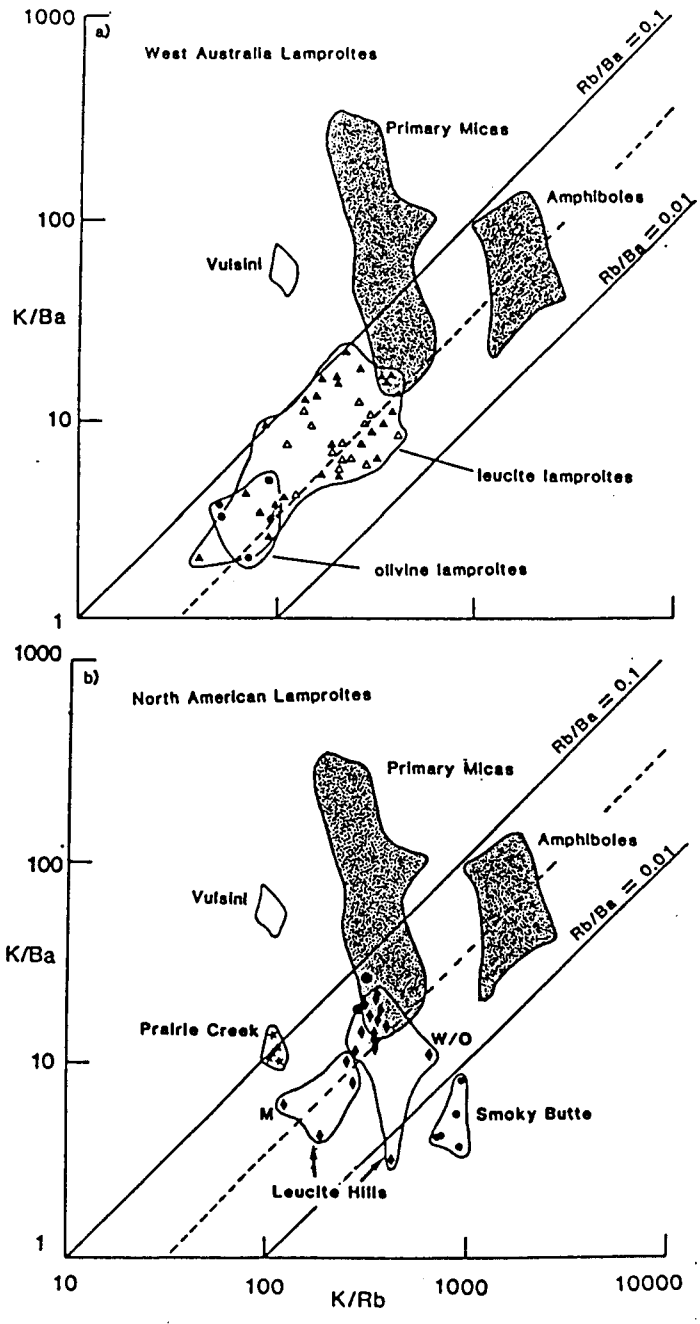

Figure 5.16 K/Ba vs. K/Rb for mantle phases and mantle derived rocks (symbols as in Figure 5.15) including; a) the West Kimberley lamproites; • = olivine lamproites (Jaques et al., 1984a), △ = leucite lamproites (Jaques et al., op. cit.), ▲ = leucite lamproites (this study) and d) the North American lamproites; ⋆ = Prairie Creek, ◆ = Leucite Hills (M = madupite, W/O = wyomingite/orendite), • = Smoky Butte, ● = phlogopite phenocrysts from Leucite Hills (Kuehner et al., 1981.

(all MARID micas and some primary peridotite micas). However, primary peridotite micas with K/Ba < 200 tend to exhibit lower Ti contents than those with K/Ba > 200. This lack of correlation may, at least in part, be due to variations in melt composition from which the micas stabilised. Moreover, the partitioning of Ti into micas may be influenced by the P and T conditions of formation (Robert, 1976).

Kimberlites and lamproites are believed to originate from phlogopite (± amphibole) bearing source regions. These phases are the main carriers of the alkalies (K, Ba, Rb) within the mantle (Beswick, 1976; Matson et al., 1986). Comparing kimberlite and lamproite trends with primary peridotite micas (Figure 5.15 and 5.16) it is apparent that the mica compositions in the source region of the two rock-types were characterised by different trace element ratios. The steep positive kimberlite trend (Figure 5.15b)intersects the peridotite phlogopite field at the high K/Ba, low K/Rb end. In contrast, the lamproite suites generally plot on shallow positive trends which parallel the main Rb/Ba trend. The lamproite variations (Figure 5.16) could be due either to high K/Rb, low K/Ba micas, or to amphibole. The depth of diamondiferous lamproite generation is deeper than the amphibole stability field. Furthermore, only at Smoky Butte is there evidence for the presence of amphibole within their source region. The low K/Ba ratios at Smoky Butte reflects their very high Ba content (Figure 5.6) and may result from another Ba-bearing phase within the source region. Mica compositions from kimberlites and lamproites also support the view that their source regions were distinguished by micas of different trace element composition. Mica macrocrysts, which may be high pressure phenocrysts of kimberlites (Smith et al., 1979) exhibit high K/Ba, low K/Rb ratios and hence extremely high Rb/Ba ratios. The two mica phenocrysts from the Leucite Hills lamproites (Kuehner et al., 1981) have K/Ba, K/Rb and Rb/Ba ratios which plot in the main Rb/Ba trend. These differences might indicate that phlogopites within the source regions of kimberlites stabilised from fluid dominated media, while those within lamproites source regions stabilised from melt dominated media.

The division into fluid and melt dominated processes is probably oversimplistic. All the peridotite micas have low Ti contents and low Ti/K ratios compared to the high Ti phlogopite, kaersutite and pargasite inclusions in alkali basalts. Hawkesworth et al. (1984) suggest the latter are due to melt dominated processes. Also, both lamproites and the majority of kimberlites exhibit Rb/Ba ratios within the range = 0.03 to 0.1, and have high HFSE contents, suggestive of melt-related processes. This could be explained if the events which stabilised phlogopite within the kimberlite and lamproite source regions were predominantly melts, but with varying amounts of H_2O- and alkali-rich fluids. The range of primary peridotite mica K/Rb and K/Ba

ratios may indicate a continuum of volatile/melt compositions.

If kimberlite and lamproite source regions were enriched by volatile bearing melts from the asthenospheric mantle, these must also explain the inferred parent/daughter ratios of these source regions. The positive correlation between εNd and $(^{206}Pb/^{204}Pb)_i$ shown by kimberlites and lamproites (Figure 5.9) intimates at related enrichment processes, even though these processes can generate a wide range in Rb/Sr and hence with time εSr (Figure 5.7). For the reasons outlined in Section 5.3.1, it is believed that the correlation on Figure 5.12 cannot be controlled by simple partial melting of a garnet peridotite source. Kimberlites and lamproites are derived from trace element enriched sources in which phases such as phlogopite, apatite $\pm$ amphibole appear to have been stabilised. Such phases carry significant amounts of incompatible trace elements. These phases could therefore influence the source composition either at the time of trace element enrichment, by crystallising preferentially from a trace element enriched melt/fluid migrating through the lithosphere, or alternatively, during magma genesis by non-modal melting. Possible mineralogical control of the isotopic trends is now discussed.

Phlogopite: Since phlogopite has been invoked almost ubiquitously within the source region of kimberlites and lamproites as a host for K and various incompatible trace elements, it is of interest to assess whether this phase was instrumental in determining the distribution of U/Pb and Sm/Nd. MORB, OIB, kimberlites and lamproites form a broad negative trend on a plot of U/Pb vs. K/Nb (Figure 5.17), which Hawkesworth et al. (1987) proposed may be consistent with a model, whereby phlogopite (high K/Nb, low U/Pb) controls the distribution of U/Pb within the mantle. Published trace element data for mineral fractions from metasomatised xenoliths from Bultfontein, South Africa, reveals that phlogopites have low Sm/Nd values = 0.026 to 0.175 (Kramers et al., 1983). Kramers et al. (op. cit.) also quoted a U/Pb ratio of 0.27 for one phlogopite separate, but this is too high for phlogopite to control the U/Pb vs. K/Nb trend on Figure 5.17, or the Sm/Nd vs. U/Pb trend on Figure 5.12. U and Pb data for phlogopite phenocrysts from the Leucite Hills lamproites give a significantly lower U/Pb ratio = 0.05 and $K_D^U/K_D^{Pb} = 0.29$ (P. Kempton, pers. comm.). These latter values suggest that at least some phlogopites may exhibit low U/Pb and Sm/Nd ratios. There is, however, a problem in progressing from this observation to proposing that phlogopite determines the U/Pb, Sm/Nd ratios within kimberlite and lamproite source regions. If phlogopite is the main host for U and Pb in these sources, then the Leucite Hills data give $D_U = 0.10$ and $D_{Pb} = 0.34$. Adopting these above values and a simple batch melting model (Section 2.10.3), then the U and Pb contents in the majority of the kimberlites and lamproites studied here (1.1 to 10.3 pm and 4.5 to 50 ppm

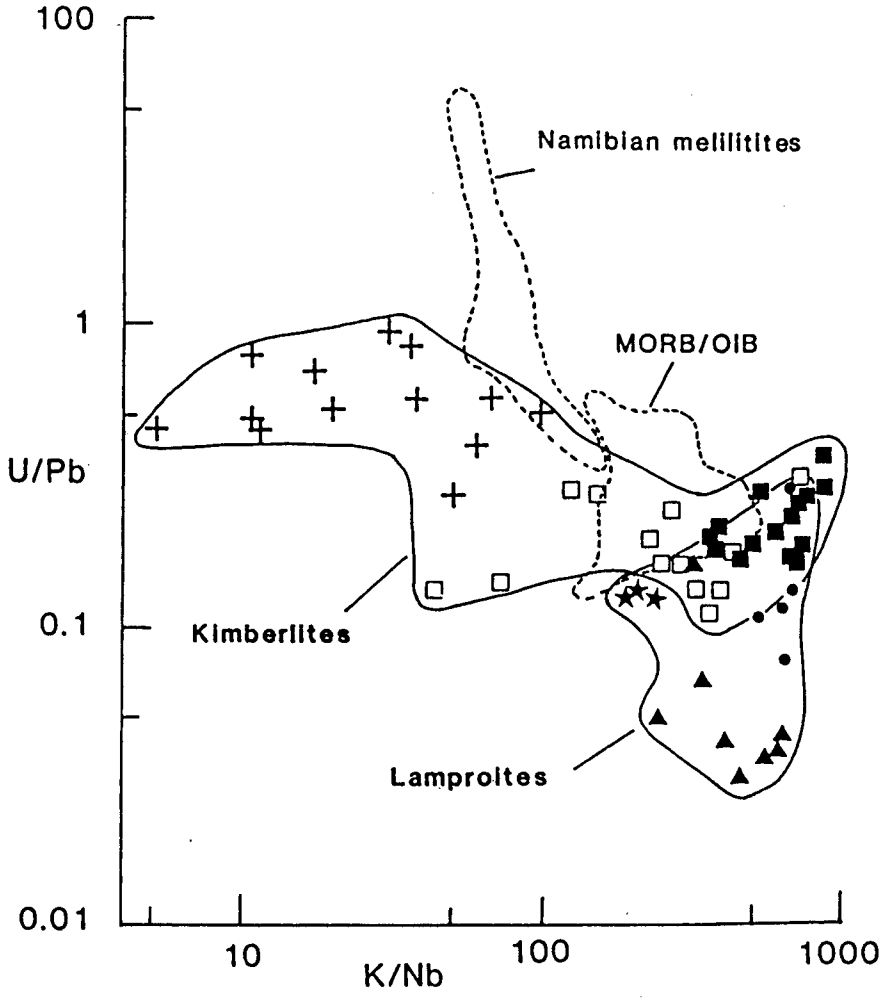

Figure 5.17 U/Pb vs. K/Nb for kimberlites and lamproites (including kimberlite data from Smith et al., 1985). Symbols as in Figure 5.7, • = Smoky Butte. These are compared with fields for Namibian Melilitites (Palacz, unpub. data) and MORB/OIB (Newsom et al., 1986) (after Hawkesworth et al., 1987).

respectively) indicate that for very small degrees of partial melting (limiting case F = 0) the source phlogopites must have contained around 0.11 to 1.0 ppm U, and 1.5 to 20 ppm Pb. However Kramers et al. (1983) quoted values of U = 0.03 ppm and Pb = 0.11 ppm from a peridotite phlogopite. However, the available U and Pb analyses in such phlogopites is evidently sparse and further work is required to determine the characteristic range of U and Pb abundance in mantle phlogopites.

Amphibole: K-richterites from mantle xenoliths exhibit low Sm/Nd = 0.085 to 0.18, extremely low U/Pb = 0.006 to 0.044 and they contain significant abundances of Pb = 1.70 to 8.39 ppm, Sm = 0.43 to 11.0 ppm and Nd = 2.9 to 65.9 ppm (Kramers et al., 1983). With the exception of Smoky Butte samples there is no evidence to suggest that kimberlites and lamproites originate from sources which contained K-richterite. Furthermore, diamondiferous kimberlites and lamproites were generated from depths ($\geq$ 150km) greater than the depths of amphibole stability ($<$ 100km).

Apatite: Kimberlites and lamproites have high P_2O_5 contents (= 0.2 to 4.0 wt%) which indicates melting of a P_2O_5 bearing phase, such as apatite. Yet, some residual apatite during melting might be inferred from troughs at P and Sr on mantle normalised trace element abundance diagrams (Figure 5.6, Section 5.2). Is it possible that apatite could control U/Pb and Sm/Nd ratios ? Beswick and Carmichael (1978) suggested that the LREE content of kimberlites could be derived from disequilibrium melting of a mantle source involving a LREE-rich accessory such as apatite. Mantle apatites contain high abundances of Sm = 194 ppm, Nd = 1285 ppm, U = 5.39 ppm and Pb = 4.6 ppm (Kramers et al., 1983). However, although the apatite analysed by Kramers et al. (op. cit.) has a low Sm/Nd ratio = 0.15, the U/Pb is extremely high = 1.17, with an effective μ = 76. Kleeman et al. (1969) also report high U contents in lherzolite apatites (U = 5.8 to 38.4 ppm). No further Pb data from apatites is known. Thus, it is considered that neither the stabilisation of apatite during the trace element enrichment in the source regions of kimberlites and lamproites, nor melting of apatite during magma genesis, controlled the distribution of U/Pb and Sm/Nd and hence the isotope systematics.

The troughs observed at P and Sr on mantle normalised trace element abundance diagrams of lamproites pose an interesting problem. Little is known about the nature and stability of apatite at depth. Residual apatite during melting is, in itself, considered unusual (Frey et al., 1980). Apatites can contain appreciable amounts of F, H_2O and CO_2 (Deer et al., 1966), all features of kimberlites and lamproites, but the effects of these volatile species on apatite at mantle depths is unknown. It is possible, however, that the troughs at P and Sr are not due to residual apatite. Rather, during trace element enrichment of the source regions, not all the P and Sr was

stabilised in apatite, but continued in a melt or fluid through the system. It might be inferred that further crystallisation at a later stage should result in a P-bearing phase such as apatite. Thus, as a complement to lamproite trace element profiles, entrained metasomatised xenoliths with peaks at P and Sr might be expected. Barton and van Bergen (1981) reported apatite xenocrysts and apatite-bearing xenoliths from Hatcher Mesa, Leucite Hills, but they did not observe that apatite was unusually abundant within the xenoliths.

In general, the above discussion seems to indicate that if the negative correlation between εNd and $(^{206}Pb/^{204}Pb)_i$ observed in kimberlites and lamproites can be attributed to mineralogical control, the only possible phase is phlogopite. However, the data as yet are inadequate to fully assess this proposition. As an alternative, it is possible that the apatite, phlogopite $\pm$ amphibole inferred to be in the enriched source regions of kimberlites and lamproites crystallised from melts that had already developed low U/Pb and Sm/Nd. The negative correlation between U/Pb and K/Nb (Figure 5.17) could just further reflect that, at least in some portions of the upper mantle, the behaviour of U relative to Pb is opposite to that generally assumed (e.g. Newsom et al., 1986).

If the source regions to kimberlites and lamproites were enriched by essentially very similar mantle processes, then the observed variations in trace element and isotope geochemistry would relate to one or more of the following; the age and/or degree of enrichment, depth and degree of melting. Kimberlites and lamproites form a broad negative trend on diagrams of K_2O wt % vs. εNd and $(^{206}Pb/^{204}Pb)_i$ (Figure 5.18). The Smoky Butte samples are displaced as a result of melting a source which contained amphibole in addition to phlogopite. The depth of melting can explain the variation in K_2O content since the phase field of phlogopite increases with depth (Foley et al., 1986b; Section 5.1.1). With increasing depth of melting, smaller degrees of partial melting might be expected and accordingly higher incompatible trace element contents should be found in melts from greater depth. The Smoky Butte lamproites however, contain exceedingly high trace element contents, comparable and higher than those in the other rocks, even when consideration is made for the dilution effect of abundant mantle peridotite in some kimberlites and lamproites e.g. Nd in Smoky Butte = 292–379 ppm, while the Nd content of the melt component in the Finsch kimberlites was probably around 200 ppm (Section 2.10.4). Moreover, at shallower depths, the degree of melting is probably higher, in which case, the kimberlite melts might be expected to have higher trace element abundances, if similar source compositions are assumed. Thus, the degree of source enrichment appears to have varied between source regions. Also shown on Figure 5.18 are the inferred ages of source enrichment events. With the exception of Prairie

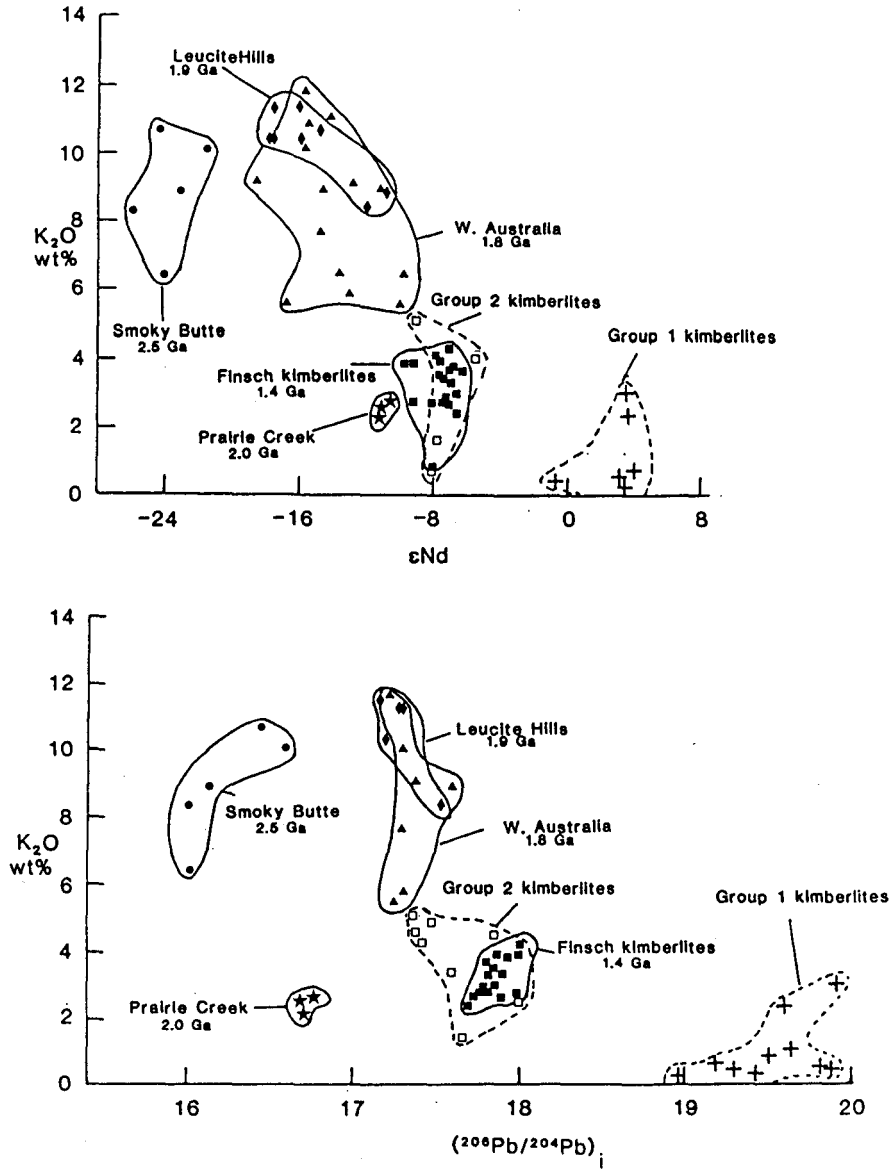

Figure 5.18 K_2O vs. a) εNd and b) $(^{206}Pb/^{204}Pb)_i$ for kimberlites and lamproites. Symbols as in Figure 5.7.

Creek, there is a general correlation such that the older the source region the higher the observed K_2O and the less radiogenic the Pb and Nd isotope ratios. An interesting corollory to these observations is that age and depth of the source regions are related. The shallower the source the older its age. The extent to which a mantle derived melt, incapable of reaching the surface, can penetrate the subcontinental lithosphere will relate to the intersection of the geothermal gradient and ambient solidus. It has been argued that intracratonic geothermal gradients have been low since Archaean times (Bickle, 1986). Thus, it may be that the older the event the higher the temperature of the enriching melt and hence the further the ascent into the lithosphere. However, Group 1 kimberlites such as Premier in South Africa are of Precambrian age and formation of enriched lithospheric portions of the mantle will probably relate to the tectonic evolution of specific cratonic areas. Hence, the correlation between age and depth of source may be accidental.

To summarise, the composition of Group 2 kimberlites and lamproites is indicative of an origin from ancient trace element enriched source regions situated within the subcontinental mantle lithosphere. The cause of these enrichment events is disputed. Arguments have tended to focus on whether they originate from recycled sediment, or extreme intra-mantle processes. The above discussion has shown how each of the models can, at least to some extent explain the characteristics of kimberlite and lamproite magmatism. However, trace element and radiogenic isotope data alone, do not appear adequate to decide between the models. However, despite a wide range in composition (e.g. εSr), the Group 2 kimberlites and lamproites exhibit a positive correlation between εNd and $(^{206}Pb/^{204}Pb)_i$, indicative of related enrichment processes. The above trend contrasts with inferred bulk distribution coefficients during mantle melting (e.g. Newsom et al., 1986). Thus, providing an explanation for this relationship may be the key to understanding the cause of the inferred trace element enrichment events in the source regions of these rocks. Proponents of recycled crust models, would argue that this trend reflects subduction of low U/Pb, low Sm/Nd pelagic sediment. Those preferring mantle processes, however, would suggest that it could be due to the stabilisation of low U/Pb, low Sm/Nd phlogopite. At present, there are insufficient data on, either the nature and composition of subducted sediments at deep mantle levels, or on U and Pb abundances and distribution within mantle phlogopite, to be able to determine which is correct.

Chapter 6

Conclusions

Combined geochemical (radiogenic isotopes, major and trace elements) and petrographic evidence has been used to evaluate whether the unusual compositions of Group 2 kimberlites and lamproites are source and/or extraction phenomena. The main conclusions of this work are;

1. Group 2 kimberlites and lamproites are generally unfractionated mantle derived igneous rocks. They are characterised by a wide range in composition and are highly enriched in trace elements. Nd and Sr isotope data encompasses much of that reported for various upper and lower crustal rocks. Yet, these magmas do not appear to have been significantly contaminated by crust.

2. They result from very small degrees of partial melting ($< 1\%$) of ancient trace element enriched source regions which are believed to be situated within the subcontinental mantle lithosphere. Enrichment events occurred from ($\simeq$ 1.0 to 2.5 Ga).

3. These source regions are situated at various mantle depths, from within the amphibole stability field ($<$ 100 km) to within the diamond stability field ($>$ 150 km).

4. Volatile compositions and depth of melting influenced the composition of primary kimberlite and lamproite melts.

5. Kimberlite and lamproite magmas from within the diamond stability field contain a high proportion of entrained and disaggregated mantle peridotite. This is a feature of melt migration and ascent to the surface from these mantle depths.

6. The wide range in Sr, Nd and Pb isotope ratios demonstrate that each kimberlite and lamproite suite was derived from an isotopically distinct source. This cannot be wholly due to variations in age and different

styles of trace element enrichment are identified on a regional basis. However, the Nd and Pb isotope data indicate an affinity between all the enrichment styles recorded.

7. The origin of the trace element enrichment events is unresolved. The available data are arguably compatible with a component from either recycled crust (e.g. pelagic sediment), or intra-mantle processes, which entailed the migration and crystallisation of small volume silicate melts with variable volatile compositions.

Appendix A

Sample localities

A.1 Finsch mine kimberlites, South Africa

Sample	Location within pipe
CRC 1	Internal dyke
CRC 2	Globular segregation – unknown locality
CRC 3	F2 intrusion
CRC 4	Tuffisitic Kimberlite breccia (TKB) – unknown locality
CRC 6	Internal dyke
CRC 7	Internal dyke
Finsch B	hypabyssal kimberlite – unknown locality
F287	F3 intrusion
F340	F(5-6) intrusion
F652	F4 intrusion
F653	F2 intrusion
F656	F2 intrusion
F659	F2 intrusion
F660	F4 intrusion
F661	F4 intrusion
F664	F2 intrusion
F667	F(5-6) intrusion
F756	External Precursor Dyke (EPD)
F757	F4 intrusion
F758	External Precursor Dyke (EPD)
F765	F3 intrusion
F766	F3 intrusion
F767	F3 intrusion
Country rocks	
F760	Karoo basalt
F769	Precambrian dolomite
Miscellaneous	
F689	Peridotite xenolith from the Finsch pipe
F750	Peridotite xenolith from the Finsch pipe
CRC 5	Unknown locality; probably from the Kimberley pool

A.2 West Kimberley Province lamproites, Western Australia

Sample	Area	Intrusion
WA A1/2	Ellendale field	Ellendale pipe A
WA A3/2	Ellendale field	Mount North
WA A3/3	Ellendale field	Mount North
WA A3/8	Ellendale field	Mount North
WA A3/16a	Ellendale field	Mount North
WA A3/16b	Ellendale field	Mount North
WA A7/1	Eastern Lennard Shelf	Mount Rose
WA A7/2	Eastern Lennard Shelf	Mount Rose
WA A9/1	Eastern Lennard Shelf	Old Leopold Hill
WA A11/1	Fitzroy Trough	Seltrust pipe 1
WA A12/1	Ellendale field	Seltrust pipe 2
WA A12/2	Ellendale field	Seltrust pipe 2
WA A12/26	Ellendale field	Seltrust pipe 2
WA A12/30	Ellendale field	Seltrust pipe 2
WA A12/31	Ellendale field	Seltrust pipe 2
WA A12/49	Ellendale field	Seltrust pipe 2
WA A12/50	Ellendale field	Seltrust pipe 2
WA A12/72	Ellendale field	Seltrust pipe 2
WA A13/1	Ellendale field	Seltrust pipe 3
WA A13/2	Ellendale field	Seltrust pipe 3
WA B3/8	Noonkanbah field	Walgidee Hills
WA B3/9	Noonkanbah field	Walgidee Hills
WA B5/5	Noonkanbah field	Noonkanbah Hill
WA B5/6	Noonkanbah field	Noonkanbah Hill
WA B8/2	Noonkanbah field	Machells Pyramid
WA B9/3	Noonkanbah field	Mount Cedric
WA B9/4	Noonkanbah field	Mount Cedric
WA B12/1	Noonkanbah field	Mount Gytha
WA B19/2	Fitzroy Trough	Oscar Plug
WA B19/3	Fitzroy Trough	Oscar Plug
WA B20/1	Noonkanbah field	The Sisters West
WA B20/2	Noonkanbah field	The Sisters West

A.3 Leucite Hills lamproites, (Wyoming) North America

Sample	Intrusion
LH2/9	Boars Tusk
LH3/11	Matthews Hill
LH4/7	North Table Mountain
LH5/7	Middle Table Mountain
LH5/9	Middle Table Mountain
LH6/12	South Table Mountain
LH6/15	South Table Mountain
LH7/1	Iddings Butte
LH8/3	Endlich Hill
LH9/1	Endlich Hill
LH11/1	Spring Butte
LH12/1	Black Rock
LH13/18	Deer Butte
LH15/1	Hatcher Mesa
LH16/8	Emmons Mesa
LH16/14	Emmons Mesa
LH17/3	Zirkel Mesa
LH17/19	Zirkel Mesa
LH17/26	Zirkel Mesa
LH17/28	Zirkel Mesa
LH17/34	Zirkel Mesa
LH17/48	Zirkel Mesa
LH19/25	Pilot Butte
LH19/26	Pilot Butte

Appendix B

Analytical techniques

B.1 Modal analyses

The modal proportions of minerals in the lamproites and kimberlites analysed are presented in Appendix C1. The Finsch data were acquired using a Swift Model E pointcounter fitted with an automated stage. At least 1500 points were counted on each sample. 'tr' signifies that a particular mineral was observed, but not pointcounted. Lamproite data was obtained by visual estimation.

B.2 Wavelength Dispersive microprobe analysis

Data were collected at the Open University on a Cambridge Instruments Microscan 9 (M9) microprobe. The M9 is fully computerised and enables all spectrometer settings, count times, crystal selections, sample movement and ZAF corrections to be controlled automatically. Standard silicate analyses were analysed in fully automated mode at an accelerating potential of 20 kV, a beam current of 30.5 nA and a typical spot size of 10–15 microns. The instrument is calibrated daily using mineral standards; Wollastonite (Si, Ca), Rutile (Ti), metal (Cr, Mn, Ni), Jadeite (Al, Na), Fayalite (Fe) and Forsterite (Mg). The consistency of the data is checked by analysing an internal standard; ABG, a basaltic glass (Table B.1).

B.3 Wavelength dispersive x-ray fluorescence analyses

X-ray fluorescence data were determined by wavelength dispersive x-ray fluorescence (WD-XRF) techniques at the Grant Institute, Edinburgh University. Sample preparation and techniques are described fully in Fitton et al. (1984). Major elements were analysed using glass beads. These were made

Oxide wt%	Observed ABG	2σ	Expected ABG	2σ
SiO_2	51.56	1.87	51.53	0.48
TiO_2	1.31	0.04	1.32	0.05
Al_2O_3	14.87	0.64	15.01	0.20
FeO	9.03	0.28	9.05	0.13
MgO	0.18	0.005	0.18	0.03
MnO	7.88	0.43	7.96	0.16
CaO	10.98	0.43	11.15	0.15
Na_2O	2.74	0.19	2.76	0.09
K_2O	0.07	0.003	0.07	0.01
Total	98.62		99.03	

Table B.1 Analytical data for basaltic glass ABG. Observed values equal the mean of 6 analyses. Expected values equal the mean of 54 analyses.

by mixing Johnson Matthey spectroflux 105 with pre-ignited rock powder in the ratio 5:1 and fusing in Pt-Au crucibles at 1100°C for 20 minutes. On cooling, flux was added to correct for flux weight loss during fusion. Further fusion was achieved by heating over a meker burner. Discs were formed by casting the fused mixture onto graphite moulds (45 mm in diameter) on a hot-plate at 220°C. Loss-on-ignition data were acquired by heating pre-dried powder in a silica crucible at 1000°C for 40 minutes.

Trace elements were analysed using pressed powder pellets. These were made by thoroughly mixing $\simeq$ 7 g of rock powder with 6 drops of binder (mowiol) and compressing, with a surround and base of boric acid powder, into a 45 mm diameter disc using a hydraulic press.

Analysis takes place in three stages;

1. SiO_2, Al_2O_3, total Fe expressed as Fe_2O_3, MgO, CaO, Na_2O, K_2O, TiO_2, MnO and P_2O_5 using the Cr X-ray tube and program 90.

2. Sc, V, Cu, Ba, La using the Cr X-ray tube and program 91.

3. Ni, Zn, Pb, Th, Sr, Y, Zr, Nb, Cr, Ce, Nd using the W X-ray tube and program 92.

   The results of several international standards analysed as unknowns are presented in Table B.2. and are compared with analyses taken from Abbey (1983). Table B.3 compares repeat XRF runs from this work. Three internal kimberlite standards from De Beers Mining Corporation, analysed by XRF and wet chemical techniques at AARL (Anglo American Research Laboratories) are compared with results for data from the Edinburgh XRF on Table B.4.

Std.	SiO_2	Al_2O_3	Fe_2O_{3T}	MgO	CaO	Na_2O	K_2O	TiO_2	MnO	P_2O_5	Total
G2[1]	69.22	15.40	2.69	0.75	1.96	4.06	4.46	0.48	0.03	0.13	99.18
G2[2]	69.20	15.29	2.70	0.78	1.91	3.97	4.48	0.49	0.03	0.14	98.97
GSP1[1]	67.32	15.28	4.30	0.97	2.03	2.81	5.51	0.66	0.04	0.28	99.20
GSP1[2]	67.35	14.99	4.31	1.00	1.99	2.76	5.50	0.66	0.04	0.28	98.89
AGV1[1]	59.61	17.19	6.78	1.52	4.94	4.32	2.92	1.06	0.10	0.51	98.95
AGV1[2]	59.88	17.25	6.78	1.56	4.88	4.17	2.93	1.05	0.10	0.49	99.10
BCR1[1]	54.53	13.72	13.41	3.48	6.97	3.30	1.70	2.26	0.18	0.36	99.91
BCR1[2]	54.81	13.58	13.43	3.49	6.89	3.31	1.71	2.24	0.18	0.36	100.00
PCC1[1]	42.10	0.73	8.28	43.50	0.55	0.01	0.00	0.01	0.12	0.01	95.31
PCC1[2]	41.73	0.75	8.29	43.63	0.58	0.004	-0.007	0.01	0.1	0.01	95.11
DTS1[1]	40.61	0.25	8.70	49.80	0.14	0.01	0.00	0.00	0.12	0.00	99.63
DTS1[2]	40.39	0.31	8.66	49.65	0.20	0.09	-0.002	0.01	0.12	0.01	99.42
GA[1]	69.96	14.51	2.77	0.95	2.45	3.55	4.03	0.38	0.09	0.12	98.81
GA[2]	69.95	14.75	2.78	0.88	2.43	3.62	4.07	0.36	0.09	0.13	99.06
GH[1]	75.85	12.51	1.36	0.03	0.69	3.85	4.76	0.08	0.05	0.01	99.19
GH[2]	75.73	12.51	1.34	-0.04	0.75	3.86	4.73	0.08	0.04	0.00	99.01
BEN[1]	38.39	10.12	12.89	13.22	13.94	3.20	1.40	2.62	0.20	1.06	97.04
BEN[2]	38.38	10.12	12.89	13.36	13.95	3.12	1.40	2.64	0.20	1.05	97.10
ANG[1]	46.35	29.83	3.36	1.80	15.92	1.63	0.13	0.22	0.04	0.01	99.29
ANG[2]	46.80	29.86	3.33	1.74	15.97	1.68	0.13	0.22	0.04	0.01	99.80
MAN[1]	66.74	17.66	0.47	0.04	0.59	5.85	3.19	0.01	0.04	1.39	95.98
MAN[2]	66.46	17.81	0.49	-0.004	0.64	6.01	3.16	0.01	0.04	1.40	96.03

Table B.2 Analyses of internal standards taken from Abbey (1983) = 1, compared with results from this work = 2.

	F756		F758		WA A12/50	
	1985	1986	1985	1986	1985	1986
SiO_2	32.51	32.93	27.63	27.75	48.63	48.48
Al_2O_3	3.42	3.47	3.31	3.38	8.62	8.69
MgO	12.66	12.70	10.44	10.41	6.78	6.77
CaO	19.93	20.04	24.48	24.54	2.32	2.32
Na_2O	-	0.02	-	0.13	-0.1	0.12
K_2O	3.83	3.89	2.71	2.79	9.02	8.95
TiO_2	1.50	1.51	1.57	1.59	6.75	6.73
MnO	0.46	0.48	0.33	0.34	0.05	0.05
P_2O_5	1.03	1.03	1.18	1.21	1.64	1.64
Total	75.34	76.01	71.65	72.02	83.81	83.75

	LH9/1		LH17/19		LH17/28	
	1985	1986	1985	1986	1985	1986
SiO_2	51.33	51.73	53.30	53.98	53.78	54.28
Al_2O_3	9.15	9.23	9.73	9.94	9.87	10.03
MgO	8.76	8.68	6.80	6.72	6.52	6.57
CaO	5.63	5.69	3.68	3.74	3.85	3.90
Na_2O	1.20	1.51	1.28	1.60	1.23	1.44
K_2O	10.42	10.39	11.33	11.37	11.28	11.32
TiO_2	2.22	2.23	2.46	2.47	2.51	2.52
MnO	0.06	0.07	0.06	0.06	0.06	0.06
P_2O_5	1.82	1.84	1.69	1.71	1.57	1.60
Total	90.59	91.37	90.33	91.59	90.67	91.72

Table B.3 Comparison of repeat XRF runs carried out during this work

B.4 Atomic Absorption Spectrometry

Data for Na were obtained using a Varian Techtron type AA-4 atomic absorption spectrophotometer at the Grant Institute, University of Edinburgh. Accurately weighed, pre-dried rock powders, were digested in Pt crucibles for several hours with 4 ml conc. HNO_3, 2 ml, H_2SO_4 and 5 ml HF. They were then evaporated to dryness overnight on a hotplate. The residue was placed into solution with the addition of deionised water and five drops H_2SO_4. These solutions were then diluted to 200 ml in pyrex flasks, with deionised water. Estimating roughly from XRF results, where possible, it was aimed to have < 5 ppm Na_2O in 200 ml solution.

Measurements were made by comparing each sample with pre-prepared standard solutions of known Na concentration and linearly extrapolating between the data. A number of standard solutions were made up, in order to closely bracket the sample values;

(a) 0, 1.0, 2.0, 3.0, 3.5, 4.0, 4.5 and 5.0 ppm Na_2SO_4 and 0 wt% K_2O, in 200 ml solution.

Oxide	Finsch K1/402		St. Augustine K2/6		Wesselton K4/423	
wt %	De Beers	Edin.	De Beers	Edin.	De Beers	Edin.
SiO_2	38.51–38.9	38.39	31.10–31.55	30.90	33.66–34.88	33.98–34.05
TiO_2	0.82–0.87	0.85	1.64–1.84	1.66	2.1–2.57	2.20–2.24
Al_2O_3	3.34–3.4	3.51	1.80–1.95	2.06	3.08–3.54	3.59–3.60
Fe_2O_3	8.19–8.48	8.34	8.94–9.34	9.10	8.99–9.55	9.20–9.36
MnO	0.13–0.16	0.14	0.14–0.16	0.15	0.12–0.16	0.15–0.16
MgO	29.0–29.9	29.50	32.60–33.71	32.81	29.88–30.33	29.90–30.03
CaO	5.38–5.69	5.49	7.43–8.77	8.39	7.19–8.82	8.41–8.46
Na_2O	0.15–0.3	0.02	0.10–0.20	-0.06	0.20–0.60	0.20–0.38
K_2O	3.88–4.33	4.12	0.08–0.18	0.15	1.82–2.10	1.99–2.00
P_2O_5	0.61–0.66	0.62	0.82–0.93	0.86	0.77–1.03	0.95–0.96

Table B.4 Comparison of results for three De Beers internal standards with Edinburgh XRF data.

Sample	Na_2O wt%			
	A.A.			XRF
	1	2	3	
SB59	1.29	1.30		1.26
PK1/4	0.35	0.32	0.32	0.20
PK1/18	0.34	0.32		0.08
F287	0.12	0.09	0.10	-0.08
F758	0.08	0.08		-0.18
F767	0.06	0.06		-0.12
LH5/7	0.92	0.95		0.72
LH17/48	0.87	0.77		0.76
WA A12/26	0.35	0.37		0.11
WA B19/3	0.39	0.39		0.17

Table B.5 Repeat analyses for Na by Atomic Absorption (= A.A.). The XRF results are also shown.

(b) 0.1, 0.2, 0.5 and 1.0 ppm Na_2SO_4 and 1 wt% K_2O, in 200 ml in solution (made up by H. Downes).

(c) 0, 0.5, 1.0, 2.0, 3.0, 3.5, 4.0 and 5.0 ppm Na_2SO_4 and 8 wt% K_2O, in 200 ml solution.

A combination of the first two sets of standards were used to measure the Finsch kimberlites and Prairie Creek lamproites, and the last set to measure the high K_2O leucite Hills, Smoky Butte and West Australia lamproites. A number of analyses were repeated to confirm reproducibility and these are given in Table B.5, together with the results from the Edinburgh XRF.

B.5 Instrumental Neutron Activation analysis

REE (La, Ce, Nd, Sm, Eu, Tb, Yb, Lu) and a number of trace elements (Cs, Hf, Ta, Th, U, Sc) were determined by Instrumental Neutron Activation analysis (INAA) following the techniques reported in Potts et al. (1981, 1985). Rock powders were dried overnight at 105°C, and 0.3 g of each powder were then weighed onto polythene capsules. The capsules were sealed by soldering. Ten capsules were placed in a polythene irradiation 'can', together with an international (Whin Sill) and internal (Ailsa Craig) standard in a pre-designated order. Capsules were separated by laquered iron foils.

Samples were irradiated within a core tube at the University of London Reactor Centre, Ascot in a thermal flux of 5×10^{12} n cm^{-2} s^{-1} for 24–30 hours of reactor time. After 'cooling' for 5 days, they were counted at the Open University, using two detectors; a planar low-energy photon spectrometer (LEPS) and a coaxial Ge(Li) detector. Data were processed using spectroscopy amplifiers and a multichannel analyser. Full details of counting conditions for the foils and samples, peak fitting, corrections for overlaps and neutron flux discrepencies and calibration are given in Potts et al. (1981, 1985).

Data for the Whin Sill, measured with each batch of samples from this work are shown in Table B.6 and compared with values from Potts et al. (1985).

B.6 Inductively Coupled Plasma Spectrometry

Six samples were analysed for REE by Inductively Coupled Plasma Spectrometry (ICP) by J.N. Walsh at Kings College, London (analyist was Jan Barker) utilising the procedure described by Walsh et al. (1981). These results were obtained because REE analyses by XRF

Element	83/84	June 1984	Sept 1984	Sept 1984	Feb 1985	Feb 1985	Oct 1985	Jan 1986	Jan 1986	Expected WS	1σ
La	25.6	25.9	25.8	29.0	25.5	25.5	26.2	26.2	25.4	22.5	2.6
Ce	58.8	58.0	57.9	58.3	58.5	57.3	59.6	58.9	58.4	57.5	3.1
Nd	33.8	34.5	33.9	33.1	34.5	36.0	32.6	35.6	33.9	32.9	3.5
Sm	7.33	7.13	7.22	7.79	7.10	7.47	7.51	7.35	7.50	7.27	2.1
Eu	2.34	2.25	2.27	2.18	2.24	2.25	2.32	2.31	2.30	2.25	3.9
Gd										7.50	11.0
Tb	1.19	1.08	1.18	1.11	1.17	1.14	1.09	1.14	1.14	1.09	3.9
Ho			1.4	1.4				1.34	1.22		
Tm		0.43	0.45					0.48	0.43	0.41	5.9
Yb	2.67	2.53	2.58	2.59	2.58	2.58	2.61	2.66	2.60	2.54	3.1
Lu	0.41	0.40	0.40	0.37	0.40	0.38	0.39	0.39	0.40	0.39	1.7
Na			2.71	2.80	2.70	2.85	2.74	2.70	2.77	2.7	6.5
Fe		13.05	12.83	13.12	12.9	13.1	12.72		13.07	12.62	3.1
Co	48.9	48.6	47.5	49.6	48.5	48.5	47.9		48.7	47.4	3.1
Rb	44	33	35	40	52	40.6	28.6		33	35.3	11
Cs	1.4	1.1	0.94		1.12	1.16	1.09	1.06	1.03	1.03	9.5
Hf	5.35	4.92	4.82	5.03	5.40	5.38	5.19	5.08	5.01	4.93	3.0
Ta	1.29	1.26	1.28	1.34	1.31	1.24	1.26	1.26	1.27	1.26	4.7
Th	3.16	3.06	3.01	3.25	3.2	3.04	3.09	3.20	3.01	3.05	4.3
U	0.92	0.8	0.6	0.9	0.8	0.6	0.7	0.9	0.8	0.90	26.5

Table B.6 INAA results for the Whin Sill, compared with those reported in Potts et al. (1985).

	PK1/20			LH5/7			WA A3/2		
REE	INAA	XRF	ICP	INAA	XRF	ICP	INAA	XRF	ICP
La	144	97.8	125	260	215	241		467	475
Ce	277	169	242	516	440	495		1012	1025
Pr			25.7			46.1			68.5
Nd	107	59.4	95.9	204	193	180		357	316
Sm	13.4		11.3	23.7		22.5			38.0
Eu	3.15		2.77	5.5		5.00			8.66
Gd			6.70			11.7			20.1
Dy			3.02			4.47			7.16
Ho			0.64			1.04	1.09		1.48
Er			2.08			3.22			5.21
Yb	0.90		0.90	1.3		1.24			1.83
Lu	0.12		0.14	0.18		0.17			0.24
	F653			LH 17/48			SB70		
REE	INAA	XRF	ICP	INAA	XRF	ICP	INAA	XRF	ICP
La	57.5	41.7	55.7	147	118	131	437	375	420
Ce	126	82.6	111	312	294	274	930	853	949
Pr			13.4			29.3			70.9
Nd	52.6	33.2	50.5	129	122	117	379	370	358
Sm	7.35		6.71	16.5		15.1	43.1		41.5
Eu	1.71		1.69	3.85		3.54	9.50		8.97
Gd			4.20			8.69			22.4
Dy			1.93			3.76			10.1
Ho			0.60			0.79			2.20
Er			1.50			2.40			6.96
Yb	0.73		0.79	1.44		1.13	3.19		3.02
Lu			0.15			0.16	0.41		0.42

Table B.7 Comparison of REE abundances in selected samples, each measured by INAA, XRF and ICP techniques.

were found to be significantly lower than those measured on the same samples by INAA. D. James (pers. comm.) believes this may be due to REE-bearing perovskite not grinding well during temaing, and hence migrating away from the analytical surface under pressure, to below the depth of penetration in powder pellets. The ICP data is compared with results from XRF and INAA in Table B.7 and confirms that generally the XRF data give low analyses.

B.7 Chondrite normalising values

All data portrayed in chondrite normalised diagrams are normalised to the values of Nakamura (1974); Ba = 3.85, Rb = 0.35, Th = 0.042, K = 120, Nb = 0.35, Ta = 0.02, La = 0.329, Ce = 0.865, Sr = 11.8, Nd = 0.63, P = 46, Sm = 0.203, Zr = 6.84, Hf = 0.2, Ti = 620, Tb = 0.052, Y = 2.0, Yb = 0.22, Lu = 0.0339, Pb = 0.12, Eu = 0.077.

B.8 Sr-, Nd- and Pb- chemistry and Mass Spectrometry

B.8.1 Chemistry

General chemistry

All the chemical dissolutions described below were carried out in laminar flow cupboards within the Open University laboratory under a positive pressure generated by filtered air. Sample dissolutions are carried out in teflon bombs and beakers. All teflon ware was cleaned following a standard procedure; thorough cleansing in cold 1.5 M HNO_3 until visibly clean, then soaked in hot (80 °C) conc. HNO_3 for 24 hours, rinsed with RO water and soaked for a further 24 hours in RO water. Reagents were all of Analar grade and were further purified as follows; HCl by a two-stage quartz distillation, HNO_3 by sub-boiling in a quartz distill, HF by distillation in a teflon two bottle still and HBr by sub-boiling in a teflon still. H_2O was purified by a Milli Q reverse osmosis procedure.

Sr- and Nd- chemistry

50-200 mg of rock powder was weighed into a teflon beaker. Sample dissolution was accomplished by first adding $\simeq$ 8 mls 40% Hf and $\simeq$ 2 mls 15 M TD HNO_3 and leaving overnight. The sample was then dried under an evaporation hood. A further 2 mls of 15 M TD HNO_3 was added and when again dry, the sample was put completely into solution with $\simeq$ 6 mls TD 6 M HCl. This was evaporated to dryness. To remove any possible insoluble residue, the sample was dissolved in 2 ml 2.5 M HCl and centrifuged. About 1–1.5 ml of the resulting clear solution were loaded onto pre-conditioned cation exchange columns containing 10 ml Bio-Rad AG 50 W$\times$ 200–400 mesh Resin. The sample was

washed in with 2 × 1 ml 2.5 ml HCl and then eluted with a further 43 ml 2.5 M HCL. The following 10 mls of 2.5 M HCl contained the Sr fraction and was collected in a teflon beaker and evaporated to dryness. Nd was collected by further washing with 1 ml RO H_2O and eluting 21 mls 3 M HNO_3 . The subsequent 20 mls of 3 M HNO_3 contained the Nd fraction, which was collected in a teflon beaker and evaporated to dryness. The Nd columns were changed half-way through this work and both techniques are outlined below:

(a) The dry Nd fraction was dissolved in $\simeq$ 1 ml Solution 1 (75% CH_3OH, 10% 8 M CH_3COOH, 10% 5 M HNO_3, 5% H_2O) and loaded onto a second set of preconditioned temperature controlled anion exchange columns, containing 3 ml Bio-Rad AG1×8 200–400 mesh resin.The temperature was set at 25°C. The sample was washed in with 2 × 1 ml Solution 1. 32 ml of Solution 1 were eluted and the temperature then raised to 35°C. 15 mls of Solution 2 (75% CH_3OH, 10% 8 M CH_3COOH, 5% HNO_3, 10% H_2O) were eluted and the subsequent 29 mls of Solution 2 containing the Nd fraction were collected in a teflon beaker. This was then evaporated to dryness.

(b) The dry Nd fraction was dissolved in $\simeq$ 1 ml of 2.5 M HCl and loaded onto a set of pre-conditioned ion-exchange-reverse chromatography columns containing teflon powder coated with HD-EDP.The sample was washed in with 2 × 1 ml 2.5 M HCl, and then eluted with a further 8 mls of 2.5 MHCl. The following 4 mls of 2.5 M HCl contained the Nd fraction, which was collected in a teflon beaker. This was then evaporated to dryness.

Sr concentrations were measured by accurately spiking the sample during weighing with 1–2 drops of ^{84}Sr spike solution. Dissolution and chemical separations were performed as above.

Handpicked (from the < 1 mm sieve fraction) clinopyroxene mineral separates from the Finsch garnet peridotites, were cleaned as follows: 30 minutes in 2.5 M HCl in an ultrasonic bath, 30 minutes in 5% HF under an evaporation hood, 30 minutes in 2.5 M HCl in an ultrasonic bath and 30 minutes in RO water in an ultrasonic bath. The mineral separates were re-handpicked between each stage. Dissolution and chemical separation were achieved using the techniques outlined above.

Pb chemistry

All chemistry separations of Pb were carried out in a laminar flow cupboard in a laboratory under a positive pressure generated by filtered air, and specifically reserved for Pb chemistry.

All Pb chemistry was done in sevalex bombs. These were cleaned as follows: 1) rinsed in RO H_2O, 2) 24 hours in hot conc. HNO_3 (main Laboratory), 3) rinsed in RO H_2O, 4) 24 hours in RO H_2O (Pb laboratory), 5) 24 hours in RO H_2O and some 6 M HCl, 6) rinsed in RO H_2O, 7) $\simeq$ 3 mls of SB 16 M HNO_3 were added, the bombs sealed and left on a hot-plate for 4–5 hours and 8) rinsed in TD H_2O and finally dried.

Sample dissolutions were carried out following similar procedures to those described above for Nd and Sr chemistry, except samples were not centrifuged and the final dissolution in 2 ml 2.5 M HCl was replaced by dissolution of the dry sample in 1 ml HBr. This was left overnight.

The sample in HBr was loaded onto pre-conditioned columns prepared from PVP disposable pipette tips fitted with a 2 mm diameter teflon plug and 3–4 drops of resin (Dowex 1 $\times$ 8, 200–400 mesh anion exchange resin) 4 $\times$ 1 cv (column volume) 1 M HBr were eluted. The Pb fraction is then collected with 2 cv TD H_2O into a clean sevalex bomb, a few drops of TD 16 M HNO_3 were added and the solution evaporated to dryness.

Samples, for measurement of Pb concentration were accurately spiked during weighing, with a few drops of ^{207}Pb spike solution (NBS 991). Dissolution and chemical separations were performed as above.

B.8.2 Mass spectrometry

Samples were loaded onto outgassed filaments of Re and/or Ta ribbon welded onto pins mounted in glass beads. Sr dissolved in a drop of TD H_2O was loaded onto a single Ta filament, on which a drop of 1 M H_3PO_4 had been pre-dried. Nd dissolved in a large drop of TD H_2O was loaded onto the two Ta side filaments of a triple filament (the centre filament was Re). Pb dissolved in a small drop of 1 M H_3PO_4 was loaded onto a single Re filament on which a large drop of silica gel had been dried to incipient dryness.

The filaments were placed in batches of six, in a turret in a Vacuum Generators Isomass 54E thermal ionisation mass spectrometer equiped with a Solitron 7060 DVM incorporating a real time clock. Sr, Nd and

Pb isotopic abundances and Sr and Pb concentrations are run automatically by software predominantly developed by P. van Calsteren and D. Wright on a HP 9845T computer. All elements are analysed at $< 10^{-7}$ atmospheres and accelerating potential of 8 kV.

Sr isotopic abundances

Sr beams are managed to give an intensity of > 15 pA at a filament current of $\simeq 2.5$ A using a 10 ohm resistor. The measuring cycle is; 88, 87, 86, 86.5, 85, 84. The 85 peak is eliminated when the Rb contribution to the 87 peak is 0.01 % and peak 84 is eliminated after the first set. All peaks are counted for four periods of 1.28 seconds. Peak intensities are calculated using a double interpolation algorithm (Dodson, 1978) corrected for zero, dynamic memory and Rb interference if necessary. The $^{87}Sr/^{86}Sr$ ratio is corrected for fractionation assuming that the fractionation is linearly dependant on mass difference and assuming $^{86}Sr/^{88}Sr = 0.1194$. Ratios are collected in sets of 10. The mean and error are calculated and ratios rejected if they do not satisfy Chauvenet's criteria. A total error for a set of > 100 ppm effects rejection of the whole set and when it exceeds 500 ppm, then the set is ignored. Chauvenet's criterion is retested on all the stored accepted and rejected ratios to calculate a running mean. The run is terminated when at least a 100 ratios are accumulated and the error is < 20 ppm (2σ). The NBS 987 standard gives $^{87}Sr/^{86}Sr = 0.71024 \pm 4$. Sr concentrations are obtained as above, but the 84 peak is not eliminated.

Nd isotope abundances

A stable Nd beam is managed to produce an intensity of $\simeq 7$ pA, by holding centre and side filaments at 3.9 and 2.0 A respectively. The measuring cycle is 146, 144, 143, 142.5, 142, 147. The 147 peak is eliminated when the contribution of Sm to the 144 peak is less than 0.01 %. The $^{143}Nd/^{144}Nd$ ratio is corrected for mass fractionation assuming $^{146}Nd/^{144}Nd = 0.7219$. A run is terminated when at least 200 ratios are accumulated and the error is < 20 ppm (2σ). BCR-1 gives $^{143}Nd/^{144}Nd = 0.512638 \pm 15$.

Pb isotopic analyses

A stable dying Pb beam is achieved by holding the filament at 2.25 A. The measuring cycle is 207, 206, 204, 204.5, 205, 208. The 208 peak is eliminated when the error on $^{207}Pb/^{206}Pb$ is acceptable. No correction for fractionation is made to the $^{206}Pb/^{204}Pb$, $^{207}Pb/^{204}Pb$ and $^{208}Pb/^{204}Pb$ ratios, during the run. Fractionation was monitored and amended by repeated measurement of the NBS 981 standard and normalising values to $^{206}Pb/^{204}Pb = 16.9371$, $^{207}Pb/^{206}Pb = 0.914637$, $^{207}Pb/^{204}Pb = 15.4913$ and $^{208}Pb/^{204}Pb = 36.7213$. A run is terminated when at least 60 ratios are accumulated and the error is < 100 ppm (2σ) on $^{207}Pb/^{204}Pb$.

B.8.3 Data representation

For principles of isotope systematics, the reader is referred to Faure and Powell (1972), Faure (1977) and Hawkesworth and van Calsteren (1984). All measured isotope whole-rock data are recalculated to initial ratios at time (t), the age of emplacement, using the following isochron equations:

$$\left(\frac{^{143}Nd}{^{144}Nd}\right)_m = \frac{^{147}Sm}{^{144}Nd}(e^{\lambda t} - 1) + \left(\frac{^{143}Nd}{^{144}Nd}\right)_i$$

$$\left(\frac{^{87}Sr}{^{86}Sr}\right)_m = \frac{^{87}Rb}{^{86}Sr}(e^{\lambda t} - 1) + \left(\frac{^{87}Sr}{^{86}Sr}\right)_i$$

$$\left(\frac{^{206}Pb}{^{204}Pb}\right)_m = \mu(e^{\lambda t} - 1) + \left(\frac{^{206}Pb}{^{204}Pb}\right)_i$$

$$\mu = \frac{^{238}U}{^{204}Pb}$$

$$\left(\frac{^{207}Pb}{^{204}Pb}\right)_m = \kappa(e^{\lambda t} - 1) + \left(\frac{^{207}Pb}{^{204}Pb}\right)_i$$

$$\kappa = \frac{^{235}U}{^{204}Pb}$$

$$\left(\frac{^{208}Pb}{^{204}Pb}\right)_m = \frac{^{232}Th}{^{204}Pb}(e^{\lambda t} - 1) + \left(\frac{^{208}Pb}{^{204}Pb}\right)_i$$

For Sr- and Nd- isotopes, the ε notation of DePaolo and Wasserburg (1976) is generally employed for representation of isotopic data formed at time (t) relative to a uniform reservoir (UR) at that same time. For Nd analyses the UR is assumed to be chondritic (CHUR). Thus;

$$\varepsilon Nd = \left[\frac{(^{143}Nd/^{144}Nd)_{sample(t)}}{(^{143}Nd/^{144}Nd)_{CHUR(t)}} - 1\right] \times 10^4$$

$$\varepsilon Sr = \left[\frac{(^{87}Sr/^{86}Sr)_{sample(t)}}{(^{87}Sr/^{86}Sr)_{CHUR(t)}} - 1\right] \times 10^4$$

The T^{Nd}_{CHUR} age is the time at which a sample of particular present day Sm/Nd and $^{143}Nd/^{144}Nd$ ratios has the same $^{143}Nd/^{144}Nd$ ratio as CHUR (Hawkesworth and van Calsteren, 1984). Thus,

$$T^{Nd}_{CHUR} = 1/\lambda \ln\left[\frac{(^{143}Nd/^{144}Nd)_m - (^{143}Nd/^{144}Nd)_{CHUR}}{(^{147}Sm/^{144}Nd)_m - (^{147}Sm/^{144}Nd)_{CHUR}} + 1\right]$$

where:

- $\lambda\ ^{147}Sm = 6.54 \times 10^{-12}\ y^{-1}$
- $(^{143}Nd/^{144}Nd)_{CHUR} = 0.51264$
- $(^{147}Sm/^{144}Nd)_{CHUR} = 0.1967$
- $\lambda\ ^{87}Sr = 1.42 \times 10^{-11}$
- $(^{87}Sr/^{86}Sr)_{UR} = 0.7047$
- $(^{87}Rb/^{86}Sr)_{UR} = 0.0847$
- $\lambda\ ^{238}U = 1.55125 \times 10^{-10}\ y^{-1}$
- $\lambda\ ^{235}U = 9.8485 \times 10^{-10}\ y^{-1}$
- $\lambda\ ^{232}Th = 4.948 \times 10^{-11}\ y^{-1}$

Appendix C

Analytical data

Abbreviations

O	=	olivine
Ph	=	phlogopite
Sp	=	spinel
Cpx	=	clinopyroxene
Opx	=	orthopyroxene
Gnt	=	garnet
M	=	macrocryst
P	=	phenocryst
G	=	groundmass
c	=	centre
r	=	rim

C.1 Modal Analyses

Finsch mine kimberlites, South Africa

sample	F653	F656	F659	F287	F652	F660	F661	F340
Intrusion	F2	F2	F2	F3	F4	F4	F4	F5-6
points ctd.	1506	1616	1566	1551	1633	1582	1557	1557
olivine (M)	19.1	28.4	13.4	34.1	8.27	19.9	15.9	45.3
olivine (P)	10.8	20.2	20.4	10.1	8.39	22.9	15.0	11.3
phlogopite	29.9	17.8	36.4	20.6	31.2	31.0	27.3	14.8
calcite	4.38	0.80	3.32	5.93	8.14	3.48	10.1	9.31
serpentine	13.5	11.4	14.4	1.10	21.7	10.0	28.7	8.09
diopside	17.0	8.97	6.38	22.9	14.0	4.43	-	-
apatite	tr	tr	1.40	tr	1.53	tr	0.96	tr
opaques	4.32	8.97	2.11	4.3	5.81	2.15	1.86	5.78
perovskite	1.06	0.68	1.53	tr	0.18	1.20	0.13	0.71
garnet	-	-	-	0.97	-	-	-	-
miscell	-	2.7	0.70	-	0.80	-	-	-
Total %	100.1	100	100	100	100	99.9	99.9	100
Ol M/P	1.77	1.41	0.66	3.38	0.98	0.87	1.06	4.01
Ol M % serp	27.1	33.8	62.9	35.2	100	100	100	27.8
Ol P % serp	65.2	58.9	89.4	86.8	100	100	100	61.9
Phlog G/P %	100	83.1	100	88.8	100	100	100	100

West Kimberley lamproites, Western Australia

	WA;-					
sample	A3/2	A3/8	A3/16a	A3/16b	A12/26	A12/30
Olivine (M)	-	-	-	-	-	-
Olivine (P)	$\leq$5	-	3-5	5	15-20	10-15
Leucite	$\simeq$50	$\geq$50	45-50	$\geq$30	50	35-40
Phlogopite	5-10	20-25	5	10	-	2-3
K-richterite	2-3	-	15-20	10-15	-	-
Diopside	2-3	-	2-3	2-3	-	-
Apatite	2-3	-	-	-	2-3	-
Perovskite	-	-	-	-	-	-
Priderite	10-15	5-10	5-10	10-15	10	10
Glass	-	-	-	-	-	-
Miscellaneous	10-15	10-15	20	25-30	5-10	35-40
Vesicles	-	10	-	-	5-10	-

WA;-						
sample	A3/2	A3/8	A3/16a	A3/16b	A12/26	A12/30
Olivine (M)	-	-	-	-	-	-
Olivine (P)	≤5	-	3-5	5	15-20	10-15
Leucite	≃50	≥50	45-50	≥30	50	35-40
Phlogopite	5-10	20-25	5	10	-	2-3
K-richterite	2-3	-	15-20	10-15	-	-
Diopside	2-3	-	2-3	2-3	-	-
Apatite	2-3	-	-	-	2-3	-
Perovskite	-	-	-	-	-	-
Priderite	10-15	5-10	5-10	10-15	10	10
Glass	-	-	-	-	-	-
Miscellaneous	10-15	10-15	20	25-30	5-10	35-40
Vesicles	-	10	-	-	5-10	-

WA ;-						
sample	A12/31	A12/49	A12/50	A12/72	A13/2	A19/3
Olivine (M)	-	-	-	-	-	-
Olivine (P)	-	15-20	2-5	5	20	10-15
Leucite	15-20	75	≥20	≥35-40	55-60	50
Phlogopite	2-3	-	5	10	1	5-10
K-richterite	-	tr	-	-	5-10	-
Diopside	-	-	-	-	5	5
Apatite	-	tr	-	tr	-	tr
Perovskite	-	-	-	-	-	-
Priderite	10	3-5	10-15	5-10	5-10	-
Glass	-	-	-	-	-	-
Miscellaneous	60	-	60	30-35	-	25-30
Vesicles	-	-	-	5	-	-

Leucite Hills lamproites, North America

sample	LH 5/7	LH 5/9	LH 6/12	LH 6/15	LH 8/3	LH 8/8
Phlogopite	25	15	15	15	15	40
Clinopyroxene	15-20	10	-	-	1	5
Leucite	30	40	25	25	40	25
Sanidine	-	-	35	25	20	25
K-richterite	-	-	10	10-12	20	tr
Glass	20	25	-	-	-	-
Priderite	-	-	-	-	-	-
Olivine	-	-	tr	1	tr	tr
perovskite	1-3	5	-	tr	-	tr
Apatite	-	tr	tr	-	-	-
Miscellaneous	5	5	4	-	4	5
Vesicles	-	-	10	15	-	-
xenoliths	-	-	-	-	-	tr
Cpx (X)	-	-	1	tr	-	-

sample	LH 9/1	LH 11/1	LH 12/1	LH 12/16	LH 13/18	LH 15/1
Phlogopite	5-10	10-15	10	10	20	5
Clinopyroxene	1-2	10	-	10-15	20	10-15
Leucite	30-35	20-25	-	45	30	25-30
Sanidine	25-30	20-25	-	10	-	tr
K-richterite	10-15	2-3	-	-	-	10-15
Glass	-	-	-	-	15	-
Priderite	tr	tr	-	tr	-	-
Olivine	-	-	-	1-2	-	-
Perovskite	-	-	-	-	-	-
Apatite	tr	-	-	tr	-	tr
Miscellaneous	10	-	-	-	15	-
Vesicles	-	25	-	15	-	10-15
xenoliths	-	-	-	-	-	-
Cpx (X)	-	-	-	-	-	1-2

sample	LH 17/19	LH 17/26	LH 17/28	LH 17/34	LH 17/48	LH 19/26
Phlogopite	25-30	15	15	20	15-20	-
Clinopyroxene	-	-	-	15	1-2	-
Leucite	-	-	-	50	10	-
Sanidine	-	-	-	tr	40-45	-
K-richterite	-	-	-	-	tr	-
Glass	-	-	-	10	-	-
Priderite	-	-	-	-	tr	-
Olivine	-	-	-	-	-	-
Perovskite	-	-	-	-	tr	-
Apatite	-	-	-	-	-	-
Miscellaneous	70-75	65	60-65	5	-	100
Vesicles	-	20	20-25	-	25	-
Xenoliths	-	2-3	2-3	-	-	-
Cpx (X)	-	-	-	-	-	-

Smoky Butte lamproites, North America

sample	SB11	SB45	SB59	SB 66	SB70
Phenocrysts					
Olivine	5	tr	10-15	5-10	-
Phlogopite	20	-	20	25	-
Gmass phenocrysts					
Clinopyroxene	10	10	3	5	<1
Armalcolite	15	25	10	10	25
Analcite	-	-	15-20	-	-
Groundmass					
Sanidine	-	30	3-5	40	-
Glass	45	-	30	5-10	40
Phlogopite	-	25	-	-	-
K-richterite	-	-	-	tr	-
Vesicles	-	10	5	-	35
Miscellaneous	5	-	5	-	-

Prairie Creek lamproites, North America

sample	PK1/4	PK1/18	PK1/20
Olivine/M	20	25	20
Olivine/P	15-20	15	15-20
Clinopyroxene	10-15	15-20	10-15
K-richterite	1-2	tr	5-10
Glass	25		25
Perovskite	5	5-10	$\simeq$ 5
Oxides	5	5-10	$\simeq$ 5
Phlogopite	5	2-3	3-5

C.2 Microprobe analyses of Finsch kimberlites

Olivine analyses

	F287							
	O/M1	O/M1	O/M1	O/M1	O/M1	O/M1	O/M1	O/M2
SiO_2	41.13	41.13	41.07	41.02	41.30	41.54	41.40	41.86
TiO_2	0.02	0.02	0.02	0.02	0.02	0.02	0.02	0.02
FeO	7.04	7.15	7.11	7.14	7.15	7.16	7.12	6.33
MnO	0.09	0.11	0.08	0.09	0.08	0.09	0.09	0.08
MgO	50.94	51.08	51.04	50.97	51.21	51.32	51.16	51.95
Total	99.22	99.51	99.32	99.26	99.76	100.15	99.82	100.26

	F287						
	O/M2	O/M3	O/M4	O/M5	O/M6	O/P1	O/P2
SiO_2	41.86	41.50	40.92	41.41	41.24	40.90	41.05
TiO_2	0.02	0.02		0.04	0.02	0.02	0.04
FeO	6.33	8.45	9.28	7.16	8.51	7.69	9.62
MnO	0.08	0.11	0.12	0.09	0.13	0.11	0.14
MgO	51.95	50.11	49.40	51.10	50.07	50.81	49.03
Total	100.26	100.26	99.74	99.83	99.69	99.89	99.75

	F653							
	O/M1	O/M1	O/M2	O/M2	O/M3	O/M3	O/M3	O/M3
SiO_2	41.37	41.48	41.54	41.43	41.99	41.92	41.39	41.54
TiO_2	0.02	0.02	0.02	0.04	0.02	0.02	0.02	0.02
FeO	6.60	6.64	6.78	7.01	7.00	7.11	7.11	7.07
MnO	0.11	0.11	0.11	0.11	0.11	0.13	0.13	0.11
MgO	51.70	51.54	51.40	50.52	51.75	51.58	50.99	51.37
Total	100.25	100.27	100.27	99.60	101.36	101.22	100.08	100.55

	F653				F656		
	O/M4	O/M4	O/M4	O/M5	O/M1	O/M1	O/M2
SiO_2	41.68	41.25	41.71	41.49	41.36	41.52	41.10
TiO_2	0.02	0.04	0.04	0.04	0.02	0.02	0.02
FeO	6.93	6.97	6.90	7.68	6.37	6.39	6.49
MnO	0.09	0.11	0.09	0.09	0.09	0.08	0.08
MgO	51.39	51.36	51.02	50.84	51.13	51.00	50.85
Total	100.56	100.19	100.17	100.59	99.43	99.41	98.93

	F656						F659	
	O/M3	O/M3	O/P1	O/P2	O/P3	O/P4	O/M1	O/M2
SiO_2	41.18	41.20	40.97	41.20	41.32	41.20	41.74	41.50
TiO_2	0.02	0.02	0.02	0.04	0.04	0.02	–	0.02
FeO	7.23	7.09	8.01	7.48	7.54	7.93	6.89	7.81
MnO	0.13	0.11	0.09	0.09	0.13	0.11	0.08	0.11
MgO	50.20	50.39	49.58	50.16	50.09	49.89	50.98	50.13
Total	99.15	99.25	99.20	99.49	99.67	99.69	100.15	100.00

F656				F664		
	O/M3	O/M4	O/M5	O/M1	O/M1	O/M2
SiO_2	41.61	40.90	41.46	41.87	42.60	42.54
TiO_2	0.02	0.04	0.02	0.02	0.02	0.02
FeO	10.21	9.77	7.48	7.18	7.25	6.55
MnO	0.09	0.09	0.11	0.11	0.13	0.09
MgO	49.10	48.37	50.05	51.32	51.82	52.40
Total	101.49	99.61	99.56	100.89	102.25	102.28

Phlogopite analyses

	F287	F656							
	Ph P1	Ph P2	Ph P3	Ph P1	Ph P2	Ph P3	Ph P4	Ph P5	Ph P6
SiO_2	42.38	42.34	42.62	41.23	42.59	42.51	39.34	42.04	42.29
TiO_2	1.47	1.12	1.34	1.72	1.27	1.62	2.76	1.25	1.49
Al_2O_3	11.59	12.09	12.11	14.97	10.40	13.57	10.05	13.54	14.21
FeO	3.99	3.11	3.67	4.67	4.08	4.28	7.77	5.12	4.67
MnO	0.03	0.05	0.02	0.05	0.04	0.02	0.08	0.03	0.02
MgO	24.37	25.22	24.78	23.57	26.84	24.16	23.46	24.12	23.80
Na_2O	0.06	0.07	0.06	0.02	0.04	0.05	0.02	0.02	
K_2O	10.24	10.37	10.41	10.29	9.96	10.54	10.22	10.57	10.26
Cr_2O_3	1.09	0.87	0.98	0.41	1.43	1.89	0.12	0.34	1.51
Total	95.22	95.24	96.03	96.93	96.65	98.64	93.82	97.25	98.25

	F659							
	Ph Gc1	Ph Gr1	Ph Gc2	Ph Gr2	Ph Gc3	Ph Gr3	Ph Gc4	Ph Gr4
SiO_2	42.69	41.48	43.61	43.63	42.99	42.73	43.50	42.13
TiO_2	1.44	1.19	1.24	0.74	1.06	0.85	0.84	2.07
Al_2O_3	8.96	0.61	8.24	6.45	8.04	6.16	7.40	0.50
FeO	9.21	17.77	9.20	10.53	9.01	11.73	9.29	17.09
MnO	0.08	0.25	0.06	0.06	0.08	0.09	0.09	0.39
MgO	25.06	4.56	25.11	25.68	25.69	25.55	25.78	24.40
Na_2O	-	0.02	0.02	0.02	-	0.02	0.02	0.05
K_2O	10.27	9.88	10.42	10.46	10.42	10.36	10.37	9.94
Cr_2O_3	0.20	0.07	0.07	0.07	0.22	0.10	0.15	0.03
Total	97.91	75.83	97.97	97.64	97.51	97.59	97.44	96.60

	F660							
	Ph Gc1	Ph Gr1	Ph Gc2	Ph Gr2	Ph Gc3	Ph Gr3	Ph Gc4	Ph Gr4
SiO_2	41.02	42.16	43.74	41.96	43.01	42.44	41.38	42.08
TiO_2	1.86	0.75	1.50	0.84	2.33	1.96	1.90	1.17
Al_2O_3	7.40	0.99	7.63	2.93	8.65	7.85	7.33	7.22
FeO	9.28	18.48	9.84	15.32	9.80	10.97	11.04	9.84
MnO	0.06	0.18	0.11	0.12	0.08	0.09	0.11	0.08
MgO	25.39	23.93	25.23	24.98	24.26	24.24	24.18	25.21
Na_2O	-	0.04	0.03	0.03	0.03	0.02	-	0.02
K_2O	9.23	9.74	10.15	10.18	10.23	10.15	10.15	10.24
Cr_2O_3	0.02	-	0.07	0.02	0.05	0.03	0.03	0.15
Total	94.26	96.27	98.30	96.38	98.44	97.75	96.12	96.01

	F664		
	Ph G1	Ph G2	Ph G3
SiO_2	41.17	40.54	40.92
TiO_2	1.86	1.45	2.22
Al_2O_3	7.06	8.16	7.98
FeO	9.99	8.90	8.85
MnO	0.09	0.11	0.06
MgO	23.91	24.57	23.90
Na_2O	0.05	0.08	0.08
K_2O	10.52	10.09	9.93
Cr_2O_3	0.08	0.10	0.05
Total	95.03	94.47	94.88

Garnet and Spinel analyses

	F287	F340				F653	F664	
	Gnt M	Sp G	Sp G	Sp M	Sp M	Sp G	Sp G	Sp G
SiO_2	42.13	0.23	0.26	0.13	0.11	0.36	0.34	1.22
TiO_2	0.34	0.17	0.17	1.53	0.67	1.00	0.96	1.05
Al_2O_3	18.56	6.60	6.48	5.29	8.50	8.00	8.41	6.47
FeO	6.12	15.47	15.54	16.83	14.72	20.90	19.57	18.65
MnO	0.34	0.39	0.40	0.42	0.39	0.60	0.39	0.53
MgO	21.09	13.58	13.42	13.32	13.56	11.68	13.64	13.61
CaO	5.21	0.03	0.03	0.06	0.03	0.05	0.05	0.09
Na_2O	0.05	–	–	–	–	–	–	–
Cr_2O_3	7.10	63.72	63.84	61.14	61.01	56.99	54.13	58.41
NiO	–	0.11	0.09	–	–	0.13	0.12	0.12
Total	100.94	100.30	100.23	98.72	98.99	99.73	97.62	100.51

Garnet Peridotite analyses

	F689					
	Opx			Cpx	Gnt1	Gnt2
SiO_2	56.66	57.85	57.78	55.21	42.39	42.63
TiO_2	0.15	0.13	0.13	0.33	0.57	0.55
Al_2O_3	0.63	0.62	0.63	2.65	21.88	21.88
FeO	5.35	5.57	5.49	2.97	7.78	7.81
MnO	0.09	0.11	0.13	0.11	0.30	0.33
MgO	33.99	34.32	34.17	17.14	21.06	21.39
CaO	0.67	0.69	0.69	18.93	4.34	4.37
Na	0.19	0.16	0.16	2.08	–	–
K	–	–	–	0.03	–	–
Cr	–	0.15	0.15	0.79	1.71	1.73
Total	97.85	99.79	99.47	100.24	100.03	100.69

C.3 XRF and AA analyses

Finsch mine kimberlites

	CRC 1	CRC 2	CRC 3	CRC 4	CRC 6	CRC7	Finsch B	F653	F656	F659	F664	F287
SiO_2	38.83	41.93	41.75	40.59	38.37	40.15	40.40	39.01	39.16	38.33	37.94	37.74
Al_2O_3	3.21	3.94	4.50	5.67	2.83	3.60	3.75	3.66	3.58	3.29	3.28	3.19
Fe_2O_3	8.44	8.42	6.70	11.92	8.41	8.13	8.40	8.31	8.52	8.52	8.35	8.06
MgO	31.18	28.62	26.80	22.53	33.38	31.22	28.23	29.51	30.47	31.27	30.57	31.97
CaO	6.20	5.67	5.30	6.15	3.31	6.22	5.53	5.47	5.59	4.02	4.33	5.38
Na_2O	0.21	0.36	0.49	0.32	0.11	0.07	0.16	0.17	0.58	0.18	0.14	0.10
K_2O	2.66	3.53	3.38	1.38	2.91	2.64	3.92	4.23	3.09	3.94	3.37	3.77
TiO_2	0.84	0.81	0.81	0.63	0.82	0.82	0.81	0.85	0.87	0.86	0.85	0.88
MnO	0.14	0.14	0.13	0.14	0.15	0.14	0.13	0.14	0.14	0.13	0.14	0.14
P_2O_5	0.59	0.54	0.49	0.3	0.65	0.60	0.54	0.56	0.59	0.58	0.54	0.86
LOI	7.50	5.28	6.43	8.57	7.62	5.60	-	6.72	6.40	7.62	9.13	6.57
Total	99.80	99.24	96.78	98.21	98.56	99.19	-	98.63	99.09	98.74	98.64	98.66
Rb	122	139	128	42	137	131	157	157	149	160	151	136
Sr	736	771	736	771	897	837	675	775	796	623	645	784
Ba	290	567	384	496	2129	1751	-	1590	1711	1798	1698	2395
Y	9	7	9	9	7	10	-	9.2	9.1	9.4	8.5	12.9
Zr	179	144	150	93	195	164	-	164	172	160	170	232
Nb	48	39	44	21	62	54	-	38.6	41.9	41.2	38.6	59.5
V	136	102	1206	82	134	6	-	128	127	139	147	134
Cr	1772	1796	1420	759	2051	1828	-	1814	1814	1725	1628	1903
Ni	1337	1236	1228	979	1473	1333	-	1279	1368	1380	1360	1396

	F765	F766	F767	F652	F660	F661	F757	F340	F667	F756	F758	F760	F769	CRC 5
SiO_2	37.33	40.69	37.37	38.04	36.87	36.99	35.68	33.24	30.83	32.51	27.63	47.15	8.42	20.54
Al_2O_3	2.83	3.75	2.52	3.65	2.54	2.44	2.73	1.94	1.62	3.42	3.31	14.55	1.66	5.29
Fe_2O_3	8.47	8.84	7.98	8.14	7.95	7.82	8.59	7.80	6.71	6.12	5.68	10.21	1.65	9.50
MgO	30.22	26.59	29.40	28.66	32.73	31.33	28.91	32.81	29.91	12.66	10.44	7.72	0.69	19.39
CaO	4.64	4.39	5.14	5.16	3.29	4.10	5.68	8.54	9.60	19.93	24.48	7.85	47.68	16.70
Na_2O	0.08	0.09	0.06	0.11	0.16	0.08	0.11	0.07	0.03	0.09	0.08	4.91	–	0.54
K_2O	3.32	3.71	2.99	3.85	2.82	2.39	3.63	2.68	0.81	3.83	2.71	1.67	0.72	1.14
TiO_2	0.79	1.03	0.63	0.82	0.64	0.60	0.96	1.00	0.80	1.50	1.57	0.83	0.05	4.44
MnO	0.15	0.18	0.20	0.13	0.13	0.15	0.16	0.26	0.28	0.46	0.33	0.18	0.76	0.25
P_2O_5	0.52	0.67	0.44	0.53	0.46	0.43	0.83	0.74	0.33	1.03	1.18	0.12	0.02	1.90
LOI	10.53	8.75	12.04	9.79	11.10	12.54	11.19	10.72	17.01	16.67	21.47	4.19	38.04	16.29
Total	98.73	98.69	98.77	–	98.69	98.87	98.47	99.80	97.93	98.22	98.88	99.38	99.69	95.98
Rb	141	182	128	157	121	107	152	133	42.9	187	140	40.6	2.5	82
Sr	611	840	520	476	473	487	842	919	416	926	1423	21.3	15.1	739
Ba	1254	1418	884	1125	1231	667	1689	2454	2590	1691	1306	280	28.0	1587
Y	74?	10.1	7.0	8.0	5.9	6.8	12.8	10.3	9.1	16.7	15.8	23.1	6.7	38
Zr	152	208	118	161	127	110	290	237	248	320	359	74.8	22.5	655
Nb	35.9	51.9	26.5	40.6	32.2	28.6	77.2	54.8	43.6	82.7	92.6	4.7	1.9	321
V	123	153	108	140	120	137	126	127	74.8	196	285	217	10.0	137
Cr	1898	1737	1839	1806	1828	1782	1835	1914	1514	1409	1429	331	11.8	1994
Ni	1499	1544	1455	1386	1475	1502	95.2	21.4	369	1204	1276	1063	719	485

	WA A3/2	WA A3/3	WA A3/8	WA A3/16a	WA A3/16b	WA A7/1	WA A7/2	WA A9/1	WA A11/1
SiO_2	44.76	48.97	50.97	47.15	46.75	52.50	48.28	57.41	49.09
Al_2O_3	5.94	6.83	8.51	5.73	5.70	8.95	7.94	7.31	7.06
Fe_2O_3	8.52	7.77	5.71	7.43	7.38	6.49	8.50	6.44	6.42
MgO	11.44	8.56	7.42	12.50	12.27	7.40	8.26	5.97	10.91
CaO	3.68	3.69	2.48	3.94	3.93	2.19	3.63	3.47	3.23
Na_2O	0.80	0.77	0.09	0.75	0.74	0.52	0.36	0.64	0.25
K_2O	7.10	9.10	11.12	6.71	6.87	9.81	9.02	8.43	8.94
TiO_2	7.55	6.04	6.61	6.71	6.69	4.90	5.89	5.37	5.01
MnO	0.07	0.08	0.02	0.05	0.05	0.05	0.07	0.07	0.05
P_2O_5	1.73	1.63	2.01	1.33	1.33	0.83	0.97	0.67	1.91
LOI	5.01	3.45	2.96	5.24	4.97	4.34	3.97	2.25	5.39
Total	96.60	96.89	97.90	97.54	96.68	97.98	96.89	98.03	98.21
Rb	610	440	406	544	564	262	360	273	512
Sr	1728	2004	1922	1746	1756	1058	1004	1127	1479
Ba	16509	14100	3588	14925	14034	9200	14000	8900	8000
Y	26.2	20	21.8	23.4	21.9	12	11	12	16
Zr	2317	1625	2057	1721	1718	1141	1288	1216	1307
Nb	244	230	176	203	197	101	192	130	165
V	181	110	214	131	132	140	110	99	169
Cr	424	330	299	460	446	373	380	178	392
Ni	270	450	514	350	336	920	220	100	440

	WA A12/1	WA A12/2	WA A12/26	WA A12/30	WA A12/31	WA A12/49	WA A12/50	WA A12/65	WA A12/72	WA A13/1	WA A13/2
SiO_2	47.72	46.30	52.18	47.52	47.86	51.41	48.63	48.37	47.45	53.28	51.79
Al_2O_3	9.01	7.80	9.36	8.36	9.44	9.89	8.62	8.29	8.70	8.39	8.29
Fe_2O_3	8.50	6.98	6.88	8.34	9.82	7.56	9.24	8.16	8.67	6.94	6.67
MgO	3.99	6.70	7.17	8.01	6.60	7.65	6.78	8.74	7.63	7.13	7.25
CaO	2.20	5.23	2.66	2.58	2.62	2.50	2.32	2.16	2.59	2.92	2.76
Na_2O	0.06	0.01	0.36	0.15	0.08	0.23	0.10	0.17	0.11	0.72	0.67
K_2O	9.68	8.94	7.64	6.37	5.32	5.51	9.02	10.05	9.87	9.74	9.13
TiO_2	6.37	5.07	4.83	6.47	7.46	5.43	6.75	6.39	6.70	5.32	5.75
MnO	0.10	0.06	0.05	0.03	0.03	0.05	0.05	0.06	0.05	0.06	0.05
P_2O_5	1.60	4.03	0.96	1.65	1.73	1.02	1.64	1.62	1.94	0.67	0.53
LOI	6.46	6.31	5.73	7.26	6.75	7.46	4.99	3.74	3.96	3.76	4.97
Total	95.69	97.43	97.82	96.74	97.71	98.71	98.14	97.75	97.67	98.93	97.86
Rb	497	357	588	580	471	653	833	500	583	398	267
Sr	1266	1837	1022	1496	1363	932	1288	1536	1485	1085	983
Ba	6200	4600	12590	16730	6131	8357	7287	5038	5738	5500	7900
Y	28	28	19.4	27.4	35	13.7	34.2	13.1	29.2	10	10
Zr	1634	1371	1200	1565	1853	1313	1745	1656	1754	1245	1269
Nb	279	209	110	218	260	107	254	248	254	111	109
V	340	190	234	136	174	476	152	230	394	140	119
Cr	68	378	478	426	5454	525	364	468	507	401	407
Ni	570	510	388	565	547	482	440	414	507	410	440

	WA B3/8	WA B3/9	WA B5/5	WA B5/6	WA B8/2	WA B9/3	WA B9/4	WA B12/1	WA B19/2	WA B19/3	WA B20/1	WA B20/2
SiO_2	36.60	29.48	52.08	51.41	50.48	51.64	51.16	61.83	51.77	60.02	45.85	54.00
Al_2O_3	4.55	3.28	9.38	9.49	7.84	8.68	7.36	8.36	10.10	8.20	6.51	9.00
Fe_2O_3	6.75	6.48	6.55	6.73	7.51	6.99	6.42	6.69	8.13	7.27	7.14	6.76
MgO	8.44	9.86	6.26	6.60	6.82	7.61	10.86	2.42	5.13	3.09	14.54	6.30
CaO	14.69	17.15	1.93	1.75	7.02	2.40	3.53	1.30	0.41	1.50	3.39	1.81
Na_2O	0.19	0.29	0.05	0.09	0.44	0.53	0.61	0.14	0.05	0.39	0.44	0.50
K_2O	6.42	5.48	11.44	11.77	8.96	10.09	8.29	8.34	10.98	8.86	5.78	10.80
TiO_2	4.48	5.43	5.72	5.90	4.93	5.32	5.32	5.19	6.20	4.93	4.75	4.47
MnO	0.10	0.07	0.05	0.06	0.10	0.06	0.06	0.04	0.05	0.05	0.08	0.04
P_2O_5	0.45	1.39	1.45	1.31	1.60	0.89	0.72	1.06	0.67	0.95	0.85	0.71
LOI	14.40	16.62	3.82	3.45	2.86	3.56	4.72	3.80	4.41	2.37	9.02	2.75
Total	97.07	95.53	98.73	98.56	98.56	97.77	99.05	99.17	97.90	97.63	98.35	97.14
Rb	435	382	246	290	191	244	188	255	344	214	225	277
Sr	1590	2349	1434	862	1011	1377	1152	801	549	802	1249	1427
Ba	9200	18100	5900	6010	6910	8500	4400	4001	11900	6993	7100	14000
Y	10	11	24	26	25	26	16	17	26	19.1	20	-
Zr	1905	1471	1273	1291	1148	1220	1090	1168	1518	1199	1049	1100
Nb	147	168	140	148	163	137	122	176	163	123	133	-
V	40	50	440	280	98	140	100	109	170	139	80	130
Cr	161	142	235	244	1931	349	323	284	416	523	593	173
Ni	225	170	300	310	190	440	401	90	530	367	1090	275

C.3.1 Leucite Hills, Smoky Butte and Prairie Creek lamproites

	LH 2/9	LH 3/11	LH 4/7	LH 5/7	LH 5/9	LH 6/12	LH 6/15	LH 7/1	LH 8/3	LH 8/8	LH 9/1	LH 11/1
SiO_2	51.89	49.57	53.01	47.79	47.52	53.43	52.73	51.35	50.60	51.92	51.33	51.67
Al_2O_3	10.15	10.53	10.09	8.99	9.16	9.52	9.23	9.26	8.89	9.42	9.15	9.99
Fe_2O_3	4.96	4.42	3.89	5.59	5.52	4.68	4.70	5.10	5.00	4.79	4.69	4.55
MgO	7.27	6.88	6.54	9.46	9.15	9.98	9.92	10.65	10.20	9.61	8.76	7.64
CaO	5.72	4.92	4.87	8.54	8.49	3.77	4.12	4.61	4.94	4.48	5.63	5.60
Na_2O	1.80	0.85	0.71	0.94	0.75	1.13	1.24	1.14	1.43	0.88	1.31	1.10
K_2O	9.97	8.85	11.16	8.40	8.88	10.30	10.40	9.98	10.86	10.29	10.42	10.64
TiO_2	2.21	2.25	2.31	2.48	2.36	2.20	2.25	2.33	2.09	2.24	2.22	2.25
MnO	0.06	0.03	0.05	0.10	0.08	0.05	0.06	0.06	0.06	0.06	0.06	0.06
P_2O_5	1.87	1.98	1.90	1.47	1.53	1.18	1.35	1.46	1.84	1.69	1.82	1.57
LOI	1.55	4.09	3.20	3.71	4.02	1.61	1.70	1.97	1.57	2.92	2.28	2.54
Total	97.45	94.37	97.73	97.47	97.46	97.85	97.70	97.91	97.48	98.30	97.67	97.61
Rb	127	180	265	257	283	276	249	211	254	276	242	260
Sr	2206	2209	1933	3169	2581	1737	1760	2238	2609	2207	2156	2349
Ba	7800	24800	7300	8861	7400	4411	4524	5500	7100	5400	5162	7700
Y	12	10	11	19.2	12	15	17.9	16	11	12	17.9	11
Zr	1361	1458	1428	1557	1420	1470	1503	1461	1340	1401	1466	1390
Nb	64	51	33	88.3	81	38	42.8	44	40	36	45.6	42
V	110	111	70	113	100	70	86.7	98	88	100	93.6	95
Cr	338	336	257	420	305	408	532	448	427	398	481	344
Ni	170	161	255	159	171	411	398	429	410	170	313	231

	LH 12/1	LH 12/16	LH 13/18	LH 15/1	LH 16/8	LH 16/14	LH 17/3	LH 17/19	LH 17/26	LH 17/28	LH 17/34	LH 17/48
SiO_2	49.75	51.02	51.83	48.83	52.63	51.50	54.10	53.30	–	53.78	53.90	54.10
Al_2O_3	8.75	8.90	9.77	9.84	9.96	9.63	9.90	9.73	–	9.87	10.19	10.58
Fe_2O_3	4.69	4.85	4.59	5.49	4.52	4.54	4.26	4.30	–	4.47	4.17	4.32
MgO	9.26	9.59	7.44	8.06	7.81	7.57	6.09	6.81	–	6.52	6.17	6.15
CaO	4.87	4.29	4.80	7.18	4.38	5.01	3.13	3.68	–	3.85	3.40	3.86
Na_2O	1.22	1.39	1.33	1.91	1.21	1.33	1.39	1.51	1.46	1.36	1.91	0.81
K_2O	9.31	10.64	11.23	9.73	11.41	10.74	12.34	11.33	–	11.28	11.78	11.52
TiO_2	2.30	2.32	2.43	2.24	2.37	2.36	2.42	2.46	–	2.51	2.58	2.62
MnO	0.06	0.06	0.06	0.07	0.05	0.06	0.05	0.06	–	0.06	0.05	0.05
P_2O_5	1.91	1.85	1.97	1.69	1.69	1.64	1.79	1.69	–	1.57	1.86	1.36
LOI	5.60	3.04	2.46	1.47	1.61	2.82	2.47	2.13	–	2.66	2.41	2.15
Total	97.72	97.95	97.91	96.51	97.64	97.20	97.94	97.00	–	97.93	98.42	97.52
Rb	215	295	263	288	290	270	285	253	268	259	279	303
Sr	2545	2258	2495	2703	2210	2240	1911	2110	1972	1772	1937	2152
Ba	5400	6400	6500	7500	5650	6300	4800	7013	6679	5188	4700	6033
Y	14	12	14	13	10	10	13	17.2	17.4	17.4	14	18
Zr	1494	1513	1380	8139	1511	1386	1608	1633	1730	1725	1651	1368
Nb	46	48	45	52	53	38	40	45	49	48	47	37
V	41	80	70	98	85	69	70	83	81	79	60	65
Cr	364	367	303	305	355	315	268	409	441	402	262	354
Ni	320	351	240	135	250	221	190	255	271	254	220	215

	LH19/25	LH19/26	SB11	SB35	SB45	SB59	SB66	SB70	PK1/4	PK1/18	PK1/20
SiO_2	37.99	42.10	50.85	51.32	47.78	50.76	51.52	46.85	39.91	39.33	41.10
Al_2O_3	7.84	7.02	7.99	10.94	8.92	8.78	8.78	11.06	3.88	3.85	3.90
Fe_2O_3	5.21	5.71	5.66	4.65	5.19	5.56	5.53	5.29	8.71	8.65	8.92
MgO	8.70	10.51	9.19	3.64	5.41	8.42	8.21	0.98	27.11	27.92	27.81
CaO	15.23	11.88	4.34	3.78	7.74	4.61	4.28	5.20	5.16	5.53	5.00
Na_2O	0.82	0.75	2.34	0.40	0.58	1.30	0.80	0.13	0.32	0.40	0.33
K_2O	4.23	7.20	2.34	10.69	8.86	6.38	8.31	10.08	2.69	2.48	2.27
TiO_2	2.05	2.06	5.56	6.28	5.68	5.30	5.32	6.38	2.89	2.30	2.88
MnO	0.22	0.10	0.06	0.04	0.09	0.06	0.05	0.04	0.13	0.13	0.12
P_2O_5	2.99	3.64	2.49	2.87	2.48	2.26	2.23	2.81	0.35	0.65	0.29
LOI	12.70	6.78	6.05	1.62	4.17	4.70	1.85	5.22	8.63	8.26	8.65
Total	97.98	97.75	96.87	96.23	96.90	98.13	96.88	94.04	99.78	99.50	101.30
Rb	276	316	39.0	118	104	59	74	90	191	176	166
Sr	3950	4420	3150	2928	2332	2686	2915	2226	1040	1002	972
Ba	13300	14400	10300	11912	9584	9673	8867	23108	1624	1790	1761
Y	12	15	27.2	31.2	26.8	24.5	24.4	47	13.4	13.7	13.6
Zr	1290	1230	1786	2023	1828	1708	1723	2005	744	662	745
Nb	79	99	109	123	111	101	102	120	102	86.7	101
V	41	10	124	131	137	121	129	99	56.1	40	68.3
Cr	322	353	420	512	457	365	389	520	1500	1485	1440
Ni	120	140	341	115	251	289	296	148	1285	1443	1340

C.4 INAA analyses

Finsch mine kimberlites

	CRC 1	CRC 2	CRC 3	CRC 4	CRC 6	CRC 7	Finsch B	F653	F656
La	55.7	49.2	50.3	33.5	61.4	59.4	50	57.5	56.7
Ce	117	107	103	67.7	134	124	102	126	123
Nd	52.7	47.8	44.0	28.8	57.2	56.1	46.5	52.6	51
Sm	7.31	6.76	6.70	4.90	8.10	7.67	6.79	7.35	7.25
Eu	1.61	1.49	1.55	1.14	1.73	1.72	1.36	1.71	1.68
Tb	0.37	0.37	0.34	0.49	0.59	0.38	0.47	0.4	0.49
Yb	0.65	0.77	0.93	1.36	0.65	0.9	0.70	0.73	0.65
Lu	–	–	–	0.22	–	–	–	–	–
Cs	1.86	2.00	1.82	1.83	2.24	2.20	2.47	2.69	2.90
Hf	4.4	3.8	3.8	3.4	4.94	4.80	3.65	4.10	4.33
Ta	3.04	2.60	2.62	1.66	3.51	3.19	2.40	3.18	3.18
Th	7.99	6.52	7.78	5.76	8.93	8.03	7.12	8.71	8.45
U	2.4	2.1	2.4	1.7	3.6	2.8	3.3	2.9	2.45
Sc	17.1	18.2	17.3	18.7	17.7	18.2	16.5	17.4	18.7

	F659	F664	F287	F765	F766	F767	F652	F660	F661
La	55.1	50.9	77.1	48.7	62.1	42.2	49.4	42.4	40.8
Ce	118	112	164	106	141	91.5	107	93.5	89.5
Nd	50.3	46.5	62.8	42.5	47.5	32.2	48.4	45.0	42.5
Sm	7.10	6.59	9.12	6.1	7.88	4.75	6.4	5.43	5.13
Eu	1.66	1.56	2.12	1.48	1.96	1.20	1.48	1.28	1.21
Tb	–	0.52	0.61	0.48	0.54	0.41	0.42	0.32	0.36
Yb	–	0.69	0.74	0.81	0.72	0.37	0.55	0.47	0.42
Lu	–	–	–	–	–	–	–	–	–
Cs	2.64	2.73	2.8	2.67	3.27	2.40	2.49	1.85	1.75
Hf	4.1	4.98	6.22	4.3	5.27	3.29	3.90	3.47	2.82
Ta	3.13	3.08	4.21	2.86	3.86	2.13	2.70	2.28	1.96
Th	7.50	7.25	10.7	6.69	9.0	5.08	6.99	5.47	4.82
U	2.4	2.1	2.5	1.8	2.7	1.6	2.5	2.0	1.6
Sc	17.1	17.4	19.4	16.3	21.2	11.8	17.3	13.6	12.8

	F757	F340	F667	F756	F758	F760	F769	CRC 5
La	105	73.3	56.3	110	108	7.4	10.3	250
Ce	227	157	120	235	227	17.4	19.3	572
Nd	94.2	62.3	55	90	78.0	9.7	8.8	250
Sm	11.97	8.7	6.14	12.8	11.74	2.67	1.22	39.5
Eu	2.87	2.0	1.52	3.10	2.92	1.01	0.28	9.86
Tb	0.91	0.53	0.47	0.85	0.98	0.66	0.17	3.01
Yb	1.02	0.70	0.49	1.08	1.11	2.43	0.44	2.02
Lu	0.14	–	0.60	–	–	–	–	0.37
Cs	3.00	2.46	0.90	2.80	3.26	0.86	0.59	10.8
Hf	7.18	6.05	6.48	8.51	9.97	2.15	0.51	16.8
Ta	5.90	3.80	3.4	5.43	5.50	0.30	0.11	20.4
Th	15.7	9.4	6.94	15.6	11.4	1.04	1.55	36.1
U	4.0	2.8	1.6	4.4	4.2	–	0.6	7.5
Sc	16.9	17.0	14.4	21.35	23.35	36.0	1.63	27.7

West Kimberley lamproites

	WA A 1/2	WA A 3/3	WA A 3/16a	WA A 7/1	WA A 11/1	WA A 12/2	WA A 12/26	WA A 12/30	WA A 12/31
La	290	425	280	213	323	402	239	509	596
Ce	601	825	569	340	602	727	495	878	975
Nd	191	276	179	121	209	243	143	280	334
Sm	22.1	29.3	22.2	14.6	24.7	29.1	18.4	35.2	40.5
Eu	4.55	7.00	5.32	3.46	5.70	6.96	4.38	8.47	9.93
Tb	1.24	1.91	1.57	0.91	1.58	1.78	1.29	2.43	2.81
Yb	1.66	1.78	1.97	1.14	1.31	1.66	1.87	2.14	2.61
Lu	–	0.2	–	0.15	–	0.25	0.19	0.2	0.26
Cs	3.84	1.1	0.98	1.79	2.19	0.68	0.75	3.55	
Hf	24.0	44.2	51.2	31.1	35.1	37.7	31.6	44.0	49.2
Ta	15.9	13.3	15.0	5.54	7.92	10.4	6.34	11.8	13.8
Th	69.1	55.5	40.4	15.8	37.3	47.4	27.6	61.9	71.3
U	10.3	6.3	6.1	1.8	5.2	9.3	1.9	5.4	6.4
Sc	19.2	18.4	17.9	14.2	14.3	14.9	13.9	17.7	19.9

	WA A 12/49	WA A 12/50	WA A 12/65	WA A 12/72	WA A 13/2	WA B 3/8	WA B 3/9	WA B 5/6	WA B 8/2
La	232	563	392	580	182	160	108	322	254
Ce	407	1017	807	1035	338	239	170	526	376
Nd	143	316	230	371	118	73.5	54.5	192	133
Sm	17.2	38.6	26.7	39.1	13.8	10.6	7.56	23.0	16.5
Eu	3.92	9.64	6.14	9.70	3.27	2.91	2.10	5.64	4.02
Tb	1.13	2.78	1.58	2.74	0.84	0.95	0.70	1.64	1.30
Yb	1.28	2.64	1.26	2.36	1.07	1.33	1.34	1.60	1.89
Lu	–	0.33	–	–	–	–	0.18	0.19	0.21
Cs	1.11	33.3	2.60	43.8	–	1.54	2.09	0.46	–
Hf	35.7	48.1	45.5	49.2	35.8	64.2	43.0	29.1	33.0
Ta	6.83	13.5	13.1	13.9	6.67	6.24	5.06	6.41	9.00
Th	24.9	75.6	66.1	75.5	17.6	23.2	15.4	23.9	22.3
U	2.0	5.4	4.3	7.1	2.2	5.1	4.4	2.2	1.9
Sc	15.0	19.5	16.9	19.9	14.0	17.6	17.6	12.7	15.9

	WA B 9/3	WA B 9/4	WA B 19/2	WA B 20/1	WA B 20/2
La	319	206	252	234	273
Ce	495	351	450	403	458
Nd	180	112	161	129	153
Sm	21.2	13.2	20.2	15.2	19.5
Eu	5.23	3.28	4.89	3.71	4.67
Tb	1.55	1.01	1.39	0.97	1.36
Yb	2.06	1.48	1.58	1.42	1.80
Lu	0.24	0.17	0.20	0.20	0.27
Cs	1.74	–	9.34	0.48	–
Hf	32.0	35.0	39.6	28.8	23.5
Ta	6.72	7.44	8.88	7.08	4.68
Th	26.9	22.0	25.3	23.5	28.0
U	2.4	1.4	9.6	3.1	3.1
Sc	15.1	13.5	16.2	15.3	14.6

Leucite Hills lamproites

	LH 5/7	LH 5/9	LH 6/12	LH 6/15	LH 8/3	LH 8/8	LH 9/1	LH 11/1
La	260	273	147	141	182	167	166	165
Ce	516	554	304	290	366	342	324	333
Nd	204	228	125	119	133	131	127	115
Sm	23.7	24.7	16.0	16.0	16.7	16.2	16.5	14.4
Eu	5.5	5.61	3.73	3.7	4.05	3.94	3.86	3.43
Tb	1.47	1.45	1.04	1.04	1.18	1.17	1.10	1.01
Yb	1.3	1.45	1.30	1.0	1.25	1.28	1.04	1.27
Lu	0.18	0.17	0.13	0.15	0.14	0.13	0.15	0.12
Cs	3.18	3.02	1.97	1.99	2.34	1.94	2.23	2.19
Hf	43.3	43.2	41.5	41.6	39.8	40.1	40.5	39.7
Ta	4.92	5.28	2.21	2.17	2.50	2.40	2.33	2.72
Th	32.8	34.00	16.0	16.04	22.9	19.0	19.1	20.2
U	8.2	8.6	4.5	4.4	4.6	4.9	7.4	4.5
Sc	–	18.4	11.9	–	12.9	12.2	–	13.6

	LH 17/19	LH 17/26	LH 17/28	LH 17/48	LH 19/26
La	140	113	112	147	357
Ce	289	235	232	312	722
Nd	111	92.4	91.2	129	251
Sm	13.9	12.2	12.5	16.5	32.7
Eu	3.44	3.02	3.06	3.85	7.48
Tb	1.07	0.94	0.90	1.09	1.91
Yb	1.41	1.40	1.38	1.44	1.49
Lu	0.13	0.13	0.15	–	–
Cs	2.02	2.01	2.10	1.80	7.04
Hf	44.3	45.7	46.9	37.7	38.3
Ta	2.42	2.46	2.51	2.10	7.06
Th	15.9	13.1	13.2	15.1	45.0
U	4.2	3.7	3.7	2.8	8.7
Sc	12.1	12.5	13.0	12.3	20.4

Smoky Butte and Prairie Creek lamproites

	SB11	SB35	SB45	SB59	SB66	SB70	PK 1/4	PK 1/18	PK 1/20
La	364	410	366	332	337	437	142	147	144
Ce	803	874	821	716	746	930	275	280	277
Nd	329	361	328	292	300	379	106	109	107
Sm	36.7	40.8	37.0	32.6	33.5	43.1	13.3	13.3	13.4
Eu	7.80	8.77	7.79	6.84	7.02	9.50	3.11	3.15	3.15
Tb	1.96	2.09	1.91	1.69	1.76	2.59	0.86	0.86	0.82
Yb	1.87	2.21	1.90	1.73	1.69	3.19	0.96	0.95	0.90
Lu	0.23	0.28	0.22	0.18	0.19	0.41	0.12	0.12	0.12
Cs	2.13	–	–	2.55	0.34	0.39	0.82	1.38	1.20
Hf	44.9	50.9	46.1	41.6	42.5	53.8	17.66	15.98	18.3
Ta	5.91	6.79	5.64	5.08	5.23	6.22	6.58	5.33	6.44
Th	6.66	7.76	6.41	5.29	5.26	7.33	10.98	11.6	11.2
U	1.4	1.9	1.4	1.1	1.3	4.0	2.7	2.5	2.6
Sc	14.0	17.2	14.6	13.0	13.3	15.4	–	–	–

C.5 Isotope analyses

C.5.1 Sr and Nd isotopes

Finsch mine kimberlites

Sample	Rb	Sr	$(^{87}Sr/^{86}Sr)_m$	2σ	$(^{87}Sr/^{86}Sr)_i$	ϵSr	Sm	Nd	$(^{143}Nd/^{144}Nd)_m$	2σ	$(^{143}Nd/^{144}Nd)_i$	ϵNd
CRC 1	122	736	0.71064	5	0.70983	74.8	7.31	52.7	0.51217	1	0.51210	-7.5
CRC 2	139	771	0.70956	3	0.70869	58.6	6.76	47.8	0.51217	1	0.51210	-7.8
CRC 3	128	736	0.70957	3	0.70873	59.1						
CRC 4	42	771	0.71188	3	0.71162	100	4.90	28.8	0.51217	2	0.51209	-7.8
CRC 6	137	897	0.70949	2	0.70875	59.4	8.10	57.2	0.51224	2	0.51217	-6.2
CRC 7	131	837	0.70959	3	0.70883	60.6	7.67	56.1	0.51219	2	0.51212	-7.1
Finsch B	157	675	0.70968	3	0.70855	56.6	6.79	46.5	0.51217	3	0.51210	-7.6
F653	157	775	0.70946	4	0.70847	55.6	7.35	52.6	0.51219	1	0.51212	-7.1
F656	149	796	0.70953	4	0.70861	57.5	7.25	51	0.51216	2	0.51209	-7.7
			0.70952	4								
F659	160	623	0.70998	3	0.70873	59.2	7.10	50.3	0.51216	1	0.51209	-7.7
F664	151	645	0.70891	3	0.70777	45.6	6.59	46.5	0.51219	1	0.51212	-7.2
F287	136	784	0.70996	5	0.70912	64.7	9.12	62.8	0.51206	2	0.51199	-9.7
F765	141	611	0.71034	2	0.70922	66.1	6.1	42.5	0.51221	1	0.51214	-6.8
F766	182	840	0.70976	3	0.70871	58.8	7.88	47.5	0.51223	2	0.51215	-6.6
F767	128	520	0.71017	3	0.70898	62.7	4.75	32.2	0.51222	1	0.51215	-6.6
			0.71017	3								
F652	157	476	0.71001	2	0.70841	54.6	6.4	48.4	0.51216	1	0.51210	-7.6
F660	121	473	0.70991	3	0.70867	58.3	5.43	45.0	0.51218	2	0.51212	-7.2
F661	107	487	0.71047	3	0.70899	62.9	5.13	42.5	0.51223	3	0.51215	-6.6
			0.70965	4					0.51221			
F757	152	842	0.70959	3	0.70871	58.9	12.0	94.2	0.51219	2	0.51213	-7.0
			0.70959	3								
F340	133	919	0.70962	4	0.70892	61.9	8.7	62.3	0.51215	2	0.51208	-7.9
F667	43	416	0.70954	3	0.70904	63.6	6.14	55	0.51213	2	0.51208	-8.0
F756	187	926	0.70988	3	0.70890	61.6	12.8	90	0.51209	2	0.51202	-9.1
F758	140	1423	0.71009	3	0.70961	71.7	11.7	78.0	0.51209	1	0.51202	-9.2
F760	21.3	364	0.70890				2.67	9.7	0.51249	1		
CRC 5	82	739	0.70524	4			39.5	250	0.51271	3		
F689wr			0.70784	3								
F750wr			0.70754	3								
F689di			0.70244	6								
F750di			0.70395	9								

Sample	Rb	Sr	$(^{87}Sr/^{86}Sr)_m$	2σ	$(^{87}Sr/^{86}Sr)_i$	ϵSr	Sm	Nd	$(^{143}Nd/^{144}Nd)_m$	2σ	$(^{143}Nd/^{144}Nd)_i$	ϵNd
WA A1/2	614	1346	0.71134	2	0.71096	89.1	22.1	191	0.51198	2	0.51197	-12.5
WA A3/3	440	2004	0.71471	2	0.71453	140	29.3	276	0.51197	1	0.51196	-12.7
WA A7/1	262	1058	0.72039	2	0.72018	220	14.6	121	0.51181	2	0.51180	-15.8
WA A11/1	512	1479	0.71807	2	0.71779	186	24.7	209	0.51164	2	0.51163	-19.1
WA A12/2	357	1837	0.71811	2	0.717995	188	29.1	243	0.51187	2	0.51186	-14.6
WA A12/26	588	1022	0.71847	3	0.71799	189	18.4	143	0.51186	2	0.51185	-14.8
WA A12/30	580	1496	0.71811	4	0.71779	186	35.2	280	0.51192	3	0.51191	-13.6
WA A12/49	653	932	0.71841	4	0.71783	187	17.2	143	0.51176	2	0.51175	-16.8
WA A13/2	267	983	0.71878	2	0.71855	197	13.8	118	0.51167	2	0.51166	-18.5
WA B3/8	435	1590	0.71251	2	0.70228	108	10.6	73.5	0.51211	2	0.51210	-9.95
WA B3/9	382	2349	0.71258	2	0.71245	110	7.56	54.5	0.51209	2	0.51209	-10.1
WA B5/6	290	862	0.72093	2	0.72065	227	23.0	192	0.51182	9	0.51181	-15.6
WA B8/2	191	1011	0.71500	2	0.71484	144	16.5	133	0.51204	1	0.51203	-11.3
WA B9/3	244	1377	0.71959	2	0.71944	209	21.2	180	0.51182	1	0.51181	-15.6
WA B19/2	344	549	0.72089	2	0.72038	223	20.2	161	0.51189	2	0.51188	-14.2
WA B20/1	225	1249	0.71746	2	0.71731	179	15.2	129	0.51194	1	0.51195	-12.9
									0.51199	2		
WA B20/2	277	1427	0.71916	2	0.71900	203	19.5	153	0.51183	2	0.51182	-15.4

Sample	Rb	Sr	$(^{87}Sr/^{86}Sr)_m$	2σ	$(^{87}Sr/^{86}Sr)_i$	ϵSr	Sm	Nd	$(^{143}Nd/^{144}Nd)_m$	2σ	$(^{143}Nd/^{144}Nd)_i$	ϵNd
LH5/7	257	3169	0.70560	4	0.70560	12.8	23.7	204	0.51203	2	0.51203	-11.9
LH5/9	283	2581	0.70556	2	0.70556	12.2	24.7	228	0.51207	1	0.51207	-11.1
LH6/12	276	1737	0.70574	3	0.70575	14.9	16.0	125	0.51182	2	0.51182	-16.0
			0.70577	3								
LH6/15	249	1760	0.70576	3	0.70575	14.9	16.0	119	0.51172	3	0.51172	-17.9
LH8/3	254	2609	0.70574	4	0.70574	14.7						
LH8/8	276	2207	0.70588	2	0.70587	16.6						
LH9/1	242	2156	0.70568	2	0.70580	15.6	16.5	127	0.51175	2	0.51175	-17.4
LH11/1							14.4	115	0.51188	2	0.51188	-14.8
LH17/19	253	2110	0.70565	2	0.70564	13.3	13.9	111	0.51174	1	0.51174	-17.6
LH17/26	268	1972	0.70571	3	0.70570	14.2	12.2	92.4	0.51183	1	0.51183	-15.8
LH17/28	259	1772	0.70587	4	0.70586	16.5	12.5	91.2	0.51182	1	0.51182	-16.0
LH17/48	303	2152	0.70575	5	0.70569	14.0	16.5	129	0.51186	1	0.51186	-15.2
SB11	39	3150	0.70592	2	0.70591	17.6	36.7	329	0.51137	1	0.51136	-24.3
SB35	118	2928	0.70587	4	0.70583	16.4	40.8	361	0.51137	1	0.51136	-24.2
SB45	104	2332	0.70604	4	0.70599	18.7	37.0	328	0.51143	2	0.51142	-23.1
SB59	59	2686	0.70633	4	0.70631	23.2	32.6	292	0.51138	1	0.51136	-24.1
SB66	74	2915	0.70628	4	0.70625	22.4	33.5	300	0.51128	1	0.51127	-25.9
SB70	90	2226	0.70630	3	0.70626	22.5	43.1	379	0.51151	2	0.51149	-21.6
PK 1/4	191	1040	0.70751	5	0.70670	29.8	13.3	106	0.51201	2	0.51196	-10.6
			0.70750	4								
			0.70751	2								
PK 1/16	176	1002	0.70780	4	0.70703	34.5	13.3	109	0.51199	1	0.51194	-11.0
PK1/20	166	972	0.70742	4	0.70667	29.4	13.4	109	0.51198	2	0.51193	11.2

C.5.4 Pb isotopes

Finsch mine kimberlites

Sample	U ppm	Th ppm	Pb ppm	$(^{206}Pb/^{204}Pb)_m$	2σ	$(^{207}Pb/^{204}Pb)_m$	2σ	$(^{208}Pb/^{204}Pb)_m$	2σ
CRC 1	2.4	7.99	14.11	17.74	1	15.48	1	37.70	1
CRC 2	2.1	6.52	8.53	17.87	1	15.54	1	37.90	3
CRC 3	2.4	7.78	12	17.91	1	15.52	1	37.94	2
CRC 4	1.7	5.7	9.04	18.24	2	15.57	2	38.23	4
CRC 6	3.6	8.93	18.52	17.80	2	15.52	2	37.80	5
CRC 7	2.8	8.03	13.00	17.89	2	15.57	1	37.95	3
Finsch B	3.3	7.12	9.48	17.99	1	15.53	1	37.98	1
F653	2.9	8.71	7.89	18.04	1	15.54	1	37.98	2
F656	2.45	8.45	12.99	17.83	1	15.50	1	37.77	1
F659	2.4	7.50	11.48	17.86	1	15.53	1	37.82	2
F664	2.1	7.25	7.84	17.92	1	15.52	1	37.93	3
F287	2.5	10.7	15.18	17.82	1	15.55	1	38.06	5
			15.62						
F765	1.8	6.69	10.09	17.84	1	15.54	1	37.84	1
F766	2.7	9.0	15.32	17.83	1	15.53	1	37.81	1
F767	1.6	5.08	5.72	17.87	2	15.51	2	37.82	5
F652	2.5	6.99	8.94	17.94	2	15.55	2	37.98	3
F660	2.0	5.47	10.14	17.82	1	15.51	1	37.72	1
F661	1.6	4.82	10.33	17.69	2	15.44	2	37.48	5
F757	4.0	15.7	17.36	17.88	1	15.51	1	37.91	2
F340	2.8	9.4	15.26	17.77	1	15.53	1	37.82	5
F667	1.6	6.94	4.55	17.96	1	15.51	1	38.04	2
F756	4.4	15.6	24.96	18.00	1	15.58	1	37.86	1
F758	4.2	11.4	24.02	18.00	1	15.54	1	37.72	2
CRC 5	7.5	36.1	24	20.05	2	15.66	1	39.83	3
				20.08	2	15.67	2	39.90	3

Sample	U ppm	Th ppm	Pb ppm	$(^{206}Pb/^{204}Pb)_m$	2σ	$(^{207}Pb/^{204}Pb)_m$	2σ	$(^{208}Pb/^{204}Pb)_m$	2σ
West Kimberley									
WA A1/2	10.3	69.1	47.7	17.56	1	15.74	1	38.36	1
				17.57	1	15.75	1	38.42	1
WA A3/3	6.3	55.5	39.7	17.38	1	15.71	1	38.31	1
WA A12/26	1.9	27.6	52.0	17.29	1	15.70	1	38.31	1
WA A12/30	5.4	61.9	110	17.28	1	15.71	1	38.05	2
WA A12/49	2.0	24.9	49.0	17.27	1	15.70	1	38.33	1
				17.27	1	15.69	1	38.32	2
WA B5/6	2.2	23.9	48.0	17.23	2	15.76	2	37.87	4
WA B8/2	1.9	22.3	48.4	17.58	1	15.74	1	38.18	1
WA B9/3	2.4	26.9	59.5	17.29	1	15.74	1	37.89	1
WA B20/1	3.1	23.5	47.1	17.27	1	15.73	1	37.94	2
Leucite Hills									
LH5/7	8.2	32.8	40.05	17.54	1	15.50	1	37.55	1
LH6/15	4.4	16.04	28.62	17.19	1	15.47	1	37.18	1
LH9/1	7.4	19.1	32.29	17.19	1	15.47	1	37.21	2
LH17/19	4.2	15.9	28.2	17.28	2	15.47	1	37.34	1
LH17/26	3.7	13.1	27.99	17.15	1	15.43	1	37.18	1
LH17/28	3.7	13.2	29.49	17.28	1	15.45	1	37.27	1
LH17/48	2.8	15.1	28.37	17.18	1	15.43	1	37.17	1
				17.17	1	15.43	1	37.16	3
Smoky Butte									
SB11	1.4	6.66	12.45	16.14	1	15.19	1	36.27	3
SB35	1.9	7.76	14.94	16.47	1	15.26	1	36.58	2
SB45	1.4	6.41	12.54	16.15	1	15.22	1	36.37	1
SB59	1.1	5.29	10.5	16.04	1	15.21	1	36.25	1
SB66	1.3	5.26	17.22	16.02	1	15.19	1	36.20	2
SB70	4.0	7.33	14.53	16.64	1	15.28	1	36.68	1
Prairie Creek									
PK 1/4	2.7	10.98	20.98	16.77	1	15.37	1	36.80	1
PK 1/18	2.5	11.6	20.8	16.70	1	15.35	1	36.76	1
PK 1/20	2.6	11.2	21.72	16.70	1	15.31	1	36.66	2

References

Abbey S. (1983) Studies in "standard samples" of silicate rocks and minerals. Geol. Surv. Canada. paper, 83–115.

Alibert C., Michard A. and Albèrede F. (1983) The transition from alkali basalts to kimberlites: isotopic and trace element evidence from melilitites. Contrib. Mineral. Petrol. 82, 176–186.

Allègre C.J. (1982) Chemical geodynamics. Tectonophysics 81, 109–132.

Allsopp H.L. and Kramers J.D. (1977) Rb-Sr and U-Pb age determinations on the Southern African kimberlite pipes. 2nd Int. Kimberlite Conf. Santa Fe, Ext. Abs.

Allsopp H.L., Bristow J.W., Skinner E.M.W., Scott Smith B.H. and Danchin R.V. (1985) Rb-Sr geochronology of some Miocene West Australian lamproites. Trans. Geol. Soc. S. Afr. 88, 341–345.

Anderson O.L. (1979) The role of fracture dynamics in kimberlite pipe formation. In: Kimberlites, Diatremes and Diamonds: Their Geology, Petrology and Geochemistry. (Eds: F.R. Boyd and H.O.A. Meyer) AGU Washington, 344–353.

Arima M. and Edgar A.D. (1983) A high pressure experimental study on a magnesian-rich leucite lamproite from the West Kimberley area, Australia: petrogenetic implications. Contrib. Mineral. Petrol. 84, 224–234.

Artyushkov E.V. and Sobolev S.V. (1984) Physics of the kimberlite magmatism. In: Kimberlites I: Kimberlites and Related Rocks. (Ed: J. Kornprobst) Developments in Petrology 11A, Elsevier, Amsterdam, 309–322.

Atkinson, W.J., Hughes F.E. and Smith C.B. (1982) A review of the kimberlitic rocks of Western Australia. Terra Cognita 2, 204.

Atkinson W.J., Hughes F.E. and Smith C.B. (1984) A review of the kimberlitic rocks of Western Australia. In: Kimberlites I: Kimberlites and Related Rocks. (Ed: J. Kornprobst) Developments in Petrology 11A, Elsevier, Amsterdam, 195–224.

Bailey D.K. (1980) Volatile flux, geotherms and the generation of the kimberlite-carbonatite-alkaline magma spectrum. Mineral. Mag. 43, 695–699.

Bailey D.K. (1982) Mantle metasomatism—continuing chemical change within the earth. Nature 296, 525–530.

Bailey D.K. (1984) Kimberlite "the mantle sample" formed by ultrametasomatism. In: Kimberlites I: Kimberlites and Related Rocks. (Ed: J. Kornprobst) Developments in Petrology 11A, Elsevier, Amsterdam, 323–333.

Bailey D.K. (1985) Fluids, melts, flowage and styles of eruption in alkaline ultramafic magmatism. Trans. Geol. Soc. S. Afr. 88, 449–457.

Barrett D.R. and Berg G.W. (1975) Complementary petrographic and strontium isotope ratio studies of South African kimberlites. Phys. Chem. Earth 9, 619–635.

Barton M. (1979) A comparative study of some minerals occurring in the potassium-rich alkaline rocks of the Leucite Hills, Wyoming, the Vico volcano, Western Italy and the Toro-Ankole region, Uganda. N. Jb. Miner. Abh. 137, 113–134.

Barton M. and Hamilton D.L. (1978) Water-saturated melting relations to 5 kilobars of three Leucite Hills lavas. Contrib. Mineral. Petrol. 66, 41–49.

Barton M. and Hamilton D.L. (1979) The melting relationships of a madupite from the Leucite Hills, Wyoming to 30 Kb. Contrib. Mineral. Petrol. 69, 133–142.

Barton M. and Hamilton D.L. (1982) Water-undersaturated melting experiments bearing upon the origin of potassium-rich magmas. Mineral. Mag. 45, 267–278.

Barton M. and van Bergen M.J. (1981) Green clinopyroxenes and associated phases in a potassium-rich lava from the Leucite Hills, Wyoming. Contrib. Mineral. Petrol. 77, 101–114.

Basu A.R. (1978) Trace elements and Sr-isotopes in some mantle derived hydrous minerals and their significance. Geochim. Cosmochim. Acta 42, 659–668.

Basu A.R. and Murthy V.R. (1977) Kaersutites, suboceanic low-velocity zone, and the origin of mid-oceanic ridge basalts. Geology 5, 365–368.

Basu A.R. and Tatsumoto M. (1980) Nd-isotopes in selected mantle derived rocks and minerals and their implications for mantle evolution. Contrib. Mineral. petrol. 75, 43–54.

Berg G.W. (1986) Evidence for carbonate in the mantle. Nature 324, 50–51.

Berg G.W. and Allsopp H.L. (1972) Low $^{87}Sr/^{86}Sr$ ratios in fresh South African kimberlites. Earth Planet. Sci. Lett. 16, 27–30.

Bergman S.C., Foland K.A. and Spera F.J. (1981) On the origin of an amphibole-rich vein in a peridotite inclusion from the Lunar Crater volcanic field, Nevada, USA. Earth Planet. Sci. Lett. 56, 343–361.

Bergman S.C. (1987) Lamproites and other potassium-rich igneous rocks; a review of their occurrence, mineralogy and geochemistry. In: Alkaline Igneous Rocks. (Eds: J.G. Fitton and B.G.J. Upton) Geol. Soc. Spec. Publ. 30, 103–190.

Beswick A.E. (1976) K and Rb relations in basalts and other mantle-derived materials. Is phlogopite the key? Geochim. Cosmochim. Acta 40, 1167–1183.

Beswick A.E. and Carmichael I.S.E. (1978) Constraints on mantle source compositions imposed by phosphorous and the rare-earth elements. Contrib. Mineral. Petrol. 67, 317–330.

Bickle M.J. (1978) Heat loss from the earth: a constraint on Archaean tectonics from the relation between geothermal gradients and the rate of plate production. Earth Planet. Sci. Lett. 40, 301–315.

Bickle M.J. (1986) Implications of melting for stabilisation of the lithosphere and heat loss in the Archaean. Earth. Planet. Sci. Lett. 80, 314–324.

Boettcher A.L., O'Neill J.R., Windom K.R., Stewart D.C. and Wilshire H.G. (1979) Metasomatism of the upper mantle and the genesis of kimberlites and alkali basalts. In: The Mantle Sample: Inclusions in Kimberlites and Other Volcanics. (Eds: F.R. Boyd and H.O.A. Meyer) AGU Washington), 173–182.

Bolivar S.L. and Brookins D.B. (1979) Geophysical and Rb-Sr study of Prairie Creek, Arkansas kimberlites. In: Kimberlites, Diatremes and Diamonds: Their Geology, Petrology and Geochemistry. (Eds:. F.R. Boyd and H.O.A. Meyer) AGU Washington, 289–299.

Bonney T.G. (1899) The parent rock of the diamond in South Africa. Proc. Roy. Soc. 65, 223–236.

Boyd F.R. and Clement C.R. (1977) Compositional zoning of olivines in kimberlite from the De Beers Mine, Kimberley, South Africa. Carnegie Institute Washington Yearbook 76, 485–493.

Boyd F.R. and Finnerty A.A. (1980) Conditions of origin of natural diamonds of peridotite affinity. J. Geophys. Res. 85, 6911–6918.

Boyd F.R. and Nixon P.H. (1973) Origin of the ilmenite-silicate nodules in kimberlites from Lesotho and South Africa. In: Lesotho Kimberlites (Ed. P.H. Nixon) Lesotho National Development Corporation, Maseru. 254–268.

Boyd F.R. and Nixon P.H. (1978) Ultramafic nodules from the Kimberley pipes, South Africa. Geochim. Cosmochim. Acta 42, 1367–1382.

Boyd S.R., Seal M., Mattey D.P., Mendelssohn M.J., Milledge H.J. and Pillinger C.T. (1986) Zoned diamonds: records of mantle volatile activity. Terra Cognita 6, 191.

Brey G. (1978) Origin of olivine melilitites – chemical and experimental constraints. J. Volc. and Geotherm. Res. 3, 61–88.

Brey G. and Green D.H. (1975) The role of CO_2 in the genesis of olivine melilitite. Contrib. Mineral. Petrol. 49, 93–103.

Brey G., Brice W.R., Ellis D.J., Green D.H., Harris K.L. and Ryabchikov I.D. (1983) Pyroxene-carbonate reaction in the upper mantle. Earth Planet Sci. Lett. 62, 63–74.

Brookins D.G. (1967) The strontium geochemistry of carbonates in kimberlites and limestones from Riley County, Kansas. Earth Planet. Sci. Lett. 2, 235–240.

Brown L., Klein J., Middleton R., Sacks I.S. and Tera F. (1982) ^{10}Be in island arc volcanoes and implications for subduction. Nature 299, 718–720.

Burke K. and Kidd W.S.F. (1978) Were Archaean continental geothermal gradients much steeper than those of today? Nature 272, 240–241.

Carlson R.W. (1984) Isotopic constraints on Columbia River flood basalt genesis and the nature of the subcontinental mantle. Geochim. Cosmochim. Acta 48, 2357–2372.

Carmichael I.S.E. (1967) The mineralogy and petrology of the volcanic rocks from the Leucite Hills, Wyoming. Contrib. Mineral. Petrol. 15, 24–66.

Carmichael I.S.E., Turner F.J. and Verhoogen (1974) Igneous petrology. McGraw- Hill, New York. 739pp.

Carswell D.A. (1975) Primary and secondary phlogopites and clinopyroxenes in garnet lherzolite xenoliths. Phys. Chem. Earth 9, 417–429.

Carswell D.A. and Gibb F.G.F. (1987) Evaluation of mineral thermometers and barometers applicable to garnet lherzolite assemblages. Contrib. Mineral. Petrol. 95, 499–511.

Chapman D.S. and Pollack H.N. (1977) Regional geotherms and lithospheric thickness. Geology 5, 265–268.

Clague D.A. and Frey F.A. (1982) Petrology and trace element geochemistry of the Honolulu volcanics, Oahu. Implications for the oceanic mantle below Hawaii. J. Petrol. 23, 447–504.

Clement C.R. (1975) The emplacement of some diatreme facies kimberlites. Phys. Chem. Earth 9, 51–59.

Clement C.R. (1982) A comparative geological study of some major kimberlite pipes in the Northern Cape and Orange Free State. Ph.D. Thesis, Univ. Capetown.

Clement C.R. and Skinner E.M.W. (1985) A textural-genetic classification of kimberlites. Trans. Geol. Soc. S. Afr. 88, 403–409.

Clement C.R., Skinner E.M.W. and Scott Smith B.H. (1984) Kimberlite redefined. J. Geol. 32, 223–228.

Cohen R.S. and O'Nions R.K. (1982) Identification of recycled continental material from Sr, Nd and Pb isotope investigations. Earth Planet. Sci. Lett. 61, 73–84.

Cohen R.S., O'Nions R.K. and Dawson J.B. (1984) Isotope geochemistry of xenoliths from East Africa: implications for development of mantle reservoirs and their interaction. Earth Planet Sci. Lett. 68, 209–220.

Collerson K.D. and McCulloch M.T. (1983) Nd and Sr isotope geochemistry of leucite bearing lavas from Gaussberg, East Antarctica. Proc. 4th Symp. Antarctic Earth Sci. 676–680.

Cox K.G. (1983) The Karoo province of Southern Africa: origin of trace element enrichment patterns. in Continental Basalts and Mantle Xenoliths. (Eds: C.J. Hawkesworth and M.J. Norry) Shiva Publishing Limited, UK), 139–157.

Cox K.G., Bell J.D. and Pankhurst R.J. (1979) The interpretation of igneous rocks. George Allen and Unwin Ltd., London, 450pp.

Cross W. (1897) The igneous rocks of the Leucite Hills and the Pilot Butte, Wyoming. Am. J. Sci. 4, 115–141.

Cullers R.L., Ramakrishnan S., Berendsen P. and Griffin T. (1985) Geochemistry and petrogenesis of lamproites, Late Cretaceous age, Woodson County, Kansas, U.S.A. Geochim. Cosmochim. Acta 49, 1383–1402.

Cundari A. (1973) Petrology of the leucite-bearing lavas in New South Wales. J. Geol. Soc. Australia 20, 465–492.

Davis G.L. (1977a) The ages and uranium contents of zircon from kimberlites and associated rocks. 2nd Int. Kimberlite Conf., Extended Abstracts.

Davis G.L. (1977b) The ages and uranium contents of zircon from kimberlites and associated rocks. Carnegie Inst. Washington Yearbook 76, 631–635.

Davis G.L. (1978) Zircons from the mantle. United States Geol. Surv. Open-File Report 78–701, Ed: R.E. Zartman, 86–88.

Dawson J.B. (1967a) 1) A review of the geology of kimberlites. In: Ultramafic and related rocks (Ed. P.J. Wyllie) Wiley, New York, 241–251.

Dawson J.B. (1967b) 2) Geochemistry and origin of kimberlite. In: Ultramafic and related rocks (Ed. P.J. Wyllie) Wiley, New York, 269–278.

Dawson J.B. (1971) Advances in kimberlite geology. Earth Sci. Rev. 7, 187–214.

Dawson J.B. (1972) Kimberlites and their relationship to the upper mantle. R. Soc. London Philos. Trans. Ser. A 271, 297–311.

Dawson J.B. (1980) Kimberlites and Their Xenoliths. Springer-Verlag, Berlin, New York, 250pp.

Dawson J.B. (1984) Contrasting types of upper-mantle metasomatism ? In: Kimberlites II: The Mantle and Crust-Mantle Relationships. (Ed: J. Kornprobst) Developments in Petrology 11B, Elsevier, Amsterdam, 289–294.

Dawson J.B. (1987) The kimberlite clan: relationship to olivine and leucite lamproites and inferences for upper mantle metasomatism. In Alkaline Igneous Rocks (Eds: J.G. Fitton and B.G.J. Upton) Geol. Soc. Lond. Spec. Publ. 30, 95–101.

Dawson J.B. and Hawthorne J.B. (1973) Magmatic sedimentation and carbonatite differentiation in kimberlite sills at Benfontein, South Africa. J. Geol. Soc. London 129, 61–85.

Dawson J.B. and Smith J.V. (1975a) Occurrence of diamond in a mica-garnet lherzolite. Nature 254, 580–581.

Dawson J.B. and Smith J.V. (1975b) Chemistry and origin of phlogopite megacrysts in kimberlite. Nature 253, 336–338.

Dawson J.B. and Smith J.V. (1977) The MARID (mica-amphibole-rutile-ilmenite-diopside) suite of xenoliths in kimberlites. Geochim. Cosmochim. Acta 41, 309–323.

Dawson J.B. and Stevens W.E. (1975) Statistical analysis of garnets from kimberlites and associated xenoliths. J. Geol. 83, 589–607.

Deer W.A., Howie R.A. and Zussman J. (1966) An Introduction to the Rock Forming Minerals. Longman Group Ltd., London, 528pp.

Deines P. and Gold D.P. (1973) The isotopic composition of carbonatite and kimberlite carbonates and their bearing on the isotopic composition of deep seated carbon. Geochim. Cosmochim. Acta 37, 1709–1733.

Deines P., Gurney J.J. and Harris J.W. (1984) Associated chemical and carbon isotopic composition variations in diamonds from the Finsch and Premier kimberlites, South Africa. Geochim. Cosmochim. Acta 45, 325–342.

Delaney J.S., Smith J.V., Carswell D.A. and Dawson J.B. (1980) Chemistry of micas from kimberlites and xenoliths– 11. Primary- and secondary-textured micas from peridotite xenoliths. Geochim. Cosmochim. Acta 44, 857–872.

DePaolo D.J. and Wasserburg G.J. (1976) Nd isotopic variations and petrogenetic models. Geophys. Res. Lett. 3, 249–252.

DePaolo D.J. and Wasserburg J.G. (1979) Petrogenetic mixing models and Nd-Sr isotopic patterns. Geochim. Cosmochim. Acta 43, 615–627.

Doe B.R., Leeman W.P., Christiansen K.L. and Hedge C.E. (1982) Lead and strontium isotopes and related trace elements as genetic tracers in the upper Cenozoic rhyolite-basalt association of the Yellowstone Plateau volcanic field. J. Geophys. Res. 86, 4785–4806.

Dodson M.H. (1978) A linear method for second-degree interpolation in cyclical data collection. J. Phys. E. Sci. Instrum. 11, 296.

Dudás, F.O., Carlson R.W. and Eggler D.H. (1987) Regional Middle Proterozoic enrichment of the subcontinental mantle source of igneous rocks from central Montana. Geology 15, 22–25.

Duncan A.R., Erlank A.J. and Marsh J.S. (1984) Regional geochemistry of the Karoo igneous province. Spec. Publ. Geol. Soc. S. Afr. 13, 355–388.

Duncan R.A., Hargreaves R.B. and Brey G.P. (1978) Age, palaeomagnetism and chemistry of melilite basalts in the Southern Cape, South Africa. Geol. Mag. 115, 317–327.

Dupuy C., Dostal J., Marcelot G., Bougault H., Joron J.L. and Treuil M. (1982) Geochemistry of basalts from central and southern New Hebrides arc: implication for their source rock composition. Earth Planet. Sci. Lett. 60, 207–225.

Eggler D.H. (1974) Effects of CO_2 on the melting of peridotite. Carnegie Inst. Washington Yearbook 74, 468–474.

Ellis D.J. and Green D.H. (1979) An experimental study of the effect of Ca upon garnet-clinopyroxene Fe-Mg exchange equilibria. Contrib. Mineral. Petrol. 71, 13–22.

Erlank A.J. and Rickard R.S. (1977) Potassic richterite bearing peridotites from kimberlite and the evidence they provide for mantle metasomatism. 2nd Int. Kimberlite Conf. Santa Fe, Ext. Abs.

Erlank A.J., Allsopp H.L., Hawkesworth C.J. and Menzies M.A. (1982) Chemical and isotopic characteristion of upper mantle metasomatism in peridotite nodules from the Bultfontein kimberlite. Terra Cognita 2, 261–263.

Erlank A.J., Waters F.G., Hawkesworth C.J., Haggerty S.E., Allsopp H.L., Rickard R.S. and Menzies M. (1987) Evidence for mantle metasomatism in peridotite nodules from the Kimberley pipes, South Africa. In: Mantle Metasomatism. (Eds: M.A. Menzies and C.J. Hawkesworth) Academic Press Geology Series), 221–311.

Exley R.A. and Jones A.P. (1983) $^{87}Sr/^{86}Sr$ in kimberlitic carbonates by ion microprobe: hydrothermal alteration, crustal contamination and relation to carbonatite. Contrib. Mineral. Petrol. 83, 288–292.

Exley R.A., Mattey D.P., Pillinger C.T. and Sinton J.M. (1986) Carbon isotope geochemistry of basalts from the Lau and North Fiji marginal basins. Terra Cognita 6, 324.

Faure G. (1977) Principles of Isotope Geology. Wiley, New York, 464pp.

Faure G. and Powell J.L. (1972) Strontium Isotope Geology. Springer-Verlag, Berlin, 188pp.

Fesq H.W., Kable E.J.D. and Gurney J.J. (1975a) Aspects of the geochemistry of kimberlites from the Premier mine, and other selected South African occurrences with particular reference to the rare-earth elements. Phys. Chem. Earth 9, 687–707.

Fesq H.W., Bibby D.M., Erasmus C.S., Kable E.J.D. and Sellschop J.P.F. (1975b) A comparative trace element study of diamonds from Premier, Finsch and Jagersfontein mines, South Africa. Phys. Chem. Earth 9, 817–836.

Fitton J.G., James D.E. and Thirlwall M.F. (1984) A users' guide to the X-ray fluorescence analysis of rock samples. Grant Institute, Edinburgh University, 34pp.

Foley S.F. (1986) The oxidation state of lamproite magmas. Tsch. Min. Pet. Mitt. 34, 217–238.

Foley S.F., Taylor W.R. and Green D.H. (1986a) The effects of fluorine on phase relationships in the system $KAlSiO_4$-Mg_2SiO_4-SiO_2 at 28 Kb and the solution mechanism of fluorine in silicate melts. Contrib. Mineral. Petrol. 93, 46–55.

Foley S.F., Taylor W.R. and Green D.H. (1986b) The role of fluorine and oxygen fugacity in the genesis of the ultrapotassic rocks. Contrib. Mineral. Petrol. 94, 183–192.

Franz G.W. and Wyllie P.J. (1967) Experimental studies in the system CaO-MgO-SiO_2-CO_2-H_2O. In: Ultramafic and related rocks. (Ed. P.J. Wyllie), Wiley, New York, 323–326.

Fraser K.J., Hawkesworth C.J, Erlank A.J., Mitchell R.H. and Scott Smith B.H. (1985) Sr, Nd and Pb isotope and minor element geochemistry of lamproites and kimberlites. Earth Planet. Sci. Lett. 76, 57–70.

Frey F.A. and Green D.H. (1974) The mineralogy, geochemistry and origin of lherzolite inclusions in Victorian basalts. Geochim. Cosmochim. Acta 38, 1023–1059.

Frey F.A., Green D.H. and Roy S.D. (1978) Integrated models of basalt petrogenesis: a study of quartz tholeiites to olivine melilitites from south eastern Australia utilising geochemical and experimental petrological data. J. Petrol. 19, 463–513.

Frey F.A., Roden M.F. and Zindler A. (1980) Constraints on mantle source compositions imposed by phosphorous and the rare-earth elements. Contrib. Mineral. Petrol. 75, 165–173.

Gallimov E.M. (1984) $^{13}C/^{12}C$ of diamonds, vertical zonation of diamond formation in the lithosphere. (Cbophur 3ak 1174) xxvii, IGC Moscow, Doklady 11, 110–123 Geochemistry and cosmochemistry.

Gaspar J.C. and Wyllie P.J. (1984) The alleged kimberlite-carbonatite relationship: evidence from ilmenite and spinel from Premier and Wesselton mines and Benfontein sill, South Africa. Contrib. Mineral. Petrol. 85, 133–140.

Gogineni S.V., Melton C.E. and Giardini A.A. (1978) Some petrological aspects of the Prairie Creek diamond-bearing kimberlite diatreme, Arkansas. Contrib. Mineral. Petrol. 66, 251–261.

Green ii H.W. and Gueguen Y. (1974) Origin of kimberlite pipes by diapiric upwelling in the upper mantle. Nature 249, 617–619.

Green D.H., Falloon T.J., Brey G.P. and Nickel K.G. (1986) Peridotite melting to 6 GPa and genesis of primary mantle-derived magmas. Fourth Int. Kimb. Conf., Ext. Abs., Geol. Soc. Aust. Abstract Series 16), 181–183.

Gurney J.J. and Harte B. (1980) Chemical variation in upper mantle nodules from Southern African kimberlites. R. Soc. London Philos. Trans. 297A, 273–293.

Gurney J.J. and Switzer G.S. (1973) The discovery of garnets closely related to diamonds in the Finsch pipe, South Africa. Contrib. Mineral. Petrol. 39, 103–116.

Gurney J.J., Jakob W.R.O. and Dawson J.B. (1979a) Megacrysts from the Monastery kimberlite pipe, South Africa. In: The Mantle Sample: Inclusions in Kimberlites and Other Volcanics. (Eds: F.R. Boyd and H.O.A. Meyer) AGU Washington), 227–243.

Gurney J.J., Harris J.W. and Rickard R.S. (1979b) Silicate and oxide inclusions in diamonds from the Finsch kimberlite pipe. In: Kimberlites, Diatremes and Diamonds: Their Geology, Petrology and Geochemistry. (Eds: F.R. Boyd and H.O.A. Meyer) AGU Washington, 1–15.

Gurney J.J., Siebert J.C. and Whitfield G.G. (1968) A diamondiferous eclogite from the Roberts Victor mine. Geol. Soc. S. Afr. Spec. Publ. 2, 352–357.

Haggerty S.E. (1986) Diamond genesis in a multiply-constrained model. Nature 320, 34–38.

Hancock S.L. and Rutland R.W.R. (1984) Tectonics of an early Proterozoic geosuture: the Halls Creek orogenic sub-province, northern Australia. Jour. Geodynamics 1, 387–432.

Harley S.L. and Green D.H. (1982) Garnet-orthopyroxene barometry for granulites and peridotites. Nature 300, 697–701.

Harper F.J. (1981) Petrographic examination of kimberlite from Finsch mine with special reference to the mica content (173/24/K1/391). Unpublished Anglo American Research Laboratories report no. 337 m/81/430 GD/81/468 DB/81/82.

Harris J.W. and Collins A.T. (1985) Studies of Argyle diamonds. Industrial Diamond Review 3/85, 128–130.

Harris J.W., Hawthorne J.B. and Oosterveld M.M. (1979) Regional and local variations in the characteristics of diamonds from some Southern African kimberlites. In: Kimberlites, Diatremes and Diamonds: Their Geology, Petrology and Geochemistry. (Eds: F.R. Boyd and H.O.A. Meyer) AGU Washington, 27–41.

Harris J.W., Hawthorne J.B., Oosterveld M.M. and Wehmeyer E. (1975) A classification scheme for diamond and a comparative study of South African diamond characteristics. Phys. Chem. Earth 9, 765–783.

Harris P.G. and Middlemost E.A.K. (1969) The evolution of kimberlites. Lithos 3, 77–88.

Hart S.R. (1984) A large-scale isotope anomaly in the Southern Hemisphere mantle. Nature 309, 753–757.

Hart S.R. and Staudigel H. (1987) Isotopic characterization and identification of recycled component. Crust/mantle recycling at convergence zones. NATO Advanced Research Workshop, Antalya, Turkey, 2–10.

Harte B. (1983) Mantle peridotites and processes—the kimberlite sample. In: Continental Basalts and Mantle Xenoliths. (Eds: C.J. Hawkesworth and M.J. Norry) Shiva Publishing Limited, UK), 46–91.

Harte B., Cox K.G. and Gurney J.J. (1975) Petrography and geological history of upper mantle xenoliths from the Matsoku kimberlite pipe. Phys. Chem. Earth 9, 477–506.

Harte B., Winterburn P.A. and Gurney J.J. (1987) Metasomatic and enrichment phenomena in garnet peridotite facies mantle xenoliths from the Matsoku kimberlite pipe, Lesotho. In: Mantle Metasomatism. (Eds: M.A. Menzies and C.J. Hawkesworth) Academic Press Geology Series), 145–220.

Hawkesworth C.J. and van Calsteren P. (1984) Radiogenic isotopes – some geological applications. In: Rare Earth Element Geochemistry. (Ed: P. Henderson), Elsevier, Oxford, 375–421.

Hawkesworth C.J., Erlank A.J., Marsh J.S., Menzies M.A. and van Calsteren P.W.C. (1983) Evolution of the continental lithosphere: evidence from volcanics and xenoliths in Southern Africa. In: Continental Basalts and Mantle Xenoliths. (Eds: C.J. Hawkesworth and M.J. Norry) Shiva Publishing Limited, UK), 111–138.

Hawkesworth C.J., Fraser K.J. and Rogers N.W. (1985) Kimberlites and lamproites: extreme products of mantle enrichment processes. Trans. Geol. Soc. S. Afr. 88, 439–447.

Hawkesworth C.J., Kempton P.D., Mattey D.P., Palacz Z., Rogers N. and van Calsteren P.W.C. (1987) Intra-mantle fractionation vs. lithosphere recycling: some geochemical evidence. Crust/mantle recycling at convergence zones. NATO Advanced Research Workshop, Antalya, Turkey, 139–144.

Hawkesworth C.J., Norry M.J., Roddick J.C. and Vollmer R. (1979) $^{143}Nd/^{144}Nd$ and $^{87}Sr/^{86}Sr$ ratios from the Azores and their significance in LIL-element enriched mantle. Nature 280, 28–31.

Hawkesworth C.J., Rogers N.W. van Calsteren P.W.C. and Menzies M.A. (1984) Mantle enrichment processes. Nature 311, 331–335.

Hawthorne J.B. (1975) Model of a kimberlite. Phys. Chem. Earth 9, 1–15.

Helmstaedt H. and Gurney J.J. (1984) Kimberlites of Southern Africa — Are they related to subduction processes. In: Kimberlites I: Kimberlites and Related Rocks. (Ed: J. Kornprobst) Developments in Petrology 11A, Elsevier, Amsterdam,425–434.

Helz R.T. (1979) Alkali exchange between hornblende and melt: a temperature sensitive reaction. Am. Mineral. 64, 953–965.

Henderson P. (1982) Inorganic Geochemistry (1982) Pergamon Press, Oxford, 353pp.

Hervig R.L., Smith J.V., Steele I.M., Gurney J.J., Meyer H.O.A. and Harris J.W. (1980) Diamonds: minor elements in silicate inclusions: pressure-temperature implications. J. Geophy. Res. 85, 6919–6929.

Hofmann A.W. and White W.M. (1982) Mantle plumes from ancient oceanic crust. Earth Planet. Sci. Lett. 57, 421–436.

Hole M.J., Saunders A.D. and Marriner G.F. (1984) Subduction of pelagic sediments: implications for the origin of Ce-anomalous basalts from the Mariana islands. J. Geol. Soc. Lond. 141, 453–472.

Holmes A. (1936) A contribution to the petrology of kimberlite and its inclusions. Trans. Geol. Soc. S. Afr. 39, 379–427.

Hunter R.H. and Taylor L.A. (1984) Magma-mixing in the low velocity zone: kimberlitic megacrysts from Fayette county, Pennsylvania. Am. Mineral. 69, 16–29.

Ilupin I.P. and Lutz B.G. (1971) The chemical composition of kimberlite and questions on the origin of kimberlite magmas. Sovetskaya Geol. 6, 61–73.

Jaques A.L., Gregory C.P., Lewis L.D. and Ferguson J. (1982) The ultrapotassic rocks of the West Kimberley region, Western Australia, and a new class of diamondiferous kimberlites. Terra Cognita 2, 251–252.

Jaques A.L., Lewis J.D. and Smith C.B. (1986a) The kimberlites and lamproites of Western Australia. Geol. Survey Western Aust. Bulletin 132, Government Printing Office, Perth, 268pp.

Jaques A.L., Lewis J.D., Smith C.B., Gregory G.P., Ferguson J., Chappell B.W. and McCulloch M.T. (1984a) The diamond-bearing ultrapotassic (lamproitic) rocks of the West Kimberley region, Western Australia. In BIKC, 225–254.

Jaques A.L., Sheraton J.W., Hall A.E., Smith C.B., Sun S.S., Drew R. and Foudoulis C. (1986a) Composition of crystalline inclusions and C-isotopic composition of Argyle and Ellendale diamonds. Fourth Int. Kimb. Conf., Ext. Abs., Geol. Soc. Aust. Abstract Series 16), 426–428.

Jaques A.L., Webb A.W., Fanning C.M., Black L.P., Pidgeon R.T., Ferguson J., Smith C.B. and Gregory G.P. (1984b) The age of the diamond bearing pipes and associated leucite lamproites of the West Kimberley region, Western Australia. J. Aust. Geol. and Geophy. 9, 1–7.

Jones A.P., Smith J.V. and Dawson J.B. (1982) Mantle metasomatism in 14 veined peridotites from Bultfontein mine, South Africa. J. Geol. 90, 435–453.

Jordan T.H. (1978) Composition and development of the continental tectosphere. Nature 274, 544–548.

Kable E.J.D., Fesq H.W. and Gurney J.J. (1975) The significance of the inter-element relationships of some minor and trace elements in South African kimberlites. Phys. Chem. Earth 9, 709–734.

Kay R.W. and Gast P.W. (1973) Rare earth content and origin of alkali-rich basalts. J. Geol. 81, 653–682.

Kemp J.F. (1897) The Leucite Hills of Wyoming. Geol. Soc. Am. 8, 169–182.

Kemp J.F. and Knight W.C. (1903) Leucite Hills of Wyoming. Bull. Geol. Soc. Am. 14, 305–336.

Kempton P.D. (1987) Metasomatism and enrichment in lithospheric peridotites. In: Mantle Metasomatism. (Eds: M.A. Menzies and C.J. Hawkesworth) Academic Press Geology Series), 45–89.

Kleeman J.D., Green D.H. and Lovering J.F. (1969) Uranium distribution in ultramafic inclusions from Victorian basalts. Earth Planet. Sci. Lett. 5, 449–458.

Kornprobst J. (1984a) Kimberlites I: Kimberlites and related rocks. Developments in Petrology 11A, Elsevier Press, Amsterdam, 446pp.

Kornprobst J. (1984b) Kimberlites II: the mantle and crust-mantle relationships. Developments in Petrology 11B, Elsevier, Amsterdam, 393pp.

Kramers J.D. (1977) Lead and strontium isotopes in Cretaceous kimberlites and mantle derived xenoliths from Southern Africa. Earth Planet. Sci. Lett. 34, 419–431.

Kramers J.D. (1979) Lead, uranium, strontium, poassium and rubidium in inclusion-bearing diamonds and mantle-derived xenoliths from Southern Africa. Earth Planet. Sci. Lett. 42, 58–70.

Kramers J.D., Roddick J.C.M. and Dawson J.B. (1983) Trace element and isotope studies on veined, metasomatic and 'MARID' xenoliths from Bultfontein, South Africa. Earth Planet. Sci. Lett. 65, 90–106.

Kramers J.D., Smith C.B., Lock N.P., Harmon R.S. and Boyd F.R. (1981) Can kimberlites be generated from an ordinary mantle? Nature 291, 53–56.

Kretz R. (1982) Transfer and exchange equilibria in a portion of the pyroxene quadrilateral as deduced from natural and experimental data. Geochim. Cosmochim. Acta 46, 411–421.

Kuehner S.M., Edgar A.D. and Arima M. (1981) Petrogenesis of the ultrapotassic rocks from the Leucite Hills, Wyoming. Am. Mineral. 66, 663–677.

Kushiro I. (1968) Compositions of magma formed by partial zone melting of the earth's upper mantle. J. Geophys. Res. 73, 619–637.

Kushiro I. (1972) Effect of water on the compositions of magmas formed at high pressures. J. Petrol. 13, 311–334.

Kushiro I. (1980) Changes with pressure of degree of partial melting and K_2O content of liquids in the system Mg_2SiO_4–$KAlSiO_4$–SiO_2. Carnegie Inst. Washington Yearbook 79, 267–271.

Leeman W.P. (1982) Olivine tholeiite basalts of the Snake River Plain, Idaho. In: Cenozoic geology of Idaho. Eds. B. Bonnichsen and R.M. Breckenridge. Idaho Bureau of Mines and Geology Bulletin 26, 181–191.

Le Bas M.J. (1984) Oceanic carbonatites. In: Kimberlites I: Kimberlites and Related Rocks. (Ed: J. Kornprobst) Developments in Petrology 11A, Elsevier, Amsterdam, 169–178.

Le Roex A. (1986) Geochemical correlation between southern African kimberlites and South Atlantic hotspots. Nature 324, 243–245.

Lewis H.C. (1888) The matrix of diamond. Geol. Mag. 5, 129–131.

Lloyd F.E. and Bailey D.K. (1975) Light element metasomatism of the continental mantle: the evidence and the consequences. Phys. Chem. Earth 9, 389–416.

Lucas H., Ramsay R., Hall A.E., Smith C.B. and Sobolev N.V. (1986) Garnets from Western Australian kimberlites and associated rocks. Fourth Int. Kimb. Conf., Ext. Abs., Geol. Soc. Aust. Abstract Series 16), 270–272.

Luth W.C. (1967) Studies in the system $KAlSiO_4$–Mg_2SiO_4–SiO_2–H_2O. 1. Inferred phase relations and petrologic applications. J. Petrol. 8, 372–416.

MacDowell F.W. (1966) Potassium-argon dating of Cordilleran intrusives. Ph.D. thesis, Columbia University, New York.

MacGregor I.D. (1974) The system MgO–Al_2O_3–SiO_2: solubility of Al_2O_3 in enstatite for spinel and garnet peridotite compositions. Am. Mineral. 59, 110–119.

MacGregor I.D. and Manton W.I. (1986) Roberts Victor eclogites: ancient oceanic crust. J. Geophys. Res. 91, 14,063–14,079.

Mantovani, M.S.M., Marques L.S., De Sousa M.A., Civetta L., Attalla L. and Innocenti F. (1985) Trace element and strontium isotope constraints on the origin and evolution of Paran'a continental flood basalts of Santa Catarina State (Southern Brazil). J. Petrol. 26, 187–209.

Marvin R.F., Hearn B.C.Jr., Mehnert H.H., Naeser C.W., Zartman R.E. and Lindsay D.A. (1980) Late Cretaceous-Paleocene-Eocene igneous activity in North-Central Montana. Isochron/West No. 29, 5–25.

Mathez E.A., Dietrich V.J. and Irving A.J. (1984) The geochemistry of carbon in mantle peridotites. Geochim. Cosmochim. Acta 48, 1849–1859.

Matson R.E. (1960) Petrography and petrology of Smoky Butte intrusives, Garfield County, Montana. M.Sc. thesis, Montana State Univ. Missoula.

Matson D.W., Muenow D.W. and Garcia M.O. (1986) Volatile contents of phlogopite micas from South African kimberlite. Contrib. Mineral. Petrol. 93, 399–408.

Mattey D.P. (1987) Carbon isotopes in the mantle. Terra Cognita 7, 31–37.

Mattey D.P., Carr R.H., Wright I.P. and Pillinger C.T. (1984) Carbon isotopes in submarine basalts. Earth Planet. Sci. Lett. 70, 196–206.

Mattey D.P., Exley R.A., Pillinger C.T., Menzies M.A., Porcelli D.R., Galer S. and O'Nions R.K. (1987) Relationships between C, He, Sr and Nd isotopes in mantle diopsides. Spec. Publ. Geol. Soc. Aust. (in Press).

McCallister R.H., Meyer H.O.A. and Aragon R. (1979) Partial thermal history of two evolved clinopyroxenes from the Thaba Putsoa kimberlite pipe, Lesotho. In: The Mantle Sample: Inclusions in Kimberlites and Other Volcanics. (Eds: F.R. Boyd and H.O.A. Meyer) AGU Washington), 244–248.

McCallum M.E. and Eggler D.H. (1976) Diamonds in an upper mantle peridotite nodule from kimberlite in southern Wyoming. Science 192, 253–256.

McCulloch M.T. (1987) Crust mantle recycling: inputs and outputs. Crust/-mantle recycling at convergence zones. NATO Advanced Research Workshop, Antalya, Turkey, 127–136.

McCulloch M.T., Jaques A.L., Nelson D.R. and Lewis J.D. (1983) Nd and Sr isotopes in kimberlites and lamproites from Western Australia: an enriched mantle origin. Nature 302, 400–403.

McGetchin T.R. and Besancon J.R. (1973) Carbonate inclusions in mantle-derived pyrope. Earth Planet Sci. Lett. 18, 408–410.

McIver J.R. (1981) Aspects of ultrabasic and basic alkaline intrusive rocks from Bitterfontein, South Africa. Contrib. Mineral. Petrol. 78, 1–11.

McIver J.R. and Ferguson J. (1979) Kimberlitic, melilititic, trachytic and carbonatite eruptives at Saltpetre Kop, Sutherland, South Africa. In: Kimberlites, Diatremes and Diamonds: Their Geology, Petrology and Geochemistry. (Eds: F.R. Boyd and H.O.A. Meyer) AGU Washington, 111–128.

McKenzie D. (1985) The extraction of magma from the crust and mantle. Earth Planet. Sci. Lett. 74, 81–91.

McLennan S.M. and Taylor S.R. (1981) Role of subducted sediments in island-arc magmatism: constraints on REE patterns. Earth Planet. Sci. Lett. 54, 423–430.

Meen J.K. (1983) Isotopic compositions of some Laramide volcanics, Absaroka Mountains, Montana. Carnegie Institute of Washington Yearbook 82, 481–486.

Menzies M. (1983) Mantle ~~ultramafic~~ xenoliths in alkaline magmas: evidence for mantle heterogeneity modified by magmatic activity. Continental Basalts and Mantle Xenoliths. (Eds: C.J. Hawkesworth and M.J. Norry) Shiva Publishing Limited, UK), 92–110.

Menzies M.A. and Hawkesworth C.J. (1987) Mantle metasomatism. Academic Press Geology Series, 472pp.

Menzies M. and Murthy V.R. (1980) Enriched mantle: Nd and Sr isotopes in diopsides from kimberlite nodules. Nature 283, 634–636.

Menzies M.A. and Wass S.Y. (1983) CO_2 and LREE-rich mantle below eastern Australia: a REE and isotopic study of alkaline magmas and apatite-rich mantle xenoliths from the Southern Highlands Province, Australia. Earth Planet Sci. Lett. 65, 287–302.

Menzies M.A., Rogers N., Tindle A. and Hawkesworth C.J. (1987) Metasomatic and enrichment processes in lithospheric peridotites, an effect of asthenosphere–lithosphere interaction. In: Mantle Metasomatism. (Eds: M.A. Menzies and C.J. Hawkesworth) Academic Press Geology Series), 313–361.

Meyer H.O.A. (1976) Kimberlites of the continental United States: a review. J. Geol. 84, 377–403.

Meyer H.O.A. (1985) Genesis of diamond: a mantle saga. Am. Mineral. 70, 344–355.

Miser H.D. and Purdue A.H. (1929) Geology of the De Queen and Caddo Gap quadrangle, Arkansas. U.S. Geol. Survey Bull. 808, 195pp.

Miser H.D. and Ross C.S. (1923) Diamond-bearing peridotite in Pike County, Arkansas. U.S. Geol. Surv. Bull. 735, 279–322.

Mitchell R.H. (1979) The alleged kimberlite-carbonatite relationship: additional contrary evidence. Am. J. Sci. 279, 570–589.

Mitchell R.H. (1981) Titaniferous phlogopite from the leucite lamproites of the West Kimberley area, Western Australia. Contrib. Mineral. Petrol. 76, 243–251.

Mitchell R.H. (1985) A review of the mineralogy of lamproites. Trans. Geol. Soc. S. Afr. 88, 411–437.

Mitchell R.H. (1986) Kimberlites. Mineralogy, geochemistry and petrology. Plenum Press, New York and London. 442pp.

Mitchell R.H. and Brunfelt A.O. (1975) Rare earth element geochemistry of kimberlite. Phys. Chem. Earth 9, 671–685.

Mitchell R.H. and Crocket J.H. (1971) The isotopic composition of strontium in some South African kimberlites. Contrib. Mineral. Petrol. 30, 277–290.

Mitchell R.H. and Hawkesworth C.J. (1984) Geochemistry of potassic lavas from Smoky Butte. Abs. w/prog. Geol. Soc. Am. Ann. Mtg. Reno 16, 507 (abstract).

Mitchell R.H. and Lewis R.D. (1983) Priderite-bearing xenoliths from the Prairie Creek mica peridotite, Arkansas. Canad. Mineral. 21, 59–64.

Mitchell R.H., Platt R.G. and Downey M. (1987) Petrology of lamproites from Smoky Butte, Montana. J. Petrol. 28, 645–677.

Moorbath S. and Taylor P.N. (1985) Geochronology and related isotope geochemistry of high-grade metamorphic rocks from the lower continental crust. In: The Nature of the Lower Continental Crust. (Eds: J.B. Dawson, D.A. Carswell, J. Hall and K.H. Wedepohl) Geol. Soc. Spec. Publ. No. 24, Blackwell Scientific Publications, UK, 211–220.

Morgan J.W. (1982) Hotspot tracks and the opening of the Atlantic and Indian Oceans. In: The Sea, V. 7.(Ed: C. Emiliani) Wiley, New York, 434–487.

Morris J.D. and Hart S.R. (1983) Isotopic and incompatible element constraints on the genesis of island arc volcanics from Cold Bay and Amak Island, Aleutians and implications for mantle structure. Geochim. Cosmochim. Acta 47, 2015–2030.

Nakamura N. (1974) Determination of REE, Ba, Fe, Mg, Na and K in carbonaceous and ordinary chondrites. Geochim. Cosmochim. Acta 39, 757–775.

Nelson D.R. and McCulloch M.T. (1987) Enriched mantle components and mantle recycling of sediments. Proc. 4th Int. Kimb. Conf., (in press).

Nelson D.R., McCulloch M.T. and Ringwood A.E. (1986b) Ultrapotassic magmas: end-products of subduction and mantle recycling of sediments? Fourth Int. Kimb. Conf., Ext. Abs., Geol. Soc. Aust. Abstract Series 16), 196–198.

Nelson D.R., McCulloch M.T. and Sun S.S. (1986a) The origins of ultrapotassic rocks as inferred from Sr, Nd and Pb isotopes. Geochim. Cosmochim. Acta 50, 231–245.

Newsom H.E., White W.M., Jochum K.P. and Hofmann A.W. (1986) Siderophile and chalcophile element abundances in oceanic basalts, Pb isotope evolution and growth of the Earth's core. Earth Planet. Sci. Lett. 80, 299–313.

Nickel K.G., Brey G.P. and Kogarko L. (1985) Orthopyroxene-clinopyroxene equilibria in the system CaO-MgO-Al_2O_3-SiO_2 (CMAS): new experimental results and implications for two pyroxene thermometry. Contrib. Mineral. Petrol. 91, 44–53.

Niggli P. (1923) Gesteins-und Mineral provinzen. Bd. 1. Verlag Gebruder. Gebruder Borntraeger, Berlin, 602pp.

Nixon P.H. and Boyd F.R. (1973a) Petrogenesis of the granular and sheared ultrabasic nodule suite in kimberlite. In: Lesotho Kimberlites. (Ed. P.H. Nixon), Lesotho National Development Corporation, Maseru, 48–56.

Nixon P.H. and Boyd F.R. (1973b) The discrete nodule (megacryst) association in kimberlites from Northern Lesotho. In Lesotho Kimberlites (Ed. P.H. Nixon) Lesotho National Development Corporation, Maseru, 67–75.

Nixon P.H., Rogers N.W., Gibson I.L. and Grey A. (1981) Depleted and fertile mantle xenoliths from Southern African kimberlites. Ann. Rev. Earth Planet. Sci. 9, 285–309.

Nixon P.H., Thirlwall M.F., Buckley F. and Davies C.J. (1984) Spanish and Western Australian lamproites: aspects of whole rock geochemistry. In: Kimberlites I: Kimberlites and Related Rocks. (Ed: J. Kornprobst) Developments in Petrology 11A, Elsevier, Amsterdam, 285–296.

Norry M.J. and Fitton J.G. (1983) Compositional differences between oceanic and continental basic lavas and their significance. In: Continental Basalts and Mantle Xenoliths. (Eds: C.J. Hawkesworth and M.J. Norry) Shiva Publishing Limited, UK), 5–19.

Ogden P.R.Jr. (1979) The geology, major element geochemistry and petrogenesis of the Leucite Hills volcanic rocks, Wyoming. Ph.D. thesis, Univ. Wyoming.

O'Hara M.J. and Yoder H.S. (1967) Formation and fractionation of basic magmas at high pressure. Scottish J. Geol. 3, 67–117.

Olafsson M. and Eggler D.H. (1983) Phase relations of amphibole, amphibole-carbonate and phlogopite-carbonate peridotite: petrologic constraints on the asthenosphere. Earth Planet Sci. Lett. 64, 305–315.

O'Neill H.St.C., Jaques A.L., Smith C.B. and Moon J. (1986) Diamond-bearing peridotite xenoliths from the Argyle (AKI) pipe. Fourth Int. Kimb. Conf., Ext. Abs., Geol. Soc. Aust. Abstract Series 16), 300–302.

O'Nions R.K., Carter S.R., Evensen N.M. and Hamilton P.J. (1979) Geochemical modelling of mantle differentiation and crustal growth. J. Geophys. Res. 84, 6091–6101.

Palacz Z.A. and Saunders A.D. (1986) Coupled trace element and isotope enrichment in the Cook-Austral-Samoa islands, Southwest Pacific. Earth Planet. Sci. Lett. 79, 270–280.

Parmentier E.M., Turcotte D.L. and Torrance K.E. (1975) Numerical experiments on the structure of mantle plumes. J. Geophys. Res. 80, 4417–4424.

Pasteris J.D. (1980) The significance of groundmass ilmenite and megacryst ilmenite in kimberlites. Contrib. Mineral. Petrol. 75, 315-325.

Pearce J.A. (1983) Role of the sub-continental lithosphere in magma genesis at active continental margins. In: Continental Basalts and Mantle Xenoliths. (Eds: C.J. Hawkesworth and M.J. Norry) Shiva Publishing Limited, UK), 330–349.

Pearce J.A., Harris N.B.W. and Tindle A.G. (1984) Trace element discrimination diagrams for the tectonic interpretation of granitic rocks. J. Petrol. 25, 956–983.

Peterman Z.E. (1979) Geochronology and the Archaean of the United States. Econ. Geol. 74, 1544–1562.

Pidgeon R.T., Smith C.B. and Fanning C.M. (1986) The ages of kimberlite and lamproite emplacement in Western Australia. Fourth Int. Kimb. Conf., Ext. Abs., Geol. Soc. Aust. Abstract Series 16), 136–138.

Potts P.J., Thorpe O.W. and Watson J.S. (1981) Determination of the rare-earth element abundances in twenty-nine international rock standards by instrumental neutron activation analysis: a critical appraisal of calibration errors. Chem. Geol. 34, 331–352.

Potts P.J. Thorpe O.W., Issacs M.C. and Wright D.W. (1985) High-precision instrumental neutron-activation analysis of geological samples employing simultaneous counting with both planar and coaxial detectors. Chem. Geol. 48, 145–155.

Powell J.L. (1966) Isotopic composition of strontium in carbonatites and kimberlites. Mineral. Soc. India-Internat. Mineral. Soc. Papers 4th Gen. Mtg., 58–66.

Powell J.L. and Bell K. (1970) Strontium isotopic studies of alkalic rocks: localities from Australia, Spain and the Western United States. Contrib. Mineral. Petrol. 27, 1–10.

Prider R.T. (1960) The leucite lamproites of the Fitzroy Basin, Western Australia. J. Geol. Soc. Australia 6, 71–118.

Prider R.T. (1982) A glassy lamproite from the West Kimberley area, Western Australia. Mineral. Mag. 45, 279–282.

Prinz M., Manson D.V., Hlava P.F. and Keil K. (1975) Inclusions in diamonds: garnet lherzolite and eclogite assemblages. Phys. Chem. Earth 9, 797–816.

Reid A.M., Brown R.W., Dawson J.B., Whitfield G.G. and Siebert J.C. (1976) Garnet and pyroxene compositions in some diamondiferous eclogites. Contrib. Mineral. Petrol. 58, 203–220.

Richardson S.H. (1986) Latter-day origin of diamonds of eclogite paragenesis. Nature 322, 623–626.

Richardson S.H. (1986) Origin of diamonds of peridotitic and eclogitic paragenesis. Fourth Int. Kimb. Conf., Ext. Abs., Geol. Soc. Aust. Abstract Series 16), 418–420.

Richardson S.H., Erlank A.J., Duncan A.R. and Reid D.L. (1982) Correlated Nd, Sr and Pb isotope variation in Walvis Ridge basalts and implications for the evolution of their mantle source. Earth Planet. Sci. Lett. 59, 327–342.

Richardson S.H., Erlank A.J. and Hart S.R. (1985) Kimberlite-borne garnet peridotite xenoliths from old enriched subcontinental lithosphere. Earth Planet. Sci. Lett. 75, 116–128.

Richardson S.H., Gurney J.J., Erlank A.J. and Harris J.W. (1984) Origin of diamonds in old enriched mantle. Nature 310, 198–202.

Richter F.M. (1985) Models for the Archean thermal regime. Earth Planet. Sci. Lett. 73, 350–360.

Rickwood P.C. and Mathias M. (1970) Diamondiferous eclogite xenoliths in kimberlite, Lithos 3, 223–225.

Ridley W. and Dawson J.B. (1975) Lithophile trace element data bearing on the origin of peridotite xenoliths, ankaramite and carbonatite from Lashaine volcano, Tanzania. Phys. Chem. Earth 9, 559–570.

Ringwood A.E. (1975) Composition and Petrology of the Earth's Mantle. McGraw-Hill, United States. 618pp.

Robert J.L. (1976) Titanium solubility in synthetic phlogopite solid solutions. Chem. Geol. 17, 213–227.

Robey J.V.A. (1982) Petrography of lamproites from Ellendale A pipe – 601/126/PK/1/1 to 4 DB/82/37. De Beers Internal Report, Ref. No. PI/82–45.

Rogers N.W., Hawkesworth C.J., Parker R.J. and Marsh J.S. (1985) The geochemistry of potassic lavas from Vulsini, central Italy and implications for mantle enrichment processes beneath the Roman region. Contrib. Mineral. Petrol. 90, 244–257.

Ruotsala A.P. (1975) Alteration of the Finsch kimberlite pipe, South Africa. Econ. Geol. 70, 587–590.

Salters V.J.M. and Barton M. (1985) The geochemistry of ultrapotassic lavas from the Leucite Hills, Wyoming. EOS 66, 1109.

Saxena S.K. (1979) Garnet-clinopyroxene geothermometer. Contrib. Mineral. Petrol. 70, 229–235.

Schulze D.J. (1986) Calcium anomalies in the mantle and a subducted metaserpentinite origin for diamonds. Nature 319, 483–485.

Scott B.H. (1979) Petrogenesis of kimberlites and associated potassic lamprophyres from Central West Greenland. In: Kimberlites, Diatremes and Diamonds: Their Geology, Petrology and Geochemistry. (Eds: F.R. Boyd and H.O.A. Meyer) AGU Washington, 190–205.

Scott Smith B.H. and Skinner E.M.W. (1984a) A new look at Prairie Creek, Arkansas. In: Kimberlites I: Kimberlites and Related Rocks. (Ed: J. Kornprobst) Developments in Petrology 11A, Elsevier, Amsterdam, 255–283.

Scott Smith B.H. and Skinner E.M.W. (1984b) Diamondiferous lamproites. J. Geol. 92, 433–438.

Scott Smith B.H., Danchin R.V., Harris J.W. and Stracke K.J. (1984) Kimberlites near Orroroo, South Australia. In: Kimberlites I: Kimberlites and Related Rocks. (Ed: J. Kornprobst) Developments in Petrology 11A, Elsevier, Amsterdam, 121–142.

Shee S.R. (1984) The oxide minerals of the Wesselton mine kimberlite, Kimberley, South Africa. In: Kimberlites I: Kimberlites and Related Rocks. (Ed: J. Kornprobst) Developments in Petrology 11A, Elsevier, Amsterdam, 59–73.

Shee S.R., Gurney J.J. and Robinson D.N. (1982) Two diamond-bearing peridotite xenoliths from the Finsch kimberlite, South Africa. Contrib. Mineral. Petrol. 81, 79–87.

Sheppard S.M.F. and Dawson J.B. (1975) Hydrogen, carbon and oxygen isotope studies of megacryst and matrix minerals from Lesothan and South African kimberlites. In: Phys. Chem. Earth 9, 747–763.

Shimizu N. (1975) Rare earth elements in garnets and clinopyroxenes from garnet lherzolite nodules in kimberlites. Earth Planet. Sci. Lett. 25, 26–32.

Shimizu N. and Richardson S.H. (1987) Trace element abundance patterns of garnet inclusions in peridotite-suite diamonds. Geochim. Cosmochim. Acta 51, 755–758.

Skinner E.M.W. (1982) Core drilling on the Seltrust Pipe 2 lamproite (601,126,PK12) Australia. Geology Dept., De Beers Consolidated Mines Ltd.

Skinner E.M.W. (1986) Contrasting Group 1 and Group 2 kimberlite petrology: towards a genetic model for kimberlites. Fourth Int. Kimb. Conf., Ext. Abs., Geol. Soc. Aust. Abstract Series 16), 202–204.

Skinner E.M.W. and Clement C.R. (1979) A mineralogical classification of Southern African kimberlites. In: Kimberlites, Diatremes and Diamonds: Their Geology, Petrology and Geochemistry. (Eds: F.R. Boyd and H.O.A. Meyer) AGU Washington, 129–139.

Skinner E.M.W., Smith C.B., Bristow J.W., Scott Smith B.H. and Danchin R.V. (1985) Proterozoic kimberlites and lamproites and a preliminary age for the Argyle lamproite pipe, Western Australia. Trans. Geol. Soc. S. Afr. 88, 335–340.

Smith C.B. (1983a) Pb, Sr and Nd isotopic evidence for sources of Southern African Cretaceous kimberlites. Nature 304, 51–54.

Smith C.B. (1983b) Rubidium-strontium, Uranium-lead and samarium-neodymium isotopic studies of kimberlites and selected mantle-derived xenoliths. Ph.D. thesis, unpublished, Bernard Price Institute of Geophysical Research, Johannesburg.

Smith C.B., Gurney J.J., Harris J.W., Robinson D.N., Shee S.R. and Jagoutz E. (1986) Sr and Nd isotopic systematics of diamond-bearing eclogite xenoliths and eclogitic inclusions in diamond from Southern Africa. Fourth Int. Kimb. Conf., Ext. Abs., Geol. Soc. Aust. Abstract Series 16), 332–334.

Smith C.B., Gurney J.J., Skinner E.M.W., Clement C.R. and Ebrahim (1985) Geochemical character of Southern African kimberlites: a new approach based on isotopic constraints. Trans. Geol. Soc. South Afr. 88, 267–281.

Smith J.V., Brennescholtz R. and Dawson J.B. (1978) Chemistry of micas from kimberlites and xenoliths—1. Micaceous kimberlites. Geochim. Cosmochim. Acta. 42, 959–971.

Smith J.V., Hervig R.L., Ackermand D. and Dawson J.B. (1979) K, Rb and Ba in micas from kimberlite and peridotitic xenoliths and implications for the origin of basaltic rocks. In: Kimberlites, Diatremes and Diamonds: Their Geology, Petrology and Geochemistry. (Eds: F.R. Boyd and H.O.A. Meyer) AGU Washington, 241–251.

Sobolev V.S., Bazarova T.J. and Yagi K. (1975) Crystallisation temperature of wyomingite from Leucite Hills. Contrib. Mineral. Petrol. 49, 301–308.

Sobolev N.V., Galimov E.M., Ivanovskaya I.N. and Yefimova E.S. (1979) The carbon isotopic composition of diamonds containing crystallographic inclusions. Doklady Akedemia Nauk. SSSR 207, 164–167.

Spera F.J. (1987) Dynamics of translithospheric migration of metasomatic fluid and alkaline magma. In: Mantle Metasomatism. (Eds: M.A. Menzies and C.J. Hawkesworth) Academic Press Geology Series), 1–20.

Stacey J.S. and Kramers J.D. (1975) Approximation of terrestrial lead isotope evolution by a 2 stage model. Earth Planet. Sci. Lett. 26, 207–221.

Stecher O., Thy P. and Carlson R.W. (1987) Subcrustal metasomatism below West Greenland: Isotopic and geochemical evidence from lamproite and kimberlite dykes. Terra Cognita 7, 621.

Stille P., Unruh D.M. and Tatsumoto M. (1983) Pb, Sr, Nd and Hf isotopic evidence of multiple sources for Oahu, Hawaii basalts. Nature 304, 25–29.

Sun S.S. (1980) Lead isotopic study of young volcanic rocks from mid-ocean ridges, ocean islands and island arcs. Phil. Trans. Roy. Soc. London A297, 409–445.

Taylor S.R. and McClennan S.M. (1985) The continental crust: Its composition and evolution. Geoscience texts, Blackwell Scientific Publications, UK. 312pp.

Tröger W.E. (1935) Spezialle petrographic der eruptivgesteine, ein nomenclature kompendium. Verlag ger Deutschen mineralischan gessellschaft, Berlin 360pp.

Tsai H. and Meyer H.O.A. (1979) Mineral inclusions in diamond: Premier, Jagersfontein and Finsch kimberlites, South Africa and Williamson mine, Tanzania. In: Kimberlites, Diatremes and Diamonds: Their Geology, Petrology and Geochemistry. (Eds: F.R. Boyd and H.O.A. Meyer) AGU Washington, 16–26.

Velde D. (1975) Armalcolite-Ti-phlogopite-diopside-analcite-bearing lamproites from Smoky Butte, Garfield County, Montana. Am. Mineral. 60, 566–573.

Vollmer R., Ogden P., Schilling J.G., Kingsley R.H. and Waggoner D.G. (1984) Nd and Sr isotopes in ultrapotassic volcanic rocks from the Leucite Hills, Wyoming. Contrib. Mineral. Petrol. 87, 359–368.

Wade A. and Prider R.T. (1940) The leucite-bearing rocks of the West Kimberley area, Western Australia. Q. J. Geol. Soc. London 96, 39–98.

Wagner P.A. (1914) The diamond fields of Southern Africa. Transvaal Leader, Johannesburg.

Wagner C. and Velde D. (1986) The mineralogy of K-richterite bearing lamproites. Am. Mineral. 77, 17–37.

Walsh J.N., Buckley F. and Barker J. (1981) The simultaneous determination of the rare-earth elements in rocks using inductively coupled plasma source spectrometry. Chem. Geol. 33, 141–153.

Wass S.Y. and Rogers N.W. (1980) Mantle metasomatism – precursor to continental alkaline volcanism. Geochim. Cosmochim. Acta 44, 1811–1823.

Waters F.G. (1986) A suggested origin of MARID nodules in kimberlites by high pressure crystallisation of lamproite magma. Fourth Int. Kimb. Conf., Ext. Abs., Geol. Soc. Aust. Abstract Series 16), 352–354.

Waters F.G. (1987) A suggested origin of MARID xenoliths in kimberlites by high pressure crystallisation of an ultrapotassic rock such as lamproite. Contrib. Mineral. Petrol. 95, 523–533.

Weaver B.L. and Tarney J. (1983) Chemistry of the sub-continental mantle: inferences from Archaean and Proterozoic dykes and continental flood basalts. Continental Basalts and Mantle Xenoliths. (Eds: C.J. Hawkesworth and M.J. Norry) Shiva Publishing Limited, UK), 209–229.

Weaver B.L. and Tarney J. (1984) Empirical approach to estimating the composition of the continental crust. Nature 310, 575–577.

Weaver B.L., Wood D.A., Tarney J. and Joron J.L. (1986) Role of subducted sediment in the genesis of ocean-island basalts: geochemical evidence from South Atlantic ocean islands. Geology 14, 275–278.

Wedepohl K.H. and Muramatsu Y. (1979) The chemical composition of kimberlites compared with the average composition of three basaltic magma types. In: Kimberlites, Diatremes and Diamonds: Their Geology, Petrology and Geochemistry. (Eds: F.R. Boyd and H.O.A. Meyer) AGU Washington, 300-312.

Wells P.R.A. (1977) Pyroxene thermometry in simple and complex systems. Contrib. Mineral. Petrol. 62, 129–139.

White W.M. (1987) Geochemical evidence for crust-to-mantle recycling in subduction zones. Crust/mantle recycling at convergence zones. NATO Advanced Research Workshop, Antalya, Turkey, 165–174.

White W.M. and Hofmann A.W. (1982) Sr and Nd isotope geochemistry of oceanic basalts and mantle evolution. Nature 296, 821–825.

Windley B.F. (1977) The Evolving Continents. Wiley, London. 385pp

Wood B.J. (1974) Solubility of alumina in orthopyroxene coexisting with garnet. Contrib. Mineral. Petrol. 46, 1–15.

Wood B.J. and Banno S. (1973) Garnet-orthopyroxene and orthopyroxene-clinopyroxene relationships in simple and complex systems. Contrib. Mineral. Petrol. 42, 109–124.

Wood D.A., Tarney J., Varet J., Saunders A.D., Bougault H., Joron J.L., Treuil M. and Cann J.R. (1979) Geochemistry of basalts drilled in the North Atlantic by IPOD Leg 49: implications for mantle heterogeneity. Earth Planet. Sci. Lett. 42, 77–97.

Wyllie P.J. (1977) Mantle fluid compositions buffered by carbonated in peridotite-CO_2-H_2O. J. Geol. 84, 187–208.

Wyllie P.J. (1978) Mantle fluid compositions in peridotite-CO_2-H_2O buffered by carbonated, amphiboles and phlogopite. J. Geol. 86, 687–713.

Wyllie P.J. (1979) Kimberlite magmas from the system peridotite-CO_2-H_2O. In: Kimberlites, Diatremes and Diamonds: Their Geology, Petrology and Geochemistry. (Eds: F.R. Boyd and H.O.A. Meyer) AGU Washington, 319–329.

Wyllie P.J. (1980) The origin of kimberlite. J. Geophys. Res. 85, 6902–6910.

Wyllie P.J. and Huang W.L. (1976) Carbonation and melting reactions in the system CaO-MgO-SiO_2-CO_2 at mantle pressures with geophysical and petrological applications. Contrib. Mineral. Petrol. 54, 79–107.

Zindler A., Jagoutz E. and Goldstein S. (1982) Nd, Sr and Pb isotopic systematics in a 3-component mantle: a new perspective. Nature 298, 519–523.